OCEANOGRAPHIC AND MORPHODYNAMIC MONITORING OF A MULTI-PURPOSE REEF AT MOUNT MAUNGANUI, NEW ZEALAND

A thesis submitted in partial fulfilment
of the requirements for the Degree of

Master of Science

in Earth and Ocean Sciences
at the University of Waikato

by

SIMON BASTIEN WEPPE

THE UNIVERSITY OF
WAIKATO
Te Whare Wānanga o Waikato

2010

ABSTRACT

The innovative concept of an offshore submerged multi-purpose reef combining a coastal protection function with recreational benefits including improved surfing, diving, or fishing conditions provides an appealing solution for the management of beaches. However, since the technology is relatively recent, there is still a lack of empirical knowledge about its performance in the field. The present research monitored the effect of the prototype "research" reef constructed at Mount Maunganui in New Zealand on the local beach morphodynamics and oceanographic conditions, being primarily concerned with implications on the coastal protection function of the technology.

The beach morphodynamic response to the reef was investigated from a set of already available high resolution bathymetric surveys imaging the foreshore and surfzone morphology prior to, and throughout reef construction, and a new post-construction survey collected as a part of this research. The reef implementation was found to disturb the pre-existing beach state functioning including the onshore/offshore migration of the underlying long shore bar, rather than cause a persistent salient response. A possible additional beach width of ~ 20 m, extending ~ 150 m alongshore was identified in the lee of the reef from shoreline analysis, but the pattern was transient throughout the monitoring period since it was superimposed on comparatively large pre-existing fluctuations. In addition, the reef structure provided a control point on the offshore morphology able to trap sediment updrift and erode sediment downdrift.

Both field measurements and numerical modelling of waves and currents were used to monitor the effect of the reef on the oceanographic conditions. Wave propagation over the reef without breaking ($H < 0.5$ m) resulted in transmitted heights larger than incident by up to a factor of 2. When the reef triggered breaking, transmitted heights were reduced by up to ~40 %. A concurrent process was the shift of the wave energy spectra towards higher frequencies landward of the reef that resulted in reduced transmitted wave periods. Wave modelling showed that the wave shadowing was associated with significant wave rotation around the reef that induced two zones of divergent wave angles near the shoreline in the lee of the reef. The hydrodynamic response to the wave energy dissipation was the development of stronger onshore directed currents landward of the reef. Hydrodynamic modelling indicated that the reef-induced flow forced a cellular circulation in the lee side under shore normal waves, and an onshore deviation of the ambient (unidirectional) long-shore currents under oblique waves.

The research provided a rare empirical test to the theoretical design concepts, and potential supplements or refinements. To obtain the required beach protection, the reef impact on the beach morphodynamic coupling including wave transformation, nearshore hydrodynamics, and small/large scale beach state response needs to be carefully assessed.

ACKNOWLEDGEMENTS

This thesis would not have been possible without the help and support of many people along the way.

First thanks to Marie for her support, patience, and fun, over the years that made a difference every day. I wish to thank my parents who encouraged and supported me when I initially suggested I would be keen to go on the other side of the world in New Zealand to continue my studies. I am deeply grateful they made the whole adventure possible. I fully appreciated the great support from my two brothers although I suspect this was mostly because I would live a stone throw from the mythical waves of Raglan.

I must individually thank my thesis supervisor Professor Terry Healy for his help to define the focus of the thesis, and his efforts to develop my research skills, critical thinking, and academic writing throughout the research project. The ideas and advice of my co supervisor Dr Brad Scarfe, who kindly made available the bathymetric datasets collected as a part of his Ph.D and helped for the new bathymetric survey, are also greatly appreciated. Thanks to Dirk Immenga whose experience and help was invaluable to complete the field work undertaken as a part of this research. Environment Bay of Plenty and The Broad Memorial Fund are gratefully acknowledged for providing the financial support for this field work.

Thanks to Richard Gorman and Rob Bell from NIWA (National Institute of Water and Atmospheric Research) for providing wave and tide data at the study site. I also wish to thank Dr Kerry Black for insightful discussions and communications about the numerical modelling undertaken.

Finally, I would like to extend my appreciation to Karin Bryan and Willem De Lange from the Earth and Ocean Department, and Giovanni Coco from NIWA who definitely hooked me on coastal sciences during my Postgraduate Diploma, and eventually led me to this thesis. I also thank my fellow students who have been a great group of people to study and mix with, and made these last 2 years at the university fully enjoyable.

TABLE OF CONTENTS

LIST OF FIGURES

LIST OF TABLES

CHAPTER 1. OFFSHORE SUBMERGED MULTI-PURPOSE REEFS FOR COASTAL PROTECTION

1.1 BACKGROUND

"The relation between wave climate, beach erosion, beach defence, habitat changes and beach value, which clearly exists [...], suggests the necessity of an integrated approach to coastal defence problems examining beside structure stability and construction problems, hydro- and morpho-dynamic effects, environmental effects (biological colonisation of the structure and water quality), societal and economic impacts (recreational benefits, swimming safety, beach quality)" (LAMBERTI, 2005).

It is increasingly being recognized that offshore submerged structures may provide a solution for such an integrated coastal management. For coastal protection, the primary functions of offshore submerged structures are to reduce the amount of wave energy in their lee, and to initiate sediment deposition at the shoreline through the modification of nearshore currents (e.g. PILARCZYK, 2003; RANASINGHE and TURNER, 2006). In contrast with conventional methods such as groynes or seawalls often used to stabilize the coast, detached submerged structures could provide the required beach protection without loss of beach amenity and aesthetic. Another advantage of submerged structures is that they provide a more complex and stable habitat that can benefit the local ecology (e.g HARRIS, 2002; HIROSE *et al*., 2002; HARRIS, 2006).

Thanks to recent progress in surfing wave mechanics, along with the identification of bathymetric components required to provide suitable surfing waves (MEAD and BLACK, 2001a; MEAD and BLACK, 2001b), the innovative concept of an artificial submerged multi-purpose reef providing coastal protection, enhanced ecology, and surfable waves was proposed (BLACK, 2001a; BLACK, 2001b; MEAD, 2001).

Such a solution is obviously attractive, however, only little is known about beach system response to multi-purpose reefs to date, primarily because the concept is relatively new (RANASINGHE *et al*., 2006). From a recent review of reported

field, laboratory, and numerical modelling investigations on submerged structures, RANASINGHE and TURNER (2006) suggested that the uncertainties on the foreseen impact on the beach were more widely relevant to submerged structures in general, and noted that key response processes and their relationships to structural and environmental were still not fully understood. They found that 7 out of 10 of the major coastal engineering projects involving submerged structures to date resulted in shoreline erosion in the lee of the structures instead of the desired accretion. Encouragingly though, the first multi-purpose prototype reef constructed at Narrowneck on the Gold Coast (Australia), which was one of the projects considered, resulted in shoreline accretion (~ 20 m) (see TURNER, 2006).

The uncertainties on beach and shoreline response in the lee of submerged structures contrast with salient or tombolo features virtually always developing in the lee of offshore emerged structures (e.g. BASCO, 2006). However, it is now becoming clear that submerged structures behave in a manner fundamentally different from emerged structures (RANASINGHE and TURNER, 2006). Emergent designs induce a total or quasi total wave sheltering of the beach in their lee, and beach response is thus predominantly controlled by wave diffraction around the structure. In contrast, submerged structures such as multi-purpose reefs allow important wave transmission. This is associated with wave-induced currents and discharge of water in the lee of the structure, therefore the beach response is more likely governed by the development of "new" nearshore circulation patterns (e.g. BLACK, 2003; RANASINGHE *et al*., 2006).

Physical and numerical modelling investigations on multi-purpose reefs generally supported that the coupling between modified hydrodynamics and sediment transport could be successful in inducing the desired shoreline accretion (i.e. salient) (e.g. TURNER *et al.*, 2001; BLACK, 2003; RANASINGHE *et al*., 2006; BLACK and MEAD, 2007). Moreover, salient features are also commonly observed in the lee of offshore natural submerged reefs (BLACK and ANDREWS, 2001). The next logical step is then to monitor existing prototypes to assess their behaviour in real coastal environments.

The focus of the present research is the monitoring of the prototype multi-purpose reef constructed at Mount Maunganui in the northeastern coast of the north island of New Zealand. This prototype is relatively unique in that it was constructed to focus the research efforts on the multi-purpose reef concept (MEAD and BLACK,

1998), rather than to address a significant erosion problem. The objective to test the beach protection function of the concept was to induce formation of a small salient feature which would have negligible impact on adjacent beaches (MEAD and BLACK, 1998).

1.2 THESIS AIM AND OBJECTIVES

The aim of the research project is to monitor the effect of the prototype reef on the local beach morphodynamics and oceanographic conditions. The research is primarily concerned with the modification of the beach system with respect to the coastal protection function of the multi-purpose reef technology. Recreational or ecological impacts are therefore not treated.

To achieve this aim, specific objectives are defined:

1. Review the literature relevant to the coastal protection function of conventional and multi-purpose submerged structures to identify the dominant oceanographic and morphodynamic processes involved.

2. Test the shoreline response to the prototype reef using available shoreline contours collected prior to, and throughout reef construction (SCARFE and HEALY, 2006; SCARFE, 2008), and a new post-construction shoreline contour collected as a part of this research.

3. Undertake the detailed analysis of the concurrent beach morphodynamic adjustments using available bathymetric datasets collected prior to, and throughout reef construction (SCARFE and HEALY, 2006; and SCARFE, 2008), and a new post-construction bathymetric survey undertaken as a part of this research.

4. Investigate the wave transmission over the reef based on field measurements of incident and reef-transmitted wave conditions.

5. Investigate the concurrent hydrodynamic response based on field measurements of incident and reef-transmitted current conditions.

6. Identify the dominant reef-induced patterns of waves and currents at the study beach using numerical modelling.

1.3 THESIS STRUCTURE

In order to achieve the above objectives, the thesis is organized as follows:

Chapter 2 reviews reported field, laboratory, and numerical investigations dealing with morphodynamic and oceanographic processes in the vicinity of conventional and multi-purpose submerged structures.

Chapter 3 presents the analysis of shoreline response to the reef based on mean sea level contours collected prior to, throughout, and after reef construction. These results were peer reviewed and presented as a paper at the 2009 Coasts and Ports Conference (Wellington, New Zealand).

Chapter 4 describes the beach morphodynamic adjustments concurrent with the analyzed shoreline changes (Chapter 3) based on a set of high resolution beach bathymetric charts collected using RTK GPS and multibeam echo sounding surveying.

Chapter 5 treats the wave transmission over the prototype reef. Incident and transmitted wave fields measured during a 5 day field experiment are compared focusing on the significant wave height transmission, the wave height distribution modification, and the wave energy spectrum transformation, along with implication on the wave period.

Chapter 6 analyses the hydrodynamic conditions that developed around the reef during the 5 day field experiment. The effect of wave forcing on mean current velocity and flow discharge landward of the reef is specifically investigated.

Chapter 7 presents the results of numerical modelling of waves and currents at the study beach. Model calibration is undertaken using collected field datasets. Field experiment conditions and representative wave events are simulated to identify the main wave and circulation patterns developing at the beach.

Chapter 8 summarizes the main research findings and suggests future research directions.

1.4 THE STUDY SITE

The multi-purpose reef was constructed near Tay Street at Mount Maunganui, which is located within the long wave exposed sandy Bay of Plenty coastline on the northeastern coast of New Zealand (Figures 1.1 and 1.2). The reef is a V-shaped submerged structure, with its apex pointing seaward, made of sand-filled geotextile containers (Figures 1.3 and 1.4). The reef is located about 250 m from the shoreline. Construction began in 2005 and was put on hold for economic reasons while 70 % of the reef was completed at the end of 2006. Reef construction was completed in June 2008. Final cross and long-shore dimensions are ~ 60 m and ~ 80 m respectively.

Wave climate at the site consists predominantly of locally generated small waves ($H_{sig} < 1$ m) but with the possibility of more energetic swell events due to subtropical disturbances (PICKRILL and MITCHELL, 1979). The net drift is towards the southeast through the Bay of Plenty with magnitude of order 60 to 80.000 m^3/ year (HEALY, 1980). Frequent reversals are expected in response to reigning climatic system and/or individual high energy events (MEAD and BLACK, 1998; SCARFE, 2008). As a result, the net drift magnitude may be small relative to gross sediment movement along the site.

Antecedent coastal engineering projects in the site vicinity include maintenance dredging of the Tauranga Harbour channel, 4 km to the northwest, and subsequent dredge disposals to the north of the study area (Figure 1.5).

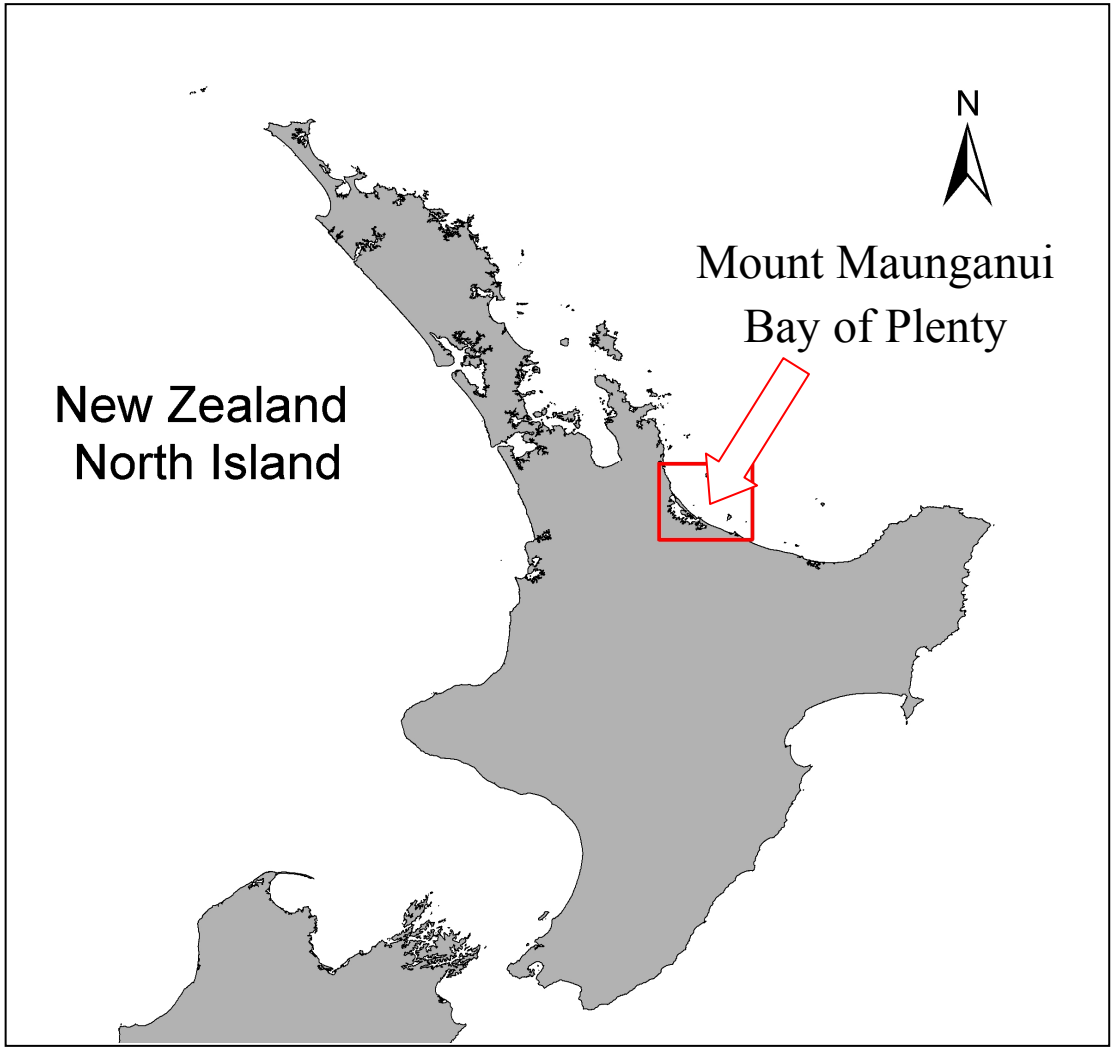

Figure 1.1. Mount Maunganui, located on southwestern Bay of Plenty on the east coast of the north island of New Zealand.

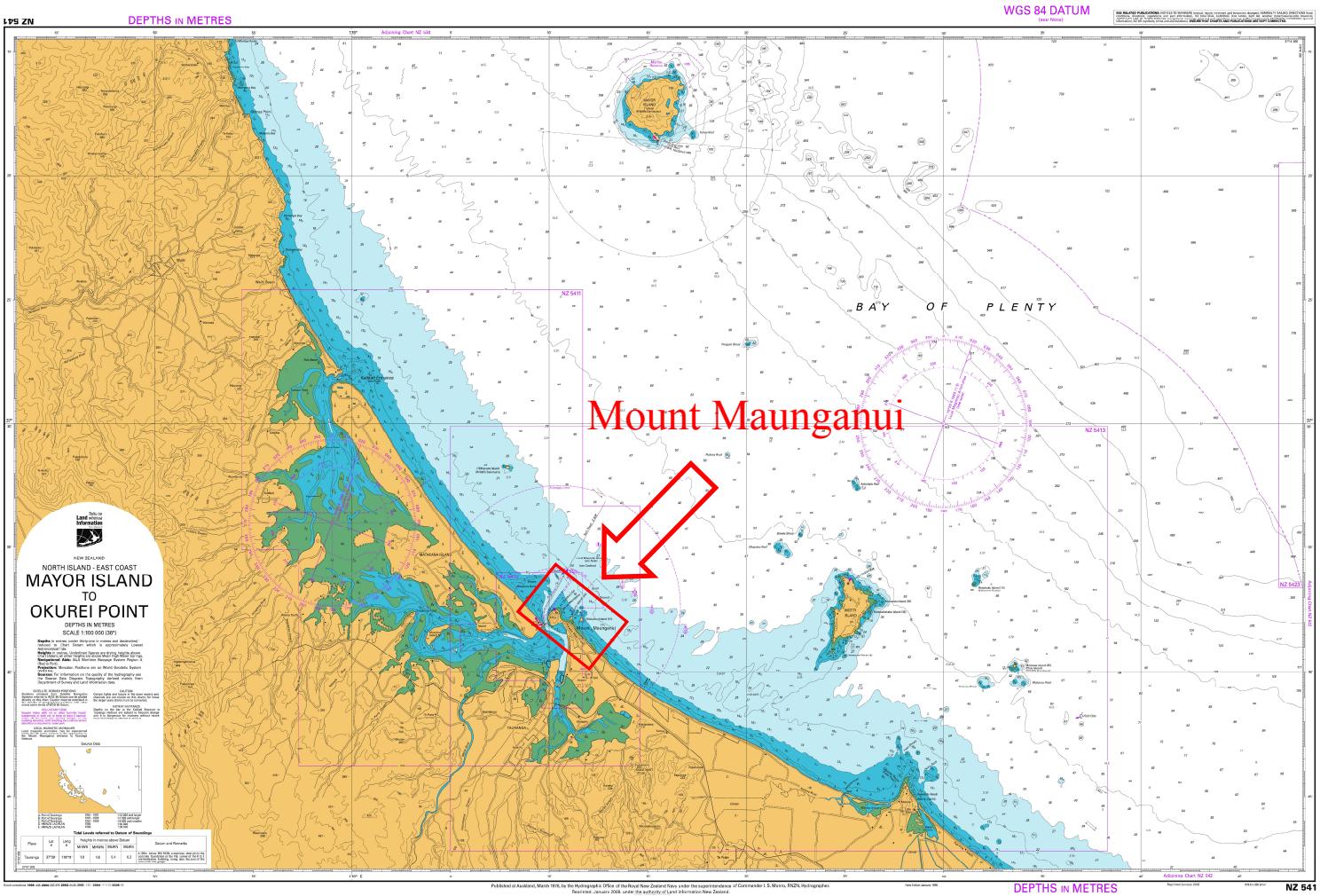

Figure 1.2. Hydrographic chart of the southwestern Bay of Plenty. (Source: Land Information New Zealand, www.linz.govt.nz).

Figure 1.3. Aerial photographs of the site during reef construction. The reef is made of sand-filled geotextile containers and is located about 250 m from the shore. (Source: Mount Reef website: www.mountreef.co.nz).

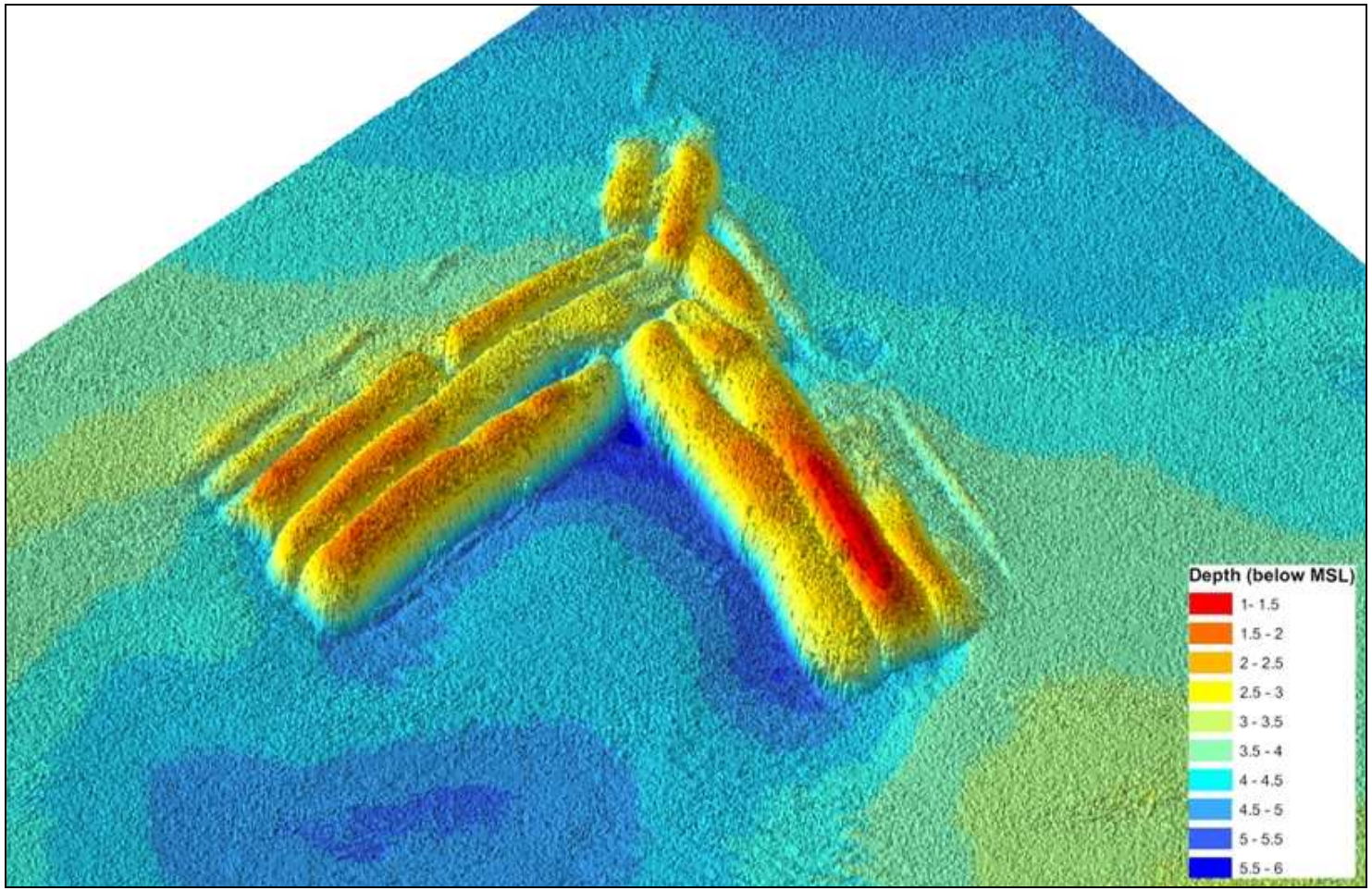

Figure 1.4. 3D view of the reef at Mount Maunganui. The image was generated using the multibeam echosoundings data collected in March 2009 (reef completed in June 2008). Depths are relative to mean sea level (Moturiki Vertical Datum, 1953). (Source: Coastal Marine Group, Earth and Ocean Sciences Department, University of Waikato).

Figure 1.5. Features of interest around the study site including the dredged channel of Tauranga Harbour, and the dredge disposal sites. (Source of aerial photo: Terralink Ltd).

1.5 REFERENCES

BASCO, D.R., 2006. Shore Protection Projects. *In*: WARD, D.L., (ed.), *Coastal Engineering Manual*, Part V, Coastal Project Planning and Design, Chapter 3, Engineering Manual 1110-2-1100, U.S. Army Corps of Engineers, Washington, DC.

BLACK, K.P., 2001a. Artificial Surfing Reefs for Erosion Control and Amenity: Theory and Application. *In:* HEALY, T.R. (ed.)*, Journal of Coastal Research, Special Issue No. 34*, 1-14.

BLACK, K.P. (ed.), 2001b. Natural and Artificial Reefs for Surfing and Coastal Protection. *Journal of Coastal Research, Special Issue No. 29*, 152 p.

BLACK, K.P., and ANDREWS, C.J., 2001. Sandy Shoreline Response to Offshore Obstacles, Part 1: Salient and Tombolo Geometry and Shape. *In:* BLACK, K.P., (ed.), Natural and Artificial Reefs for Surfing and Coastal Protection. *Journal of Coastal Research, Special Issue No. 29*, 82-93.

BLACK, K.P., 2003. Numerical Prediction of Salient Formation in the Lee of Offshore Reefs. *In:* BLACK, K.P., and MEAD, S.T., (eds.), *Artificial Surfing Reefs 2003: The 3rd International Conference,* (Raglan, New Zealand). CD publication. pp. 196-218, ISBN:0-473-09801-06.

BLACK, K.P., and MEAD, S.T., 2007. Sand Bank Responses to a Multi-Purpose Reef on an Exposed Sandy Coast. *In*: WALTHER, M., (ed.), Shore Protection and Surfing Dedicated Issue. *Shore and Beach,* 75(4), 55-66.

HARRIS, L.E., 2002. Submerged reef structures for habitat enhancement and shoreline erosion abatement. *U.S. Army Corps of Engineers, Coastal & Hydraulic Engineering Technical Note*, Vicksburg, MS.

HARRIS, L.E., 2006., Artificial Reefs for Ecosystem Restoration and Coastal Erosion Protection with Aquaculture and Recreational Amenities. *5th International Surfing Reef Conference* (Lombok, Indonesia), 12 p.

HEALY, T.R., 1980. Erosion and Sediment Drift on the Bay of Plenty coast. *Soil and Water*, August, pp. 12-14.

HIROSE, N., WATANUKI, A., SAITO, M., 2002. New type units for artificial reef development of ecofriendly artificial reefs and the effectiveness thereof. *Proceedings of the 30th International Navigation Congress*, PIANC.

LAMBERTI, A., 2005. Editorial paper on DELOS project. *Coastal Engineering,* 52, 815–818.

MEAD, S.T. and BLACK, K.P., 1998. A Multipurpose Artificial Reef at Mount Maunganui Beach, New Zealand. *Coastal Management,* 27, 335-365.

MEAD, S.T., 2001. Incorporating High-Quality Surfing Breaks into Multi-Purpose Reefs. Hamilton, New Zealand: University of Waikato, PhD Thesis, 213 p.

MEAD, S.T., and BLACK, K.P., 2001a. Field Studies Leading to the Bathymetric Classification of World-Class Surfing Breaks. *In:* BLACK, K.P., (ed.), Natural and Artificial Reefs for Surfing and Coastal Protection. *Journal of Coastal Research, Special Issue No. 29*, 5-20.

MEAD, S.T., and BLACK, K.P., 2001b. Functional Component Combinations Controlling Surfing Quality at World-Class Surfing Breaks. *In:* BLACK, K.P. (ed.), Natural and Artificial Reefs for Surfing and Coastal Protection. *Journal of Coastal Research, Special Issue No. 29*, 21-32.

PICKRILL, R. A., and J. S. MITCHELL. 1979. Ocean wave characteristics around New Zealand. *New Zealand Journal of Marine and Freshwater Research,* 1, 501–520.

PILARCZYK, K.W., 2003. Design of low-crested (submerged) structures: an overview. *Proceedings of the 6th International Conference on Coastal and Port Engineering in Developing Countries* (Colombo, Sri Lanka), 19 p.

RANASINGHE, R., and TURNER, I.L., 2006. Shoreline Response to Submerged Structures: A Review. *Coastal Engineering*, 53, 65-79.

RANASINGHE, R., TURNER, I.L., and SYMONDS, G., 2006. Shoreline Response to Multi-Functional Artificial Surfing Reefs: A Numerical and Physical Modeling Study. *Coastal Engineering,* 53, 589-611.

SCARFE, B.E., and HEALY, T.R., 2005. Baseline Bathymetric Data Collection for Monitoring of Bar, Rip and Salient Response to an Artificial Surfing Reef - Mount Maunganui, New Zealand. *In:* TOWNSEND, M. and WALKER, D. (eds.), *Proceedings for the 2005 Coasts and Ports Australasian Conference* (Adelaide, South Australia), pp. 459-464.

SCARFE, B.E., 2008. Oceanographic Considerations for the Management and Protection of Surfing Breaks. Hamilton, New Zealand: The University of Waikato, Ph.D. thesis, 307 p. + appendices.

TURNER, I., LEYDEN, V., COX, R., JACKSON, A., and MCGRATH, J., 2001. Physical Model Study of the Gold Coast Artificial Reef. *In:* BLACK, K.P. (ed.), Natural and Artificial Reefs for Surfing and Coastal Protection. *Journal of Coastal Research, Special Issue No. 29*, 131-146.

TURNER, I.L., 2006. Discriminating Modes of Shoreline Response. *Journal of Waterway, Port, Coastal and Ocean Engineering*, 132(3), 180-191.

CHAPTER 2. LITERATURE REVIEW OF OCEANOGRAPHIC AND MORPHODYNAMIC PROCESSES AROUND MULTI-PURPOSE AND CONVENTIONAL SUBMERGED STRUCTURES

2.1. INTRODUCTION

In this chapter, oceanographic and morphodynamic processes developing due to submerged structures are reviewed with respect to the coastal protection function of multi-purpose reefs. The first part of the review deals with oceanographic processes around multi-purpose reefs; field investigations as well as physical and numerical modelling studies are documented and compared with relevant works on conventional submerged structures. Investigations on the beach morphodynamic response are treated in a second part using a similar approach. Finally, results are discussed and summarized. Note that performances in terms of surfing or ecological enhancement are not considered.

2.2. OCEANOGRAPHIC PROCESSES AROUND SUBMERGED STRUCTURES

2.2.1 INTRODUCTION

Submerged structures interact with wave and hydrodynamic processes in a complex fashion (ZYSERMANN and JOHNSON, 2002). The complexity is due to (i) the natural variability of the wave field, and (ii) the interaction of the incident wave field with a given structure (FERRANTE, 2007). Here, the focus is on what happens in the vicinity of the structure and therefore we consider the second cause. This includes processes such as wave breaking over short obstacles, wave height and energy transmission, wave-driven currents development, and wave-current interaction for which understanding is still developing (DREI *et al.*, 2001; TAJZIECHI, 2006).

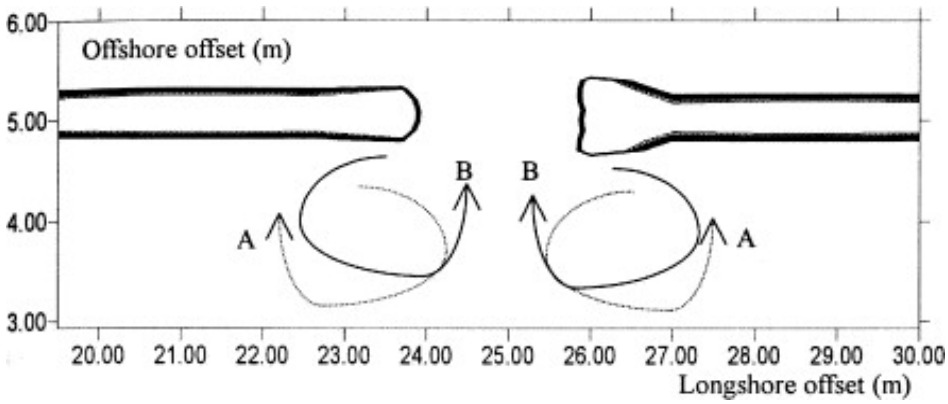

Figure 2.1. Different nearshore circulation patterns expected in the vicinity of (A) emergent, and (B) submerged breakwaters (from LOVELESS and MACLEOD, 1999). Pattern B shows the development of an offshore directed current at the gap between the structures potentially able to transport sediment offshore and induce erosion. Pattern A shows the convergence of currents in the lee of the (emerged) structure due to greater water level setup in the lee of the gap.

2.2.2. FIELD OBSERVATIONS

Field monitoring of wave and current modification by submerged structures was reported for several conventional submerged breakwater projects but there is presently no such investigation available for multi-purpose reefs.

Monitoring of a 1260 m shore parallel submerged structure, known as "PEP reef", located at about 70 m from the shoreline (Palm Beach, Florida) was reported by DEAN *et al*. (1997). Measurements of incident and transmitted wave heights at the structure indicated limited height attenuation over the structure from 5 to 15 %. The significant wave transmission resulted in strong onshore flow over the structure that diverged and was compressed in the lee of the reef. This was found to cause an aggravated erosion of the shoreline.

Monitoring of waves and currents was also undertaken in the vicinity of the submerged structures system at Lido di Dante, Italia. As the PEP reef, it is one of the ten major submerged breakwater projects to date (see RANASINGHE and TURNER, 2006). The system consists of 2 shore parallel structures and an inshore area compartmented by submerged groins. A strong increase in long-shore currents was identified within the lee area and a defined rip current developed through the gap between structures. Spectral analysis of current velocity suggested that the long-shore currents were essentially due to waves while the rip current in between the structures was governed by tide oscillations (DREI *et al*., 2001, ARCHETTI *et al*., 2003). It should be noted that the breakwater was

constructed in the Mediterranean Sea that is a relatively low wave energy environment. The tide-forced rip in the gap between the breakwaters is unlikely to be relevant for higher wave energy environment. With respect to the wave attenuation, coefficients of height transmission ranged from 0.5 to 1 for increasing water depth over the structure crest.

2.2.3. PHYSICAL MODELLING

A comprehensive review of the laboratory experiments on hydrodynamic response to conventional submerged breakwaters is provided in RANASINGHE and TURNER (2006) and not reproduced here. However, it is noted that the numerous studies described in their review, including physical modelling of the PEP reef (DEAN *et al*., 1997), experiments on a single (NOBUOKA *et al*., 1996), segmented (GROENEWOUD *et al*., 1996), or multiple (VAN DER BIEZEN *et al.*, 1998) submerged breakwaters, all reported a consistent circulation pattern of a strong onshore flow over the structure diverging into a 2-cell circulation in the inshore region.

Furthermore, comparing circulation patterns for 3 different crest heights of the same structure system, namely fully emergent, partially emergent (crest at MWL) and fully submerged, LOVELESS and MACLEOD (1999) suggested that such circulation pattern would be distinctly different to that behind an emergent structure. The wave transmission and onshore flow over the submerged crest created a setup of the water level in the lee of the structure that was balanced by divergent flows in the lee eventually returning offshore trough gaps. In contrast, the total wave shadowing in the lee of the emergent design allowed a water level smaller in the lee side than on the adjacent beach that induced the convergence of currents towards the sheltered beach (Figure 2.1).

The first published investigation on a physical model of a multi-purpose reef was TURNER *et al*. (2001). The model reproduced the proposed reef design for Narrowneck (Gold Coast Austalia) (BLACK, 1998; BLACK, 1999; BLACK and MEAD, 2001b) to assess and verify wave transformation and nearshore circulation in the vicinity of the structure. The fixed bottom beach model was plane sloping and consequently did not reproduce the long-shore bars although present in reality (see HUTT *et al*., 1999). The strong littoral drift characteristic of the site (~500,000 m^3/year, towards the north, see JACKSON *et al*., 2007) was simulated

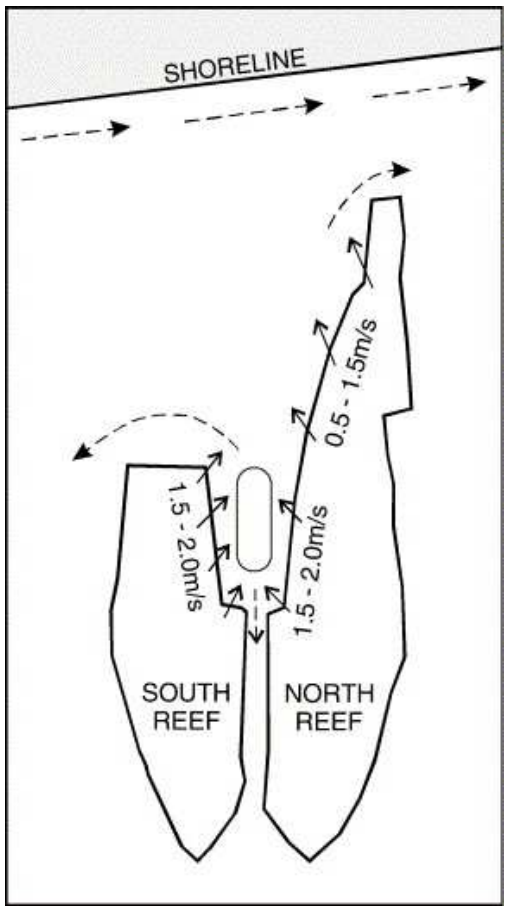

Figure 2.2. Nearshore circulation pattern observed in the vicinity of the physical model of the Narrowneck multi-purpose reef (from TURNER *et al*., 2001). Arrows indicate currents direction. The feature between the 2 arms schematizes the development of a circulation cell.

by generating obliquely incident waves. A significant reduction of incident height was observed the immediate lee of the structure (50% reduction), however, the wave sheltering was less efficient at the shoreline (10 % reduction). This was attributed to diffraction effects creating complex interference patterns (wave crest superposition) in the lee of the reef and possibly focusing wave heights. The resulting nearshore circulation pattern was consistent with the earlier observations of onshore flow divergence in the lee of the structure, although superimposed on ambient long-shore currents (Figure 2.2). The predominant return current was due to the divergent flow from the south reef limb, progressively deviated offshore by opposing long-shore currents. On the other extremity, the flow from the north reef limb reinforced the natural drift.

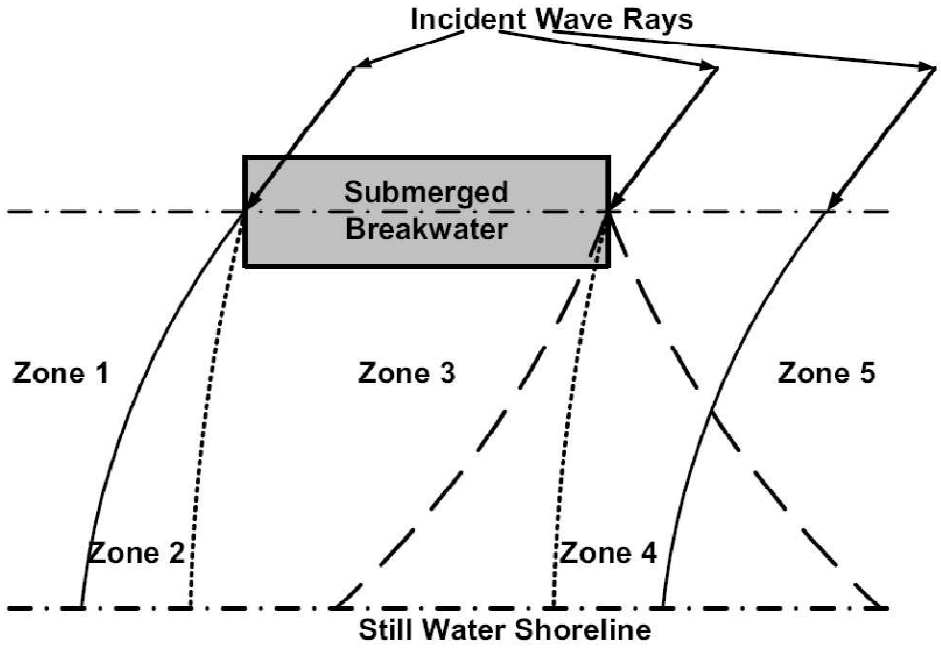

Figure 2.3. Schematic diagram of the wave field in the vicinity of a submerged breakwater under obliquely incident waves (from RANASINGHE and SATO, 2007). The wave field is divided into 5 zones. Zone 1 and 5 are unaffected by the structure. Wave refraction over the structure creates zone 3 (dotted lines). Zone 2 is sheltered from the incident rays thanks to their refraction in zone 3 therefore smaller wave height are expected in this region. On the contrary, waves tend to focus on zone 4 (dashed lines) that receives both refracted rays (from zone 3) and incident rays (from zone 5).

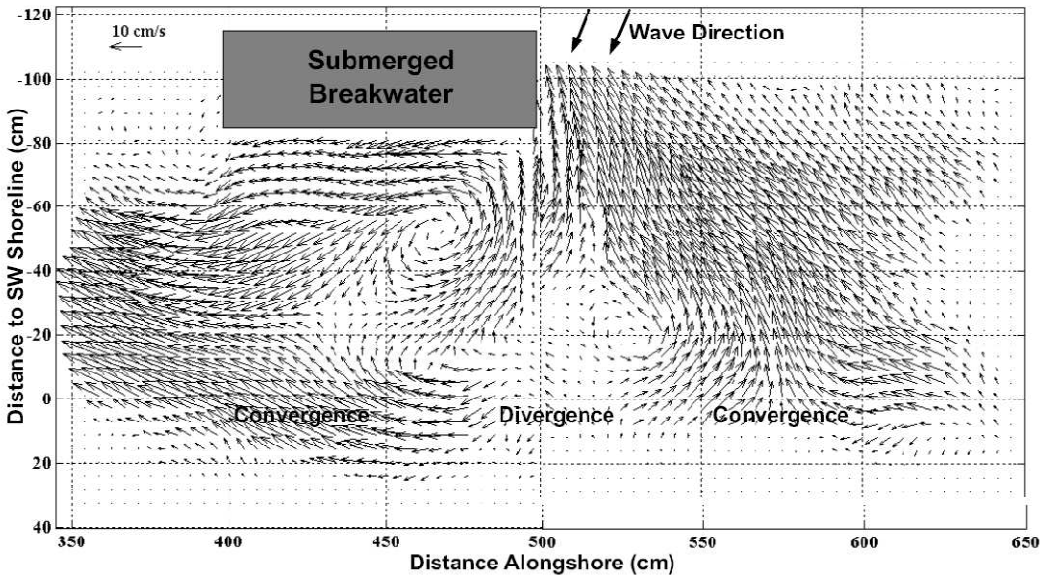

Figure 2.4. Current field in the vicinity of a submerged breakwater under obliquely incident waves (from RANASINGHE and SATO, 2007). Structure-induced currents interact with ambient long-shore currents and create a cellular circulation. Note three main features: (i) currents strengthening and convergence downdrift, (ii) rip current formation along the structure updrift, and (iii) an area of weak currents in the lee of the structure.

RANASINGHE and SATO (2007)'s experiments on single shore-parallel submerged breakwater focused on obliquely incident waves and thus reproduced a similar drift environment. Similarly to LOVELESS and MACLEOD (1999), they noted a characteristic wave and current pattern completely different compared to that for emergent breakwaters. Typically, the wave field was divided into 5 zones (Figure 2.3). Zone 1 and zone 5 are regions unaffected by the structure. The structure induces refraction of incident waves rays in zone 3 (dotted lines) and in turn creates both zone 2 and zone 4. Zone 2 is sheltered from the incident rays due to their refraction in zone 3 and not really exposed to undisturbed incident waves from zone 1 either. We can thus expect a shadow zone with smaller wave heights. On the contrary, waves tend to focus on zone 4 that receives both refracted (from zone 3) and incident rays (from zone 5). With respect to the nearshore circulation, diverging currents in the lee of the structure obstructed natural long-shore currents and induced a cellular circulation (Figure 2.4). In good agreement with TURNER *et al.* (2001) findings, the structure-induced currents and long-shore currents converged and accelerated downdrift, while circulation cells developed in the lee of the structure with formation of a rip along the updrift side of the structure.

A significant source of laboratory data on submerged breakwaters is available thanks to the DELOS project (Environmental Design of Low Crested Coastal Defence Structures) (see KRAMER *et al.*, 2005). It should be noted that the DELOS project generally focuses on low wave energy environments (such as the Mediterranean Sea) however the range of experimental wave conditions tested are also relevant to environment exposed to more significant wave energy.

Particular points of interest with respect to the multi-purpose reef technology are the experiments on the influence of wave obliquity in the mechanisms of wave transmission (transmission coefficient, spectral change, wave direction change), and the comparison of behaviour between typical rubble-mound breakwaters and smooth structures. The rotation of obliquely incident waves to reduce the long-shore currents may be one of the multi-purpose reef functions (e.g. BLACK and MEAD, 2001a) and it is then valuable to investigate further the transmission characteristics under such conditions. Likewise, the smooth surface of geo-containers used for multi-purpose reef construction contrasts with the more commonly used rubble-mound revetments and should be considered too.

Comparison of experimental results showed that wave transmission over smooth submerged structures was completely different from rubble-mound structures (VAN DE MEER *et al*., 2005). Previous equations by d'ANGREMOND *et al*. (1996) for transmission over both rubble-mound (Equation 2.1) and smooth (Equation 2.2) structures were quasi identical, suggesting similar behaviour.

Rubble-mound structures

$$K_t = -0.4(Rc/Hi) + 0.64(B/Hi)^{-0.31}[1 - \exp(-0.5\xi_{op})] \quad (2.1)$$

Smooth structures

$$K_t = -0.4(Rc/Hi) + 0.80(B/Hi)^{-0.31}[1 - \exp(-0.5\xi_{op})] \quad (2.2)$$

with a minimum $K_t = -0.075$ and maximum $K_t = 0.8$.

Rc is the crest freeboard, Hi is the incident wave height, B is crest width and ξ_{op} is a breaker parameter $\xi_{op} = \tan \propto /(s_{op})^{0.5}$, in which s_{op} is the wave steepness computed as $s_{op} = 2\pi Hi/(gT_p^2)$, and $\tan \propto$ is the structure slope (T_p is peak wave period, and g gravity constant).

VAN DE MEER *et al*. (2005) demonstrated the opposite by reanalysing all smooth structure data available and proposed a new equation (4) to be used for 1D wave height transmission over smooth structures:

Smooth structures

$$K_t = -0.3(Rc/Hi) + 0.75[1 - \exp(-0.5\xi_{op})] \text{ for } \xi_{op} < 3 \quad (2.3)$$

with a minimum $K_t = -0.075$ and maximum $K_t = 0.8$.

Using the new data obtained on oblique wave incidence, VAN DER MEER *et al*. (2005) further found that in contrast with rubble-mound structures, there was a strong dependency between transmission coefficient and angle of wave approach for smooth structures. A predictive formula for transmission coefficient over submerged smooth structures including the wave obliquity was proposed (see Figure 2.5 and Equation (2.4)).

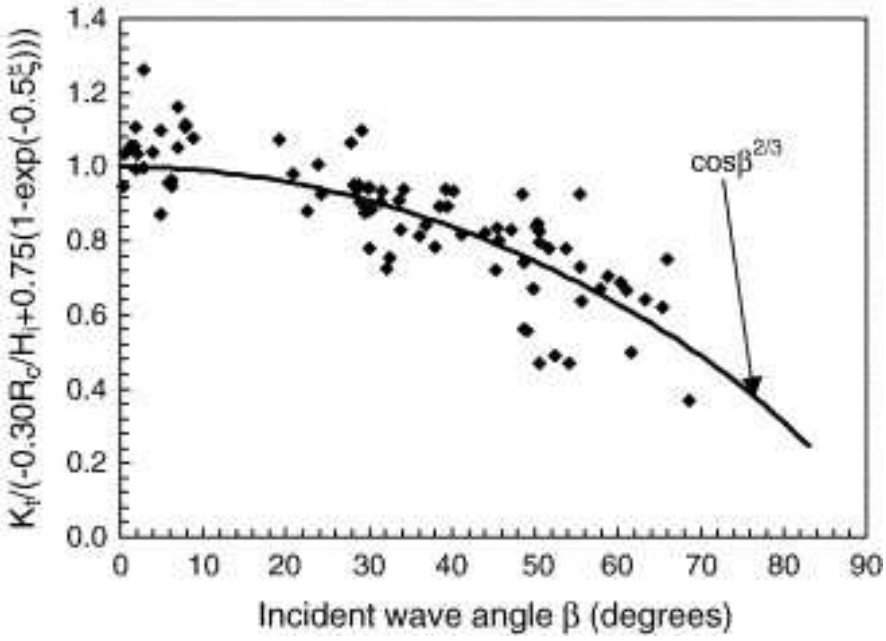

Figure 2.5. Influence of oblique wave approach on wave height transmission coefficients above smooth structures (from VAN DER MEER *et al*., 2005).

$$K_t = -0.3(Rc/Hi) + 0.75\left[1 - \exp\left(-0.5\xi_{op}\right)\right].\cos^{2/3}\beta \qquad (2.4)$$

with a minimum $K_t = -0.075$ and maximum $K_t = 0.8$.

The limits are: $1 < \xi_{op} < 3; 0° < \beta < 70°; 1 < \frac{B}{Hi} < 4$; Rc is the crest freeboard, Hi is the incident wave height, B is crest width, β incident wave angle (degrees) and ξ_{op} is a breaker parameter $\xi_{op} = \tan \propto /(s_{op})^{0.5}$, in which $s_{op} = 2\pi Hi/(gT_p^2)$, and $\tan \propto$ is the structure slope (T_p is peak wave period, and g gravity constant).

Conceptually, this equation can also be used to estimate the transmission coefficients for any configuration of wave incidence angle/structure orientation as long as the orientation difference lies within the proposed range (0-70 °). It could then be applicable to the multi-purpose V-shaped reefs.

The Narrowneck reef arms form an angle with the beach varying from 85° (offshore) to 65° (inshore) (chosen for surfing reasons, see BLACK, 1998; BLACK and MEAD, 2001b). Similarly, the Mount Maunganui reef includes a shore perpendicular focus ramp linked to 2 arms at about 60°. With respect to VAN DER MEER'S formula, such orientations would potentially allow reduced transmission coefficients for a range of wave incidence. This is also in agreement with findings

from earlier works by GODA (1996) and GODA and TAKAGI (1998) on the advantages of longitudinal versus shore-parallel breakwaters with respect to wave transmission.

The change in wave energy spectrum behind a submerged structure was another process investigated. A wave breaking over a submerged structure may generate two or more transmitted waves on the lee side. The averaged effect is that more wave energy is present at higher frequencies in the transmitted spectrum than in the incident spectrum (VAN DER MEER *et al.,* 2000; BLECK and OUMERACI, 2001; VAN DER MEER *et al*., 2005). BLECK and OUMERACI (2001) noted that this change of spectral shape cannot be neglected for the design of coastal structures as the wave frequency and thereby its period may be a measure for the wave celerity, which is a determinant for estimating the wave energy flux. Wave run-up also depends largely on the wave period (VAN DER MEER *et al*., 2000). Figure 2.6 shows an example of incident / transmitted spectrum over a submerged structure. VAN DE MEER *et al*. (2000) proposed a simple model to predict transmitted wave energy spectrum from 2D laboratory data (Figure 2.7). 60% of the transmitted energy remains at the incident peak frequency f_p and the other 40% of the energy is evenly distributed between 1.5 f_p and 3.5 f_p. The model was found to be in agreement with the new oblique wave data indicating a minimal effect of wave obliquity in wave energy transmission (VAN DE MEER *et al*., 2005). The only feature noted was that smooth structures tended to exhibit a little larger portion of energy at higher frequencies than rubble-mound breakwaters.

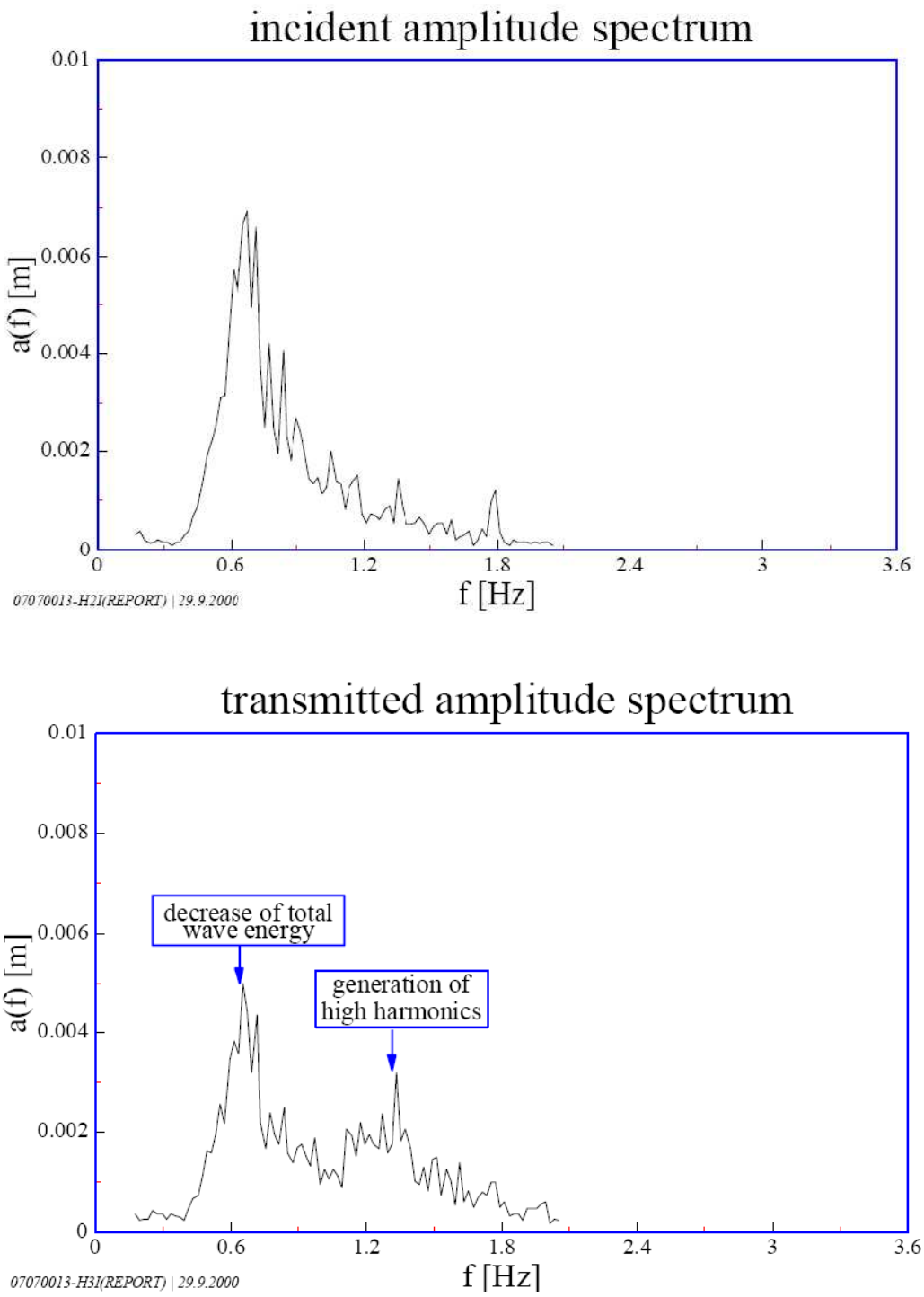

Figure 2.6. Incident and transmitted wave energy spectra over a physical model of submerged breakwater (from BLECK and OUMERACI, 2001). The incident peak wave energy mainly at 0.6 Hz is redistributed towards higher frequencies behind the structure.

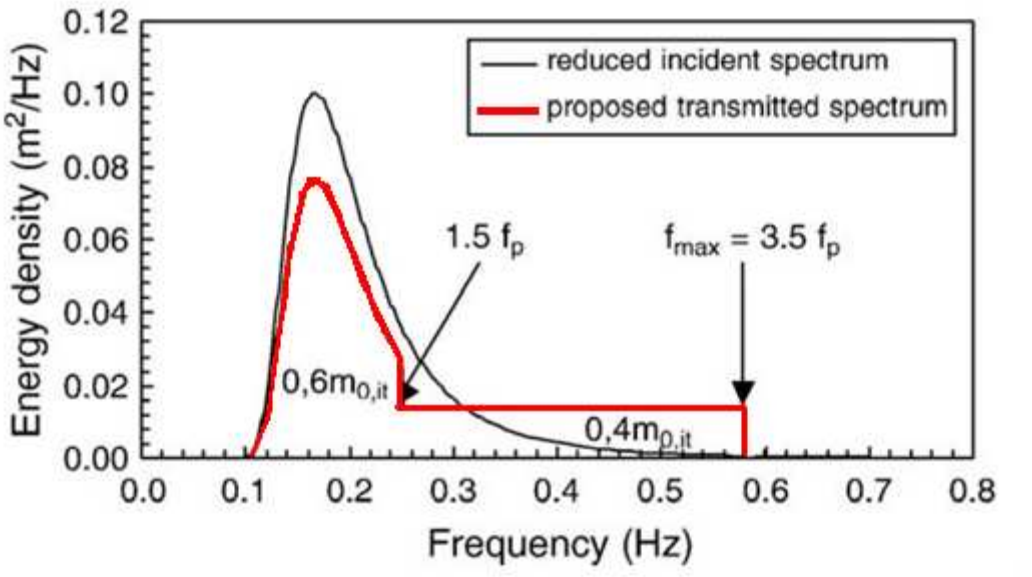

Figure 2.7. Method proposed by VAN DER MEER *et al*. (2000) to estimate transmitted wave energy spectrum behind a submerged structure (red). The model assumes that 60% of the incident energy remains at the incident peak frequency f_p while 40 % is transferred to higher frequencies, in the range 1.5 f_p - 3.5 f_p.

2.2.4. NUMERICAL MODELLING

BLACK (1999) tested the proposed design for the Narrowneck reef using Boussinesq modelling. Wave penetration and interference patterns were important for higher water levels and decreasing in magnitude for lower tides. With respect to wave rotation, the reef locally rotated northeast incident waves on the downdrift region while rotation updrift was minimal. No results on currents and water levels were presented.

BLACK (2003) investigated wave and hydrodynamic processes for 3 projected reef designs. Predicted wave heights, sea levels and current fields were presented for the case of Lyall Bay reef (New Zealand) (Figure 2.8). The project consisted of a V-shaped structure (~100 m wide) located 250 m offshore (Figure 2.8a). The reef created a shadow zone of reduced wave height in its lee, progressively diminishing as the shoreline was approached (Figure 2.8b). The wave breaking on the reef crest induced a distinct setup of the sea level its lee relative to the adjacent undisturbed areas. This gradient was inversed at the shoreline i.e. water level smaller that adjacent undisturbed shorelines (Figure 2.8c, see dashed line). This was attributed to smaller transmitted waves in the lee of the structure that induced a lessened water level setup at the shoreline. Interestingly, a reduced water level

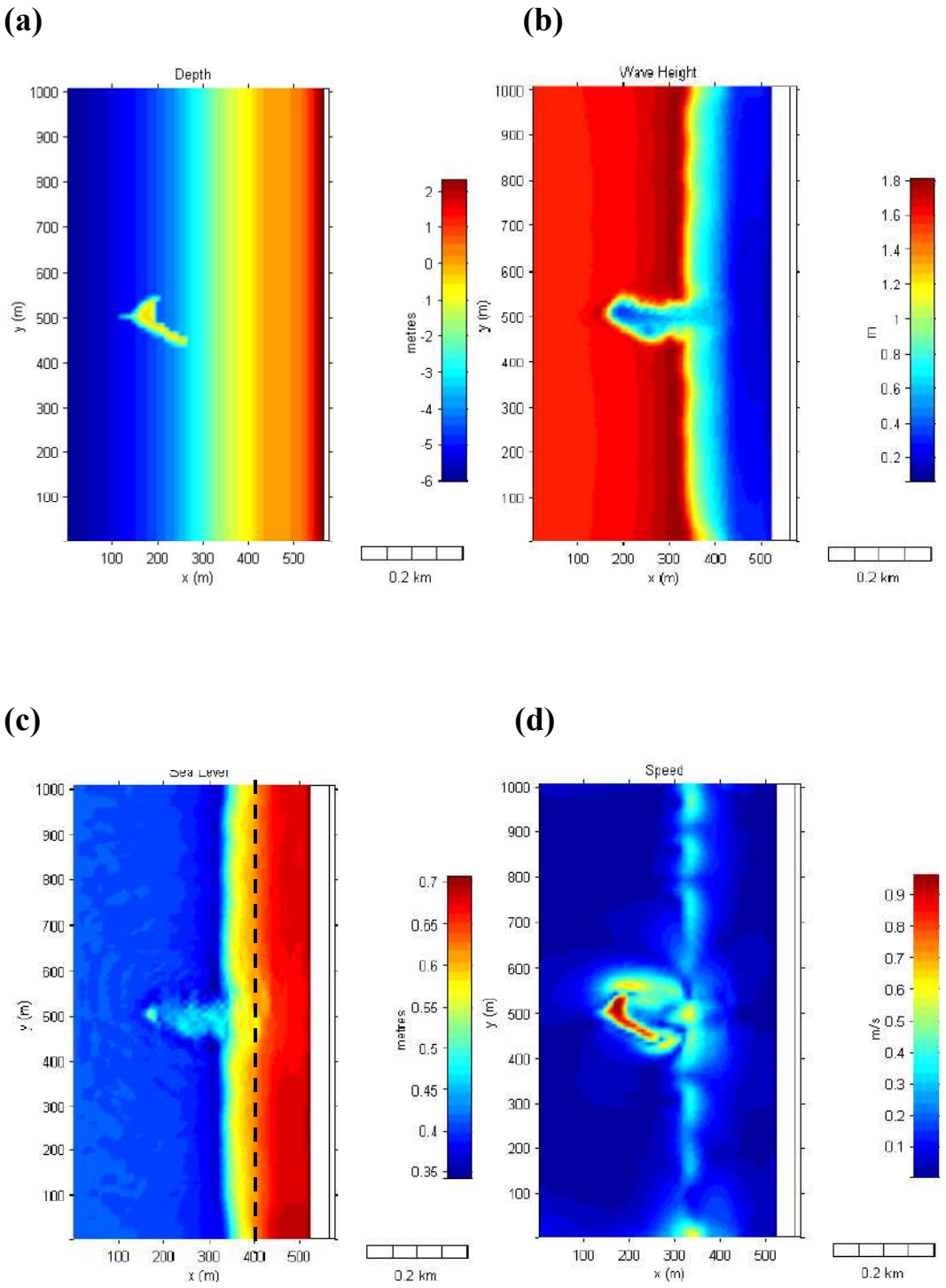

Figure 2.8. Predicted waves and hydrodynamics for the multi-purpose reef designed for Lyall Bay in New Zealand (from BLACK, 2003). (a) Idealized bathymetry, (b) Wave height attenuation, (c) Sea level; and (d) Current velocity. The dashed black line on figure (c) is used to show the relative decrease of water level at the shoreline in the lee of the structure.

would drive current convergence towards the sheltered shoreline, which contrasts with the divergent pattern reported earlier. Current velocity distribution was represented (Figure 2.8d) but the interpretation remain limited since no directional information was available. As expected, the strongest currents were found over the structure due to wave breaking (~1 m/s). High current velocities were also observed in the vicinity of the reef as well as at the shoreline in the lee.

4 important hydrodynamic processes relevant to submerged multi-purpose reefs were identified by the author. These were: (i) wave sheltering generating a shadow zone, (ii) wave rotation on the reef reducing long-shore currents by realigning wave crests with bathymetric contours (see also BLACK and MEAD, 2001a), (iii) wave breaking on the reef reducing the set-up of water level at the shoreline, (iv) counter rotating vortices in the lee of the reef. All of these processes are favourable for salient formation and will be discussed further.

RANASINGHE *et al*. (2006) tested an idealized multi-purpose reef system focusing on 3 parameters namely distance from shoreline to structure, crest submergence level, and the presence or absence of ambient long-shore currents. The most significant feature identified was the "switch" of the nearshore circulation from a 2-cell circulation pattern to a 4-cell circulation pattern as the structure was moved offshore (see Figure 2.9). The 2 contrasting circulation patterns were governed by the development of (i) a sea level at the shoreline in the lee of the reef higher than on the adjacent shorelines that would drive divergent currents (2-cell, Figure 2.9, top), or (ii) a sea level at the shoreline in the lee of the reef lower than on the adjacent shorelines that would drive convergent currents (4-cell, Figure 2.9, bottom). Regarding the two other design parameters, the symmetric pattern for shore normal waves became asymmetric for oblique waves since superimposed on ambient long-shore currents, while the crest level was found to modulate only the intensity of nearshore currents but not their pattern.

The proposed system functioning is robust in that it explains and connects the usual observations of compressed divergent currents in the lee of a submerged structure (e.g. NOBUAKA *et al*., 1996; DEAN *et al*., 1997; VAN DER BIEZEN *et al*., 1998; TURNER *et al*, 2001) and the contrasting processes identified by BLACK (2003) and RANASINGHE and SATO (2007) (e.g. weakening and convergence of currents at the shoreline).

(a) 2-cell circulation

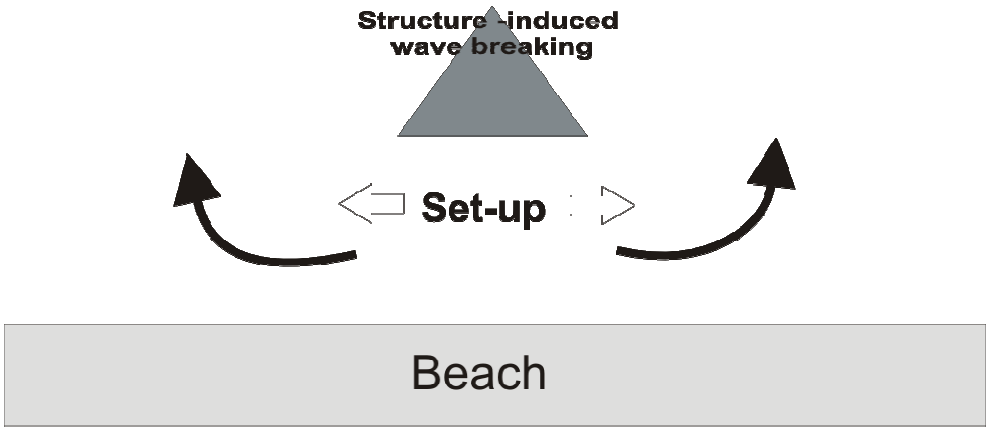

(b) 4-cell circulation

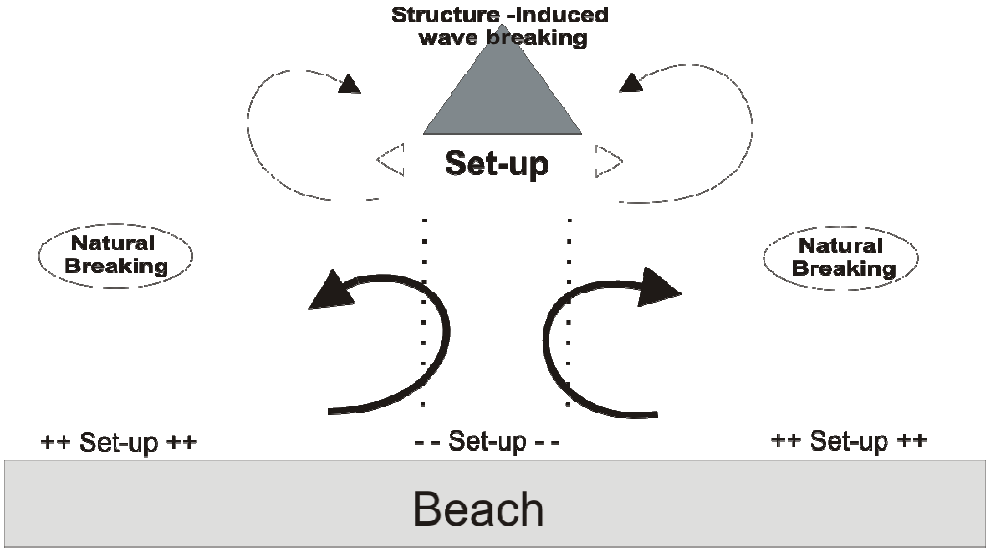

Figure 2.9. Model for nearshore circulations and water level patterns in the vicinity of a multi-purpose reef (based on findings of RANASINGHE *et al.*, 2006). (a) Structure close to the shore. The water level setup near the shoreline is compressed by the structure and causes strong divergent currents near the shoreline that organize into a 2-cell circulation. (b) Structure further offshore. The set up of water level due to structure-induced wave breaking is shifted offshore and so are the 2 diverging cells. The water level at the shoreline in the lee of the reef becomes lower than on the adjacent beach which induces convergent currents organizing in 2 counter-rotating cells. The figure presents result for the case of normally incident waves; the circulation is conserved although more asymmetric under oblique waves.

That being, numerical investigations on the prototype reef system at Mount Maunganui by BLACK and MEAD (2007) still suggested the importance to account for realistic beach morphology to correctly predict the nearshore circulation pattern. Their modelling results showed that the typical pattern of strong onshore flow over the structure and divergence in the lee did occur, however it was observed as well on the natural sand bars in the surf zone. As they were larger than the structure, they generated currents an order of magnitude higher and thus tended to govern the overall inshore circulation. As a result, it was difficult to identify a 2 or 4 -cell circulation pattern as obtained by RANASINGHE *et al*. (2006).

2.3 MORPHODYNAMIC PROCESSES AROUND SUBMERGED STRUCTURES

2.3.1. INTRODUCTION

The objective of a multi-purpose reef designed for coastal protection is to initiate salient formation in its lee, widening the subaerial beach, and providing an additional buffer of sediment during high energy erosive wave events. Salient is the preferred shoreline response as it allows a portion of the long-shore sediment transport to continue to move through the project area to downdrift beaches. In contrast, a tombolo would interrupt the natural long-shore transport with potential starvation of downdrift beaches.

Salient and tombolo formations in response to emergent breakwaters have been widely observed and quantified in the literature (see BASCO, 2006 for a review). However less information is available on offshore submerged structures (BLACK, 2001, RANASINGHE and TURNER, 2006). Observations of salient features in the lee of natural submerged reefs (BLACK and ANDREWS, 2001) provided a favourable argument for salient response to multi-purpose reefs and equations derived for shoreline response provided the basis to design existing multi-purpose reef projects (Figure 2.10).

Being of central interest for coastal management, the shoreline position is the typical proxy to design and assess a project performance. However, the strong onshore flows and cellular circulations, as documented on the first part of the review, are expected to interact with the entire nearshore beach morphology (e.g.

SHORT, 1999). There is then a need to investigate the response of the entire beach bathymetry including beach profile response, sand bar behaviour, and scour development.

Note that since numerical modelling has been the main tool to design multi-purpose reefs and test the beach response, numerical modelling studies are reviewed first to better follow the chronology of published papers. Physical experiments and field observations follow.

2.3.2. NUMERICAL MODELLING

BLACK (1999) investigated sediment dynamics around the final design of the multi-purpose Narrowneck reef. Representative wave events were simulated and output morphologies averaged to determine key features of the sedimentation patterns. Although no salient was obvious, a sedimentation trend was observed near the shoreline through the formation of a long-shore bar possibly broken into several pairs of sand bars and rip channels. The rhythmic sand bars were attributed to the wave interference patterns. Two localised scour holes were predicted near the reef arms' extremities.

Further testing the salient formation in response to different projected multi-purpose reefs, BLACK (2003) suggested that although counter intuitive, the optimal beach protection would be obtained if the reef was positioned several hundred meters offshore and outside of the natural surfzone. Such a positioning would allow increased wave shadow zone along the shoreline (if waves have broad directional spread) and the reduction of long-shore currents compression between the reef and the shoreline.

RANASINGHE *et al*. (2006) confirmed this idea demonstrating that an idealized beach system would have 2 contrasting modes of shoreline response to the reef, namely erosion or accretion, depending upon the structure distance offshore, and subsequent development of a 2 or a 4-cell circulation in the lee side (Figure 2.9). For the 2-cell circulation, compressed divergent currents caused erosion in the lee of the reef. For a reef further offshore, these 2 erosive cells were shifted offshore and 2 counter-rotating cells developed near the shoreline. The inshore cells forced current convergence at the shoreline in the lee of the reef and induced shoreline accretion. These responses were observed with both normal and oblique wave

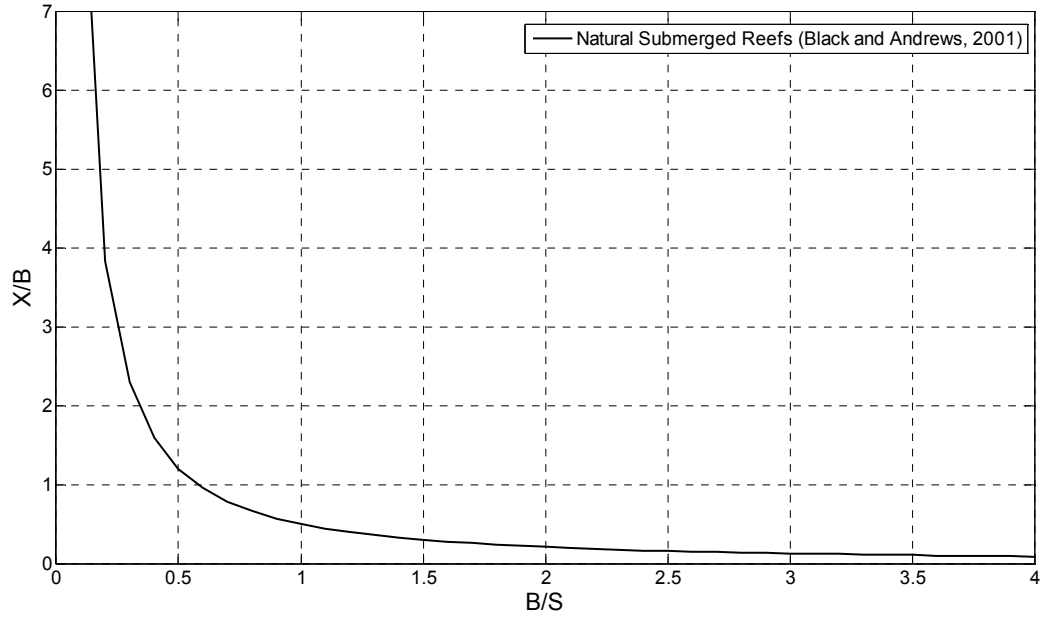

Figure 2.10. Relationship between B/S and X/B for natural offshore submerged reefs (BLACK and ANDREWS, 2001). B is the along-shore width of the structure, S is the distance from the structure to the undisturbed shoreline, and X is the distance from the salient apex to the structure. Salient cross-shore amplitude is equal to S-X. Tombolos were observed when B/S > 0.6, and salients when B/S < 2.00. The threshold for depositional conditions is B/S = 0.1.

approaches, the sedimentation patterns being asymmetric in the latter where the salient was deflected downdrift.

Based on their set of numerical simulations, design graphics were proposed to estimate the magnitude shoreline response (i.e. erosion or accretion) relative to design parameters (Figure 2.11). Since both of erosion and accretion responses have been observed for submerged structures (e.g. RANASINGHE and TURNER, 2006) and found relevant for multi-purpose reefs as well, the authors suggested that the equation of BLACK and ANDREWS (2001) for natural submerged reefs predicting only accretion or absence of accretion may not be applicable in all cases (RANASINGHE *et al*., 2006).

BLACK and MEAD (2007)'s study on the prototype reef at Mount Maunganui allowed comparison of theoretical results with surveyed beach response. Unfortunately, the structure was still uncompleted and the ratio B/S (along-shore width/distance offshore), used in BLACK and ANDREWS (2001)'s equation, was close to non-depositional conditions ($B/S_{observed} = 0.125$ with threshold of 0.1 for salient formation). Shoreline response was indeed limited but simulations showed the importance of sand bar behaviour in shoreline accretion. Under the wave

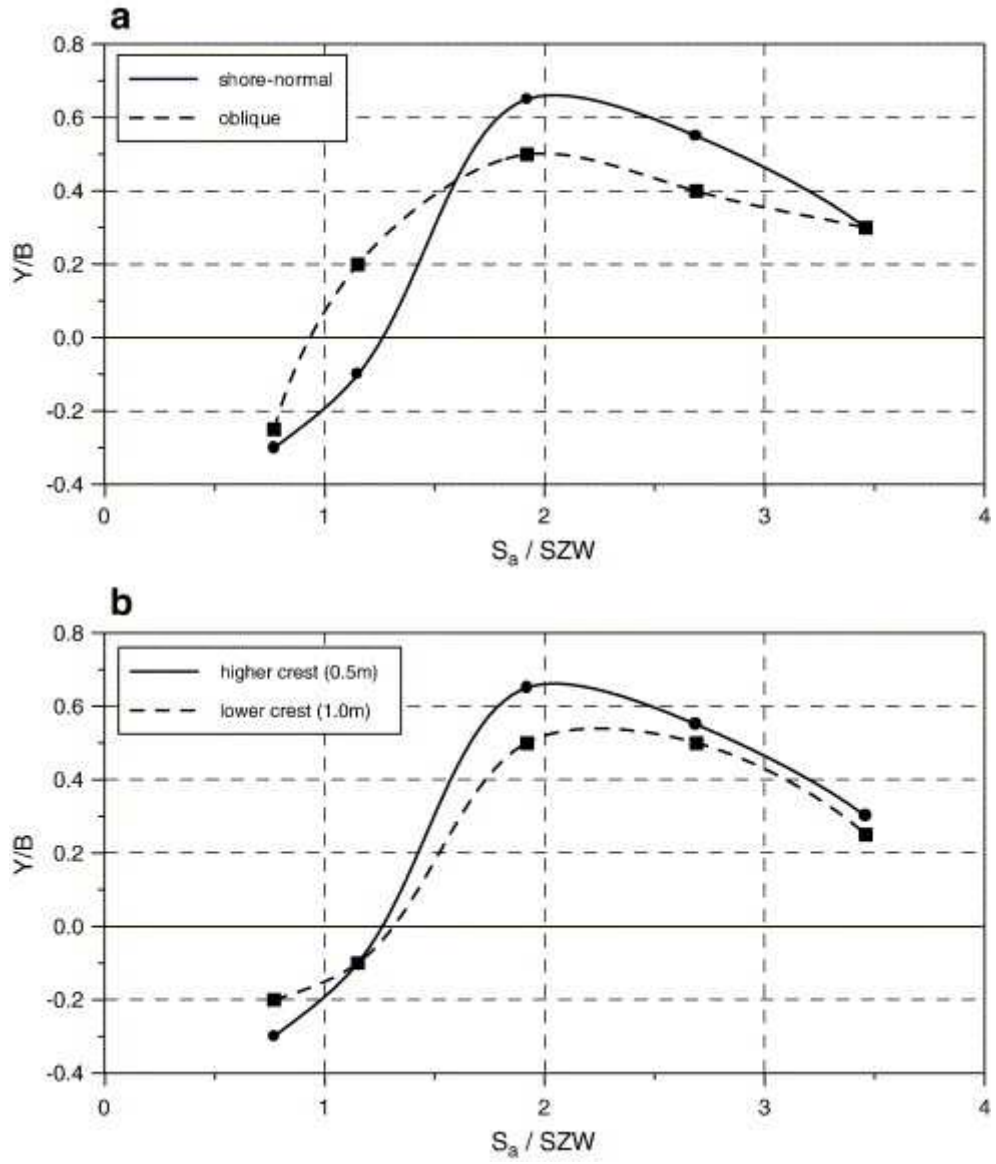

Figure 2.11. Relationships between Y/B and S_a/SZW for (a) shore normal and oblique wave incidence with structure crest level constant at 0.5 m below MWL, and (b) for higher and lower structure crest levels at shore normal wave incidence (from RANASINGHE *et al.*, 2006). Y, B, S_a, and SZW are salient cross-shore amplitude, structure along-shore width, distance of the structure apex to the undisturbed shoreline, and surf zone width respectively. Both graphics predict erosion when the structure is close to the shoreline (i.e. S_a / SZW < 0.8-1.2). The predicted shoreline response then switches to accretion as the structure is moved offshore. Salient size increases within the range S_a / SZW ~ 1.2-2. For greater offshore distances, the structure becomes increasingly transparent to incident waves and predicted salient size decreases.

events considered, the long-shore bar present in the vicinity of the reef would progressively migrate onshore and fragment into two sand banks on each side of the reef. These 2 bars eventually merged with the shoreline to create 2 more prominent shoreline features separated by a rip channel termed a "double horned salient" by the authors. No conclusions could be directly drawn with respect to equations by RANASINGHE *et al.* (2006) since the ratio distance offshore/surfzone width was found beyond range considered in the study (S_a/SZW ~ 7, see Figure 2.11). We can still expect that, as the distance offshore S_a increases, the structure would become increasingly transparent to incident waves, to finally have negligible effect on the shoreline i.e. salient size Y tending to 0. That would be in agreement with the limited to null accretion predicted by the equation of BLACK and ANDREWS (2001) for large ratios B/S.

2.3.3. PHYSICAL MODELLING

The shoreline response to the physical model of the Narrowneck reef was investigated in TURNER *et al*. (2001) using lightweight tracer on a fixed bed beach model. For the simulated wave events, salient formation was observed as the result of a merging of several individual accretive features termed "protosalients" that developed at the shoreline. These features compare well with rhythmic bar features predicted by BLACK (1999) and were likewise attributed to wave interference patterns. The salient size was found to decrease as the incident wave height increased because more wave energy was transmitted in the lee of the reef.

A process that could not be reproduced by the model used in TURNER *et al*. (2001) is scour formation. Scour has been problematic for emergent breakwaters and consequently extensively studied (see BURCHARTH and HUGHES, 2006 for a review). However, less is known about scour around submerged structures.

SUMER *et al*. (2005) compared scour development in mobile bed beach models for emergent, semi, and fully submerged structures, and identified once again fundamentally different processes. Given the small reflection coefficient of submerged structure, scour patterns were not governed by a system of resonant standing wave inducing erosion at antinodes and deposition at nodes, as for emergent structures. In contrast, it was observed that vertical circulation cells

Figure 2.12. Satellite view of the Narrowneck multi-purpose reef (yellow square) and surroundings dating from 18/09/2004 (reef completed in 2000) (Source: Google Earth).

would develop in the close vicinity of the structure, with current velocities an order of magnitude larger than for emergent structures, thus eroding the seabed.

The submerged structure system used in RANASINGHE and SATO (2007) included a sandy beach (uniform grain size) so that precise sedimentation patterns could be observed. Under oblique waves, sedimentation occurred in the lee of the structure firstly through growth of 2 depositional features, progressively merging into a broad single salient. The salient position coincided with the area of weak currents identified in Figure 2.4 (see "Divergence" zone). The adjustment sequence compares well with protosalient formation (TURNER *et al.*, 2001), and "double horned salient" (BLACK and MEAD, 2007). The salient cross-shore amplitude decreased for smaller freeboards as more wave energy was transmitted in the lee of the structure. Undesired side effects included significant erosion of the shoreline downdrift of the structure due to accelerated long-shore currents (see Figure 2.4) which was further enhanced by the limitation of sediment supply due to the structure obstruction to long-shore sediment movement. A scour hole developed in the immediate lee of the structure.

2.3.4. FIELD OBSERVATIONS

The first opportunity to empirically investigate beach system response to a multi-purpose reef was the Narrowneck reef prototype. TURNER (2006) applied an odd-even function analysis to a 2 year dataset of weekly video-extracted shorelines of

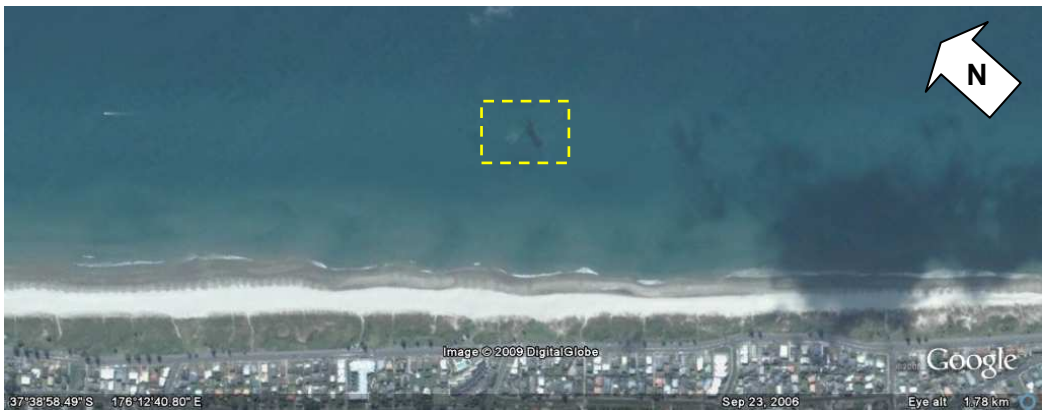

Figure 2.13. Satellite view of the Tay Street area at Mount Maunganui, New Zealand where the prototype reef was constructed (yellow square) dating from the 23/09/2006 (reef 70 % completed). Note the rhythmic bar and rip systems in the vicinity of the reef. (Source: Google Earth).

a 900 m beach segment centred on the reef. An odd-even function analysis was used to discriminate natural (e.g. erosion/accretion) and reef-induced effects (e.g. salient formation) on the shoreline position. An important standard deviation in shoreline position was found along the study site (~15 m) but an average shoreline advance of ~20 m was identified in the lee of the reef within the monitoring period. This accretion signal remains still much lower than predictions (~70 m, see BLACK, 1998). A satellite view of the beach system dating from after the monitoring study (Figure 2.12) does not show obvious salient feature and suggests a relatively dynamic shoreline response.

SCARFE and HEALY (2006) and SCARFE (2008) monitored the beach morphodynamic response to the prototype multi-purpose reef at Mount Maunganui, New Zealand using repetitive multibeam echosoundings surveys prior to, and throughout reef construction. Consecutives bathymetries at early stages of reef construction imaged the inshore migration of the underlying long-shore bar that subsequently fragmented into rhythmic rip and bar systems in the shallow surfzone. Even though the mechanism of shoreward migration and fragmentation of the long-shore bar is in agreement with BLACK and MEAD (2007), it was noted in SCARFE (2008) that this process had occurred not only in the vicinity of the reef but also on a larger scale, with 6-8 similar bar systems developing along the beach. Several bar and rip systems are visible on a satellite view of the study site (Figure 2.13). An updated calculation of the ratio B/S of BLACK and ANDREWS (2001)'s equation for the larger reef dimensions at that time yielded a value around 0.3 that potentially predicted salient formation (see Figure 2.10). The surveyed shorelines did not show obvious depositional feature

and rather oscillated around the mean preconstruction position. A scour hole ~3 times the size of the reef itself developed in the immediate lee of the structure and was attributed to the strong onshore flow over the structure.

2.4. DISCUSSION

2.4.1. OCEANOGRAPHIC PROCESSES

When waves break on a submerged structure, incident wave energy is partitioned into an onshore flow over the structure, and a water level setup directly in the lee of the structure (RANASINGHE *et al*., 2006). These 2 features are expected to govern the nearshore circulation in the lee side (see Figure 2.9). Idealized cases on plane sloping beaches showed the importance of the reef distance offshore as a design parameter (BLACK, 2003; RANASINGHE *et al.*, 2006). A structure positioned too close to the shore will result in strong divergent flow in its lee. This circulation pattern was consistently observed in the lee of conventional submerged structures (GROENEWOUD *et al.*, 1996; DEAN *et al*., 1997; LOVELESS and MACLEOD, 1999; DREI *et al.*, 2001). Moving the structure offshore, these divergent cells are shifted offshore and force inshore counter-rotating cells eventually resulting in current convergence towards at the shoreline in the lee of the structure, which is favourable for sedimentation (e.g. BLACK, 2003; RANASINGHE *et al.*, 2006).

Comparable processes are expected at natural reef systems which have been observed to provide the desired salient response (BLACK and ANDREWS, 2001). However, it was noted from field observations that an important part of the incident wave energy is actually dissipated by friction over the rough surface of the reef flat (SYMONDS *et al*., 1995; LOWE *et al.*, 2005) which is unlikely on the smooth geotextiles commonly used for multi-purpose reef construction. Application of findings from SYMONDS *et al*. (1995) to predict wave-driven currents over submerged structures (SYMONDS and BLACK, 2001) confirmed that structures that are (i) narrow, (ii) detached, (iii) fully submerged, and (iv) smooth with low frictional resistance were likely to further enhance wave-driven currents since energy dissipation through frictional resistance is minimal. This has likely implications on current patterns and magnitudes, and in turn sediment transport in the vicinity of submerged multi-purpose reefs.

With respect to wave transmission, very little is available specifically on multi-purpose reefs. Qualitatively, reef structures (i.e V-shaped) may however have some advantages as transmission coefficients are found to decrease with structure angle with the shoreline (see VAN DER MEER *et al.*, 2005). Moreover, conditioned shoaling and refraction tend to maximize the breaking wave height (e.g. GODA, 1996; BLACK, 2001) thus providing a better energy dissipation.

Another domain for which little is available is the change in wave energy spectra as waves propagate over a submerged structure. Studies on conventional submerged breakwaters predicted a shift of the wave energy spectra mostly towards high frequencies (e.g. VAN DER MEER *et al.*, 2000, BLECK and OUMERACI, 2001). This wave energy spectrum modification was also observed on barred beaches (e.g. MASSELINK, 1998; SENECHAL *et al*., 2002). The generation of high frequency energy appeared to be hardly affected by wave breaking and would delay wave energy dissipation to the beach face (SENECHAL *et al*., 2002). This contrasts with the desired shelter in the lee of the reef.

Finally, transfer of wave energy towards lower frequencies (infragravity energy) has also been observed on natural reefs (e.g. BRANDER *et al*., 2004) and barred beaches (e.g. RUESSINK, 1998; CERTAIN *et al*., 2005) and is then expected with submerged structures. Infragravity energy can be an important driver for nearshore beach morphology (e.g. bar morphology, rip formation) (e.g. AAGAARD and MASSELINK, 1999), which in turn was found to be important to understand beach response to multi-purpose reefs (BLACK and MEAD, 2007; SCARFE, 2008).

2.4.2. MORPHODYNAMIC PROCESSES

Since a multi-purpose reef interrupts the natural surf zone circulation, a modification of the beach morphodynamics is expected in addition to any shoreline effects (e.g. SHORT, 1999). Based on the WRIGHT and SHORT (1984)'s model, a decrease in wave height in the lee of a structure would result theoretically in a shift of the sheltered beach towards a more reflective state. This includes the development of more rhythmic features such as rip/bar systems, and these have indeed been observed in the vicinity of constructed reef prototypes (JACKSON *et al*., 2007; SCARFE*,* 2008). These features are found to be the result of an input of sediment in the nearshore zone due to the fragmentation and

shoreward migration of a long-shore bar (BLACK, 1999; BLACK and MEAD, 2007; SCARFE, 2008). The process is consistent with numerical modelling simulations by GARNIER *et al.* (2008) who demonstrated that a single bathymetric perturbation on an idealized uniform long-shore bar was sufficient to induce the bar onshore migration and its fragmentation into a bar/rip systems, through coupling between hydrodynamics and morphology. This further highlights the relevance of rip systems formation around narrow submerged structures. They pose potentials problems since increased rips currents can deteriorate swimming safety and may transport significant volumes of sediment offshore (e.g. AAGAARD *et al.,* 1997).

With respect to shoreline adjustments, observed responses appear to be less than predicted. Looking at either surveyed (BLACK and MEAD, 2007; SCARFE *et al.*, 2008) or modelled (BLACK, 1999; BLACK and MEAD, 2007) beach morphologies around multi-purpose reefs, an explanation could be that bars and scours that develop during adjustment periods could have adverse impacts on the processes suggested for salient formation (see BLACK, 2003). The concept of wave rotation (MEAD and BLACK, 2001a) is theoretically valid, however, SCARFE (2008) showed that wave refraction by the scour hole that developed in the lee of the Mount Maunganui reef was eventually more significant. Furthermore, the rhythmic beach system that developed inshore of the reef at the site is likely to interfere with the desired wave setup patterns at the shoreline as well as development of structure-induced counter-rotating vortices.

2.5. CONCLUSIONS

The chapter reviewed the literature dealing with oceanographic and morphodynamic processes around conventional and multi-purpose submerged structures. Main points are:

- Beach system response to submerged structures is significantly different from that for emerged structures, mainly because significant wave transmission is allowed in their lee. Moreover, for the class of submerged structures, smooth structures show a contrasting behaviour compared to typical rubble-mound breakwaters.

- The dominant hydrodynamic process at a submerged structure is the partition of incident wave energy into (i) a strong onshore flow over the structure, and (ii) a set-up of the water level in the lee that is able to drive nearshore currents. Idealized cases showed that the reef offshore distance governs the development of either divergent or convergent currents at the shoreline, inducing erosion or accretion respectively. These idealized patterns will however be superimposed on the ambient surfzone circulation that may be dominant depending on the underlying morphology. This indicates the necessity to account for pre-existing surfzone features and their perturbation post-construction.

- Wave height and energy transmission over multi-purpose reefs is poorly quantified and lacks field data. Oblique structures such as multi-purpose reef oblique arms may provide reduced transmission coefficients relative to conventional shore-parallel designs due to enhanced wave refraction and maximization of the breaking wave height allowing greater energy dissipation. Modification of wave energy spectra with a shift towards both higher and lower frequencies has been observed over both conventional submerged structures and natural reefs and is likewise expected for multi-purpose reefs.

- Physical and numerical modelling investigations provided favourable arguments for salient formation in the lee of multi-purpose reefs but shoreline responses to prototypes monitored to date remain lower than predictions. Besides shoreline effects, it appears that an important feature of the beach morphodynamic response is the shift of protected beach systems towards more reflective states which includes the development rhythmic surfzone features such as rip/bar systems. Scour formation in the vicinity of multi-purpose reefs and submerged structures has also been consistently observed.

2.6. REFERENCES

AAGAARD, T., GREENWOOD, B., and NIELSEN, J. 1997. Mean currents and sediment transport in a rip channel. *Marine Geology*, 140, 25-45.

AAGAARD, T., and MASSELINK, G., 1999. The Surf Zone. *In*: SHORT, A.D. (ed.), *Handbook of Beach and Shoreface Morphodynamics*. West Sussex, England: John Wiley & Sons Ltd, ISBN 0-471-96570-7, pp. 72-118.

D'ANGREMOND, K., VAN DER MEER, J.W., and DE JONG, R.J., 1996. Wave transmission at low crested structures. *Proceedings of 25th International Conference on Coastal Engineering* (Orlando, Florida, ASCE), pp. 2418-2427.

ARCHETTI, R., TIRINDELLI, M., and LAMBERTI, A., 2003. Field measurements of hydrodynamics around a beach defense system. *Proceedings of the 2003 Coastal Structures Conference* (Portland, Oregon, ASCE), pp. 663– 675.

BASCO, D.R., 2006. Shore Protection Projects. *In*: WARD, D.L., (ed.), *Coastal Engineering Manual*, Part V, Coastal Project Planning and Design, Chapter 3, Engineering Manual 1110-2-1100, U.S. Army Corps of Engineers, Washington, DC.

BLACK, K.P., 1998. Narrowneck Reef Report 3: Sediment Transport. Hamilton, New Zealand: Centre of Excellence in Coastal Oceanography and Marine Geology, The University of Waikato and NIWA, 162 p.

BLACK, K.P., 1999. Designing the Shape of the Gold Coast Reef: Sediment Dynamics. *Proceedings of the 1999 Coasts and Ports Conference* (Perth, Australia), pp. 58-63.

BLACK, K.P., 2001. Artificial Surfing Reefs for Erosion Control and Amenity: Theory and Application. *In:* HEALY, T.R., (ed.), International Coastal Symposium (ICS2000). *Journal of Coastal Research, Special Issue No. 34*, 1-14.

BLACK, K.P., 2003. Numerical Prediction of Salient Formation in the Lee of Offshore Reefs. *In:* BLACK, K.P., and MEAD, S.T., (eds.), *Artificial Surfing Reefs 2003: The 3rd International Conference,* (Raglan, New Zealand). CD publication. pp. 196-218, ISBN: 0-473-09801-06.

BLACK, K.P., and ANDREW, C.J., 2001. Sandy Shoreline Response to Offshore Obstacles, Part 1: Salient and Tombolo Geometry and Shape. *In:* BLACK, K.P., (ed.), Natural and Artificial Reefs for Surfing and Coastal Protection. *Journal of Coastal Research, Special Issue No. 29*, 82-93.

BLACK, K.P., and MEAD, S.T., 2001a. Wave Rotation for Coastal Protection. *Proceedings of the 2001 Coasts and Ports Conference* (Gold Coast, Australia), pp. 120-127.

BLACK, K.P. and MEAD, S.T., 2001b. Design of the Gold Coast Reef for Surfing, Public Amenity and Coastal Protection: Surfing Aspects. *In:* BLACK, K.P. (ed.), Natural and Artificial Reefs for Surfing and Coastal Protection. *Journal of Coastal Research, Special Issue No. 29*, 115-130.

BLACK, K.P. and MEAD, S.T., 2007. Sand Bank Responses to a Multi-Purpose Reef on an Exposed Sandy Coast. *In*: WALTHER, M. (ed.), Shore protection and surfing dedicated issue: *Shore and Beach*, 75(4), 55-66.

BLECK, M. and OUMERACI, H., 2001. Wave Damping and Spectral Evolution at Artificial Reefs. *Proceedings of the 4th International Symposium on Ocean Wave Measurement and Analysis* (San Francisco, California), pp. 1062-1071.

BRANDER, R.W., KENCH, P.S., and HART, D., 2004. Spatial and temporal variations in wave characteristics across a reef platform, Warraber Island, Torres Strait, Australia. *Marine Geology*, 207, 169– 184.

BURCHARTH, H.F., and HUGHES, S.A., 2006. Fundamentals of Design. *In*: HUGHES, S., (ed.), *Coastal Engineering Manual,* Part VI, Design of Coastal Project Elements, Chapter 2, Engineering Manual 1110-2-1100, U.S. Army Corps of Engineers, Washington, DC.

CERTAIN, R., MEULE, S., REY, V, AND PINAZO, C., 2005. Wave transformation on a microtidal barred beach (Sète, France). *Journal of Marine Systems*, 38, 19–34.

DEAN, R.G., CHEN, R., and BROWDER, A.E., 1997. Full scale monitoring study of a submerged breakwater. *Coastal Engineering*, 29, 291– 315.

DREI, E., TURCHETTO, A., ARCHETTI, R., and LAMBERTI, A., 2001. Wave and current field measurements around low crested structure. *Proceedings of the 4th International Sympossium on Ocean Waves Measurements and Analysis* (San Francisco, California), pp. 115– 124.

FERRANTE, V., 2007. Spectral analysis of wave transmission behind submerged breakwaters, Napoli University, Ph.D Thesis.

GARNIER, R., CALVETE, FALQUES, A.D., and DODD, N., 2008. Modelling the formation and the long-term behaviour of rip channel systems from the deformation of a long-shore bar. *Journal of Geophysical Research*, 113, C07053, doi:10.1029/2007JC004632.

GODA, Y., 1996. *Wave Damping Characteristics of Longitudinal Reef System*. Advances in Coastal Structures and Breakwaters, Thomas Telford, London, pp. 192–207.

GODA, Y., and TAKAGI, H., 1998. Lateral Versus Longitudinal Artificial Reef Systems. *Proceedings of the 26th International Conference on Coastal Engineering* (Copenhagen, Denmark, ASCE), pp. 2152-2165.

GROENEWOUD, M.D., VAN DE GRAAFF, J., CLAESSEN, E.W., and VAN DER BIEZEN, S.C., 1996. Effect of submerged breakwater on profile development. *Proceedings of the 25th International Conference on Coastal Engineering* (Orlando, USA, ASCE), pp. 2428– 2441.

HUTT, J.A., BLACK, K.P., JACKSON, A., and MCGRATH, J., 1999. Designing the Shape of the Gold Coast Reef: Field Investigations. *Proceedings of the 1999 Coasts and Ports Conference* (Perth, Australia), pp. 299-304.

JACKSON, L.A., TOMLINSON, R., MCGRATH, J., and TURNER, I., 2002. Monitoring of a multi-functional submerged geotextile reef breakwater. *Proceedings of the 28th International Conference on Coastal Engineering* (Cardiff, UK, ASCE), pp. 1923–1935.

JACKSON, L.A., and CORBETT, B.B., 2007. Review of Existing Multi-Functional Artificial Reefs. *Proceedings of the 2007 Coasts and Ports Australasian Conference* (Gold Coast, Australia). 15 p.

KRAMER, M., ZANUTTIGH, B., VAN DER MEER, J.W., VIDAL, C., and GIRONELLA, F.X., 2005. Laboratory Experiments on Low-Crested Breakwaters. *Coastal Engineering,* 52, 867-885.

LOVELESS, J., and MACLEOD, B., 1999. The influence of set-up currents on sediment movement behind detached breakwaters. *Proceedings of the 1999 Coastal Sediments Conference* (Long Island, USA), pp. 2026–2041.

LOWE, R.J., FALTER, J.L., BANDET, M.D., PAWLAK, G., ATKINSON, M.J., MONISMITH, S,G., and KOSEFF, J.R., 2005. Spectral wave dissipation over a barrier reef. *Journal of Geophysical Research,* 110, C04001, doi:10.1029/2004JC002711.

MASSELINK, G., 1998. Field investigation of wave propagation over a bar and the consequent generation of secondary waves. *Coastal Engineering*, 33, 1-9.

NOBUOKA, H., IRIE, I., KATO, H., and MIMURA, N., 1996. Regulation of nearshore circulation by submerged breakwater for shore protection. *Proceedings of the 25th International Conference on Coastal Engineering* (Orlando, USA, ASCE), pp. 2391– 2403.

RANASINGHE, R., and TURNER, I.L., 2006. Shoreline Response to Submerged Structures: A Review. *Coastal Engineering*, 53, 65-79.

RANASINGHE, R., TURNER, I.L., and SYMONDS, G., 2006. Shoreline Response to Multi-Functional Artificial Surfing Reefs: A Numerical and Physical Modelling Study. *Coastal Engineering*, 53, 589-611.

RANASINGHE, R., and SATO, S., 2007. Beach morphology behind single impermeable submerged breakwaters under obliquely incident waves. *Coastal Engineering Journal*, 49 (1), 1-24.

RUESSINK, B.G., 1998.The temporal and spatial variability of infragravity energy in a barred nearshore zone. *Continental Shelf Research*, 18, 585-605.

SCARFE, B.E., and HEALY, T.R., 2005. Baseline Bathymetric Data Collection for Monitoring of Bar, Rip and Salient Response to an Artificial Surfing Reef - Mount Maunganui, New Zealand. *In*: TOWNSEND, M. and WALKER, D., (eds.), *Proceedings for the 2005 Coasts and Ports Australasian Conference* (Adelaide, South Australia), pp. 459-464.

SCARFE, B.E., 2008. Oceanographic Considerations for the Management and Protection of Surfing Breaks. Hamilton, New Zealand: The University of Waikato, Ph.D. thesis, 307 p. + appendices.

SENECHAL, N., BONNETON, P., and DUPUIS, H., 2002. Field experiment on secondary wave generation on a barred beach and the consequent evolution of energy dissipation on the beach face. *Coastal Engineering*, 46, 233-247.

SHORT, A.D., 1999. Beach Modification: Natural impacts and beach Morphodynamics. *In*: SHORT, A.D. (ed.), *Handbook of Beach and Shoreface Morphodynamics*. West Sussex, England: John Wiley & Sons Ltd, ISBN 0-471-96570-7, pp. 253-270.

SUMER, B.M., FREDSOE, J. LAMBERTI, A., ZANUTTIGH, B., DIXEN M., GISLASON K., and DI PENTA A.F., 2005. Local scour at roundhead and along the trunk of low crested structures. *Coastal Engineering*, 52, 995-1026.

SYMONDS, G., BLACK, K. P., and YOUNG, I. R., 1995. Wave-driven flow over shallow reefs. *Journal of Geophysical Research*, 100, 2639– 2648.

SYMONDS, G. and BLACK, K.P., 2001. Predicting Wave-Driven Current on Surfing Reefs. *In:* BLACK, K.P. (ed.), Natural and Artificial Reefs for Surfing and Coastal Protection. *Journal of Coastal Research, Special Issue No. 29*, 102-114.

TAJZIECHI, M., 2006. Experimental and numerical modelling of wave induced currents and wave transformations in presence of submerged structures. School of Civil and Environmental Engineering, University of New South Wales, Australia, Ph.D Thesis.

TURNER, I., LEYDEN, V., COX, R., JACKSON, A., and MCGRATH, J., 2001. Physical Model Study of the Gold Coast Artificial Reef. *In:* BLACK, K.P. (ed.), Natural and Artificial Reefs for Surfing and Coastal Protection. *Journal of Coastal Research, Special Issue No. 29*, 131-146.

TURNER, I.L., 2006. Discriminating Modes of Shoreline Response. *Journal of Waterway, Port, Coastal and Ocean Engineering*, 132(3), 180-191.

VAN DER BIEZEN, S.C., ROELVINK, J.A., VAN DE GRAAFF, J., SCHAAP, J., and TORRINI, L., 1998. 2DH morphological modelling of submerged breakwaters. *Proceedings of the 26th International Conference on Coastal Engineering* (Copenhagen, Denmark, ASCE), pp. 2028– 2041.

VAN DER MEER, J.W., REGELING, H.J. and DE WAAL, J.P., 2000. Wave transmission: spectral changes and its effects on run-up and overtopping. *Proceedings of the 27th International Conference on Coastal Engineering* (Sydney, Australia, ASCE), pp. 2156-2168.

VAN DER MEER, J.W., BRIGANTI, R., ZANUTTIGH, B., WANG, B., 2005. Wave transmission and reflection at low crested structures: design formulae, oblique wave attack and spectral change. *Coastal Engineering*, 52, 915-929.

WRIGHT, L.D., and SHORT, A.D., 1984. Morphodynamic Variability of Surf Zones and Beaches: A Synthesis. *Marine Geology*, 56, 93–118.

ZYSERMAN, J.A., and JOHNSON, H.K., 2002. Modelling morphological processes in the vicinity of shore-parallel breakwaters. *Coastal Engineering* , 45, 261–284.

CHAPTER 3. SHORELINE RESPONSE TO AN OFFSHORE SUBMERGED MULTI-PURPOSE REEF AT MOUNT MAUNGANUI, NEW ZEALAND

3.1 INTRODUCTION

The chapter focuses on the shoreline response to the offshore submerged multi-purpose reef constructed near Tay Street at Mount Maunganui. A dataset including both pre and post reef construction shorelines is analyzed using an odd-even function analysis (see ROSATI and KRAUS, 1997) to separate natural (e.g. cyclic erosion/accretion) and structural modes (e.g. salient formation, groin effect) of shoreline response, and thus more accurately quantify the structural effects. These results have been presented as a paper at the Coasts and Ports Conference 2009 in Wellington, New Zealand. The paper in included in the Appendix A.

3.2 METHODS

3.2.1 THE SHORELINE DATASET

The study site (Figure 1.5) benefits from a pre-construction baseline bathymetric and foreshore survey datasets collected using multibeam echosoundings (MBES) and RTK GPS (SCARFE and HEALY, 2005). Throughout reef construction, SCARFE (2008) collected additional surveys for comparison with the baseline. A new survey has been undertaken in March 2009 as a part of this research, after reef completion in June 2008 (Table 3.1).

To apply the odd-even function analysis, shoreline contours, taken as mean sea level contours (MSL, Motukiri Vertical Datum, 1953), were extracted from the survey datasets. The study zone was defined as a 1400 m segment of shoreline centred on the reef axis. Six complete shoreline contours were available for this zone (Table 3.1). A reference line in the backshore provided a measure of the beach width (see Figure 3.1) and contours were then interpolated to yield evenly

Table 3.1. Dates of surveys around the Tay Street reef and stages of reef completion. Symbols * indicate surveys for which a complete shoreline contour (MSL) is available (from SCARFE, 2008).

Survey date	Reef completion
19/08/2004 *	0%
28/10/2004	0%
26/04/2005	0%
08/09/2005	0%
17/11/2005*	10%
20/04/2006	25%
15/08/2006 *	25%
23/01/2007 *	70%
15/05/2007 *	70%
14/03/2009 *	100%

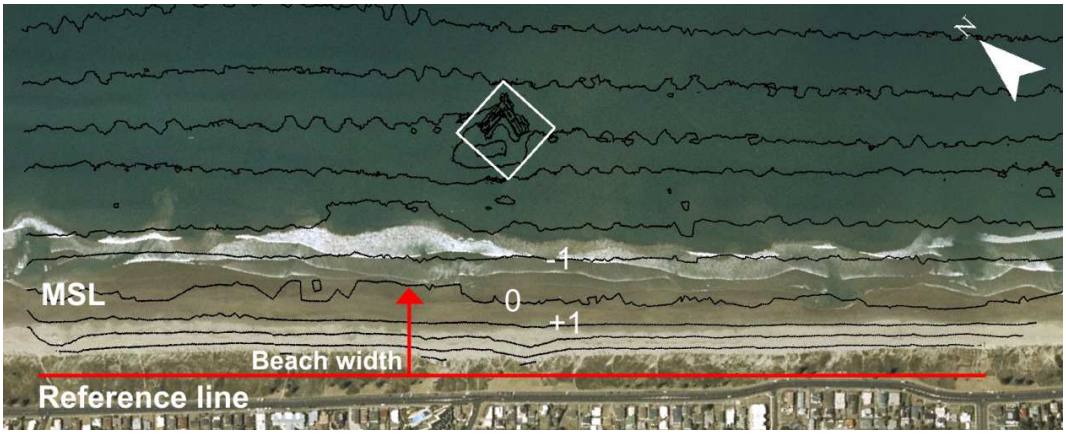

Figure 3.1. Definition of the beach width from the reference line to the mean sea level contour i.e. 0 contour (MSL, Motukiri Vertical Datum, 1953). The contours shown here are derived from the last survey undertaken in March 2009, after reef completion (see Table 3.1).

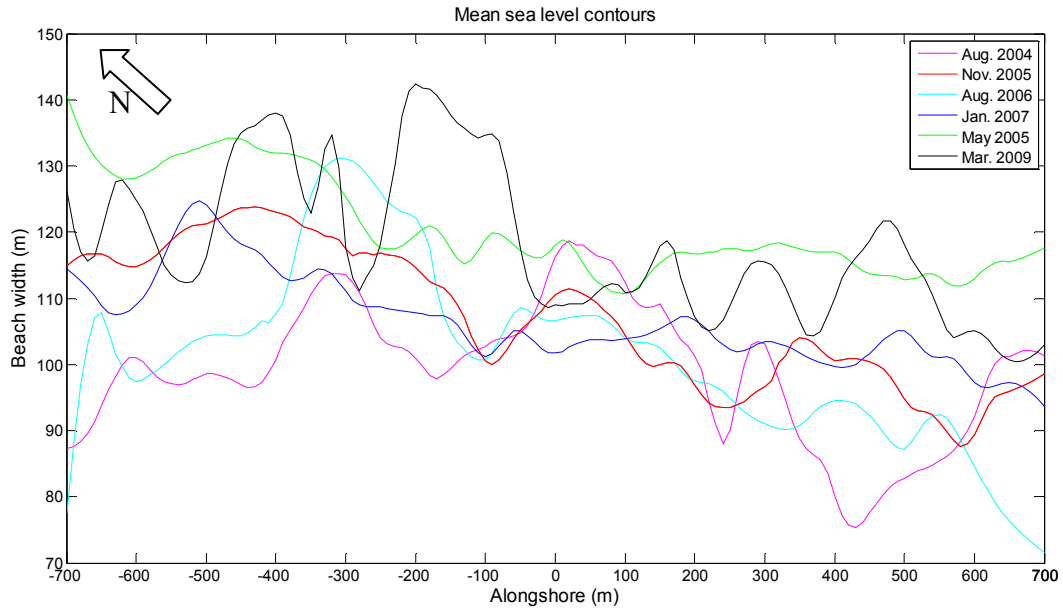

Figure 3.2. Mean sea level contours and beach widths relative to the reference line shown in Figure 3.1. The alongshore origin (x=0 m) corresponds to the reef centreline. The beach width oscillates within 50 to 60 m in the cross-shore direction depending on surveys. No obvious salient is observed but note the crenulated shoreline surveyed in March 2009.

spaced data (every 10m) as required to apply the odd-even function decomposition (Figure 3.2).

3.2.2 Odd-Even Function Analysis

3.2.2.1 Principe

The basic principle of the odd-even function analysis is to decompose shoreline change data into its symmetric and asymmetric components about a point of significance (Rosati and Ebbersole, 1998). The reference point corresponds typically to a coastal structure (here the reef) or inlet position. The method has been used previously to assess the alongshore extent of impacts of engineering projects such as inlets (e.g. Dean and Work, 1993; Rosati and Ebbersole, 1998) but application on a smaller scale to the Narrowneck reef site by Turner (2006) proved it to be a robust tool to discriminate different modes of shoreline response to offshore structures i.e. natural erosion/accretion, salient growth, and secondary groin effect (Figure 3.3)

3.2.2.2 Calculation procedure

The procedure outlined here is based on the methodology given in Rosati and Kraus (1997).

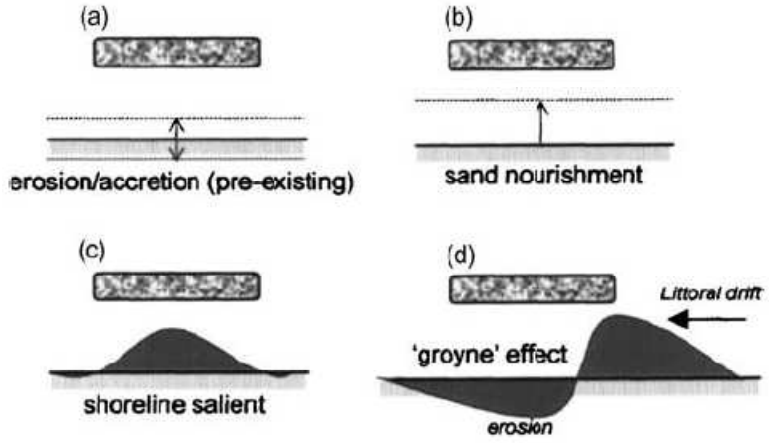

Figure 3.3. Different modes of shoreline response to offshore structures: (a) natural variability, (b) artificial nourishment, (c) salient formation, and (d) secondary groin effect (from TURNER, 2006).

First, we have to define the shoreline change function for the time interval considered, $\Delta S(x)$, where x is the alongshore direction and the reference x = 0 m is the structure centreline. Using the beach widths bw(x) at two times t_1 and t_2, the shoreline change function is:

$$\Delta S(x)=bw_{t2}(x)-bw_{t1}(x) \tag{3.1}$$

We have to decompose this shoreline change function into an even and odd function. An even function does not change sign if the argument changes sign:

$$f_{even}(-x)=f_{even}(x) \tag{3.2}$$

On the contrary, an odd function changes sign if its argument does:

$$f_{odd}(-x)=-f_{odd}(x) \tag{3.3}$$

The total shoreline change function is the sum of the even and odd components:

$$\Delta S(x)=\Delta S_{even}(x)+\Delta S_{odd}(x) \tag{3.4}$$

Using properties of the even and odd functions, (3.2) and (3.3), we have:

$$\Delta S_{even}(-x)=\Delta S_{even}(x) \tag{3.5}$$

$$\Delta S_{odd}(-x)=-\Delta S_{odd}(x) \tag{3.6}$$

Then:

$$\Delta S(-x)=\Delta S_{even}(-x)+\Delta S_{odd}(-x)=\Delta S_{even}(x)-\Delta S_{odd}(x) \tag{3.7}$$

Rearranging (3.4) and (3.7), we can solve for the even and odd functions:

$$\Delta S_{even}(x) = \frac{1}{2}.(\Delta S(x) + \Delta S(-x)) \quad (3.8)$$

$$\Delta S_{odd}(y) = \frac{1}{2}.(\Delta S(x) + \Delta S(-x)) \quad (3.9)$$

The procedure was implemented in a Matlab program used for the computation and representation of the odd-even function analysis results. The program code is given in Appendix B.

3.2.2.3 Interpretation

Although the method explicitly separates symmetric and asymmetric beach width changes, distinction of natural and engineered effects requires careful interpretation and often knowledge about the site settings (e.g. direction and magnitude of net/gross long-shore sediment transport, previous engineering projects) (ROSATI and KRAUS, 1997).

The even component describes symmetrical shoreline advance/retreat. In this function, natural effects are anticipated to occur uniformly along the study site. A simple example is an overall shoreline retreat during a storm event, or more energetic winter months. On the other hand, structural effects are expected to be localized in the vicinity of the structure. For the case of offshore structures, salient or tombolo growth is expected to occur symmetrically around the structure centreline, tapering off to zero at some distance alongshore. Thus, natural shoreline advance or retreat can be discriminated by identifying any positive or negative uniform offset in the even function shape.

A non structural engineered impact that may need to be accounted for is concurrent or antecedent sand nourishment. Shape of the expected sand nourishment signal will depend on the size of the region of interest relative to project dimension and would range from an uniform advance if the study site is focused enough (e.g. TURNER, 2006), which is preferable, to more complex adjustment curves for larger zones (see DEAN, 2002).

Asymmetrical shoreline adjustments are represented by the odd function (e.g. groin effect). The odd component may approach a negligible value at natural coastlines with either no significant drift, or no net drift (with possibly significant gross alongshore transport). In that case, natural asymmetric shoreline changes are

either absent, or compensated for by the successive reversals. Note that a groin in such a drift environment will tend to impound sediment on both of its sides. Shoreline changes are then symmetric and will be expressed in the even function (ROSATI and KRAUS, 1997).

In the case of more consistent drift direction, the odd function may still approach zero if the alongshore transport rate is homogeneous along the study site, for the study period. If we can make this assumption for the initial system (e.g. open straight coast with oblique wave incidence), the odd function can be used directly to estimate alongshore extent of the impact of a coastal engineering project such as jetty system, groin or offshore structure. The structure induces an accretion/erosion pattern in the odd component and the impact extent is defined by the alongshore points at which the function approaches a negligible value again (ROSATI and EBBERSOLE, 1997).

On more complex coasts, a pre-existing gradient in long-shore transport, in turn leading to gradient in shoreline changes may exist. These occur in places where incident wave energy is naturally modulated along the coast (e.g. offshore islands, focusing shoals) (WALTON, 2002). Then, analysis of an independent shoreline change function (i.e. pre-construction) is necessary to identify and subsequently discriminate the signal in constructed intervals. Importantly, an implicit condition for any gradient in shoreline change to be stationary in time is the assumption of stationary wave climate and sediment transport (WALTON, 2002).

Another feature particularly relevant for an offshore structure is the necessity to re-centre shoreline data relative to salient or tombolo apex in the case of an alongshore offset, as expected on littoral drift coastlines (e.g. TURNER, 2006). This is required to yield valid results with respect to both symmetrical salient deposition (even) and secondary groin effect (odd).

3.2.2.4 Application

A strength of the shoreline dataset is that the first two available contours i.e. August 2004 and November 2005, provide a shoreline change function representative of the pre-construction shoreline behaviour. Reef construction began towards the end of 2005 and 10% of the reef was actually completed during the survey in November 2005 but we can still reasonably assume minimal interaction with the beach system. Therefore, to serve as a basis for further

interpretation, we can apply the analysis to a pre-construction interval to identify any pre-existing alongshore gradient in shoreline change at the site. This is valuable as such signals may be hard to discriminate from structure effects if only a pair of pre/post construction shoreline is available (WALTON, 2002). The next logical interval to study is the period from November 2005, virtually pre-construction, to March 2009, post-construction (the reef was completed in June 2008). Salient formation and any secondary groin effect can thus be investigated on the longest term possible given the available data. This is supplemented by analysis of shoreline changes during successive intervals within the entire period to investigate the adjustment sequence.

3.3 RESULTS

3.3.1 PRE-CONSTRUCTION INTERVAL

The decomposition of the shoreline change function between August 2004 and November 2005 is given in Figure 3.4. The even function is predominantly positive indicating net accretion over the period. It is characterized by two more prominent depositional features (symmetric) located at about ± 400 m with a magnitude of about + 25 m. The central part of the function consists of two secondary symmetric peaks (+10 m) at about ± 200 m, separated by a zone of shoreline retreat (-5 m).

The offset in accretion in the central 400 m may be related to a modulation of the incident wave energy. SPIERS (2005) and SCARFE *et al.* (2009) identified distinct bands of wave focusing offshore of the site that can vary in location depending on wave direction. The localized zones of enhanced wave energy (e.g. wider surfzone as observed by SCARFE and HEALY, 2005) could have effects on the pre-construction shoreline adjustment.

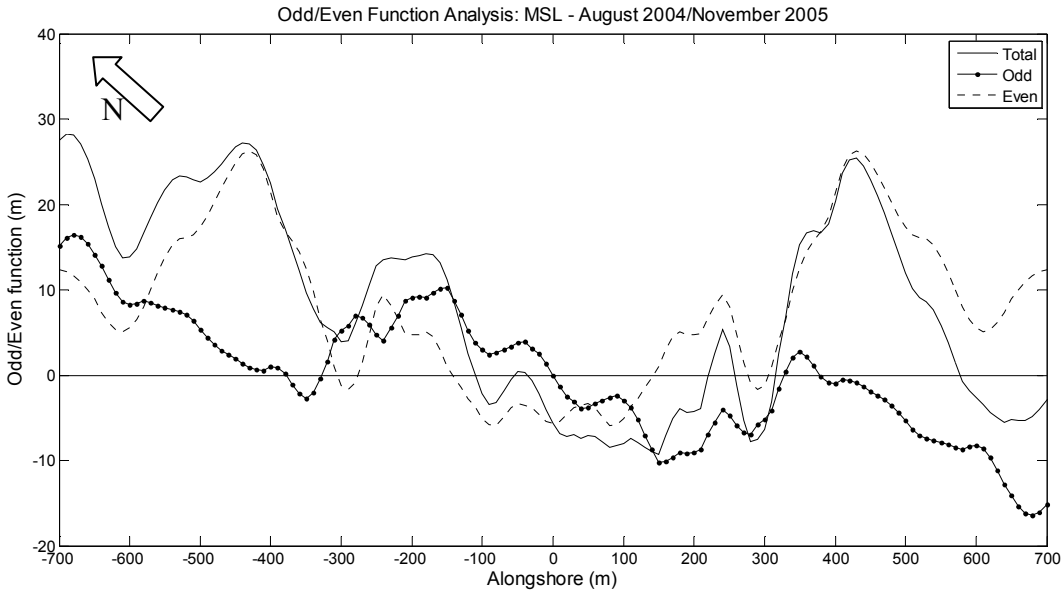

Figure 3.4 Odd-even function analysis results for the shoreline change function computed from the August 2004 and November 2005 shorelines i.e. pre construction. The total function is the sum of the odd (dotted) and even (dashed) components. The alongshore origin (x=0 m) corresponds to the reef centreline. Note the negative gradient in shoreline advance towards the southeast described by the odd function.

Focusing on asymmetrical shoreline adjustments (Figure 3.4), we can see that the odd function, although undulating, tends to indicate a negative gradient in shoreline advance as we go towards the southeast. Overall, this involves about 15 m of accretion to the northwest of the zone progressively switching to erosion of similar magnitude to the southeast. The alongshore gradient is consistent with the earlier observation of overall decrease in beach width towards the southeast (SCARFE, 2008). As a pre-existing characteristic of the system, it may potentially be present in the next applications, interwoven with structure effects. The observed gradient may arise from a sheltering effect of offshore islands (see SCARFE *et al.*, 2009 for modelling). Another likely cause is the proximity of dredge disposal site directly to the north of the study site (see Figure 1.3). The gradient may then be due or enhanced by onshore migration of this additional sediment (e.g. SPIERS and HEALY, 2007).

The total function mostly follows even component oscillations with net changes up to 25-30 m. These magnitudes of changes, along with shorelines generally oscillating within 50-60 m in the cross-shore direction (Figure 3.2), give an order of shoreline position fluctuations expected at the site.

3.3.2 PRE / POST CONSTRUCTION INTERVAL

Shoreline change from November 2005 to March 2009 allows investigating structural effects during the longest time frame allowed by the dataset. Given that the major phase of the reef construction was completed at the January 2007 survey (alongshore width of 80 m, see SCARFE, 2008), we can assume that for the last survey in March 2009 the beach has had more than 2 years to adjust to the structure. The salient was expected to form within a year (MEAD and BLACK, 1998) so this time interval is reasonable to identify the adjusted state.

Figure 3.5 presents results of the odd-even function analysis for the interval considered. The even component of shoreline change indicates a positive mean shoreline advance of about 10 m, likely associated with a natural fluctuation (e.g. Figure 3.3 a). The function is however found to significantly oscillate around this mean trend with rhythmic features spacing at 100-300 m. Features observed here appear to be more regular and closer together than they were for the pre-construction interval and this distinctive crenulated character was not as obvious in the pre-construction even function. Although undulations developed all along the study site, thus limiting direct discrimination of a structural effect, the more crenulated aspect of the even component still suggests a modification of the shoreline response which it is tempting to attribute to the structure since it coincides with its implementation. In the vicinity of the structure, two more prominent depositional features (+ 20 m) are found on both sides of the reef at approximately ± 200 m. These 2 features are separated by a low in the central 50-100 m in the immediate lee of the reef with virtually no beach width change. Here, the signal contrasts with a classic salient growth as a symmetric and localized shoreline advance (Figure 3.3 c). This consequently limits the relevance of a readjustment of shoreline data relative to salient position as in TURNER (2006). That being, the central pattern still tends to stand out from the function shape and would indicate a structural effect.

Any secondary groin effect can be investigated in the corresponding odd function (Figure 3.5). A first observation that can be made is that the negative gradient identified in the precedent interval is absent. In fact, although oscillating, the function mean trend has straightened up and thus not reproduces any distinct gradient in the alongshore direction. As mentioned previously, an implicit assumption to observe again the gradient initially identified in Figure 3.4 is a

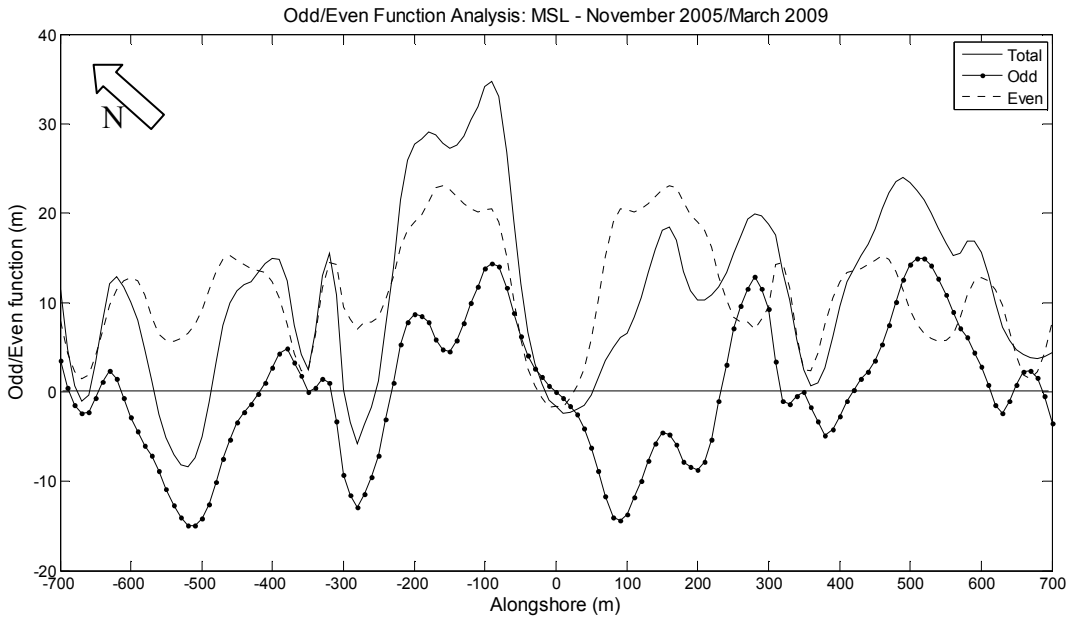

Figure 3.5. Odd-even function analysis results for the shoreline change function computed from the November 2005 (pre construction) and March 2009 (post construction) shorelines. The total function is the sum of the odd (dotted) and even (dashed) components. The alongshore origin (x=0 m) corresponds to the reef centreline. The even component is crenulated with two more prominent features in the central 400 m. They coincide with a local groin effect in the lee of the reef (odd function between ± 200 m). This explains the depositional feature to the northwest of the reef.

condition of stationary wave climate and sediment supply over the period (WALTON, 2002). The net drift through the Bay of Plenty of Plenty has consistently been found towards the southeast (HEALY, 1980; MEAD and BLACK, 1998; SPIERS, 2005). However, frequent reversals are expected in response to reigning climatic system or individual high energy events (MEAD and BLACK, 1998; SCARFE, 2008). As a result, the net movement may be small relative to gross movement along the site. Such reversals limit the validity of the stationary hypothesis and are likely to impact gradients in alongshore shoreline change. Besides, sediment supply has artificially been modified through dredging and disposals near the site. As a result, it can hardly be resolved whether the absence is induced by the structure or rather related to natural causes (e.g. better balance in gross sediment transport with less net effects, lessened supply, or ENSO effect).

Between ± 200 m alongshore, an interesting feature is the sharp gradient in shoreline position change that occurs around the reef centreline. This results in accretion of ~10 m to the north side matched by similar erosion to the south side (Figure 3.5). The odd function describes undulations at some distance of the reef,

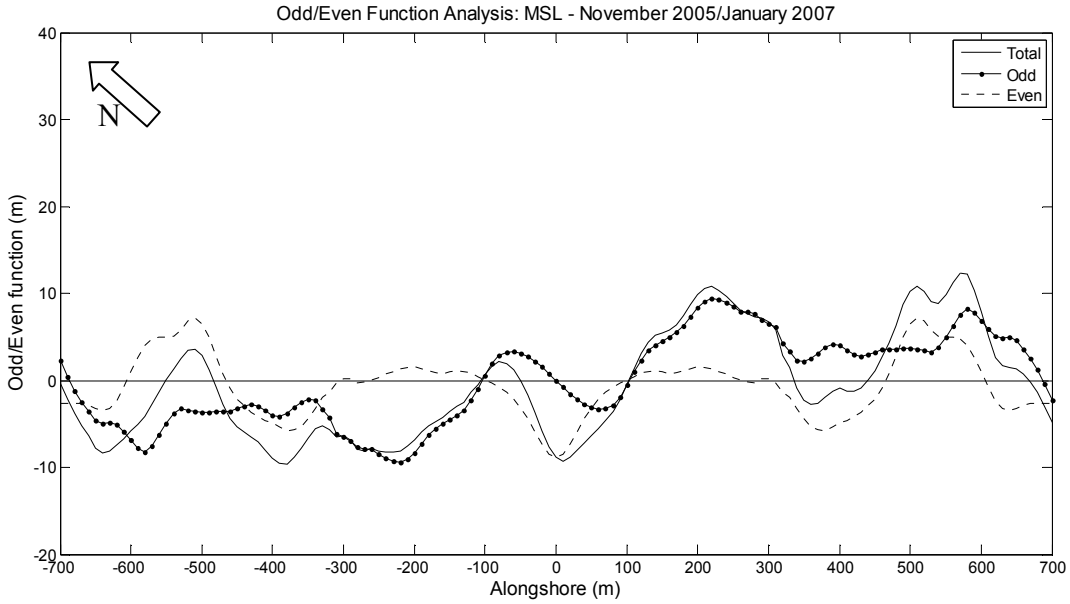

Figure 3.6. Odd-even function analysis results for the shoreline change function computed from the November 2005 and January 2007 shorelines. The total function is the sum of the odd (dotted) and even (dashed) components. The alongshore origin (x=0 m) corresponds to the reef centreline. Total, even, and odd functions have mean trends close to zero indicating very limited net changes over the period. Their relatively linear shapes indicate no significant structural effect.

however, it is stressed that no such magnitude of erosion/accretion is found further alongshore, indicating that the structure does have a role on the observed changes, even if limited. Since the net drift direction is to the southeast, the signal i.e. updrift accretion and downdrift erosion is consistent with a local groin effect.

The groin pattern coincides with the two depositional features in the lee of the reef (even function). The combined effects are shown in the total function and result in the greater growth of the depositional feature to the northwest of the reef, benefiting from additional accretion, while the symmetric feature to the southeast is offset due to the matching erosion. This yields an advance of the MSL contour of up to 35 m to the north west of the structure (total function in Figure 3.5).

The 2-feature pattern and groin effect that induce greater accretion to the north of the reef are not considered to be a coincidence. As additional shoreline contours are available within the period (see Table 3.1), it is interesting to consider shoreline adjustments over different intervals to further validate and/or refine the identified pattern.

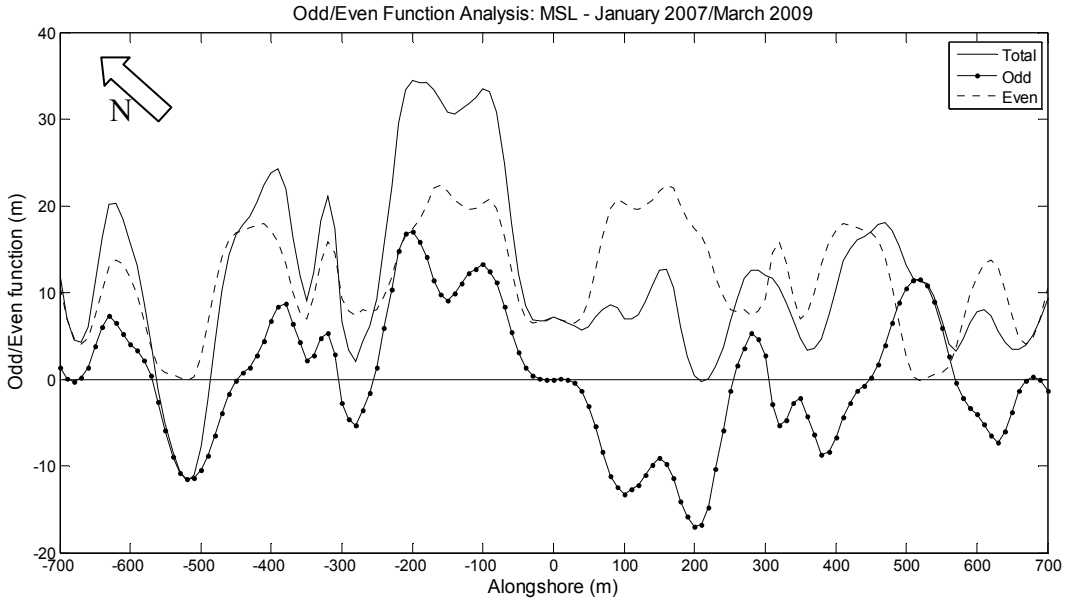

Figure 3.7. Odd-even function analysis results for the shoreline change function focusing on the post-construction interval i.e. from January 2007 to March 2009, when 70% to 100% of the structure was in place. The total function is the sum of the odd (dotted) and even (dashed) components. The alongshore origin (x=0 m) corresponds to the reef centreline. The central pattern is fully consistent with Figure 3.5 and the magnitude of changes indicates that most of the net shoreline adjustments have occurred during this interval.

Analysis of successive shorelines indicated that the central pattern observed in Figure 3.5 was not the result of a progressive adjustment through the entire pre/post construction interval. The shoreline position appears to be primarily governed by natural fluctuations for the period from November 2005 to January 2007. Shoreline contours for these dates are relatively linear and indicate beach widths of same order (see also the August 2006 shoreline within the interval) (Figure 3.2). Odd-even analysis yields very limited net changes over the period (Figure 3.6). All three functions, even, odd and total have mean trends close to zero and are relatively linear indicating no significant structural impact over the period. Note that there is no distinct alongshore gradient in change from the northwest to the southeast in the odd component as initially identified in the pre-construction interval (Figure 3.4), with even a small inverted signal (see odd function in Figure 3.6). This limits the relevance of a steady underlying gradient in shoreline change consistently interwoven with structural effects. It is more likely related to antecedent wave conditions and/or recent disposals before the study period (see SPIERS and HEALY, 2007) and will vary through the different time intervals considered. That being, it still appears to have long-term effects given the general decrease in beach width towards the southeast (see Figure 3.2).

On January 2007, the beach was in an eroded state with a linear shoreline and reduced beach width. In contrast, the last survey in March 2009 imaged a well accreted and wide beach (see Figure 3.2). Analysis of shoreline change between these two different beach states (Figure 3.7) yields odd and even functions fully consistent with Figure 3.5. Magnitudes of beach width changes indicate that most of the net accretion observed during the entire interval has occurred during this 2 year period from January 2007 to March 2009. Removing the mean "natural" advance of ~10 m from the even component, the 2 more prominent symmetric features provide additional 10 m of shoreline advance around the reef. The local groin effect superimposes and gives rise to the distinct depositional feature to the northwest of the reef, with a net additional advance estimated at ~20 m, extending ~150 m alongshore. As this happened while the structure footprint on the system was larger (70 to 100 % completion, see Table 3.1), this increases our confidence in relating the pattern to the structure.

In contrast, the linear eroded shoreline of January 2007 still suggests that the depositional features may be more prominent for accreted beach states and subsequently eroded under high wave energy conditions. This transient response may explain the relative absence of any significant shoreline adjustments over the first part of the interval (November 2005 to January 2007) that could have been masked by larger scale ambient morphology.

3.4 DISCUSSION

Although complexity of the natural shoreline has to be kept in mind, the structure impact appears to be twofold: (1) a more crenulated response associated with 2 more prominent features around the structure centreline, and (2) development of a localized groin effect.

With respect to the first impact, SCARFE (2008) already identified more prominent undulations in post-construction shorelines that were found to be linked to rhythmic bar and rip features. This evolution may be the expression in the morphology of a more cellular surfzone circulation induced by the structure (SHORT, 1999). By triggering wave breaking, the reef induces a local gradient in wave height driving strong flows over the structure (e.g. RANASINGHE *et al.*, 2006). This likely stimulates the development of circulation cells that may then be

expressed in the beach morphology into stronger rips, crescentic features, or development of crenulated shoreline (SHORT, 1999).

Furthermore, morphological modelling of the reef system at Mount Maunganui showed that the structure would drive bar formation in its vicinity much faster that on other parts of the beach (BLACK and MEAD, 2007). Two main bar features would grow along the side of the reef and migrate inshore to eventually merge with the shoreline. This is coherent with the 2 larger depositional features identified in the lee of the reef (Figures 3.5 and 3.7), possibly indicating a signature of such mechanism. That being, as the rhythmic character is consistently present in the full extents of even functions we can still expect that the proposed mechanism either has some effects at some distance from the structure, or is a localized expression of a larger scale modification of the surfzone such as more cellular circulation (SHORT, 1999; SCARFE, 2008) or development of wave interference patterns (TURNER *et al.*, 2001).

The second identified reef impact is a shoreline change signal that indicates a local groin effect. The question that arises is how the structure develops this effect on the shoreline. A first possible explanation is that the structure acts as a physical barrier to the overall motion of sediment, able to trap sediment updrift. Such effect was observed on the offshore bar (SCARFE, 2008) and although obviously expected to be greater in the direct vicinity of the reef, the process might be relevant at some distance from the structure. Secondly, the groin effect may be due to the structure-induced circulation. The strong onshore flows over the structure interact with long-shore currents to weaken currents updrift and enhance them downdrift (e.g. RANASINGHE and SATO, 2001; TURNER *et al*., 2001; RANASINGHE and TURNER, 2006). This may create a local gradient in long-shore transport rate and subsequent deposition/erosion that would be consistent with the groin signal. Finally, the pattern may be a secondary effect of the depositional features identified, acting as submerged groins.

The combination of these two effects gives rise to a distinct depositional feature to the north of the reef and thus on the updrift side of the structure (Figure 3.5 and 3.7). Although on a smaller scale and likely masked by natural variability “noise”, the pattern could then resemble an episode of proto-salient formation as observed on physical modelling of the Narrowneck site (TURNER e*t al.*, 2001) and subsequently identified during the first year of shoreline response monitoring

(TURNER, 2006). This was expected to be a temporary phase with subsequent merging of features into an equilibrium salient, offset downdrift relative to the structure centreline. With respect to our case, this may suggest a shoreline still adjusting. However, given the significant time period allowed, the identified pattern is more likely representative of the adjusted state. This would then indicate a more complex and transient character of shoreline response at the study site of Mount Maunganui.

On one hand, future shoreline surveys over the next years would be of interest to further monitor shoreline adjustment. On the other hand, more accurate understanding of the shoreline response would likely benefit from observations of the system at a higher temporal resolution, as for example through individual high energy events and recovery periods.

The existing datasets not only provide shoreline data but also image the beach foreshore and surfzone morphology evolution over the study period. As a result, the next step is to follow concurrent 3D beach morphology adjustments. 3D erosion-accretion analysis would be of particular interest to investigate expression of the pattern identified here on the full scale beach morphology. Also, odd-even analysis could be undertaken on the contour immediately offshore of the reef to help understand the groin effect identified by SCARFE (2008) on the offshore bar and seen here in the shoreline analysis.

3.5 CONCLUSIONS

Shoreline response to the multi-purpose reef constructed at Mount Maunganui has been tested using an odd-even function analysis. The shoreline dataset includes a pair of contours representative of the pre-construction behaviour along with several post-construction shorelines. This allowed application of the method to investigate the pre-existing variability of the system. Results for the pre-construction interval indicated a complex pre-existing shoreline with possible fluctuations of 20-30 m, including an underlying alongshore gradient in shoreline change from the northwest to the southeast. The gradient was not stationary in time and likely related to antecedent wave conditions and/or sediment disposals but it still appeared to have residual effects on the beach width.

Analysis of pre / post construction shoreline changes depicted a more crenulated character of shoreline adjustment with the growth of two prominent features in the lee of the structure (even component), along with the development of a localized groin effect (odd component).

Successive shoreline changes within the monitoring period indicated that the most obvious net adjustments occurred while the structure was in place, and thus provided a favourable argument to relate the pattern to the structure. However, the shoreline feature(s) are superimposed on large scale natural fluctuations, and may then be more prominent on accreted beach states and reset during eroding conditions. This transient response contrasts with equilibrium salient formation but the identified pattern still provided a net additional beach width of ~ 20 m, along ~ 150 m of shoreline (MSL) to the northwest of the reef (updrift).

3.6 REFERENCES

BLACK, K.P. and MEAD, S.T., 2007. Sand Bank Responses to a Multi-Purpose Reef on an Exposed Sandy Coast. *In*: WALTHER, M. (ed.), Shore protection and surfing dedicated issue: *Shore and Beach*, 75(4), 55-66.

DEAN, R.G., 2002. *Beach Nourishment: Theory and Practice*. Advanced Series on Ocean Engineering, Volume 18, World Scientific Publishing, Singapore, 397 p.

DEAN, R.G., and WORK, P.A., 1993. Interaction of navigational entrances with adjacent shorelines. *Journal of Coastal Research,* 18, 91–110.

HEALY, T.R., 1980. Erosion and Sediment Drift on the Bay of Plenty coast. *Soil and Water*, August, pp. 12-14.

RANASINGHE, R., and TURNER, I.L., 2006. Shoreline Response to Submerged Structures: A Review. *Coastal Engineering*, 53, 65-79.

RANASINGHE, R., TURNER, I.L., and SYMONDS, G., 2006. Shoreline Response to Multi-Functional Artificial Surfing Reefs: A Numerical and Physical Modeling Study. *Coastal Engineering*, 53, 589-611.

RANASINGHE, R., and SATO, S., 2007. Beach morphology behind single impermeable submerged breakwaters under obliquely incident waves. *Coastal Engineering Journal*, 49 (1), 1-24.

ROSATI, J. D., and EBBERSOLE, B. A., 1998. Littoral impact of Ocean City Inlet, Maryland, USA, *Proceedings of the 25th International. Conference. on Coastal Engineering*, (New York, NY, ASCE), pp. 2779–2792.

ROSATI, J. D., and KRAUS, N. C., 1997. Even–odd analysis of shoreline position and volume change, *Coastal Engineering Technical Note IV-10*, Coastal and Hydraulics Laboratory, United States Army Corps of Engineers Waterways Experiment Station, Vicksburg, Mississipi, 8 p.

SCARFE, B.E., and HEALY, T.R., 2005. Baseline Bathymetric Data Collection for Monitoring of Bar, Rip and Salient Response to an Artificial Surfing Reef - Mount Maunganui, New Zealand. *In*: TOWNSEND, M. and WALKER, D. (eds.), *Proceedings for the 2005 Coasts and Ports Australasian Conference* (Adelaide, South Australia), pp. 459-464.

SCARFE, B.E., 2008. Oceanographic Considerations for the Management and Protection of Surfing Breaks. Hamilton, New Zealand: The University of Waikato, Ph.D. thesis, 307 p. + appendices.

SCARFE, B.E., HEALY, T.R., RENNIE, H.G., and MEAD, S.T., 2009. Sustainable Management of Surfing Breaks: Case Studies and Recommendations. *Journal of Coastal Research*, 25(3), 684-703.

SHORT, A.D., 1999. Beach Modification: Natural impacts and beach Morphodynamics. *In*: SHORT, A.D. (ed.), *Handbook of Beach and Shoreface Morphodynamics*. West Sussex, England: John Wiley & Sons Ltd, pp. 253-270.

SPIERS, K.C., 2005. Continued Beach Renourishment from Dredge Spoil Disposal. Hamilton, New Zealand: University of Waikato, Master thesis, 241 p. + appendices.

SPIERS, K.C., and HEALY, T.R., 2007. Beach Renourishment through Spoil Disposal Downdrift of a Dredged Entrance Channel. *In*: KRAUS, N.C. and ROSATI, J, D. (eds.) *Coastal Sediments '07,* pp. 2358-2371.

TURNER, I., LEYDEN, V., COX, R., JACKSON, A., and MCGRATH, J., 2001. Physical Model Study of the Gold Coast Artificial Reef. *In:* BLACK, K.P. (ed.), Natural and Artificial Reefs for Surfing and Coastal Protection. *Journal of Coastal Research, Special Issue No. 29*, 131-146.

TURNER, I.L., 2006. Discriminating Modes of Shoreline Response. *Journal of Waterway, Port, Coastal and Ocean Engineering*, 132(3), 180-191.

WALTON, T.L., 2002. Even-odd analysis on a complex shoreline. *Ocean Engineering*, 29, 711–719.

CHAPTER 4. BEACH MORPHODYNAMIC RESPONSE TO AN OFFSHORE SUBMERGED MULTI-PURPOSE REEF AT MOUNT MAUNGANUI, NEW ZEALAND

4.1. INTRODUCTION

Monitoring of the beach morphodynamic response to the multi-purpose reef constructed near Tay Street at Mount Maunganui was undertaken by SCARFE (2008) using repetitive mapping of the beach foreshore and nearshore bathymetry prior to (see SCARFE and HEALY, 2005), and throughout reef construction until ~70% completion (January 2007). As a part of this present research, a new survey was undertaken in March 2009, after reef completion in June 2008.

This chapter presents analysis of the new and existing survey datasets to carry on the monitoring of the beach response post-construction and supplement the shoreline analysis (Chapter 3) with the description of the concurrent 3D beach morphology adjustments. The groin effect of the reef on the offshore morphology identified in SCARFE (2008) is investigated using an odd-even function analysis of position change of a bathymetric contour just seaward of the reef (-5.0 m, MSL). Observed post-construction beach response is finally compared to predictions obtained using available design relationships.

4.2. METHODS

The data analyzed in the chapter consists in 4 complete bathymetric survey of the study site (Figure 1.4) collected within the period from August 2004 to March 2009 (see Table 4.1). The reader is directed towards SCARFE (2008) for a full outline of the survey procedure combining multibeam echosoundings (MBES) and RTK GPS to map the nearshore bathymetry and beach foreshore. The survey data collected was processed into bathymetric charts relative to Motukiri Vertical Datum 1953 (approximately mean sea level) using ArcGIS, with general resolution of 1 m and up to 0.25 m in the close vicinity of the reef.

Table 4.1. Dates and stages of reef completion of analyzed surveys.

Survey date	Reef completion
19/08/2004	0%
17/11/2005	10%
23/01/2007	70%
14/03/2009	100%

The time intervals considered are the same as in Chapter 3, namely (i) pre-construction: August 2004 to November 2005, and (ii) pre / post construction: November 2005 to March 2009. The January 2007 survey within the pre/post construction period allows analysis of successive adjustments from November 2005 to January 2007, and from January 2007 to March 2009.

Beach bathymetric charts with concurrent erosion/accretion maps are presented to show patterns and magnitudes of morphological changes throughout the study site. An odd-even function analysis of the -5.0 m contour (located just offshore of the reef) is used to detect effect of the reef on the offshore morphology. Contours were extracted and processed as mean sea level contours used for shoreline analysis (Chapter 3). Application procedure and general interpretation of the odd-even function analysis are outlined in Chapter 3.

Hindcast wave data offshore of the site (GORMAN, 2005) provided the wave conditions over the study period. Offshore wave data (~ 20 m depth) was transformed in breaker conditions using methods of NIELSEN (1982) (Figure 4.2). To supplement the obtained wave data, a predictive model of beach state (WRIGHT and SHORT, 1985) was used to provide a proxy on wave / morphology conditions preceding the surveys. The model is further outlined in paragraph 4.3.1.

In the last part of the chapter, several structural and environmental parameters of the prototype reef are defined for use in predictive relationships of shoreline response to natural submerged reefs (BLACK and ANDREWS, 2001) and multi-purpose reefs (RANASINGHE *et al.*, 2006). Predicted and observed responses are compared.

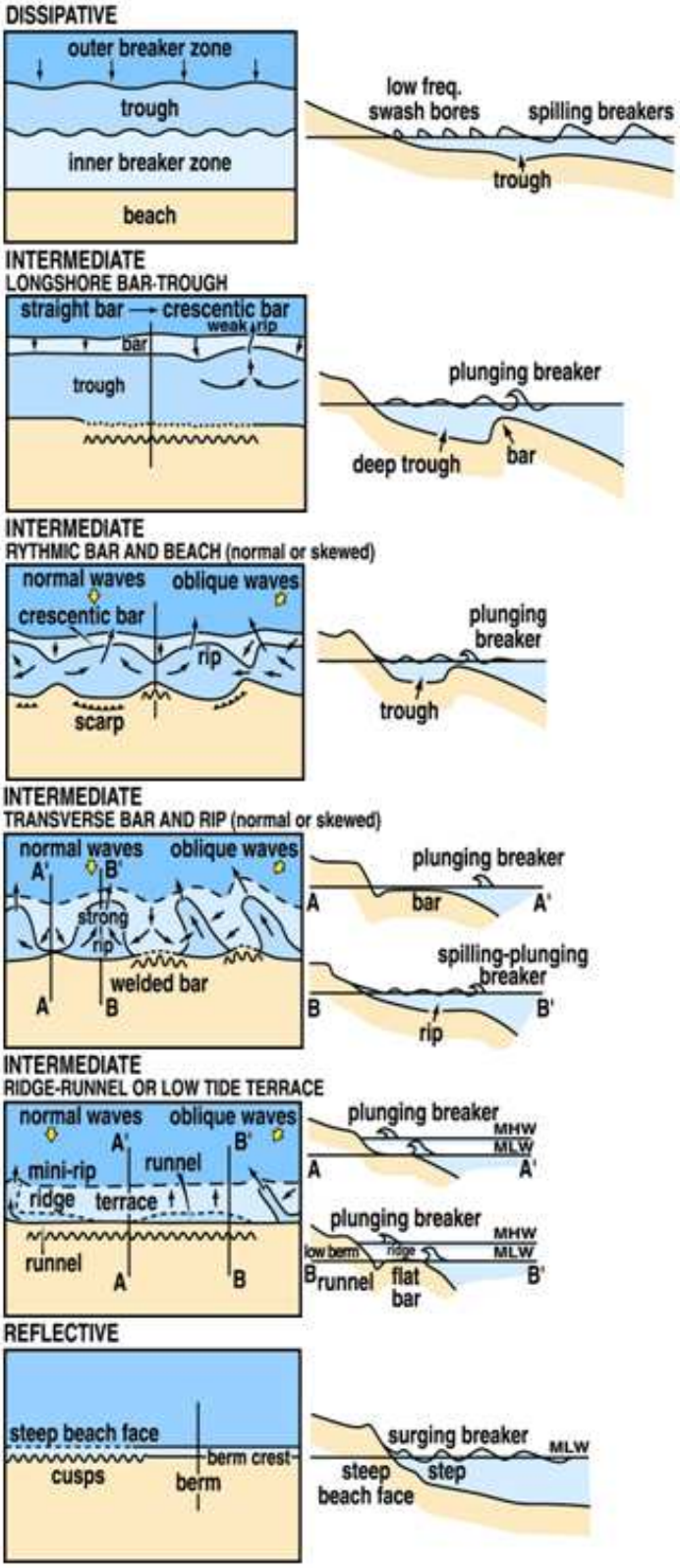

Figure 4.1. WRIGHT and SHORT's (1984) beach state classification.

4.3. RESULTS

4.3.1. BEACH STATE AND WAVE CONDITIONS

The Mount Maunganui beaches, including near Tay Street, are part of the long wave exposed sandy Bay of Plenty coastline (see Figure 1.2). Sediment at the site was found to be mostly of fine to medium sands (0.16-0.29 mm) (PICKETT, 2004; SPIERS, 2005). The north of the site was subject to recent dredge disposals in 2004 (see disposal grounds on Figure 1.4) but with grain sizes very similar to the native (SPIERS, 2005). Local wave climate consists predominantly of locally generated small waves but with the possibility of more energetic storm/swell events due to subtropical disturbances (PICKRILL and MITCHELL, 1979). This is visible in Figure 4.2 with a mean breaking height of about 1.4 m with peaks, generally brief, up to 4-5 meters.

Fine to medium sand combined with moderate wave climate generally predict a beach system oscillating between intermediate states, with well developed bar/trough and rhythmic features (WRIGHT and SHORT, 1984). WRIGHT and SHORT (1984) provide a classification of beach states that will be used through the chapter to describe the beach morphology (Figure 4.1). The beach state is related to the dimensionless fall velocity Ω (or Dean's parameter) combining wave height, period, and sediment fall velocity.

$$\Omega = H_b/(w_s T_p) \quad (4.1)$$

where H_b is the breaker height (m), w_s the fall velocity of beach sand (m/s), and T_p peak period (s).

The values of Ω indicate development of dissipative (Ω >6), intermediate (1< Ω <6), or reflective (Ω <1) beach morphology (WRIGHT and SHORT, 1985). However, the instantaneous value of the parameter supposedly predicts the equilibrium state that would develop if the instantaneous wave conditions were steady for a "sufficient" time, depending on the pre-existing beach state. This means that observations of a beach under similar instantaneous conditions may actually yield a range of different morphologies. To address this issue, WRIGHT and SHORT (1985) proposed a predictive model based on a weighted mean value

$\overline{\overline{\Omega}}$ of the parameter, accounting for antecedent values of the parameters Ω (i.e. antecedent wave forcing/beach state). The model reads:

$$\overline{\overline{\Omega}} = \left[\sum_{i=1}^{D} 10^{-i/\phi}\right] \sum_{i=1}^{D} (\Omega_i \, 10^{-i/\phi}) \qquad (4.2)$$

where i=1 on the day before observation, and i=D on D days prior observation; Ω_i indicates the parameter value at day i. The parameterϕ, in days, is a weighting factor describing the "memory" of the beach system. This weighting factor decreases to 10% at ϕ days prior present day.

The model was applied to transformed hindcast data (breaker height and peak period in Figure 4.2) at the study beach. The fall velocity (w_s) used was 0.038 m/s as found in PICKETT (2004). D=30 days and ϕ=5 days provided the best fit in WRIGHT and SHORT (1985) and have been used for the present application. The model predicts a beach system predominantly oscillating within the intermediate category still with frequent peaks at more dissipative or reflective states (Figure 4.2, bottom). The predicted modal beach state is the rhythmic bar and beach (RBB) assemblage (mean $\overline{\overline{\Omega}}$ = 3.9) occurring 32% of the time; then follows the transverse bar beach (TBR, 27%), long-shore bar and trough (LBT, 16%), dissipative (DIS, 13%) and low tide terrace (LTT, 12%). Shifts towards more dissipative or reflective states (function max/min peaks) require sustained high or low energy conditions, and typically last 10 to 15 days.

It was noted in WRIGHT and SHORT (1985) that the model had its limitations especially to differentiate intermediate states within the intermediate category. Model parameters (D, ϕ) would also require calibration against observed states to provide the best predictions. This likely limits the model ability to accurately predict the instantaneous beach state, but the weighted value of the dimensionless fall velocity $\overline{\overline{\Omega}}$ still provides a proxy to describe the combination of wave height/period and duration over which it is sustained, that will be useful to outline wave and beach morphology conditions preceding the surveys.

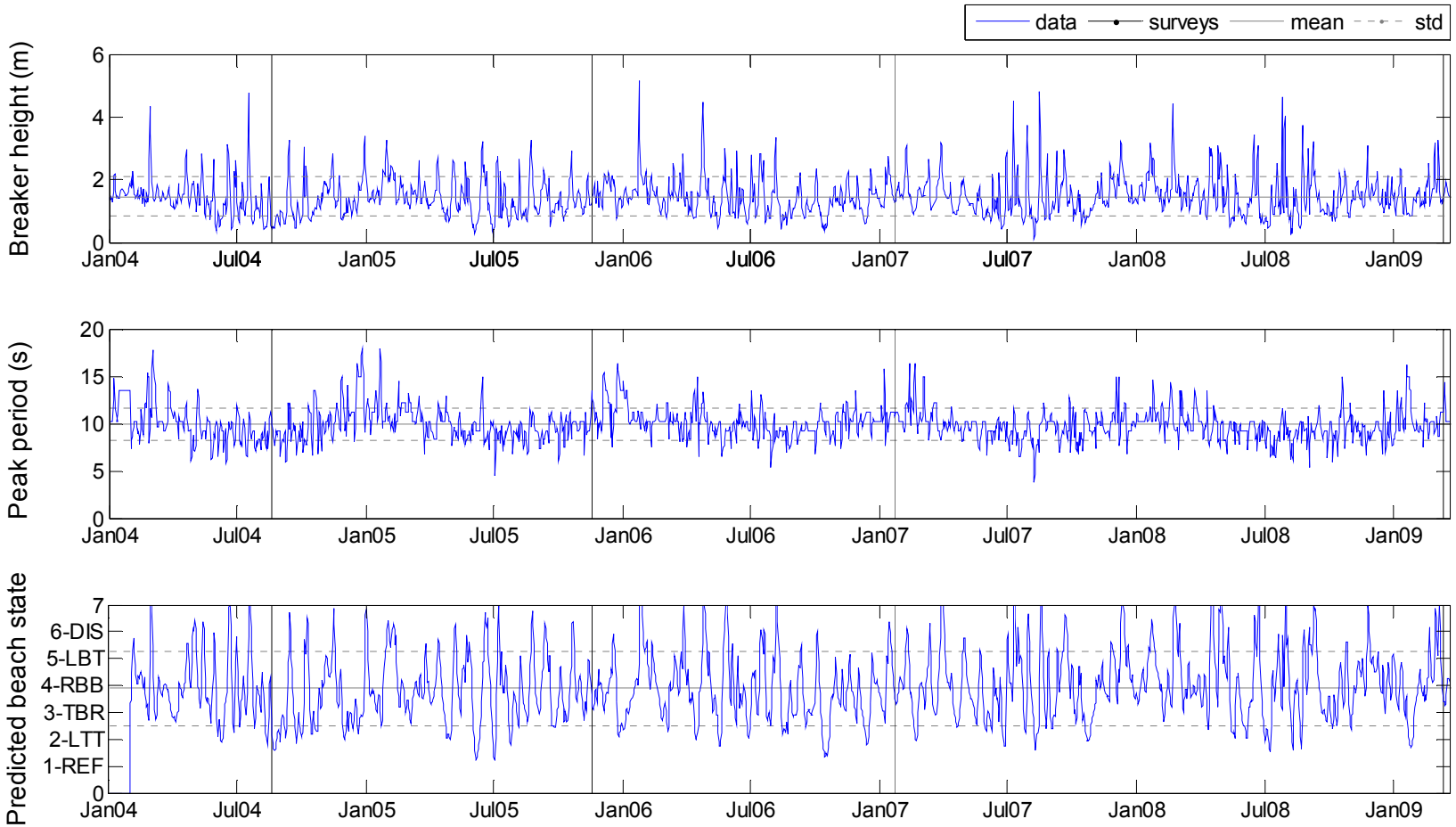

Figure 4.2. Breaking wave height, peak period, and predicted beach state according to the WRIGHT and SHORT (1985) model during the study period. Hindcast wave data offshore of the site (GORMAN, 2005) was transformed in breaking conditions using the methods of NIELSEN (1982). The time series of predicted beach states was computed using Equation 4.2. Survey dates are represented by vertical black lines. Horizontal plain and dashed lines indicate mean value and standard deviations respectively.

4.3.2. PRE-CONSTRUCTION INTERVAL

Figure 4.3 presents the pre-construction beach bathymetries of August 2004 and November 2005 with an erosion/accretion difference map. Several surfzone features are identifiable on the August 2004 survey. To the north of the site a long-shore bar protrudes at about -2 m, and two deeper rip channels (- 4 m) are found landward of the projected reef location. The intertidal area is relatively narrow (~60 m) suggesting an eroded state that could resemble a combination of RBB and LBT (see Figure 4.1). In contrast, the November 2005 survey images a fuller and smoothed state of the beach with more linear contours. There is a relict rip channel to the south of the reef and the first structure material in place induces a very slight perturbation of the -4 m contour (see the zone inside the white triangle, Figure 4.3). The intertidal area is larger with a net advance of the mean sea level (0 m) and -1 m contour of about 20-30 m over the interval (see Figure 3.4 for the odd-even decomposition of the mean sea level position change).

The bathymetric difference map computed from the two surveys (reproduced from SCARFE, 2008) suggests that these morphological changes are mostly governed by the onshore/offshore migration of a long-shore bar, either nourishing or eroding the surfzone and intertidal area. Over the 15 month interval, the surfzone has accreted. The bar feature to the north has migrated inshore merging with the intertidal area, and the rip channels have been filled. The negative alongshore gradient in shoreline advance (north to south) identified in Chapter 3 is visible on the lower part of the map with a decreasing accretion trend towards the south of the study site. The offshore part of the map indicates an alongshore uniform band of accretion (~ + 1 m, relative to chart datum). Odd-even analysis of the -5 m contour position change over the interval indicates that this accretion induced an offshore translation of ~ 15 m (even component) with no pre-existing gradient in change along the study site (i.e. linear odd function) (Figure 4.4).

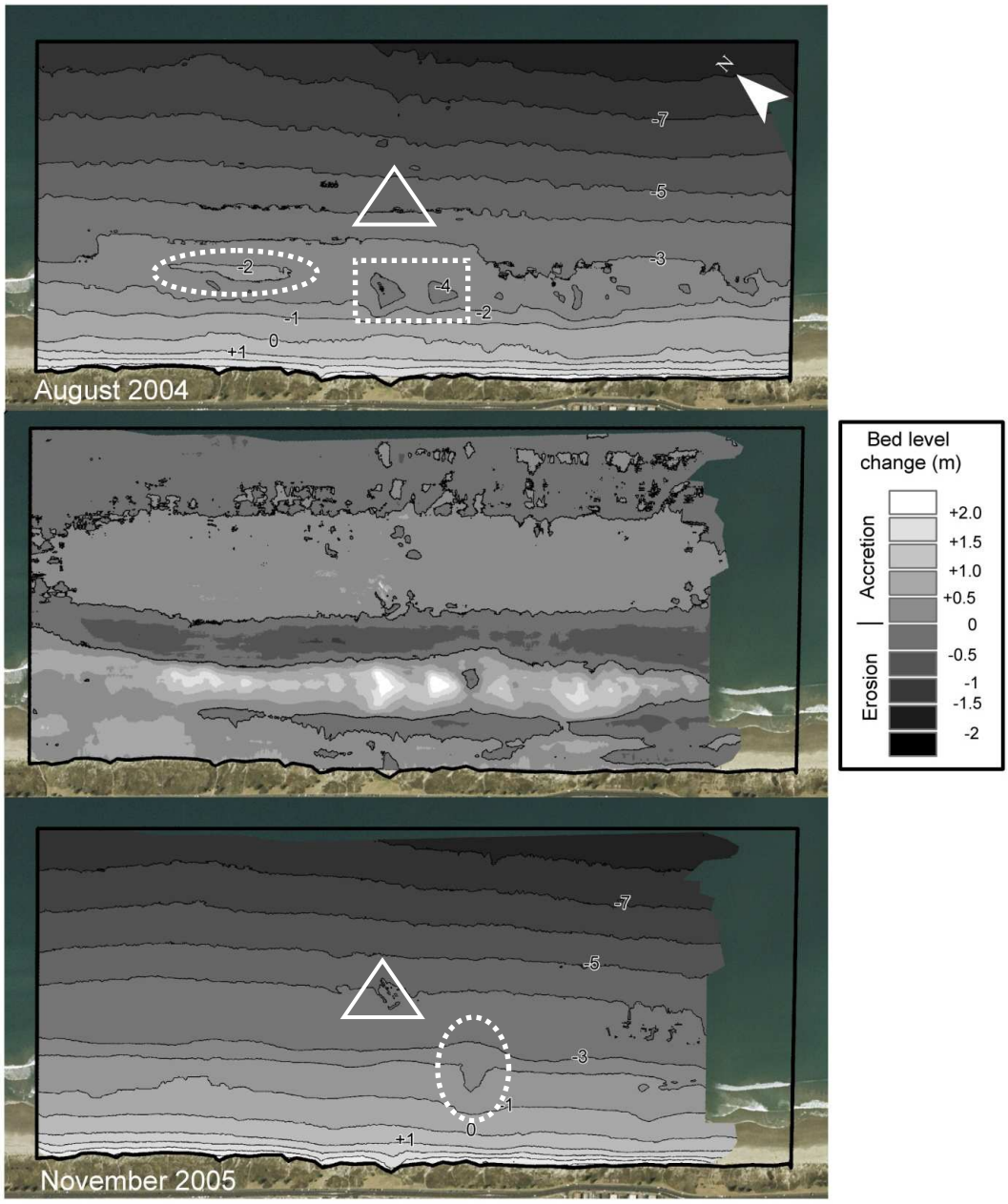

Figure 4.3 Bathymetric surveys of August 2004 (top) and November 2005 (bottom) undertaken by multibeam echo soundings (MBES) and RTK GPS. Chart datum is Moturiki Vertical Datum, 1953 (approximately mean sea level). The white triangle indicates the projected reef location. The middle chart shows the bathymetric difference between the 2 surveys, with magnitudes of erosion/accretion indicated by the colorbar; the black contour is the limit between erosion and accretion. Note the distinct beach bathymetries with several surfzone features in August 2004, reset into a more the linear state in November 2005. Features of interest including a long-shore bar and 2 deep rip channels in the August 2004 survey, and a relict rip channel in the November 2005 survey are represented by the white features (dashed). (Source: SCARFE, 2008, Coastal Marine Group, University of Waikato).

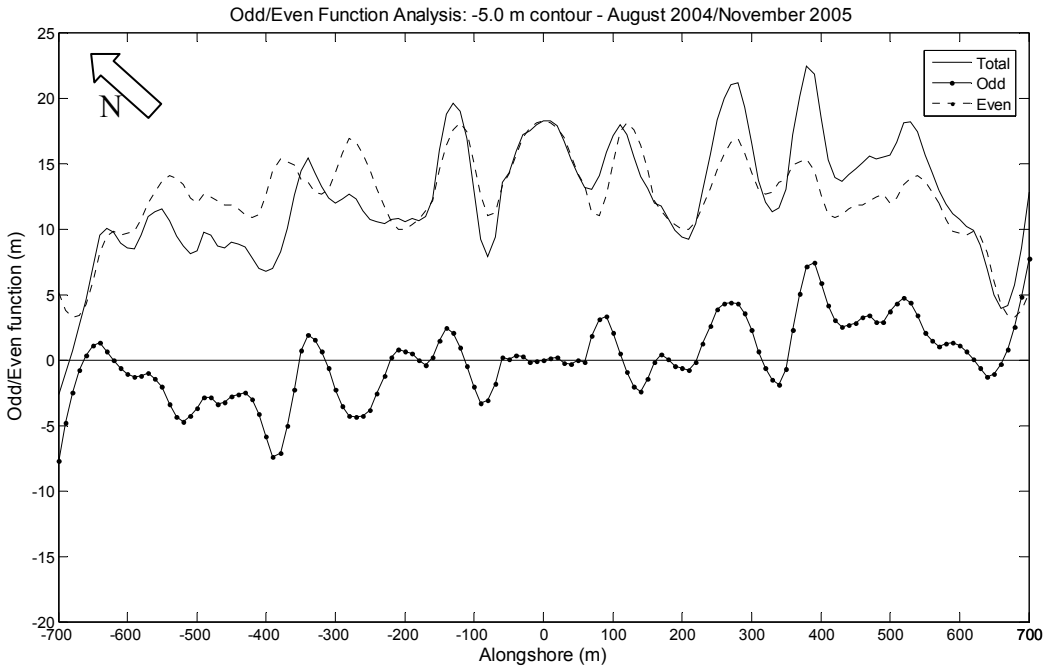

Figure 4.4. Odd-even function analysis of the -5.0 m contour position change over the pre-construction interval (August 2004 to November 2005). The total function is the sum of the odd (dotted) and even (dashed) components. The alongshore origin (x=0 m) corresponds to the reef centreline. All three functions are relatively linear indicating an offshore translation of the contour of about 10-15 m (even function), with no pre-existing alongshore gradient in change (linear odd function).

4.3.3. PRE / POST CONSTRUCTION INTERVAL

Figure 4.5 focuses on the 2 year interval from November 2005 to January 2007 (70% reef completion). In January 2007, the surfzone morphology has developed several distinct bar/rip pairs with wavelength of 100-300 m, extending some 800 m alongshore. The upper foreshore has a steep and reflective slope (0.065 while typically 0.02) all along the study site (note the 0, +1, and +2 m contours very close together). The morphology overall resembles a TBR state (see Figure 4.1). This assemblage is commonly found during an accretionary sequence when the horns of pre-existing crescentic bars weld to the beach (WRIGHT and SHORT 1984). SCARFE (2008) observed the formation of such fragmented features in a precedent survey in August 2006. From the August 2006 survey onwards, the site experienced relatively fair wave conditions with a spaced succession of moderate wave events (Figure 4.2), including clean and moderate swell events some time before the survey (H_b=1-2 m, see SCARFE, 2008, p. 242-243), that are potentially appropriate conditions for the shoreward migration of bar features (e.g. SHORT, 1999, p.196).

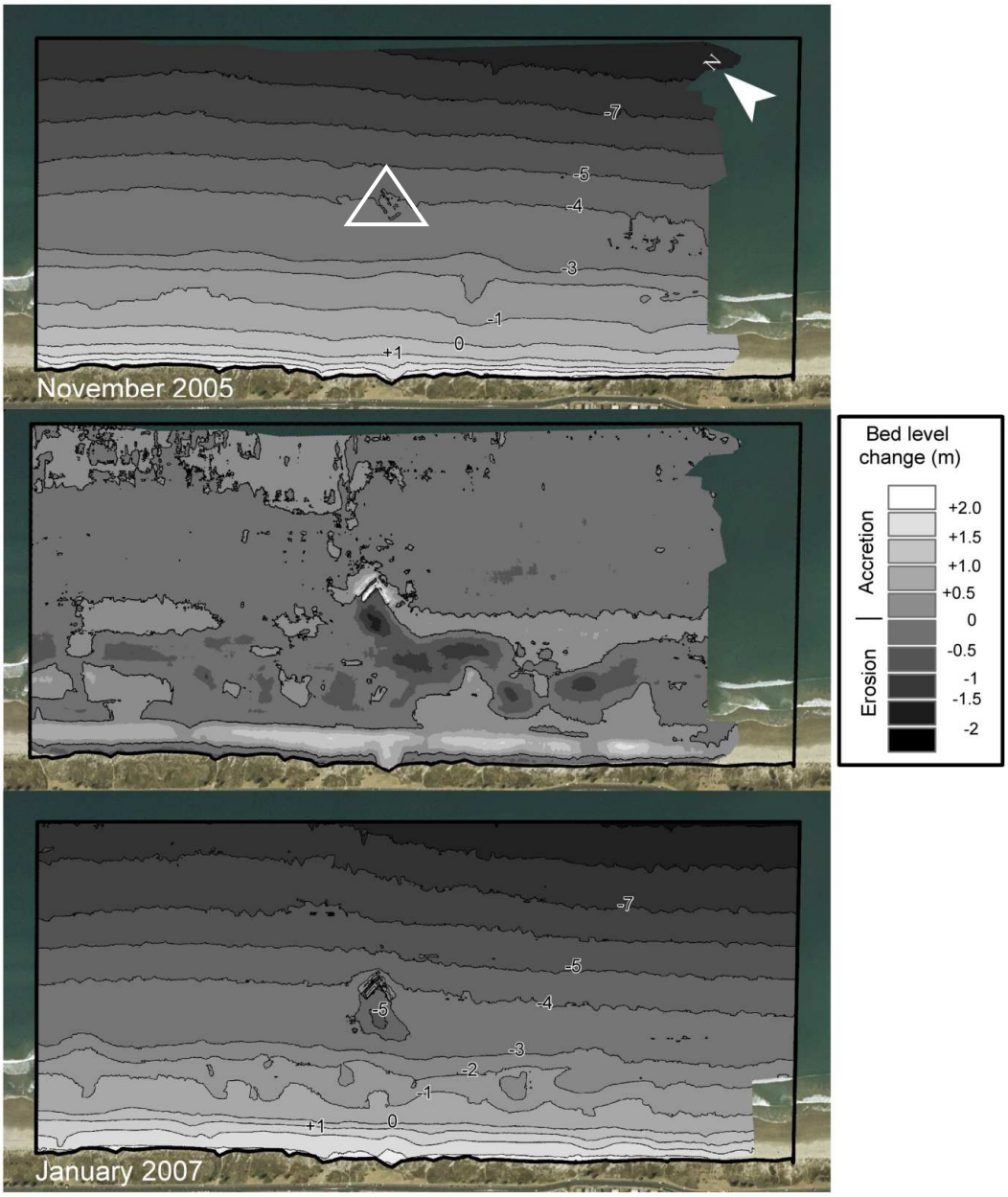

Figure 4.5 Bathymetric surveys of November 2005 (top) and January 2007 (bottom) undertaken by MBES and RTK GPS. Chart datum is Moturiki Vertical Datum, 1953 (approximately mean sea level). The white triangle indicates the projected reef location (top chart). The middle chart shows the bathymetric difference between the 2 surveys, with magnitudes of erosion/accretion indicated by the colorbar; the black contour is the limit between erosion and accretion. The morphology in January 20007 has developed a rhythmic morphology with several bar/rip pairs with wavelengths of 100-300m. A similar morphology is observable in antecedent satellite imagery (Figure 4.7). The erosion/accretion map suggests a perturbation of the onshore/offshore migration of sediment in the vicinity of the reef with rhythmic patterns due to bar/rip morphology development. Note also the difference of accretion pattern around and seaward of the reef updrift/downdrift (northwest/southeast). A large scour feature developed onshore of the reef (~7000 m², middle and bottom charts). (Source: SCARFE, 2008, Coastal Marine Group, University of Waikato).

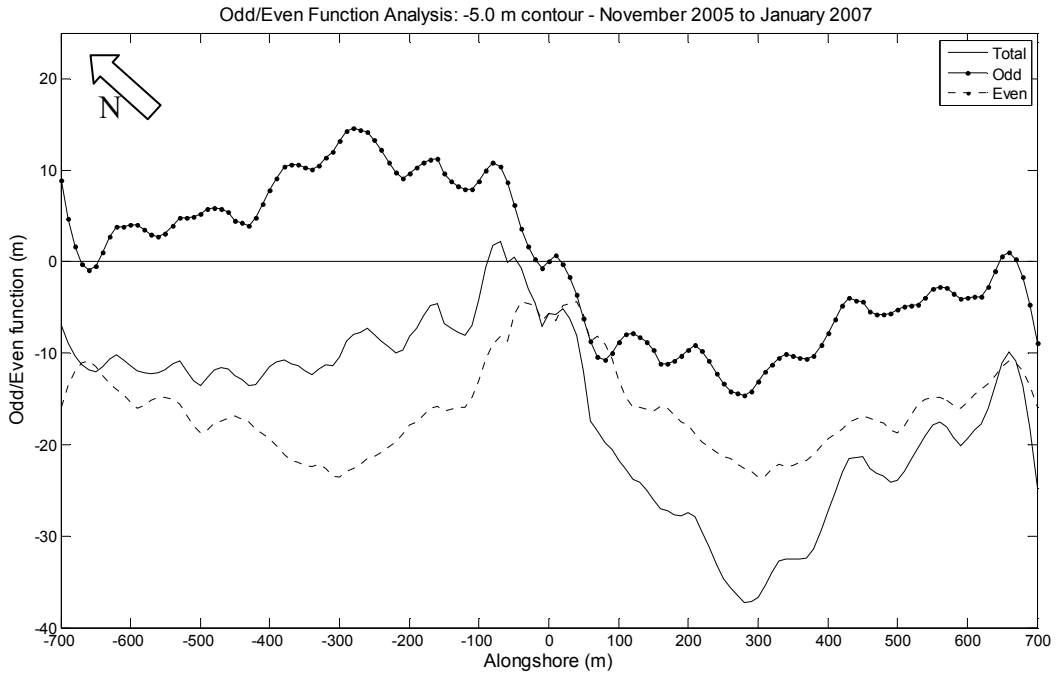

Figure 4.6. Odd-even function analysis of the -5.0 m contour position change for the interval November 2005 to January 2007. The total function is the sum of the odd (dotted) and even (dashed) components. The alongshore origin (x=0 m) corresponds to the reef centreline. The odd function shows an offshore advance of the contour to the northwest of the reef matched by an onshore deflection of the contour to the southeast. This pattern indicates a groin effect of the reef on the offshore beach morphology and extends all along the study site (1400 m). The even component shows a mean onshore migration of the contour of about 10 m likely associated with a natural fluctuation of the beach system. The high of the function around the reef centreline is attributed to short-term drift reversals accumulating sediment around the reef. Combined effects (total function) show a distinct offset in contour position change around the reef (~ 40 m).

The distinct bar/rip pairs are identifiable on a satellite picture of the beach dating from September 2006 where they have started to merge with the shoreline (Figure 4.7). This shift towards a more reflective beach state was attributed to the reef impact on surfzone hydrodynamics including reduction of wave height and more cellular circulation (see SCARFE, 2008).

The bathymetric difference map (Figure 4.5, middle) indicates significant morphological adjustments. The lower half of the map shows rhythmic patterns in the surfzone due to development of rip/bar pairs, along with the development of a large scour hole in the immediate lee of the structure (~7000 m^2). The broken long-shore band of accretion just landward of the reef suggests that the reef has disturbed the migration of the pre-existing long-shore bar, which may have served as a source for the rhythmic features in the surfzone. For this interval from November 2005 and January 2007, it was found that there was no significant net

Figure 4.7. Satellite view of the study beach near Tay Street dating from September 2006. The bar/rip pairs present in the January 2007 and August 2006 surveys (see SCARFE, 2008) are identifiable. Note the crenulated shoreline and intertidal area due the rip/bar pairs. (Source: Google Earth).

change in shoreline position (see Chapter 3, Figure 3.6). However the subaerial beach has accreted uniformly all along the study site and its level relative to the chart datum (i.e. Moturiki Vertical Datum, 1953) was raised by ~1-1.5 m (Figure 4.5, middle). This resulted in the steep and reflective slopes of the upper beach foreshore surveyed in January 2007 (Figure 4.5, bottom).

SCARFE (2008) noted the additional updrift (northwest) accretion around and seaward of the reef (Figure 4.5, middle) and further identified the development of a groin effect of the reef on the offshore bar, inducing offset in bar cross-shore position, and bar crest elevation around the structure. The odd-even analysis of the -5 m contour position change confirms the groin-like pattern around the reef (Figure 4.6). The odd component indicates 10-15 m of offshore advance of the contour to the northwest of the reef matched by similar onshore deflection to the southeast (downdrift). Extent of the groin signal is defined by the alongshore distance at which the odd function reaches a negligible value again (ROSATI and KRAUS, 1997). It encompasses here the 1400 m of the study site. The even component shows a mean onshore advance (~15 m) but a high of the function is identifiable around the reef. This signal is likely the result of progressive accumulation of sediment around the reef vicinity due to short-term sediment movement reversals, as would occur around a groin (e.g ROSATI and KRAUS, 1997). Note the similar sediment build up around the reef apex on the - 4 m contour (January 2007 chart, Figure 4.5). The total function (combined odd and even components) clearly shows the accretion/erosion pattern updrift / downdrift

of reef. The offset in contour position change of ~ 35-40 m appears to be just compensated at the southern end of the study site.

Recent sand disposal to the north of the study site before the reef construction in April/May 2004 (see SPIERS and HEALY, 2007) may have had some effects in the observed offset signal since it artificially increased the sediment supply to the north of the site. However, the absence of any obvious pre-existing gradient in neither the odd-even analysis (Figure 4.6) nor the erosion/accretion map (Figure 4.5) on the pre-construction (but post-dump) period from August 2004 to November 2005 suggests that the reef implementation has had a dominant effect in the pattern.

Figure 4.8 covers the following interval from January 2007 to March 2009 (reef completed in June 2008). The last survey in March 2009 imaged a relatively linear and accreted beach state. The intertidal area was wide (~100 m) with possible mini rip channels, generally resembling a LTT state (see Figure 4.1). The depositional feature identified in shoreline analysis is visible to the northwest of the reef on the MSL contour (0 m contour) with a coinciding advance of the -2 m contour of ~ 40 m. The absence matching signal on the LAT contour (-1 m) suggests that the feature may be due to 2 bar features rather than a typical single salient formation. The scour hole is still present with similar depth (-5 m, MSL) but slightly reduced extents (~5000 m^2). It has however changed of orientation with an axis east / west instead of north / south.

The bathymetric difference map computed from the two beach surveys of January 2007 and March 2009 (Figure 4.8, middle) shows that the full beach and surfzone in March 2009 is the result of both erosion of the subaerial beach and onshore migration of the underlying long-shore bar. This fully filled and smoothed out the prominent bar/rip morphology of January 2007. Since patterns of morphological changes in the beach and surfzone generally run all along the study site, no structural effect is readily identifiable. There is no obvious 3D expression of the shoreline pattern obtained in shoreline analysis (i.e. two depositional feature and superimposed groin effect) although it had fully developed over this time interval (see Figure 3.7).

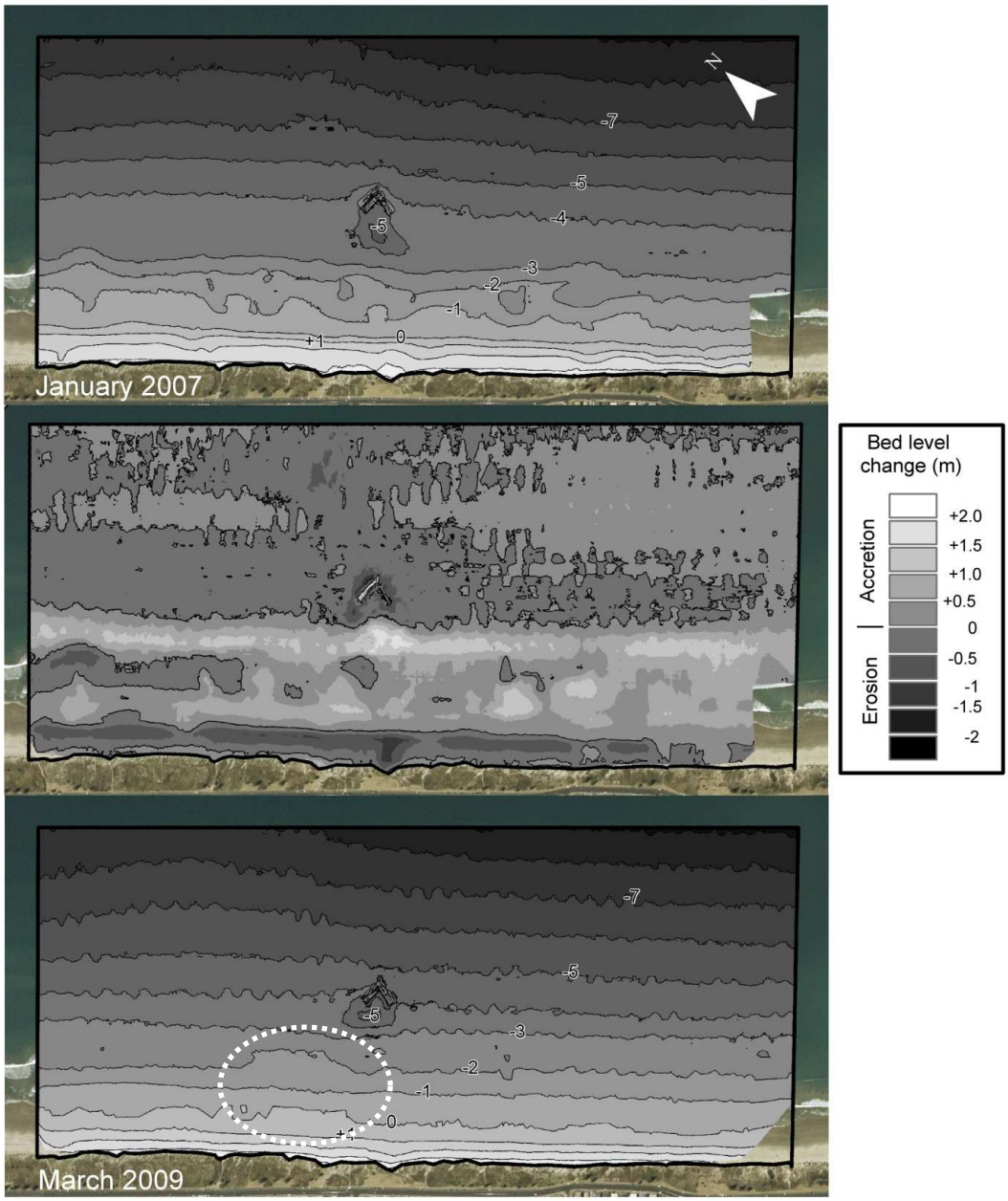

Figure 4.8 Bathymetric surveys of January 2007 (top) and March 2009 (bottom) undertaken by MBES and RTK GPS. Chart datum is Moturiki Vertical Datum, 1953 (approximately mean sea level). The middle chart shows the bathymetric difference between the 2 surveys, with magnitudes of erosion/accretion indicated by the colorbar; the black contour is the limit between erosion and accretion. The well accreted and linear beach morphology in March 2009 (bottom) contrasts with the prominent bar/rip morphology of January 2007 (top). The scour feature is still present although reoriented. The local shoreline advance identified in Chapter 3 is visible to the northwest of the reef in the March 2009 survey (dashed white feature). There is coincident advance of the -2 m contour (~ 40 m) but the -1.0 m contour is linear. (Source: SCARFE, 2008, Coastal Marine Group, University of Waikato).

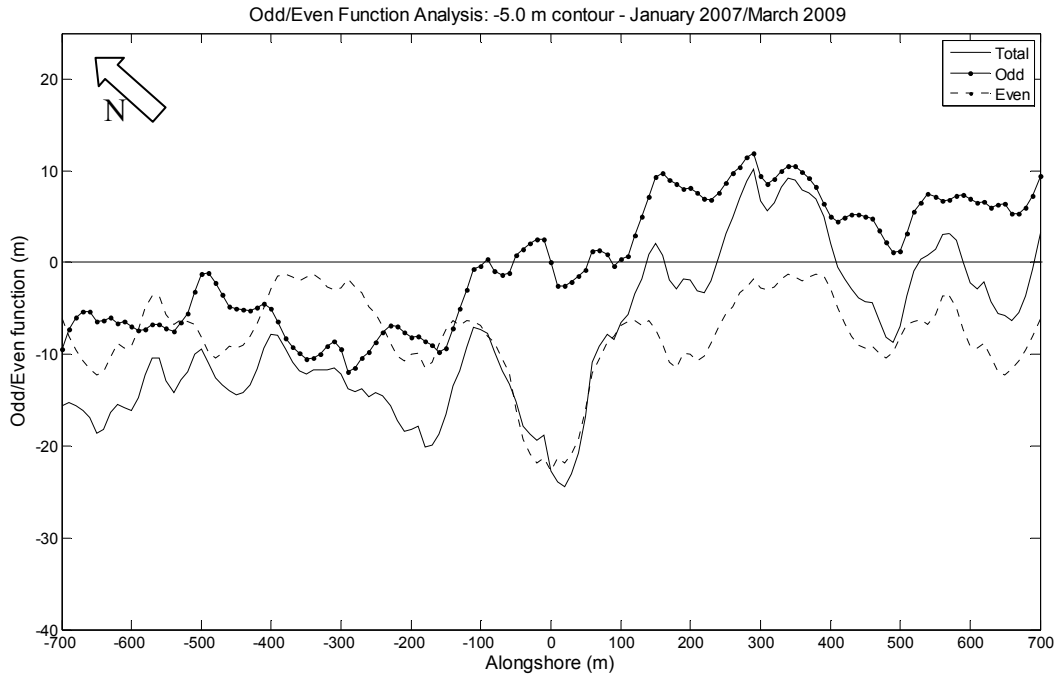

Figure 4.9. Odd-even function analysis of the -5.0 m contour position change for the interval January 2007 to March 2009. The total function is the sum of the odd (dotted) and even (dashed) components. The alongshore origin (x=0 m) corresponds to the reef centreline. The odd component yields a reversed groin pattern relative to Figure 4.6 suggesting an opposed net movement of sediment over the time interval. The mean trend of the even component indicates a new onshore migration of the contour.

Regarding differences around the reef centerline, the southern half of the map shows slightly more marked accretion. This is supported in the concurrent odd-even analysis of the -5 m contour (Figure 4.9) that depicts a "reversed" groin signal relative to precedent direction (i.e. Figure 4.6), with magnitude of about ±10 m (odd function). Here, the signal is not compensated even at some distance of the reef. The reversed pattern suggests that the net movement of sediment over the interval was towards the northwest instead of southeast. This is consistent with the reorientation of the scour hole. The even component of change indicates an onshore advance of 5 to 10 m that, along with the groin effect, induced a more significant onshore migration of the contour to the north of the reef (total function). This resulted in a straighter contour in the March 2009 survey (Figure 4.8, bottom). Note that the depositional feature initially thought to be updrift of the reef could in fact be offset downdrift, as more generally expected (e.g. TURNER, 2006), but relative to antecedent wave directions and long-shore sediment transport.

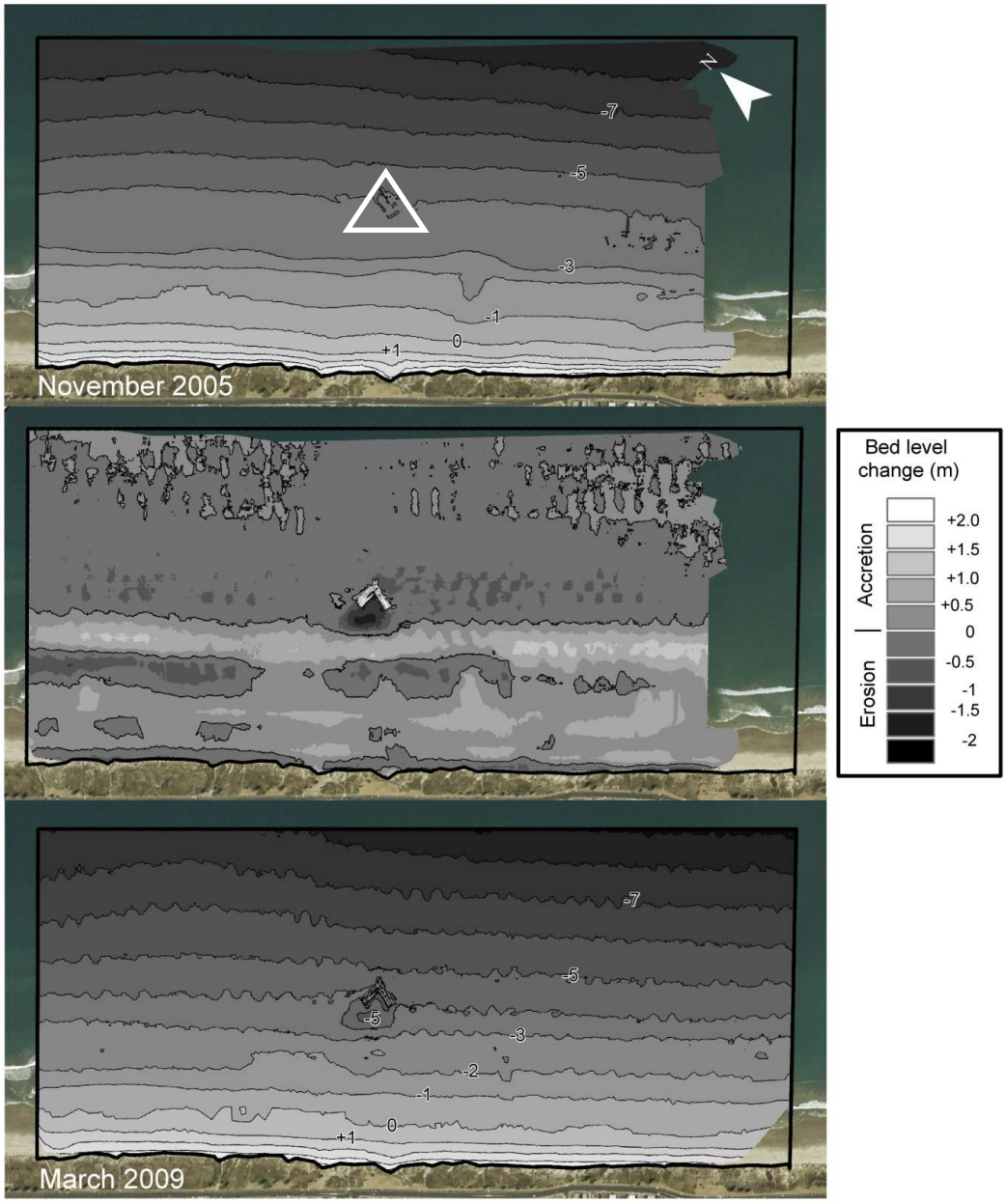

Figure 4.10 Bathymetric surveys of November 2005 (top) and March 2009 (bottom) undertaken by MBES and RTK GPS. Chart datum is Moturiki Vertical Datum, 1953 (approximately mean sea level). The white triangle indicates the projected reef location (top chart). The middle chart shows the bathymetric difference between the 2 surveys, with magnitudes of erosion/accretion indicated by the colorbar; the black contour is the limit between erosion and accretion. The figure compares pre and post construction beach bathymetries to investigate the net morphological changes over the entire study period. The scour feature is evident in the lee of the reef. The long-shore accretion band landward of the reef is due to the migration of the pre-existing long-shore bar. There are 3 main "double bar" features nourishing the intertidal and subaerial beach. (Source: SCARFE, 2008, Coastal Marine Group, University of Waikato).

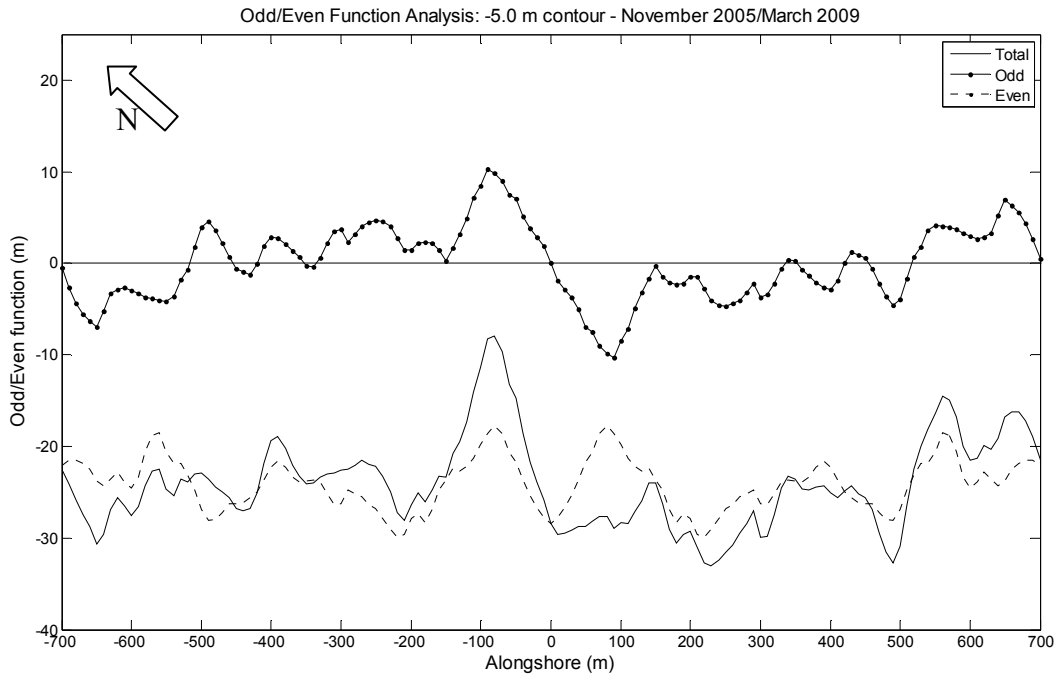

Figure 4.11. Odd-even function analysis of the -5.0 m contour position change for the entire pre/post construction interval from November 2005 to March 2009. The total function is the sum of the odd (dotted) and even (dashed) components. The alongshore origin (x = 0 m) corresponds to the reef centreline. The odd component indicates a residual advance/retreat of the contour of magnitude ± 10 extending 300 m around the reef. This is superimposed on the onshore migration of the contour of ~ 25 m over the period (even component). The residual sediment accumulation to the north (left) of the reef is evident in the total function.

The dominant morphological adjustments over the 2 successive intervals within the entire pre / post construction interval were (i) the transition from a linear beach state to a prominent rip/bar morphology (Figure 4.3) and (ii) the inverse transformation from the rhythmic beach state back to a more linear state (Figure 4.5).

The two relatively similar beach states in November and March 2009 allow having a more consistent underlying morphology to identify any residual erosion/accretion pattern (Figure 4.10). The erosion/accretion map indicates a long-shore accretion band landward of the reef that is due to the migration of the underlying bar feature. The scour development is obvious landward of the reef, with net lowering of the seabed of up to 2 m relative to pre-construction seabed level, extending ~5000 m². The pattern of beach and surfzone accretion is rhythmic with three main "double bar" features nourishing the intertidal and subaerial beach. Focusing on the 2 "double bar" features around the reef centerline near the shoreline, the pattern could resemble the symmetrical 2-feature advance signal obtained in concurrent shoreline analysis (even function, Figure

3.5). However, the third feature at the southern extremity of the study site is very similar although at some distance of the structure. This consequently limits the confidence in discriminating any net structure-induced accretion pattern from the underlying beach fluctuations.

Regarding the offshore morphology, net changes over the entire study period are limited with 2 areas of mild accretion (+0.5 m) around the -7 m contour. In the reef vicinity, small accretion patches can be seen along and near the northern arm of the reef. Odd-even analysis for the period (Figure 4.11) indicates that the 2 successive groin signals (Figures 4.6 and 4.9) resulted in a net offshore advance/onshore deflection of the contour of magnitude ±10 m extending ~300 m around the reef (odd function). The direction is consistent with the net drift direction i.e. northwest to southeast indicating that the first signal identified (Figure 4.6) has been dominant.

4.3.4. COMPARISON WITH PREDICTIONS

A range of environmental and structural parameters of the reef system are defined below to (i) provide a basis for any future verification or research on design relationships based on field data and (ii) test two available predictive relationships of shoreline response that are potentially appropriate for the study reef, namely these of BLACK and ANDREWS (2001) and RANASINGHE *et al.* (2006).

BLACK and ANDREWS (2001) established empirical relationships from field observations of natural submerged reefs which were used as a basis to design the Narrowneck and Tay Street reef prototypes (see BLACK, 1999; MEAD and BLACK, 1998). The relationship link the non dimensional ratios X/B and B/S:

$$\frac{X}{B} = 0.5\left(\frac{B}{S}\right)^{-1.27} \qquad (4.3)$$

in which X is the distance between the structure and seaward apex of the salient, B is the reef alongshore width, and S is the distance between the undisturbed shoreline and the structure (see Figure 4.12 for graphical representation). The cross-shore amplitude of the salient Y relative to undisturbed shoreline is Y=S-X.

The salient alongshore width D_{tot} can be estimated using:

$$\frac{Y}{D_{tot}} \approx 0.125 \pm 0.02 \qquad (4.4)$$

Salient formation is expected for ratios B/S < 2.0 and tombolo for B/S > 0.6. The threshold prior to depositional condition is 0.1 (BLACK and ANDREWS, 2001). Note that the formula predicts the "equilibrium" salient that would develop in response to long-term averaged wave/hydrodynamics conditions.

Predictive relationships of RANASINGHE *et al.* (2006) are based on numerical modelling of idealized beach morphology evolution in the presence of a multi-purpose reef. Design graphics provides relationships between Y/B and SZW/ S_a (Figure 4.13) in which Y is the cross shore salient amplitude from undisturbed shoreline, B is the structure alongshore width, SZW is the natural surfzone width, and S_a is the distance between the undisturbed shoreline and the apex of the structure. Two graphics are provided including two curves each; the first is for a fixed crest level of -0.5 m (MSL) under normal and oblique wave incidence, and the second is for 2 crest levels at -0.5 and -1 m (MSL) under normal wave incidence only. At the site, both shore normal and oblique wave incidences are possible and the reef crest is at -2 m (MSL). To best approach these conditions, the "oblique wave" curve in the first graphic (Figure 4.13 a) and the "lower crest" curve (-1 m) (at shore normal incidence) in the second graphic (Figure 4.13 b) were used.

The constructed alongshore width B is directly identifiable from the last survey (B = 80 m) but the definition of the other parameters involves arbitrary choices. The "undisturbed" shoreline was taken as the mean of pre-construction mean sea level contours (August 2004 and November 2005 survey). Structure distance offshore was defined from the shoreline to the apex of the reef as required by RANASINGHE *et al.* (2006) (S_a) and to the cross-shore center of the reef for BLACK and ANDREWS (2001). The surfzone width (SZW) required in the relationships of RANASINGHE *et al.* (2006) was estimated using Equation 4.5 as in BLACK and MEAD (2007):

$$SZW = H_b/(\gamma.\tan\beta) \qquad (4.5)$$

where H_b is the breaking wave height (m), γ is the breaking criterion (taken as 0.78), and tan β is the average beach slope.

Table 4.2. Structural and environmental parameters of the prototype reef at Mount Maunagnui, New Zealand.

Design parameters		**BLACK and ANDREWS (2001)**	**RANASINGHE *et al.* (2006)**
Structure alongshore width	**B = 80 m**	**Dimensionless ratio**	**Dimensionless ratios**
Structure cross-shore length	**C = 65 m**		
Crest level (freeboard)	**R = -2 m MSL**	**B/S = 0.28**	**S_a/SZW $_{mean}$ = 2.4**
Distance to undisturbed shoreline	**S = 287 m**	B/S > 0.1	**S_a/SZW $_{high}$ = 1.7**
(mean preconstruction MSL)	**S_a = 317 m**	B/S <0.6 <2.00 *Salient expected*	**S_a/SZW $_{low}$ = 4.0**
Signficant breaking wave height		**Salient amplitude Y**	**Salient amplitude Y**
Mean value	**$H_{b\ mean}$ = 1.45 m**	X/B = 2.5; X = 200 m	**Oblique waves (crest -0.5 m MSL)**
Mean + standard deviation	**$H_{b\ high}$ = 2.05 m**	where X = S-Y = 287 m-Y	Y/B $_{mean}$ = 0.45 **Y = 36 m**
Mean - standard deviation	**$H_{b\ low}$ = 0.85 m**	**Y = 87 m**	Y/B $_{high}$ = 0.45 **Y = 36 m**
		Estimated alongshore width	Y/B $_{low}$ = N/A
Natural surfzone width		$D_{tot} \approx 87/0.125 \approx 700$ m	**Normal waves (crest -1 m MSL)**
$SZW=H_b/(\gamma.\tan\beta)$	**SZW_{mean} = 133 m**		Y/B $_{mean}$= 0.53 **Y = 42 m**
H_b breaking wave height	**SZW_{high} = 188 m**	*(see Fig. 4.12 and Eq. 4.3 and 4.4)*	Y/B $_{high}$ = 0.37 **Y = 30 m**
γ breaker index (0.78)	**SZW_{low} = 78 m**		Y/B $_{low}$ = N/A
$\tan\beta$ beach slope (0.014)			*(see Figure 4. 13a and b)*

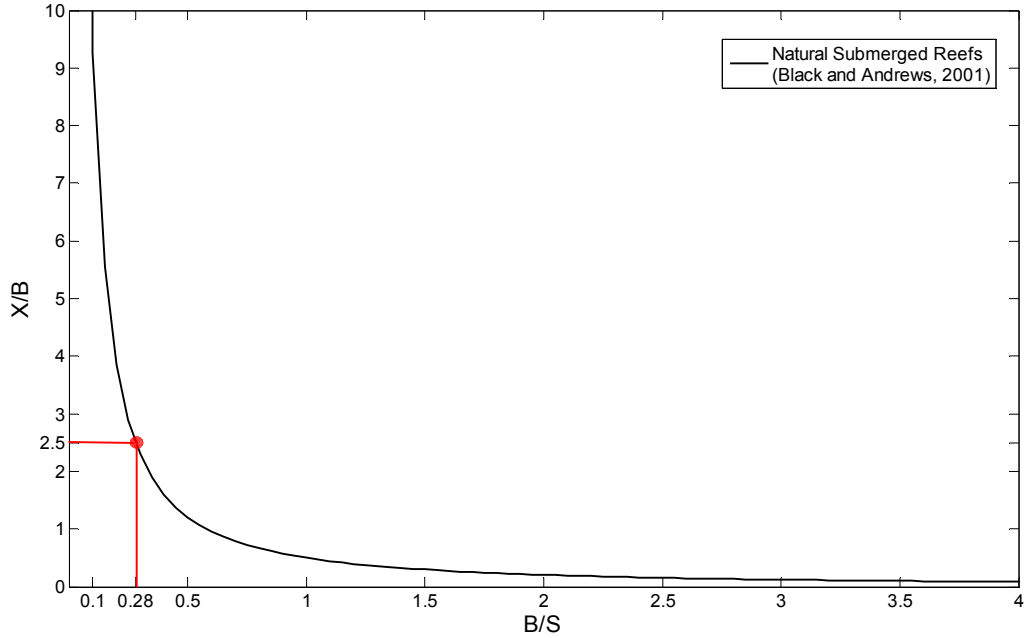

Figure 4.12. Relationship between B/S and X/B for natural offshore submerged reefs (BLACK and ANDREWS, 2001). B is the alongshore width of the structure, S is the distance of the structure to the undisturbed shoreline, and X is the distance from the salient apex to the structure. Salient cross-shore amplitude Y is equal to S-X. Tombolos were observed when B/S > 0.6 and salients when B/S < 2.00. The threshold for depositional conditions is B/S = 0.1. The studied prototype configuration is indicated in red (see Table 4.2).

The breaking wave height parameter H_b used was the mean significant breaking height over the study period (see Figure 4.2). To account for the wave climate variability, this was supplemented by lower/upper heights using the standard deviation i.e. mean value ± standard deviation. The natural seabed gradient was estimated at ~ 0.014 by averaging several pre-construction profiles at different alongshore positions. The parameters are summarized in Table 4.1 and plotted on respective design graphics on Figures 4.12 and 4.13.

Both graphics predict salient formation but diverge on the size of feature expected by a factor of about 2. Based on the final reef dimensions, BLACK and ANDREWS (2001)'s formula yields cross-shore salient amplitude of 87 m extending some 700 m alongshore. Positioning of the reef is correct according to the RANASINGHE *et al.* (2006) relationships (i.e. near the curves' peak) but they predict a smaller feature of ~ 40 m using mean wave conditions, decreasing to ~30 m under the larger breaking height considered (mean+std) (Figure 4.13b).The smaller height case (mean-std) falls just out of the range covered by the graphics. We can still reasonably assume that as the ratio S_a/SZW increases, the footprint of the reef on the beach system will decline, eventually leading to null deposition.

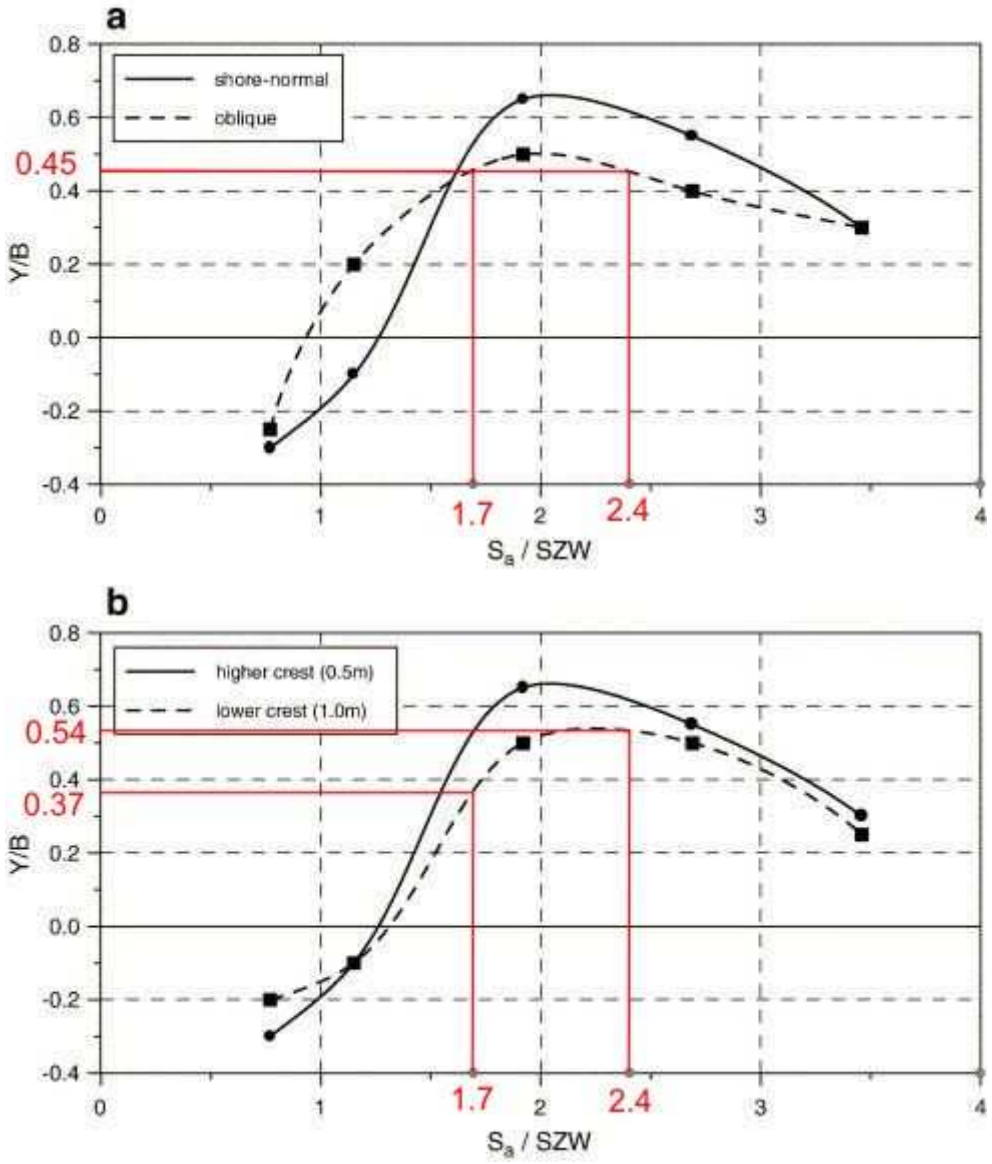

Figure 4.13. Relationships between Y/B and S_a/SZW for (a) shore normal and oblique wave incidence for a reef crest at 0.5 m below MWL, and (b) higher (plain line) and lower (dotted line) reef crest at shore normal wave incidence (from RANASINGHE *et al*., 2006). Y, B, S_a, and SZW are salient cross-shore amplitude, structure alongshore width, distance of the structure apex to the undisturbed shoreline, and surf zone width respectively. Positive or negative ratios Y/B predict shoreline accretion or erosion respectively. The studied prototype configuration is indicated in red (see Table 4.2).

This trend is suggested by the graphic curves so features expected with the lower wave height conditions considered would be very limited. Importantly, it is noted that the larger breaking wave height of 2.05 m considered in computation can easily be exceeded at the site (see Figure 4.2). This can shift the ratio S_a/SZW towards non-depositional or erosive conditions. For example, a 3 m breaking wave height yields a ratio S_a/SZW~1 that predicted shoreline erosion.

It also mentioned that the salient amplitudes are predicted for crests at - 0.5 m or -1.0 m relative to MSL while the reef at Tay Street is at -2.0 m. Salient size is expected to decrease for lower crests (see curves at different crest levels in Figure 4.13b) so feature sizes actually expected at the site could be smaller than these predictions.

Surveyed shorelines and bathymetries indicate that even though a small feature is possible (~ 20 m, see March 2009 survey, Figure 4.10), it is superimposed on the underlying beach oscillations that are generally dominant. The relationship of BLACK and ANDREWS (2001) for natural submerged reefs then significantly overestimates the salient size at the site. The range predicted by RANASINGHE *et al.* (2006) is also greater than the observed responses but less obviously. However, an interesting result obtained from the application of their design graphics is that energetic wave conditions are able to switch the predicted shoreline response from accretion to erosion (i.e. Y/B < 0). A succession of (small) salient formations and resets (i.e. erosion) in response to instantaneous wave conditions seems consistent with the transient beach response observed on the set of bathymetric surveys.

4.4. DISCUSSION

Some important characteristics of the beach morphodynamic response to a submerged multi-purpose reef can be outlined from the analyzed dataset.

The most obvious and consistent geomorphic feature in both the bathymetric charts and the erosion/accretion maps is the large scour hole onshore of the reef. The scour is larger than the structure itself (~5-7000 m²) with lowering of the seabed of up to ~2 m relative to undisturbed profiles. Scour formation has been consistently predicted in design or research studies about submerged structures or

multi-purpose reefs (e.g. BLACK, 1999, RANASINGHE *et al*., 2006; RANASINGHE and SATO, 2007; BLACK and MEAD 2007), however, modeled scour features are generally limited in size and much smaller than the structure itself. Underestimation of scour is potentially problematic since scour affects structure stability and may causes failure due to overturning/settling or sliding (e.g. BURCHART and HUGHES, 2006).

The dominant hydrodynamic mechanism responsible for the scour formation is most likely the development of strong wave-induced onshore flows over and landward of the structure (SCARFE, 2008). The onshore location of scour and absence of erosion or even accretion seaward of the structure (e.g. Figure 4.6) is consistent with recent experiments on scour around submerged structures (see SUMER *et al.,* 2001). This contrasts with emergent breakwaters that generally develop scour on their seaward side.

Regarding the surf and swash zone morphology, the response to the reef is complex. The prominent bar/rip pairs imaged by the January 2007 survey provide evidence of cellular surfzone circulation (SCARFE, 2008). However, the smoothed beach state and accreted beach of March 2009 indicates that the reset of such a rhythmic morphology is possible. This is most likely related to ambient fluctuations of the local beach system (e.g. antecedent wave conditions, position of the underlying offshore bar) and can be compared to the two different pre-construction beach states i.e. a relatively eroded state in August 2004 with several surfzone features and a more linear beach in November 2005 (see Figure 4.3).

The small salient/bar feature that was present for the March 2009 survey was not observed in any of the precedent surveys of SCARFE (2008). The formation may be the result of the "reef bar" mechanisms identified by BLACK and MEAD (2007). Alternatively, the feature may be due a more marked expression of the hydrodynamic processes favorable for salient formation, including (i) wave shadow in the lee of the reef, (ii) rotation of incident waves generating less long-shore currents; (iii) development of counter rotating cells in the lee side transporting sediment, and (iv) reduction of wave setup at the shoreline (see BLACK, 2003; BLACK and MEAD, 2007), due to appropriate antecedent wave conditions (e.g. clean swell events inducing more organized nearshore circulation pattern).

The temporal resolution of the present dataset (months to years) is insufficient to resolve such a transient beach morphology response to the reef. Any transient salient/bar feature development would require shoreline and/or beach bathymetry data every weeks or month to be correctly monitored.

The video monitoring (e.g. Argus) of the beach would be able to provide such data and seems a valuable tool to better understand the short-term beach morphodydnamics in presence of submerged multi-purpose reefs. Furthermore, the detection and tracking of nearshore bars and shoreline position allowed by the technology (e.g. LIPPMAN and HOLMAN, 1989; PLANT *et al.*, 2007) could be used to further investigate the bar mechanisms identified by BLACK and MEAD (2007) and the more crenulated/rhythmic beach response observed by SCARFE (2008).

The Narrowneck reef benefits from an extensive database of video images thanks to an Argus station (see TURNER *et al.*, 2004). Analysis of the long-term shoreline response to the reef was undertaken by TURNER (2006) but there is likely a scope for further use of the data to investigate the short-term morphodynamics in the vicinity of the reef. This has not really been addressed so far although suggested of importance for salient formation (BLACK and MEAD, 2007; SCARFE 2008).

Another important impact of the reef, initially identified by SCARFE (2008), is its groin effect on the offshore beach morphology. The reduction of the downdrift sediment supply due to the implementation of a submerged structure is one of the side effects expected since natural sediment movement is disturbed (e.g. RANASINGHE and SATO, 2007). On the -5 m contour (MSL) just offshore of the reef, the groin signal was found to possibly extend along the 1400 m of the study site. The pattern has occurred in two opposed direction further confirming the role of the reef as a control point in the long-shore sediment movement. The net groin signal from November 2005 to March 2009 is consistent with the net drift direction (northwest to southeast) (Figure 4.11).

Interestingly, there is a matching signal in shoreline change analysis (Chapter 3, Figure 3.5) for the same time interval (±15 m, 400 m alongshore), however the relationship between groin signals in offshore and shoreline contour analysis (Chapter 3) is relatively inconsistent in successive intervals within the study

period. The most obvious "offshore" groin effect is observed on the interval 2005 to 2007 but there is no concurrent signal in the shoreline analysis over this period (Figure 3.6). Then, analysis of the -5 m contour adjustment from 2007 to 2009 indicates a reversed groin effect while shoreline analysis yields a groin signal still following the long-term net drift direction. It is likely that the groin effect at the shoreline is not directly due to the physical obstruction of the structure to the offshore sediment movement and rather related to other processes (e.g. circulation-induced or secondary effect of shoreline feature, see Chapter 3).

Overall, the perturbation of the offshore sediment movement since reef implementation has not caused problematic downdrift erosion throughout the monitoring period, but this secondary effect still requires attention since the reduction of sediment supply downdrift could become more significant for projects undertaken in drift environment with greater magnitude of sediment transport, and/or involving larger structures. Basically, we can expect that the groin effect would decrease as the structure is moved from the surfzone (greater sediment movement and potential trapping) to further offshore, with finally negligible effects beyond the closure depth (i.e. on the stable profile).

For optimal coastal protection (salient), it is understood that the structure should be placed well beyond the natural surfzone (BLACK, 2003; RANASINGHE *et al.*, 2006; BLACK and MEAD, 2007) so this already limits the issue. However, it may still be relevant to consider the cross-shore dimension of the structure during design and possibly assess downdrift effects not only in terms of secondary effect of emerging salient only (e.g. MEAD and BLACK, 1998; TURNER, 2006; TURNER *et al.*, 2001) but rather of the combination of salient and submerged structure. In that sense, cross-shore positioning relative to the closure depth may be another parameter to consider, in addition to optimal offshore distance for salient formation and/or reasonable construction costs.

4.5. CONCLUSIONS

This chapter investigated the beach morphodynamic response to the multi-purpose reef constructed near Tay Street at Mount Maunganui. Pre and post construction MBES and RTK GPS charts of the nearshore bathymetry and beach foreshore concurrent with shoreline contours used in Chapter 3 were analyzed to identify the

main geomorphic features on the 3D beach morphology, and compare them with shoreline adjustments. An odd-even function analysis was applied to the -5.0 m contour (located just offshore of the reef) position change to monitor the groin effect of the reef on the offshore beach morphology identified in previous monitoring by SCARFE (2008). Hindcast wave data offshore of the site and a predictive model of beach state (WRIGHT and SHORT, 1985) were used in conjunction to provide a proxy on wave conditions over the study period. Main findings of the chapter are:

- The new post-construction survey in March 2009 imaged a smoothed and well accreted beach state that contrasted with the prominent bar/rip morphology observed previously in January 2007 (see SCARFE, 2008). A small depositional bar/salient feature matching the local shoreline advance observed in Chapter 3 was identifiable to the northwest of the reef. However, the absence of persistent salient pattern throughout the study period suggests that the feature is transient, likely related to underlying beach morphology and antecedent wave conditions.

- The large onshore scour hole of the reef identified by SCARFE (2008) was still present in March 2009 with a consistent depth (-5 m, MSL) and size (~5000 m^2), although reoriented due to antecedent wave direction.

- Odd-even analysis of the -5 m contour just offshore of the reef indicates that the structure acts as control point in the long-shore sediment movement. A groin effect consistent with the net drift direction developed over the first half of the pre / post interval with additional seaward advance of the contour of ~ 10 m to the north of the reef, matched by similar landward deflection to the south. The signal encompassed the entire study site that extends 1400 m alongshore. A reversed effect occurred over the second half of the interval with similar magnitudes, likely due to a temporary drift reversal. The two effects compensated over the full study period, with a net pattern of seaward advance/landward deflection of magnitude ± 10 m extending 300 m centred on the reef. The net signal was consistent with the net drift direction. The groin signals in contour change offshore and at the shoreline (MSL) (Chapter 3) are inconsistent suggesting different governing processes.

- Available design relationships for shoreline response to natural submerged reefs (BLACK and ANDREWS, 2001) and multi-purpose reefs (RANASINGHE *et al.*, 2006) both predict salient formation at the site but diverge on the size of the feature by a factor of ~ 2. The equation of BLACK and ANDREWS (2001) predict a salient cross-shore amplitude of 87 m extending 700 m alongshore. Equations of RANASINGHE *et al.* (2006) predict a smaller feature with cross-shore amplitude of ~ 40 m using mean wave height conditions (H_b = 1.45 m). Observed responses are lower than the predictions with a possible shoreline advance of ~ 20 m (cross-shore) extending 150 m alonghsore.

4.6. REFERENCES

BLACK, K.P., 1999. Designing the Shape of the Gold Coast Reef: Sediment Dynamics. *Proceedings of the 1999 Coasts and Ports Conference* (Perth, Australia), pp. 58-63.

BLACK, K.P., 2003. Numerical Prediction of Salient Formation in the Lee of Offshore Reefs. *In*: BLACK, K.P., and MEAD, S.T. (eds.), *Artificial Surfing Reefs 2003: The 3rd International Conference, Raglan, New Zealand.* CD publication, pp. 196-218, ISBN: 0-473-09801-06.

BLACK, K.P., and ANDREW, C.J., 2001. Sandy Shoreline Response to Offshore Obstacles, Part 1: Salient and Tombolo Geometry and Shape. *In:* BLACK, K.P., (ed.), Natural and Artificial Reefs for Surfing and Coastal Protection. *Journal of Coastal Research, Special Issue No. 29*, 82-93.

BLACK, K.P. and MEAD, S.T., 2007. Sand Bank Responses to a Multi-Purpose Reef on an Exposed Sandy Coast. *In*: WALTHER, M. (ed.), Shore protection and surfing dedicated issue: *Shore and Beach*, 75(4), 55-66.

BURCHARTH, H.F., and HUGHES, S.A., 2006. Fundamentals of Design. *In*: HUGHES, S., (ed.), *Coastal Engineering Manual,* Part VI, Design of Coastal Project Elements, Chapter 2, Engineering Manual 1110-2-1100, U.S. Army Corps of Engineers, Washington, DC.

GORMAN, R.M., 2005. Numerical wave forecasting for the New Zealand region. *In*: TOWNSEND, and M., WALKER, D. (eds), *Proceedings of the 2005 Coasts and Ports Australasian Conference*, pp.179-184.

LIPPMANN, T.C, and HOLMAN, R.A., 1989, Quantification of sand bar morphology: a video technique based on wave dissipation. *Journal of Geophysical Research*, 94(C1), 995 -1011.

MEAD, S.T. and BLACK, K.P., 1998. A Multipurpose Artificial Reef at Mount Maunganui Beach, New Zealand. *Coastal Management,* 27, 335-365.

NIELSEN P., 1982. Explicit formulae for practical wave calculations. *Coastal Engineering*, 6, 389-398.

PICKETT, V.I., 2004. The Application of Equilibrium Beach Profile Theory to Coastal Hazard Identification in the Bay of Plenty. Hamilton, New Zealand: University of Waikato, PhD thesis, 507 p.

PICKRILL, R.A., and MITCHELL, J.S., 1979. Ocean Wave Characteristics around New Zealand. *New Zealand Journal of Marine and Freshwater Research*, 13(4), 501-520.

PLANT, N. G., AARNINKHOF, S G J., TURNER I. L., and KINGSTON, K. S., 2007. The Performance of Shoreline Detection Models Applied to Video Imagery. *Journal of Coastal Research*. 23(3), 658-670

RANASINGHE, R., and TURNER, I.L., 2006. Shoreline Response to Submerged Structures: A Review. *Coastal Engineering*, 53, 65-79.

RANASINGHE, R., TURNER, I.L., and SYMONDS, G., 2006. Shoreline Response to Multi-Functional Artificial Surfing Reefs: A Numerical and Physical Modeling Study. *Coastal Engineering*, 53, 589-611.

RANASINGHE, R., and SATO, S., 2007. Beach morphology behind single impermeable submerged breakwaters under obliquely incident waves. *Coastal Engineering Journal*, 49 (1), 1-24.

SCARFE, B.E., and HEALY, T.R., 2005. Baseline Bathymetric Data Collection for Monitoring of Bar, Rip and Salient Response to an Artificial Surfing Reef - Mount Maunganui, New Zealand. *In*: TOWNSEND, M. and WALKER, D. (eds.), *Proceedings for the 2005 Coasts and Ports Australasian Conference*, pp. 459-464.

SCARFE, B.E., 2008. Oceanographic Considerations for the Management and Protection of Surfing Breaks. Hamilton, New Zealand: The University of Waikato, Ph.D. thesis, 307 p. + appendices.

SHORT, A.D., 1999. Wave-Dominated Beaches. *In*: SHORT, A.D. (ed.), *Handbook of Beach and Shoreface Morphodynamics*. West Sussex, England: John Wiley & Sons Ltd, ISBN 0-471-96570-7, pp. 173-203.

SUMER, B.M., WHITEHOUSE, J.S., and TORUM, A., 2001. Scour around coastal structures: a summary of recent research. *Coastal Engineering*, 44, 153–190.

SPIERS, K.C., and HEALY, T.R., 2007. Beach Renourishment through Spoil Disposal Downdrift of a Dredged Entrance Channel. *In*: KRAUS, N.C. and ROSATI, J, D. (eds.), *Coastal Sediments '07,* pp. 2358-2371.

TURNER, I., LEYDEN, V., COX, R., JACKSON, A., and MCGRATH, J., 2001. Physical Model Study of the Gold Coast Artificial Reef. *In:* BLACK, K.P. (ed.), Natural and Artificial Reefs for Surfing and Coastal Protection. *Journal of Coastal Research, Special Issue No. 29*, 131-146.

TURNER, I. L. AARNINKHOF, S. G. J., DRONKERS, T. D. T, and MCGRATH, J., 2004. CZM Applications of Argus Coastal Imaging at the Gold Coast, Australia. *Journal of Coastal Research*, 20(3), 739-752.

TURNER, I.L., 2006. Discriminating Modes of Shoreline Response. *Journal of Waterway, Port, Coastal and Ocean Engineering*, 132(3), 180-191.

WRIGHT, L.D., and SHORT, A.D., 1984. Morphodynamic Variability of Surf Zones and Beaches: A Synthesis. *Marine Geology*, 56, 93–118.

WRIGHT, L.D., and SHORT, A.D., 1985. Short Term Changes in Morphodynamic State of Beaches and Surf Zones: An Empirical Predictive Model. *Marine Geology*, 62, 338–364.

CHAPTER 5. WAVE TRANSMISSION OVER AN OFFSHORE SUBMERGED MULTI-PURPOSE REEF AT MOUNT MAUNGANUI, NEW ZEALAND

5.1 INTRODUCTION

Analysis of wave data collected during a 5 day field experiment in the vicinity of the multi-purpose reef near Tay Street at Mount Maunganui is presented. This is the first field investigation of wave processes around a multi-purpose reef. The instrument deployment consisted of two measuring stations located seaward and landward of the reef to measure both incident and transmitted wave fields. Incident and transmitted wave fields are compared focusing on: (i) the transmission of significant wave height, (ii) the modification of wave height distribution, and (iii) the transformation of wave energy spectrum, along with implications on wave period.

5.2 METHODS

5.2.1 FIELD EXPERIMENT

The field data analyzed was collected during a 5 day field experiment conducted from the 28th of August to the 2nd of September 2009 in the vicinity of the multi-purpose reef constructed near Tay Street at Mount Maunganui. To monitor the effect of the reef on the wave conditions, 2 Sontek Triton acoustic doppler velocimeters (ADV) equipped with pressure sensors were installed seaward and landward of the reef to measure incident and transmitted wave field characteristics (Figure 5.1). The ADVs were attached to frames anchored to the seabed in about ~5.2 m water depth relative to mean sea level (Moturiki Vertical Datum, 1953) (Figure 5.2). The pressure sensors were 0.7 m above the seabed and sampled wave-induced pressures at 4 Hz for 1024 seconds, every 30 minutes. The retrieval operation indicated no displacement of the instruments during the experiment however the site had experienced sediment accretion and frames were partially

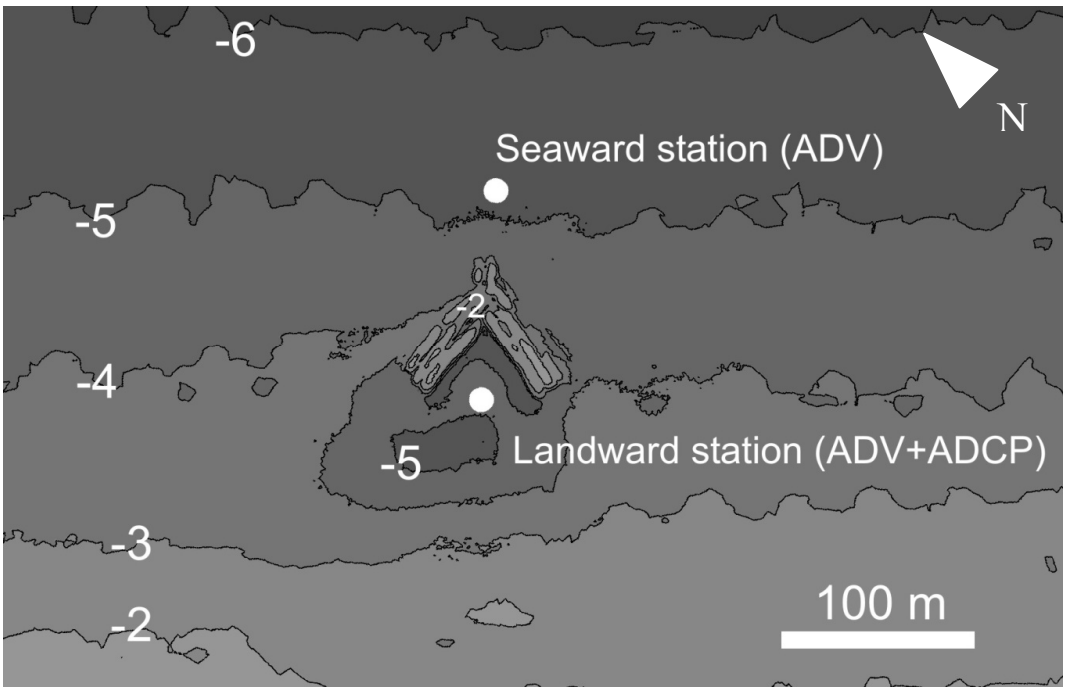

Figure 5.1. Instrument stations around the reef. The bathymetry is from March 2009 and depths are relative to mean sea level (Moturiki Vertical Datum, 1953).

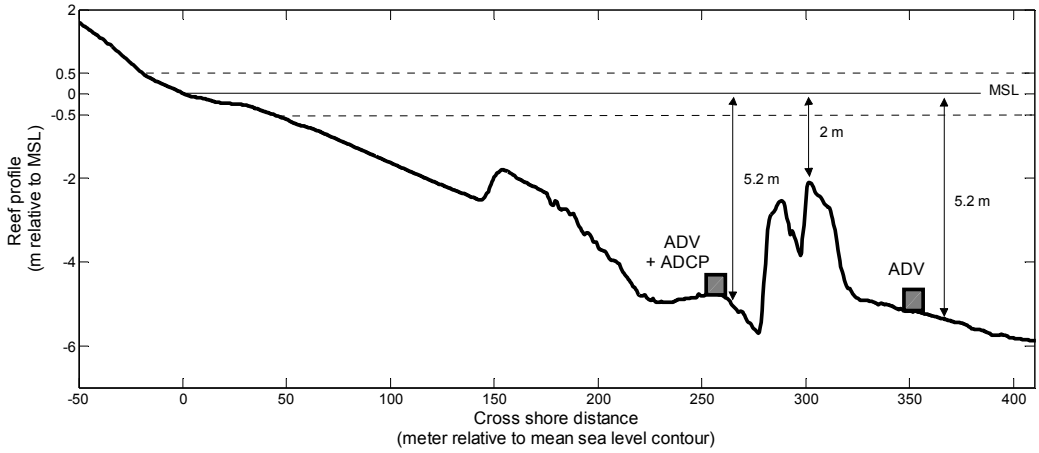

Figure 5.2. Reef profile with instrument depths and positions. Depths are relative to mean sea level (Moturiki vertical datum 1953, plain line). Highest and lowest water levels during the experiment are represented (dashed lines).

buried by about 0.2 m. This did not affect the measurements although the sensor heights above bottom were probably slightly reduced during the experiment.

The pressure dataset considered for analysis consists of 231 bursts sampled from the 28th of August 2009 at 2.30 pm to 2nd of September 2009 at 9.30 am. Hourly wind data at the Tauranga Aerodrome was obtained from the National Climate database for the experiment period (NATIONAL INSTITUTE of WATER and ATMOSPHERIC RESEARCH, 2009a). Water levels were obtained from the tide gage located at Moturiki Island (NATIONAL INSTITUTE of WATER and ATMOSPHERIC RESEARCH, 2009b).

5.2.2 DATA PROCESSING

To determine representative wave parameters, height and period distributions, and wave energy spectra, both wave-by-wave and spectral analysis were required. A set of Matlab programs was developed to undertake the processing of the pressure dataset. They are included in the Appendix C. The Sontek software ViewTritonPro (SONTEK/YSI, 2001b) was used to obtain wave directions.

For each burst, steps of the processing consisted of (i) conversion of measured pressure time series to sea surface elevation time series, (ii) zero level down crossing analysis, (iii) determination of a range of representative wave height and period parameters, (iv) determination of height and period distributions, and (v) determination of wave energy spectrum.

5.2.2.1 Pressure to Surface Elevation

The conversion of pressure time series into sea surface elevations time series was undertaken using the linear wave theory and assuming the sea-state to be a superimposition of numerous linear waves of different frequencies and amplitudes (Gaussian model).

Assuming unidirectional waves, the sea surface elevation η(t) at the instrument position can be represented by the Fourier integral:

$$\eta(t) = \int_0^{\infty} A_n . e^{i2\pi f_n t} \qquad (5.1)$$

where t is time, and A_n is the complex Fourier amplitude associated with the n-th harmonic component of frequency f_n.

In practice, since the recorded wave data is discrete, only a finite number of frequency components are considered and Equation 5.1 becomes:

$$\eta(t) = \sum_{n=1}^{N/2} A_n . e^{i2\pi f_n t} = \sum_{n=1}^{N/2} [\, a_n . \cos(2\pi f_n . t) + ib_n . \sin(2\pi f_n . t)] \qquad (5.2)$$

where t is time, N is the total number of data points, a_n and b_n are the real and imaginary components of the complex Fourier amplitude A_n of the n-th harmonic, and f_n is the n-th harmonic frequency. The frequency range (f_n) is from 1/(N/2) to F_N, where F_N is the Nyquist frequency which is equal to half the sampling frequency (F_N =2 Hz here).

Surface wave amplitude is attenuated across the water column by a factor that is depth and frequency dependent. The relationship between surface elevation η(t) and measured pressure p(t) at the instrument depth is given by:

$$\frac{p(t)}{\rho . g} = \eta(t) . \frac{\cosh(k(h+z_{instrument}))}{\cosh(kh)} \qquad (5.3)$$

where ρ is the seawater volumic mass, g is the gravitation constant, k is the wave number, h is the total water depth, and $z_{instrument}$ is the height of the instrument sensor above the seabed.

The wave number k is related to the wave frequency f by the dispersion relationship:

$$(2\pi . f)^2 = g . k . \tanh(k . h) \qquad (5.4)$$

The transfer function K (k_n) from pressure p(t) to surface elevation η(t) is then:

$$K(k_n) = \frac{1}{\rho . g} . \frac{\cosh(k_n . h)}{\cosh(k_n . (h+z_{instrument}))} \qquad (5.5)$$

where k_n is the wave number associated with frequency component f_n of the Fourier integral. The subscript n indicates the n-th wave harmonic considered.

Even though wave frequencies up to the Nyquist frequency could theoretically be considered, in practice a high frequency cut-off is used according to sensor immersion. The cut-off frequency was estimated using the depth-limited factor of HUTT and BLACK (1997):

$$f_{cut-off} = 0.282\sqrt{g/d} \quad (5.6)$$

where g is the gravity constant, and d is the water depth above the sensor (i.e. $d=h-z_{instrument}$ where h is the total water depth, and $z_{instrument}$ is the height of the instrument sensor above the seabed.).

The highest water level experienced during the experiment yielded a factor of ~0.37 Hz at both stations which was rounded to 0.35 Hz and used for the entire pressure dataset.

To apply the transfer function $K(k_n)$ to the de-trended pressure time series were transposed in the frequency domain using a Fast Fourier Transform. Each correction factor $K(k_n)$ was applied to the real (a_n) and imaginary (b_n) components of the Fourier amplitude associated with f_n (i.e. n-th harmonic). The frequency cut-off was applied by setting the amplitudes a_n and b_n associated with $f_n > 0.35$ Hz to 0. Amplitudes associated with $f_n < 0.05$ Hz were also set to 0 to remove long waves oscillations (e.g. surfbeat) (HORIKAWA, 1988). The corrected signal was transposed back in the time domain summing all the corrected frequency components (Equation 5.2) and yielded the sea surface elevation time series.

5.2.2.3 Wave Crossing Analysis

The determination of wave height and period distributions required looking at individual waves within the time series of sea surface elevation. A single wave can be determined as the signal between two successive zero level up (or down) crossings. The wave height is the difference between the peak and trough amplitude, and the wave period is the time between the successive zero level up (or down) crossings. The time series of sea surface elevation are discrete and will rarely be exactly zero so the closest point is found.

The zero-crossing analysis was undertaken using the WAFO toolbox (BRODTKORB *et al.*, 2000). The zero down-crossing method was used since it generally provides better estimates of wave heights near the break point and in the surfzone than the up-crossing method (HORIKAWA, 1988). The crossing analysis provided individual wave heights and periods within each burst from which representative wave parameters were defined. Significant heights H sig and periods T sig (i.e mean of highest one third of waves and mean of associated periods) were principally used in the analysis but H_{10}, H_{max}, H_{rms} , and T_{mean} were

also considered for comparison. (Subscripts 10, max, and rms stand for mean of highest 1/10 of waves, maximum wave height within a burst, and root mean square height respectively).

Significant wave heights were used to compute significant wave height transmission coefficients Kt_{sig} :

$$Kt_{sig} = \frac{H\,sig_{transmitted}}{H\,sig_{incident}} \quad (5.7)$$

where $H\,sig_{incident}$ is the significant wave height measured at the seaward ADV station and $H\,sig_{transmitted}$ is the significant wave height measured at the landward ADV station ($H\,sig_i$ and $H\,sig_t$ hereafter).

To obtain distributions, height and period ranges were compartmented in bins and respective probability functions, p(H) and p(T), were defined dividing the number of individual waves falling in a given bin by the total number of waves (within a burst). The sum of probabilities for a given distribution is then 1. For some applications, the incident and transmitted probability functions were computed from the time series of wave heights H normalized by the incident significant wave height $H\,sig_i$ (i.e. $p(H / H\,sig_i)$) to facilitate the comparison of distribution shapes throughout the experiment. Depending on the incident wave periods, the wave parameters and distributions were determined based on ~ 100 to 200 waves.

5.2.2.4 Spectral Analysis

Wave energy spectra were computed following methods of EMERY and THOMSON (1997). Pressure time series were de-trended and low pass filtered to apply the frequency cut-off of 0.35 Hz. Filtering was undertaken using a 4^{th} order Butterworth filter working as a succession of 2^{nd} order filter (zero phase shift). Obtained time series were divided in 7 segments of 256 seconds with 50% overlapping. Each segment was tapered using a Hanning window and transposed to the frequency domain using a Fast Fourier Transform. A correction coefficient of $(8/3)^{0.5}$ was applied to Fourier coefficients to compensate the loss of variance due to tapering. Each frequency components was then corrected for depth attenuation (Equation 5.5). The final wave energy spectrum S(f) was obtained by averaging the spectral densities of the 7 segments. The segmentation and windowing resulted in ~ 21 (equivalent) degrees of freedom and a frequency resolution of $\Delta f = 0.0039$ Hz.

Peak period were defined as the inverse of the frequency associated with the spectral peak. Spectrally-derived significant wave heights H_{mo} were also calculated to validate the crossing-derived significant wave heights:

$$H_{mo} = 4\sqrt{m_0} \quad (5.8)$$

where $m_0 = \int_{0.05\ Hz}^{0.35\ Hz} S(f).df$

The comparison of the spectrally and crossing-derived significant wave heights showed strong agreement (included in the Appendix C).

5.3 RESULTS

The analysis begins with the description of incident wave conditions during the field deployment and a qualitative comparison with transmitted conditions. The influence of incident wave height and reef crest submergence on significant wave height transmission is then specifically investigated. Effects on the transmitted height distributions are also treated. Wave energy transmission and implications on wave period are then considered. Finally, 6 representative events are selected to illustrate the main characteristics of wave height and energy transmission over the reef.

5.3.1 WAVE CONDITIONS DURING THE FIELD EXPERIMENT

Wave conditions, wind conditions, and water levels during the field experiment are presented in Figure 5.3. During the first two days of the experiment (day 240.5 to 242.5), the incident wave field consisted of small swell waves ($H\ sig_i < 0.5$ m) of period 10-12 seconds with a northeastern direction (~30-35°). The cross-shore direction at the site is 48 °N. A tide modulation of the incident wave heights is visible with generally larger heights for higher water levels. Wind was relatively light (~0-5 m/s) and mostly from the northwest. Sometime before day 242.5, the wave period drops to ~ 5-6 seconds and this is shortly followed by an increase in wind speed from a more northerly direction, and an increase in wave height. Wave period keeps decreasing to about 5 seconds and wave direction is shifted to a more northerly incidence (10°). A more energetic wave event develops from day 243.

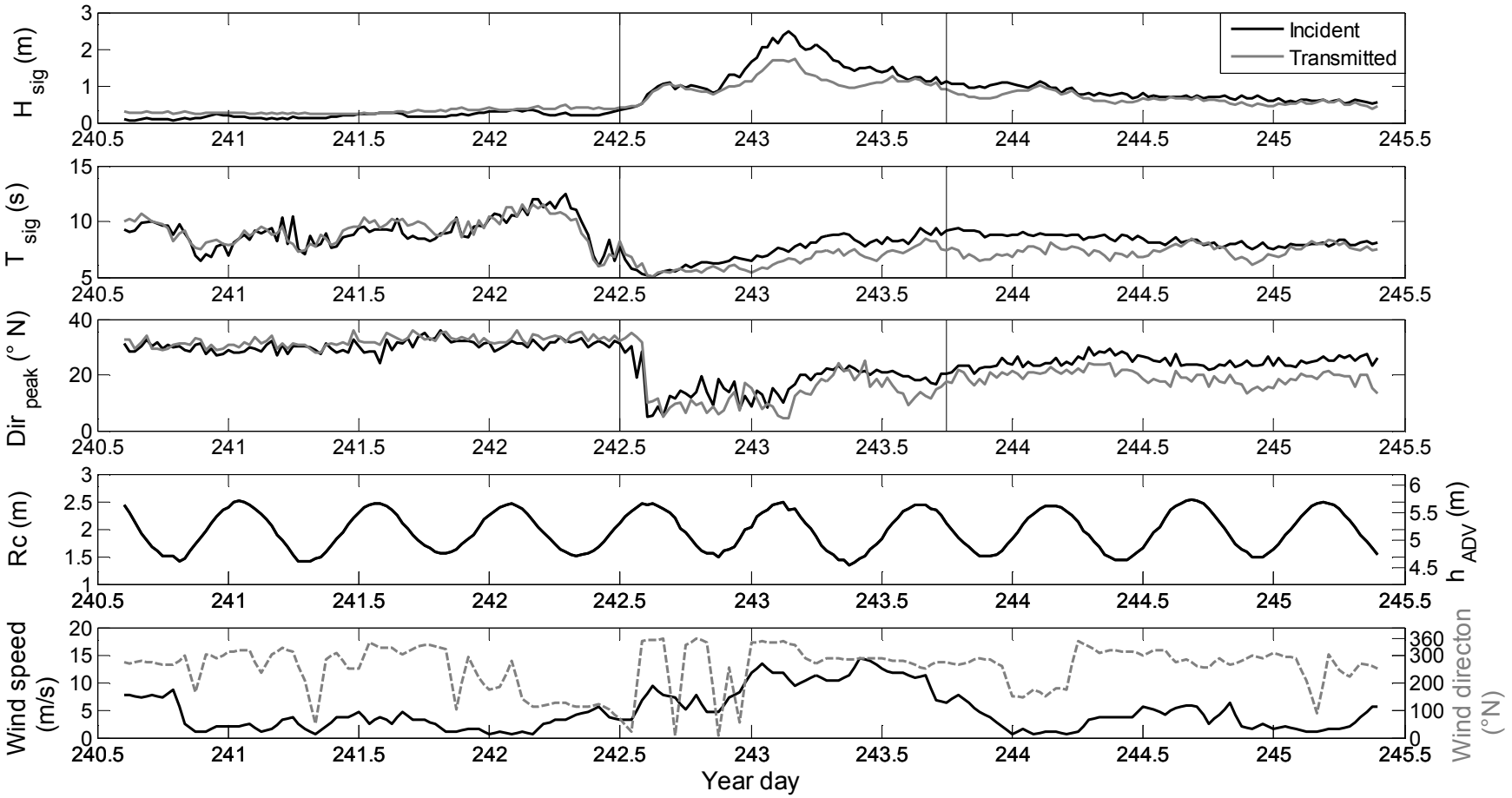

Figure 5.3. Incident (black) and transmitted (grey) wave conditions during the experiment (H_{sig}, T_{sig}, peak direction). The vertical lines separate the 3 experiment periods. Reef crest submergence Rc with corresponding water levels at the ADV stations (h_{ADV}) are represented, along with wind speed (black) and direction (grey dashed) at Tauranga Aerodrome (bottom graphic). Date is expressed as year day, 1 January 2009 being day 1. The shore-normal direction at the site is 48° N.

Incident significant height H_{sig_i} increases to 1 m in a first stage, and then up to up to 2.5 m (day 243.5). Wind becomes stronger around 10-15 m/s, firstly from the north then from the west (i.e. cross-onshore to cross-offshore). Incident heights progressively decay to ~1 m on day 244 while periods increase to ~ 8 seconds. Wave direction is shifted at 20-25 °. The end of the deployment experiences slowly easing medium waves (H_{sig_i} = 0.5-1 m) with periods of 7-8 seconds and incidence 25-30 °. Wind becomes light from the northwest.

Overall, the experiment can be divided in 3 periods (vertical lines in Figure 5.3). Period 1 is from the beginning of the deployment until day 242.5 and consists of small swell waves; period 2 is from day 242.5 to 243.75 and corresponds to more energetic wave conditions; period 3 is from day 243.5 until the end of deployment and experiences slowly easing medium waves.

Before describing the transmitted wave parameters, it seems important to gain insight into wave breaking conditions at the outer ADV station and over the reef crest. The incident significant heights H_{sig_i} are plotted against the water depth at the outer ADV station h_{ADV} and the depth over the reef crest Rc in Figure 5.4. The breaker ratio of breaker height to breaker depth $H_b / h_b = 0.78$ is represented. A ratio range from 0.65 to 1.3 found relevant to wave breaking on submerged obstacles (SMITH and KRAUS, 1991) is identified on the plot of incident height H_{sig_i} versus reef crest submergence Rc. No breaking is expected at the ADV station seaward of the reef throughout the experiment. On the other hand, waves possibly break on the reef depending of the incident conditions and crest submergence. Small waves (H_{sig_i} < 0.5-0.8 m) can propagate over the reef without breaking.

Focusing now on transmitted wave parameters on Figure 5.3 (grey lines), it is observed in period 1 that transmitted significant wave heights are consistently larger than incident for the small wave conditions experienced. More significant height amplification is observed during lower tides. This is most probably related to a more efficient wave shoaling on a shallower reef crest. Transmitted wave periods are generally similar to incident. Wave direction landward of the reef is consistently larger than the incident direction by about 2 to 4° indicating that the reef slightly refracts incident waves towards the shore normal direction (48° N).

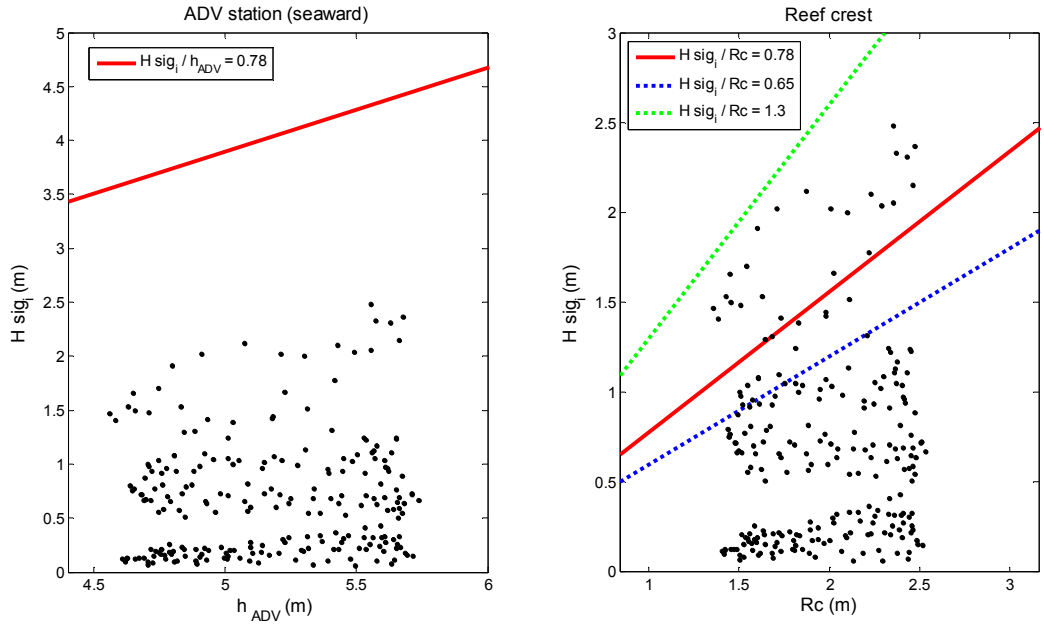

Figure 5.4. Ratios of significant wave height to water depth at the seaward ADV station (left) and over the reef crest (right). The breaker depth index of H / h = 0.78 is represented for both graphics (red line). To account for the possibly different wave breaking characteristics on the reef crest, additional ratios obtained by SMITH and KRAUS (1991) from investigations on wave breaking over submerged obstacles are represented (green and blue dashed line). No breaking is expected for data points under breaker ratio lines.

During period 2, transmitted heights are similar to incident during the first wave height increase between day 242.5 and 243. They then become significantly reduced as the second and more significant wave event develops (day 243). The transmitted heights become modulated by the crest submergence, with more important height reduction on shallow reef crests. Transmitted periods are similar to incident over the first height increase and subsequently reduced by 1 to 2 seconds as the second wave event develops. The increase in height also changes the incident/transmitted direction pattern; transmitted direction becomes generally smaller than the incident (- 4-6°) indicating waves propagating more obliquely relative to the shore after propagation over the reef.

During period 3, transmitted heights are virtually similar to incident for higher water levels but they become more significantly reduced as the water level decreases (i.e. shallower reef crest). Transmitted periods appear to be lower than incident by ~1 second at the beginning of the period and get closer to incident throughout the period. A greater period difference is observed from day 244.5 to 245 and seems to match a variation in height transmission and water level.

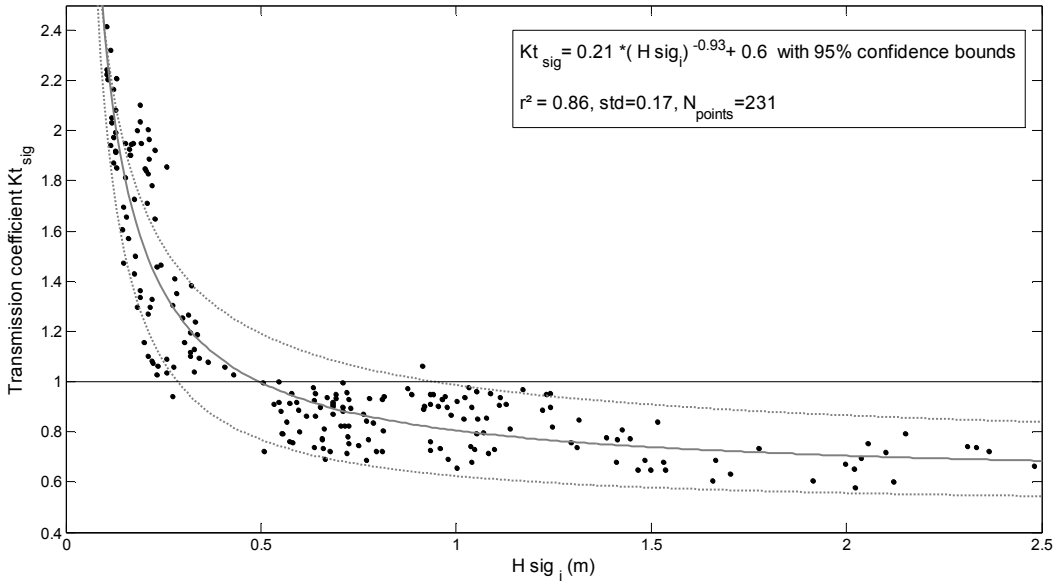

Figure 5.5. Wave height transmission coefficient Kt_{sig} as a function of incident significant wave height $H\,sig_i$. Note the switch from amplification to reduction of incident waves at $H\,sig_i \sim 0.5$ m. Three height ranges can be defined: (i) $H\,sig_i$ = 0-0.5 m, with Kt_{sig} ~1-2.5; (ii) $H\,sig_i$ = 0.5-1.5 m, with Kt_{sig} ~ 0.8-1; and (iii) $H\,sig_i$ = 1.5-2.5 m, with Kt_{sig} ~ 0.6-0.8. The dataset is correctly described by the function $Kt_{sig} = 0.21(H\,sig_i)^{-0.93} + 0.6$ (plain grey line, r^2=0.86, number of points = 231). Dashed lines represent 95 % confidence bounds.

Overall, we can distinguish 2 effects of the reef on incident wave heights during the experiment. For small incident waves ($H\,sig_i < 0.5$ m), the reef amplifies incident heights. The amplification is more significant for lower tides and thus shallower reef crests. For higher incident waves ($H\,sig_i >$ 0.5-1 m), incident heights are reduced. The reduction is more significant for lower tides and thus shallower reef crests. The switch from height amplification to reduction is reasonably explained by the start of wave breaking on the reef.

5.3.2 Significant Wave Height Transmission

The 2 different responses of reef-transmitted wave heights depending on incident heights are clearly observed in Figure 5.5 that displays significant height transmission coefficients Kt_{sig} as a function of incident significant height $H\,sig_i$. The transmission coefficient is greater than 1 for incident height $H\,sig_i \sim$ 0-0.5 m indicating that transmitted height is larger than incident. Within the range, height amplification overall increases for decreasing incident height. After the threshold height of $H\,sig_i$ = 0.5 m, transmission coefficients become consistently less than 1 indicating a switch to height reduction. There is some scatter in the data but a general decrease in transmission coefficient as the incident wave height increases is identifiable.

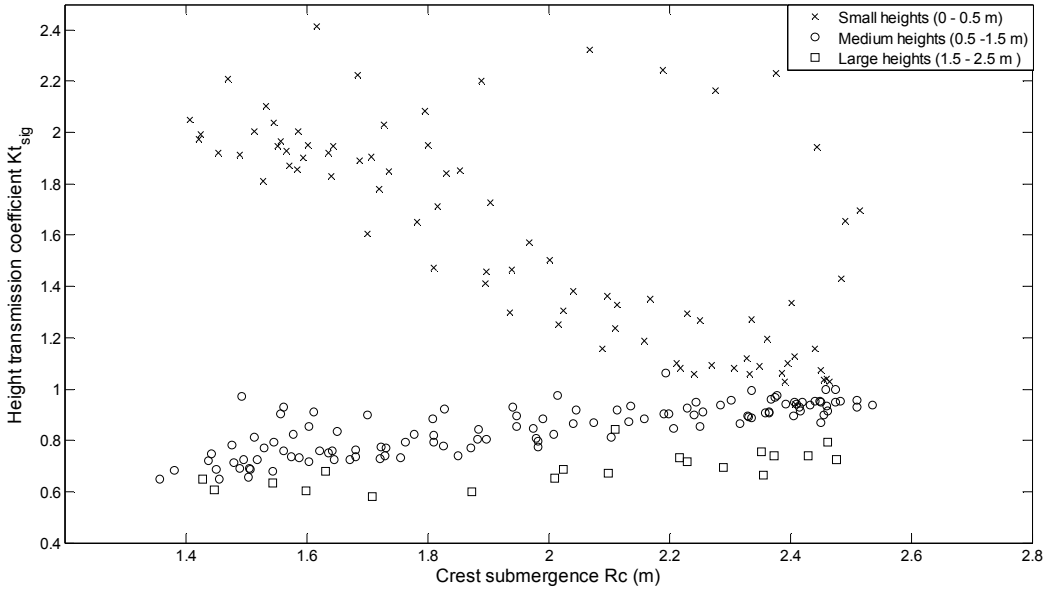

Figure 5.6. Significant wave height transmission coefficient Kt_{sig} as a function of reef crest submergence. Small, medium and large incident wave heights are indicated by cross, round and square respectively. Amplification of small incident waves increases on shallower crests. Large heights are subject to more important reduction than medium ones. Both large and medium heights describe the same trend of increased height reduction on decreasing reef crest submergence (i.e. shallower).

Two sub-groups of points can be identified for the height range $H\,sig_i$ = 0.5-1.5 m and $H\,sig_i$ = 1.5-2.5 m, with respective transmission coefficients of 0.7-1 and 0.6-0.8. Note that the 3 height ranges 0-0.5 m, 0.5-1.5 m, and 1.5-2.5 m will be used in following figures and referred to as small, medium and large respectively.

Fitting of simple functions to the dataset indicated that the relationship between Kt_{sig} and $H\,sig_i$ was well described by the power law:

$$Kt_{sig} = 0.21\,(H\,sig_i)^{-0.93} + 0.6 \qquad (r^2 = 0.86) \qquad (5.9)$$

Equation 5.9 neglects the effect of the crest submergence that has some apparent effects in Figure 5.3, however, the good correlation indicates that $H\,sig_i$ only can give a reasonable first approximation of the transmission coefficient.

The effect of reef crest submergence on height transmission coefficient is investigated in Figure 5.6. The 3 wave height ranges are represented using different symbols. For small waves, the trend of greater height increase on shallower crests is visible. Large wave heights are more reduced that medium ones, as expected from Figure 5.5, but respective data points follow the same trend of increased reduction on shallower reef crest.

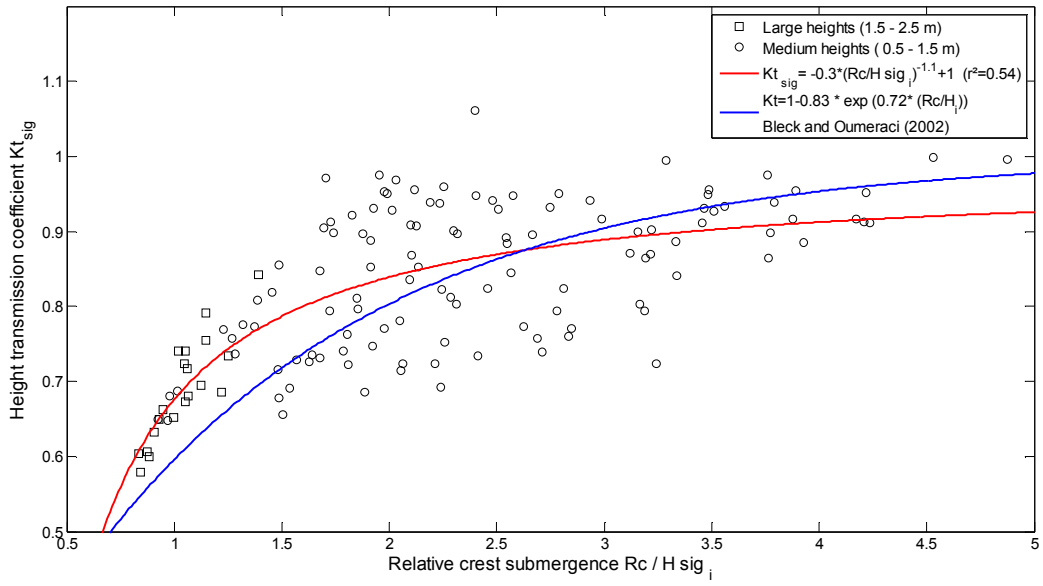

Figure 5.7 Significant wave height transmission coefficient Kt_{sig} as a function of relative crest submergence $Rc/H_{sig\,i}$. Medium (round) and large (square) incident significant heights are identified. There is a trend of increased height reduction on smaller relative crest submergence. Note the accelerated reduction of large heights with a near linear relationship (square). The main trend of the dataset (red line $r^2 = 0.54$) is comparable to the empirical relationship of BLECK and OUMEARCI (2002) (blue line) derived from experiments on a simple rectangular submerged reef.

A dimensionless parameter that is commonly used and often of dominant importance in wave transmission studies is the relative crest submergence $Rc / H_{sig\,i}$ (e.g. SEABROOK and HALL, 1998; BLECK and OUMERACI, 2002; FRIEBEL and HARRIS, 2004; BLENKINSOPP and CHAPLIN, 2008). Application of the parameter was problematic for small waves because smallest heights yielded sometimes very large ratios $Rc / H_{sig\,i}$ that scattered the data points. This complicated the interpretation and is therefore not shown. However, a more defined trend is observed for medium and large heights (Figure 5.7). The dependence of transmission coefficient on relative crest submergence is strong for large heights with is a near linear decrease of Kt_{sig} in response to decreasing relative crest submergence (square symbols). The medium wave data points (round symbols) are more scattered but it is seen that the mean trend slope is milder than for large heights. This indicates that the medium height range is relatively less sensitive to the relative crest submergence (i.e. less reduction in Kt_{sig} for same reduction of relative submergence).

For comparison, an empirical relationship obtained by BLECK and OUMERACI (2002) on a simple smooth rectangular submerged reef is represented and a fitting function of the present dataset estimated to give the main trend. Overall both

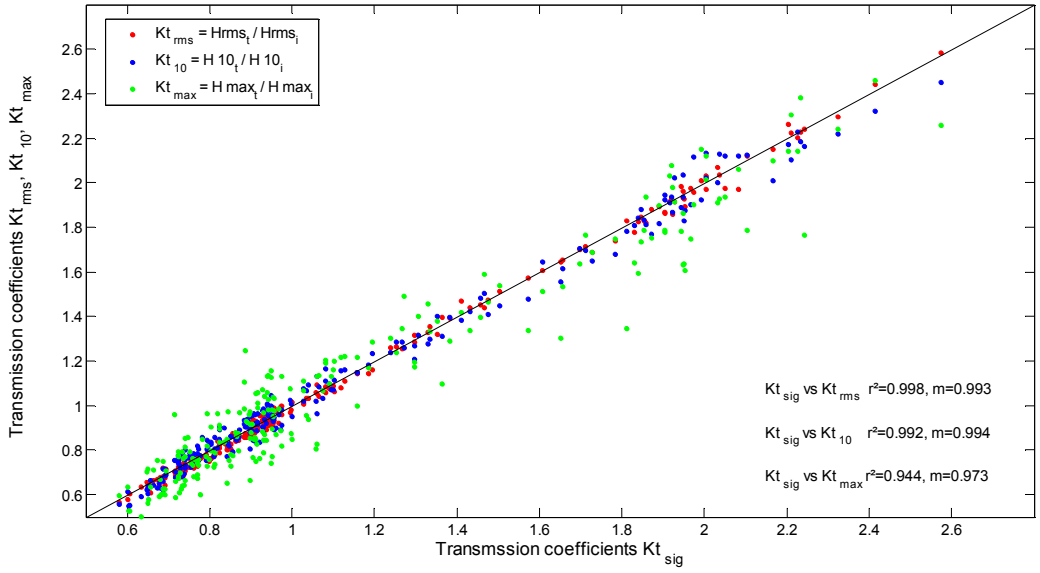

Figure 5.8. Comparison of transmission coefficients computed from incident and transmitted significant, root mean square, highest 1/10, and maximum wave heights, Kt_{sig}, Kt_{rms}, Kt_{10}, Kt_{max} respectively. A strong agreement between the coefficients is found (r^2>0.99) with slopes very close to 1 indicating virtual equality. Kt_{sig} and Kt_{rms} have the strongest correlation.

curves describe the same pattern of accelerated height reduction for decreasing relative crest submergence (i.e. height increase and/or crest submergence decrease). The main difference between the present dataset and the equation of BLECK and OUMERACI (2002) is for smallest relative crest submergences for which our measured Kt_{sig} are consistently higher and tend to increase quicker than those predicted (for a simple rectangular submerged reef).

The last 2 figures showed the relationships between significant wave height transmission coefficients Kt_{sig} and (i) incident height, and (ii) crest submergence or relative crest submergence. Since a range of different wave height parameters can easily be derived from the wave crossing analysis, it is interesting to look at how respective transmission coefficients will compare with the "significant" transmission coefficients considered so far. A comparison of Kt for H_{rms}, H_{10} and H_{max} is given in Figure 5.8. The subscripts stand for root mean square height, mean height of highest 1/10 of waves, and maximum height respectively. All 3 transmission coefficients Kt_{rms}, Kt_{10}, and Kt_{max} are found to be strongly correlated with Kt_{sig}. Slopes of linear regressions are very close to 1 indicating a quasi equality of coefficients. The consistence of the different Kt coefficients indicate that the coefficient Kt_{sig} provide a correct representation of the general height transmission characteristics of a given incident wave field, for given crest

submergence. Moreover, another implication is that the relationships identified previously apply for these parameters as well. This is particularly interesting for H_{rms} since the parameter is often used in numerical models to provide a measure of the overall energy of an irregular wave field (e.g. BATTJES and JANSEN,1978; THORNTON and GUZA, 1983). Obtained Kt_{sig} and Equation 5.9 could provide a direct calibration basis for modeled H_{rms}.

5.3.3 WAVE HEIGHT DISTRIBUTION TRANSMISSION

The coefficient of significant wave height transmission provides a compact mean to describe transmission characteristics, however, a more complete representation of the reef effect on the irregular incident wave field can be obtained comparing incident and transmitted wave height distributions. Incident and transmitted probability functions were computed from the sets of wave heights H measured within each burst normalized by the corresponding incident significant wave height $H\,sig_i$. This allows consistent comparison of wave distributions shapes and ranges with respect to $H\,sig_i$ (i.e. amplification or reduction) throughout the experiment period. Computed wave height distributions are shown in Figure 5.9. Note that according to Figure 5.4, the incident distribution describes unbroken waves while the transmitted distribution may describe, unbroken, broken or combination of both, depending on incident wave conditions and crest submergence.

The incident height distribution shape is consistent throughout the experiment. Waves are mostly comprised between 0 and 1.5 $H\,sig_i$ and peak probabilities centered around 0.5 $H\,sig_i$. In contrast, the transmitted distributions exhibit significant changes throughout the experiment period. The effect of reef crest submergence is obvious in period 1. Transmitted distributions become distributed up to about 3 $H\,sig_i$ for shallow crest submergence. For deeper reef crests though, transmitted distributions are mostly similar to incident. Incident and transmitted distributions are similar at the beginning of period 2, however, a distinct truncation of the transmitted distribution is observed as the second wave event starts. It is the most obvious on shallow reef crests between 243 and 243.5, with reduction of all waves higher that ~ 0.8 $H\,sig_i$ (see white dashed line). As the incident wave conditions decay throughout period 3, this behavior is conserved for shallow reef crests but with a larger threshold before truncation of ~ 1 $H\,sig_i$. Simultaneously, the probabilities for smaller (transmitted) waves are increased.

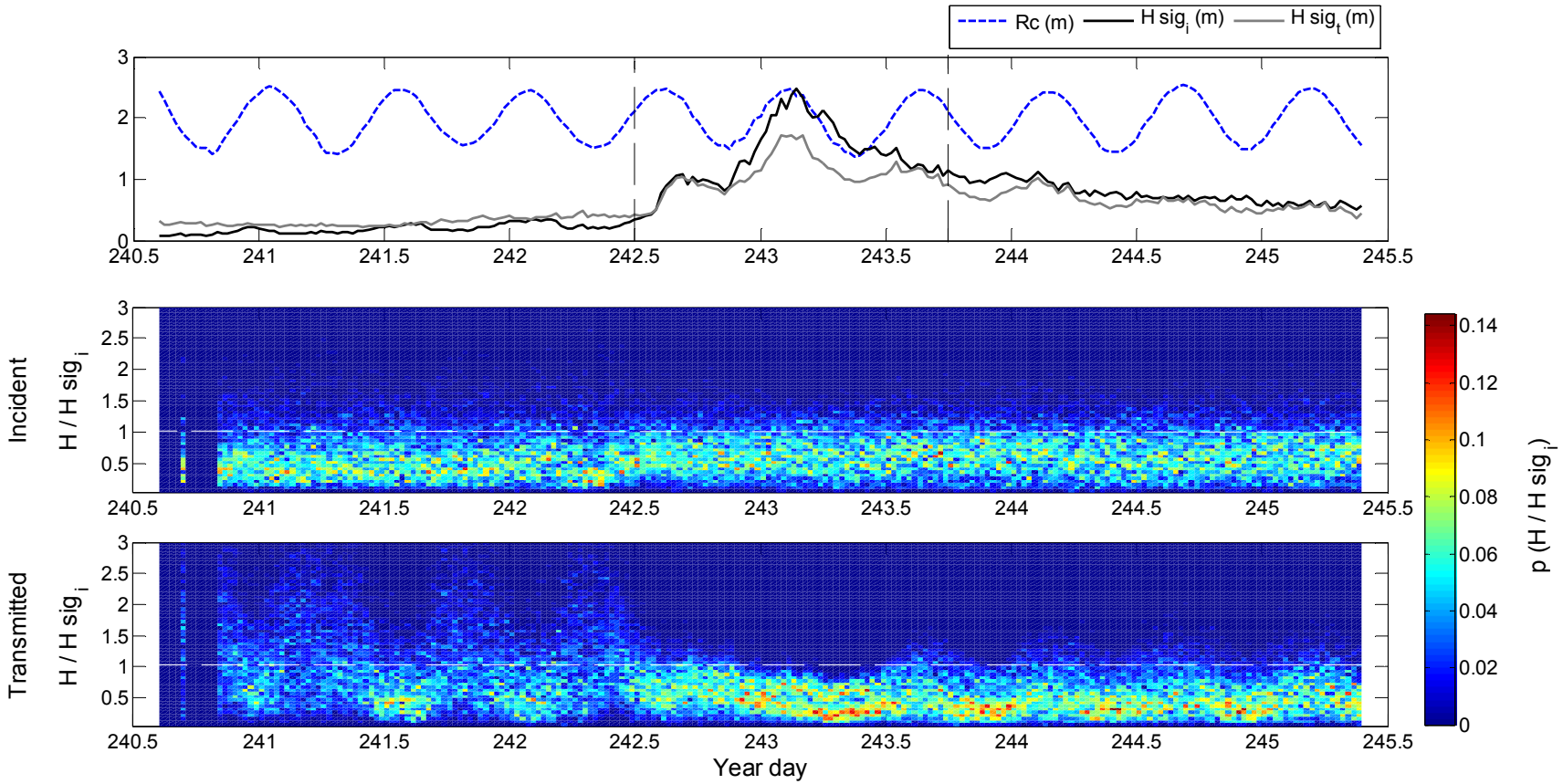

Figure 5.9. Incident and transmitted normalized wave height distributions p(H/H sig $_i$) during the experiment. Incident and transmitted significant heights and reef crest submergence Rc are shown for comparison, along with the 3 experiment periods (vertical lines) (top graphic). The horizontal white dashed line on the distribution graphics is at H/H sig $_i$= 1 and is shown for comparison of distribution ranges. Note the strong influence of the reef crest submergence in period 1 for small incident waves. Transmitted wave heights are redistributed up to 3 H sig $_i$ on shallow reef crests. A distinct truncation of the distribution above ~ 0.8 H sig $_i$ is observed for large waves and dissipative conditions around day 243-243.5 (period 2). This response is conserved on shallow reef crests for medium waves throughout the end of experiment (period 3) but with a higher truncation threshold (~1 H sig $_i$).

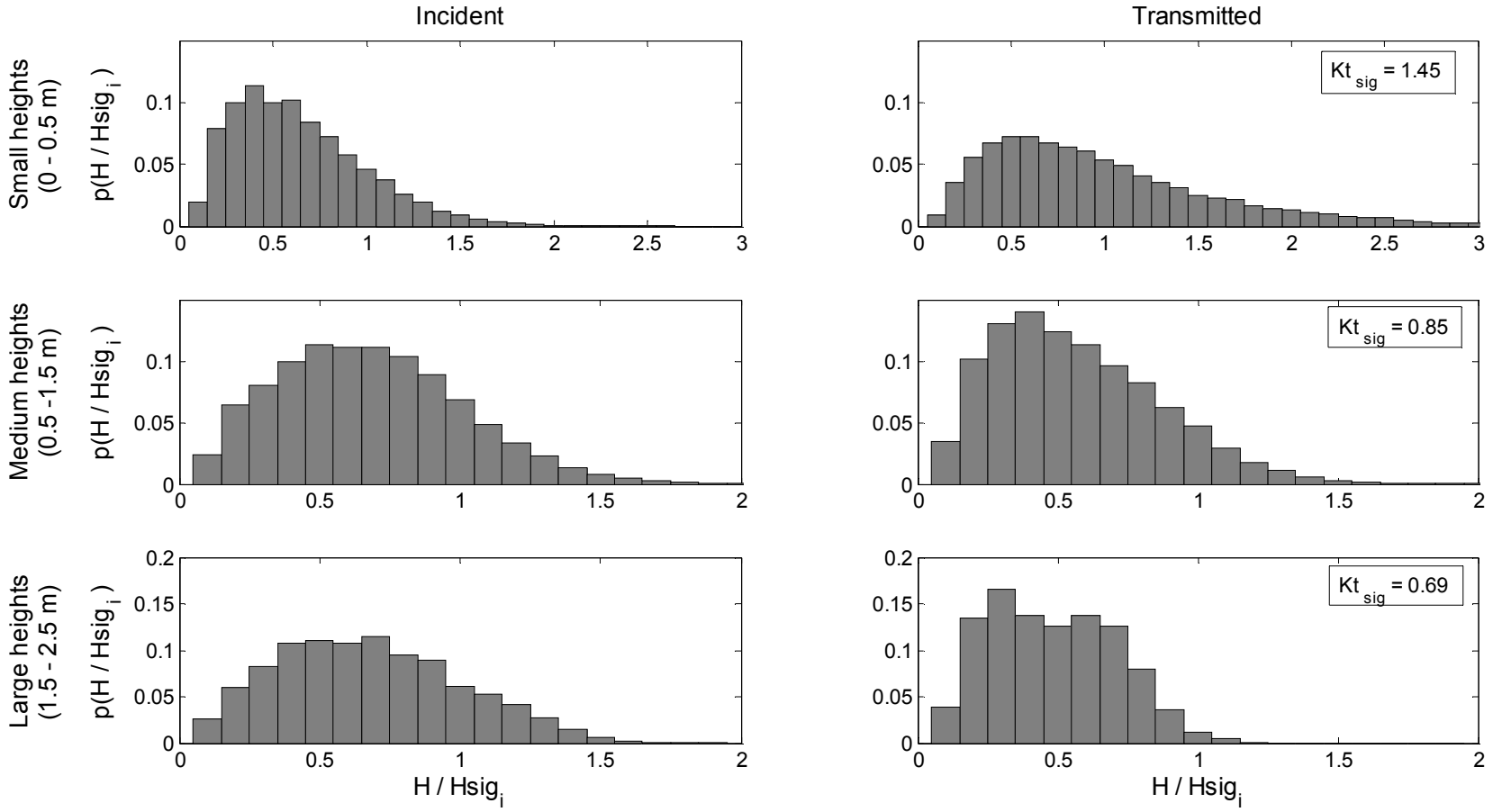

Figure 5.10. Averaged incident and transmitted normalized height distributions for small, medium and large incident waves, with associated mean significant wave height transmission coefficient Kt_{sig} .

To outline these responses, wave height distributions obtained for each of the 3 range of incident heights were separately averaged (Figure 5.10). The mean distribution obtained for the small waves (top) shows the widening of the height range towards higher heights. The probabilities of waves between 0 to 1 H sig $_i$ seaward of the reef are reduced and redistributed up to 3 H sig $_i$ landward of the reef. For medium waves (middle), the transmitted height range is similar to incident, however, the probability function peak is shifted from ~ 0.6 H sig $_i$ to ~ 0.4 H sig $_i$ and highest waves are reduced. The transmitted distribution shape is more significantly changed for large incident waves (bottom). The distribution tail is truncated at ~ 1 H sig $_i$ indicating a redistribution of all incident waves greater than this threshold to the lower range 0-1 H sig $_i$.

5.3.4 WAVE ENERGY TRANSMISSION

The comparison of incident and transmitted wave energy spectra can give information on how much of the total incident wave energy is amplified or dissipated by the reef, and also on any change of the wave energy distribution within the frequency domain. In addition to linear propagation effects prior to wave breaking such as amplitude increase and wavelength decrease due to linear shoaling, non linear interactions become increasingly important as the water depth gets shallower and may be responsible for significant transfers of energy to wave components with both higher and lower frequencies (e.g. ELGAR and GUZA, 1985; MASSELINK, 1998; RUESSINK, 1998). For the present case, the sharp depth change over the reef crest after wave propagation on a natural profile may further stimulate the non linearity of incident waves. Indeed, a common observation of waves propagating over submerged obstacles is the generation of high frequency harmonic energy (i.e. at multiple of f_{peak}) during the shoaling process and possible decomposition of incident primary waves into smaller and shorter transmitted waves in the deeper waters landward of the obstacle. These obstacles may be nearshore bars (MASSELINK, 1998; SENECHAL *et al.*, 2002), natural reefs (YOUNG, 1989), artificial reefs (BLECK and OUMERACI, 2002) or submerged breakwaters (VAN DER MEER, 2001).

The transmission of incident wave energy over the study reef is investigated comparing normalized incident and transmitted wave energy spectra during the experiment period (Figure 5.11). Both incident and transmitted spectral densities are normalized by the incident peak spectral density $(S_i)_{peak}$ so that magnitudes of

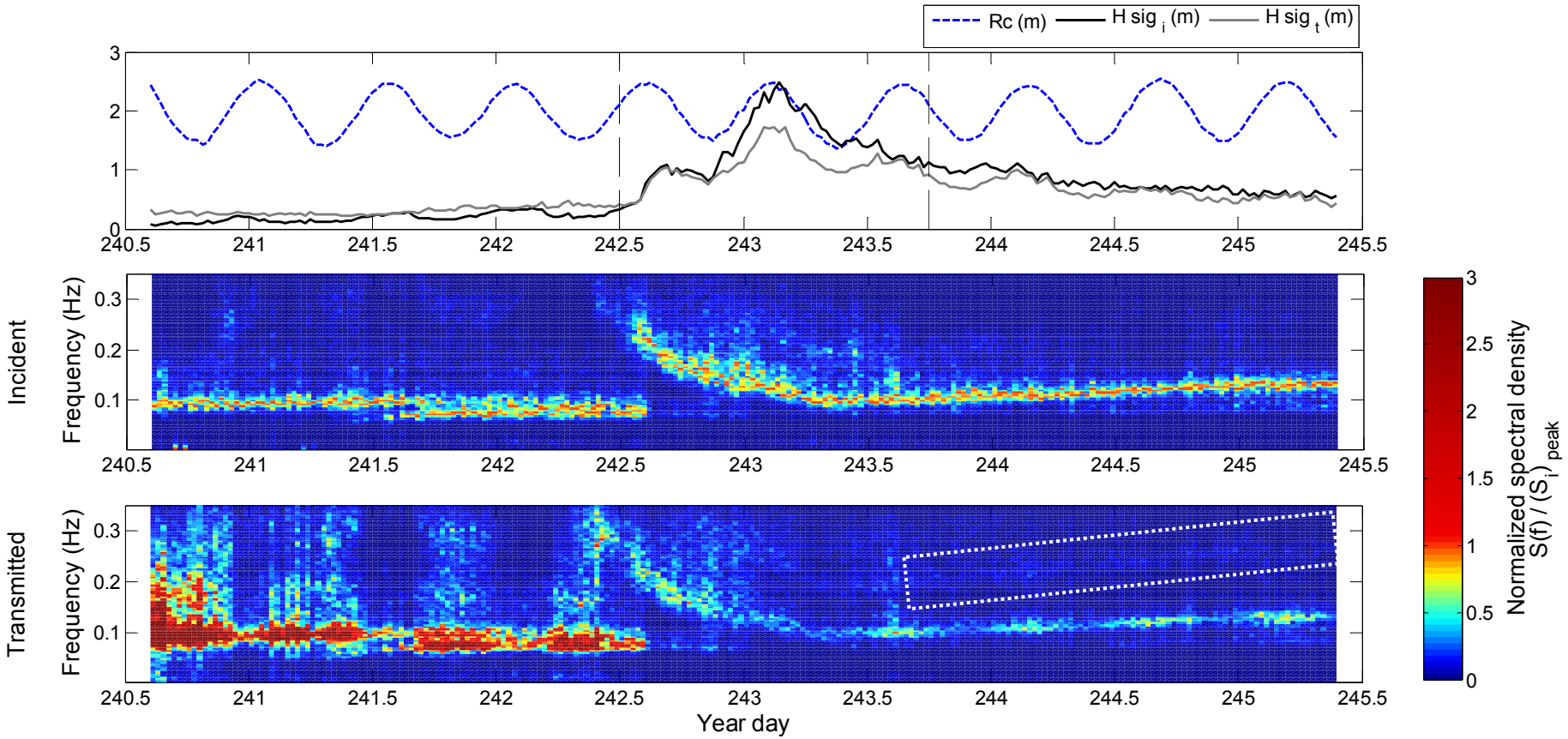

Figure 5.11. Incident and transmitted normalized wave energy spectra during the experiment. Incident and transmitted spectral density functions S(f) are normalized by the incident peak spectral density $(S_i)_{peak}$. Incident and transmitted significant heights and reef crest submergence Rc are shown for comparison, along with the 3 experiment periods (vertical lines) (top graphic). Note the strong amplification of incident peak energies in period 1 for shallow reef crests, and the development of new energy peaks near harmonic frequencies 2 f_{peak} and 3 f_{peak}.. Wave energy dissipation starts in period 2 and is the most obvious between day 243 and 243.5 for shallow reef crests. The dissipation of peak energy becomes clearly modulated by the reef crest submergence in period 3. Note the harmonic energy "line" near 2 f_{peak} throughout the period 3 in transmitted spectra (dashed white feature).

energy dissipation or amplification can be more easily identified. Focusing first on incident spectra, relatively narrow banded wave energy is observed in period 1, with peak frequency around ~ 0.1 Hz. There is some energy at higher frequencies along with several events exhibiting energy at infragravity frequencies ($f < 0.05$ Hz). A second energy peak develops slightly above 0.05 Hz on day 241.5. Spectra are double-peaked for about half a day indicating a superimposition of 2 swell fields and the peak frequency is then progressively re-centered at 0.1 Hz.

In period 1, transmitted wave energy spectra are subject to a distinct rhythmic pattern matching the oscillations of the reef crest submergence. Shallower reef crests are associated with more significant amplification of the peak energies and growth of wave energy at higher frequencies (0.15-0.35 Hz). The peak energy amplification is due to a more efficient shoaling on a shallower reef crest. This was also present in transmission coefficients and distributions (see Figure 5.6 and 5.9). Some new energy peaks seem to develop near harmonic frequencies ($2\ f_{peak}$ and $3\ f_{peak}$) indicating that some harmonic wave decoupling likely occurred as waves propagated over the reef. The shoaling of the high frequency energy initially present in the incident field may also have contributed to some extent to the apparent growth of high frequency energy. That being, the shoaling process is expected to be a lot less significant for incident short period waves than it is for longer period waves.

The rhythmic pattern stops around day 242.5 and the transition to the period 2 is marked by the development of a mixed swell/sea wave field with two spectral peaks at 0.1 Hz (swell) and 0.2-0.25 Hz (sea waves). The underlying swell has fully decayed when the first increase in wave height occur at day 242.75. Incident and transmitted spectra are then very similar with respect to peak frequency ($f_{peak} \sim 0.2$ Hz) and peak energy magnitude. The incident wave energy becomes broader banded from day 243 with most of the energy within the frequency band 0.1-0.15 Hz. The dissipation of incident energy after propagation (and breaking) over the reef is evident in the transmitted spectra. The most intense wave energy dissipation is observed between day 243 and 243.5 and coincides with shallow reef crests. This interval was associated with the lowest transmission coefficients measured over the experiment ($Kt_{sig} \sim 0.55$).

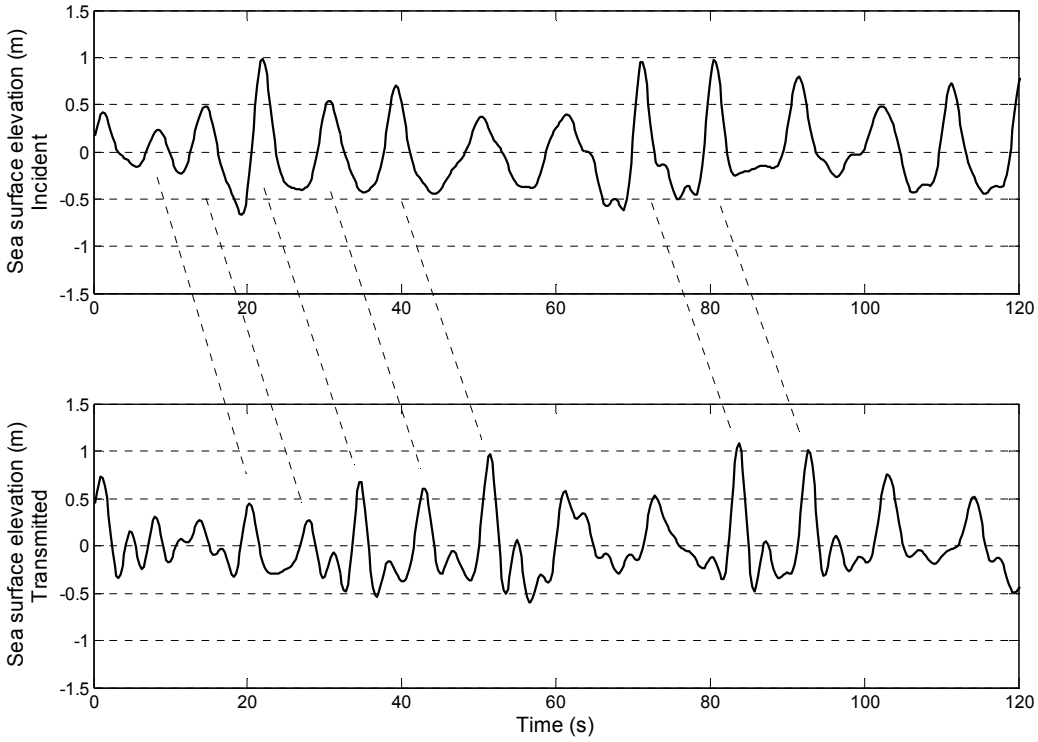

Figure 5.12. Segment of de-trended sea surface elevations time series measured seaward (top) and landward (bottom) of the reef at year day 243.9. The dotted lines follow the wave fronts along their propagation towards the beach. The incident waves are already strongly non linear and have steep and asymmetric profiles (top). The release of secondary harmonic waves landward of the reef is visible on the transmitted sea surface elevation record (bottom).

The incident wave energy slowly decays and becomes narrower banded from day 243.5 and throughout period 3, with the peak frequency f_{peak} going from 0.1 to 0.15 Hz. A rhythmic pattern reappears in the transmitted spectra consisting of more important peak energy dissipation on shallower crests and lessened dissipation on deeper crests. The peak frequencies are conserved. Concurrent with the peak energy dissipation, an interesting feature is the development of some high frequency energy predominantly at twice the peak frequency. Associated energy is still small relative to peak energy but careful observation of the transmitted wave energy spectra for the frequency band 0.15-0.25 Hz does show a line of increased energy near ~ 2 f_{peak} throughout the period (see dashed white feature in Figure 5.11). The frequency associated with this new wave energy increases simultaneously with the peak frequency confirming a predominant transfer to the harmonic frequency 2 f_{peak}. This harmonic energy seems to have maximas during milder energy dissipation as experienced over deeper reef crests. This possibly indicates that the energy transfer benefits from less intense breaking conditions. Again, it is noted that some energy was already present at higher frequencies in the incident spectra and may contribute to the transmitted high

frequency energy. However, the incident high frequency energy still appears rather uniformly distributed which contrasts with the distinct harmonic energy "line" on the transmitted spectra.

In agreement with the harmonic energy transfer, the decomposition of incident waves into smaller and shorter waves was consistently observed in respective time series of sea surface elevation. An example is given in Figure 5.12. It is seen that the incident waves are already clearly non linear with steep and asymmetric profiles. They may even naturally develop so-called tail waves (e.g. MASSELINK, 1998) right behind the primary crest (t = 60-80 h, Figure 5.12). The generation and decoupling of secondary waves from primary waves is well seen in the sea surface elevation time series measured landward of the reef.

To compare more objectively the spectral shape evolution, incident and transmitted wave energy fluxes were distributed into three components: (1) primary wave energy (0.05 Hz-1.5 f_{peak}), (2) high frequency energy (1.5 f_{peak} to 0.035 Hz), and (3) total wave energy (0.05-0.35 Hz). The flux of energy of each component was computed from the sea surface elevation spectra (assuming shoreward progressive waves without reflection) integrating the energy flux over the considered frequency band:

$$EC_g = \int_{f1}^{f2} S(f).C_g(f).df \qquad (5.10)$$

where EC_g is the energy flux, C_g (f) is the wave group velocity associated with the frequency f, S(f) is the spectral density associated with the frequency f, and f_1 and f_2 are the cut-off frequencies of each band.

The group velocity is given by:

$$C_g(f) = \frac{2\pi.f}{2k}\left(1 + \frac{2kh}{\sinh 2kh}\right) \qquad (5.11)$$

where the wave number k is related to frequency f by the dispersion relationship (Equation (5.4)).

Energy fluxes in the primary and high frequency bands for both incident and transmitted wave fields were then normalized by the total *incident* energy flux to obtain relative distributions. For the transmitted wave conditions, energy flux distributions were also determined with respect to the total *transmitted* energy

Table 5.1. Ratios of wave energy fluxes in total, primary, and high frequency bands for small, medium and large waves.

Small incident waves (H sig $_i$ = 0- 0.5 m)			
	Total	Primary	High frequency
Incident	1	0.75	0.25
Transmitted	2.6	1.9 (0.73 of total transmitted)	0.7 (0.27 of total transmitted)

Medium incident waves (H sig $_i$ = 0.5- 1.5 m)			
	Total	**Primary**	**High frequency**
Incident	1	0.86	0.14
Transmitted	0.67	0.5 (0.75 of total transmitted)	0.17 (0.25 of total transmitted)

Large incident waves (H sig $_i$ = 1.5- 2.5 m)			
	Total	**Primary**	**High frequency**
Incident	1	0.74	0.26
Transmitted	0.48	0.3 (0.63 of total transmitted)	0.18 (0.37 of total transmitted)

flux. Average distributions are given in Table 5.1 for each wave height range (small, medium, large).

Comparing first total energy ratios, we observe, as expected, the wave energy amplification for small waves, and the 2 levels of wave energy dissipation for medium and large waves. For small waves (non breaking), the high frequency energy landward of the reef becomes almost three times as much as the one seaward of the reef, thus reaching a level equivalent to the incident primary wave energy. The primary energy is increased in similar proportion (i.e. ~3 times) resulting in a transmitted energy distribution similar to the incident (primary frequency/high frequency ~ 75/25 %). For medium waves, the energy on the high frequency band is slightly increased landward of the reef while ~ 40 % of the primary energy is dissipated. This height range was mainly observed in period 3 when there was evidence of harmonic energy generation (Figure 5.11 and 5.12) so this increase seems coherent. Significant dissipation of both primary and high frequency energy is observed for large waves. The primary energy is however

much more efficiently dissipated (-60%) than that at high frequency (i.e. shorter period waves) (-30%). Overall for medium and large waves, it appears that the reef significantly filters the primary wave energy through breaking-induced dissipation, while the high frequency energy band is less impacted, and even possibly amplified for medium waves. This results for both cases in a larger proportion of high frequency energy within the transmitted wave field.

5.3.5 WAVE PERIOD TRANSMISSION

The larger proportion of high frequency wave energy indicates that there are more short-period waves in the transmitted wave field than in the incident. The implication is a possible reduction of representative wave period parameters. This is investigated in Figure 5.13 where transmitted peak, significant, and mean periods are compared to incident for small, medium and large incident wave heights. The generation of high frequency energy was the most obvious for small waves (Figure 5.11), however, the comparison of incident and transmitted period parameters do not show any defined trend (top). Peak periods are generally conserved except for the highest incident periods where some deviations occur. Significant and mean periods can be increased or reduced by up to about 2 second. In contrast, both medium and large heights (Figure 5.13, middle and bottom) show a distinct trend of reduction of mean and significant wave periods landward of the reef. For medium waves, the mean and significant wave period reduction tends to increase for increasing incident periods, with transmitted period parameters possibly up to 3 seconds smaller than incident. This seems coherent since both breaking-induced dissipation of primary energy and non linear interactions, that are responsible for the modified transmitted energy distribution, are more intense for longer period waves. Peak periods are mainly conserved except for several large wave events for which T_{peak} are reduced. This may be explained by the more intense breaking-induced dissipation of longer wave periods, possibly shifting T_{peak} to shorter values.

Since the dissipation of incident wave heights was modulated by the relative crest submergence (Figure 5.7) and that the ratio Rc / H sig $_i$ may also be regarded as a simple measure of wave non linearity (BLECK and OUMERACI, 2002), the modification of the wave energy distribution, and in turn the wave period reduction, should be related to the relative crest submergence too. This is tested for each height range in Figure 5.14 where ratios of transmitted to incident period

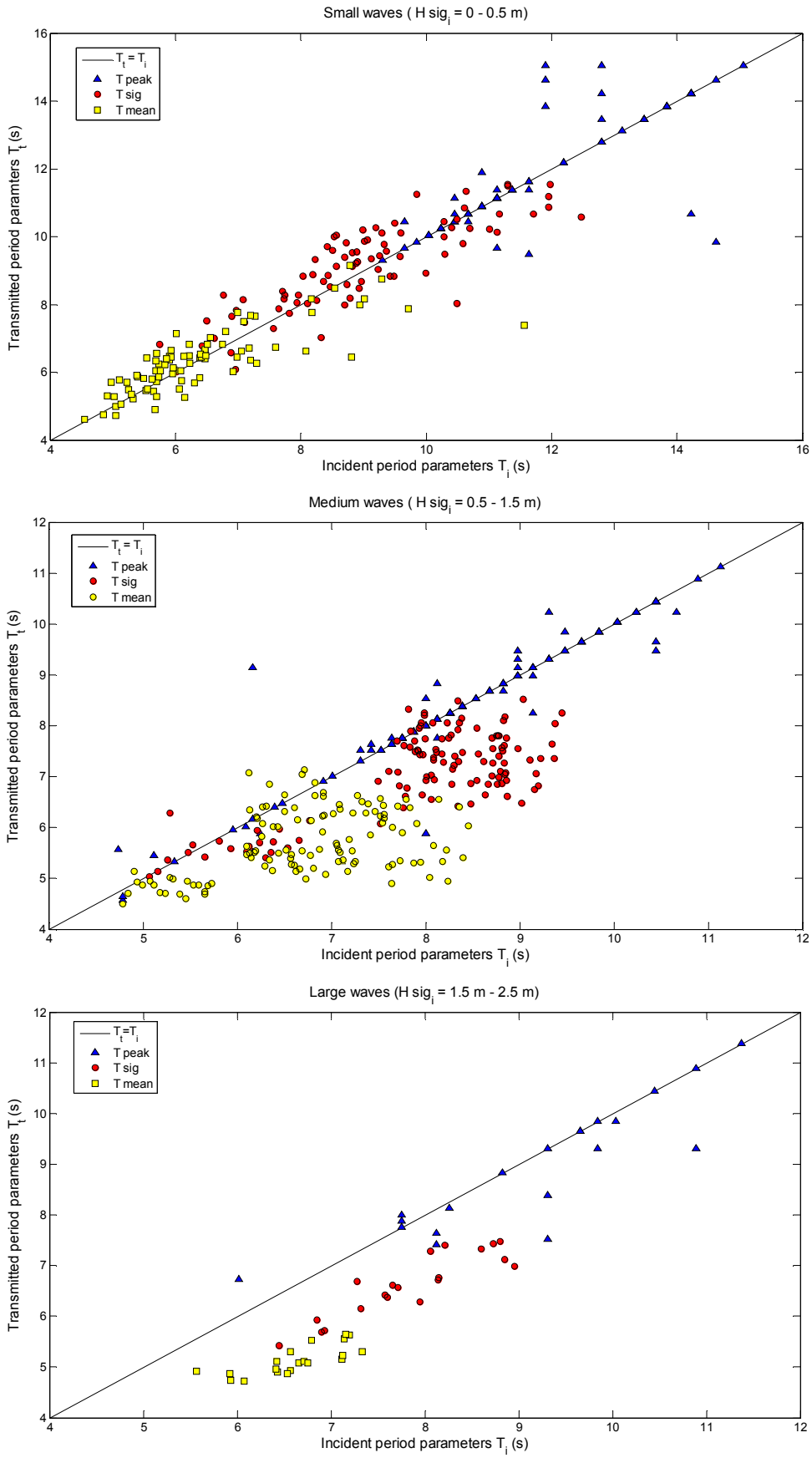

Figure 5.13. Transmitted peak, significant, and mean wave periods as a function of respective incident periods for small, medium, and large waves (top to bottom). The black line indicates period conservation. Note the consistent reduction of significant and mean wave periods for medium and large waves. Peak periods are generally conserved.

parameters (peak, significant and mean) are plotted against relative crest submergence.

For small waves, a trend that was possibly masked in the scatter obtained comparing incident and transmitted periods (Figure 5.13, top) was a predominant period reduction on shallow reef crests, when most of the high frequency energy was generated. However there is surprisingly no evidence of such relationship in Figure 5.14 (top). A possible explanation for the less evident transmitted period response of small waves is that the transmitted wave energy, although being amplified, conserved its relative distribution i.e. ratios primary/high frequency energy (Table 5.1).

A more distinct relationship is observed for medium waves with increasing mean and significant period reduction on decreasing relative crest submergence. Peak periods are mainly conserved and do not show any evident dependence on relative crest submergence. The reduction of the significant wave periods is less evident for large heights, but the mean period still tends to decreases on smaller relative crest submergence. Note that the large heights were sustained only during only about 1 tidal cycle which is not ideal to test the dependence of crest submergence.

The obtained relationships make overall sense however looking back to Figure 5.12, a relatively contradictory feature is that for medium wave heights in period 3, the harmonic energy generally had maximas on deep rather than shallow reef crests. As the period reduction overall responds to decreasing crest submergence, the modification of the wave energy distribution (which induces the period reduction) is probably predominantly due to the focus of the breaking-induced dissipation on the primary wave energy (which is increasingly efficient for decreasing relative crest submergence Figure 5.6 and 5.7) rather than to the generation of high frequency harmonic energy. That being, it is seen in Figure 5.14 (middle) that most important period reductions (- 40 %) did not occur on smallest relative crest submergences and rather for $Rc/H\,sig_i$ around 1.5. This offset may indicate that most significant period reductions would occur in intermediate submergence conditions, when both breaking of longer period waves and secondary wave generation act in combination.

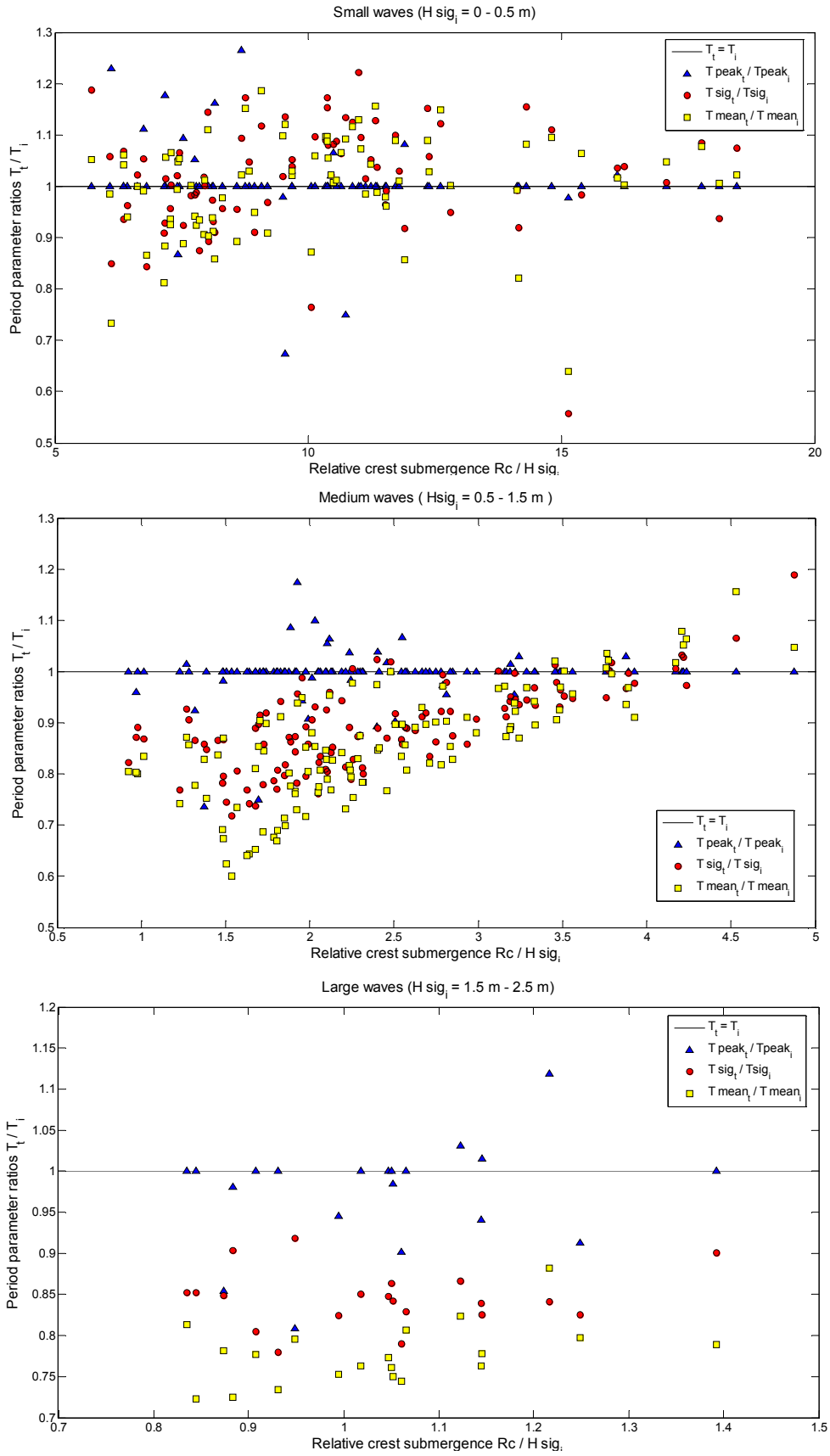

Figure 5.14. Ratios of transmitted to incident peak, significant, and mean periods as a function of relative crest submergence for small, medium and large waves (top to bottom). The black line indicates period conservation. Note the decrease of significant and mean period ratios (i.e more important period reduction) on smaller relative crest submergence for medium and large waves.

5.3.6 REPRESENTATIVE EVENTS

The relationships obtained from the precedent figures are outlined in a range of representative events. Both incident heights and crest submergence were found to have important effect on the wave transmission characteristics, therefore 2 events with shallow and deep crests are selected within each of the incident height ranges (small, medium, large).

5.3.6.1 Small Waves

a) Shallow crest Rc=1.6 m, year day 241.8 (Figure 5.15)

The 2 main transformation of the incident wave energy spectrum after wave propagation over the reef are the amplification of energy at the spectral peak and the growth of energy at higher frequencies (0.15-0.35 Hz). More defined energy bulges are present at 0.14 and 0.16 Hz, close to harmonic frequency 2 f_{peak} of the primary peaks. The wave energy amplification is visible in the transmitted height distribution that displays a reduced number of small waves (H=0-0.3 m) and the development of larger waves distributed up to 0.9 m. This is reasonably explained by the shoaling of incident heights as they propagate over the shallow reef crest. The physical effect of a wave energy transfer to harmonic frequency is that incident primary waves can decompose into smaller, shorter waves (e.g. Figure 5.12). This is observed in the greater number of waves measured at the landward station, and the development of a new peak on the transmitted period distribution at 3-4 s, which in turn induces a reduction of the significant wave period.

b) Deep crest Rc=2.5 m, year day 242 (Figure 5.16)

As seen in the rhythmic pattern present in Figure 5.11 (period 1), energy amplification is less obvious for this deep crest event. Peak energy is only slightly increased. The difference in high frequency energy seaward/landward of the reef is not obvious and less secondary waves are generated.

5.3.6.2 Medium Waves

a) Shallow crest Rc=1.5 m, year day 243,9 (Figure 5.17)

The switch to dissipative conditions is evident in the transmitted energy spectrum with reduction of the peak energy by about 70 %. On this case some high frequency energy was already present seaward of the reef with a bulge of energy centered around the harmonic frequency 2 f_{peak} = 0.22 Hz. This is less defined

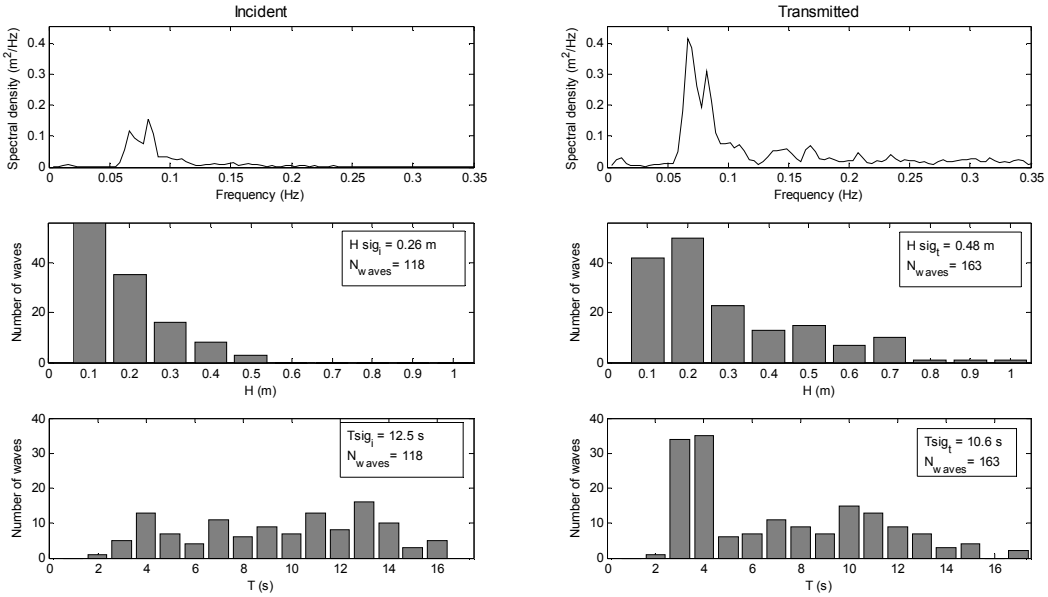

Figure 5.15. Incident and transmitted wave energy spectra, height distributions, and period distributions for small incident waves and a shallow reef crest Rc=1.6 m (year day 241.8).

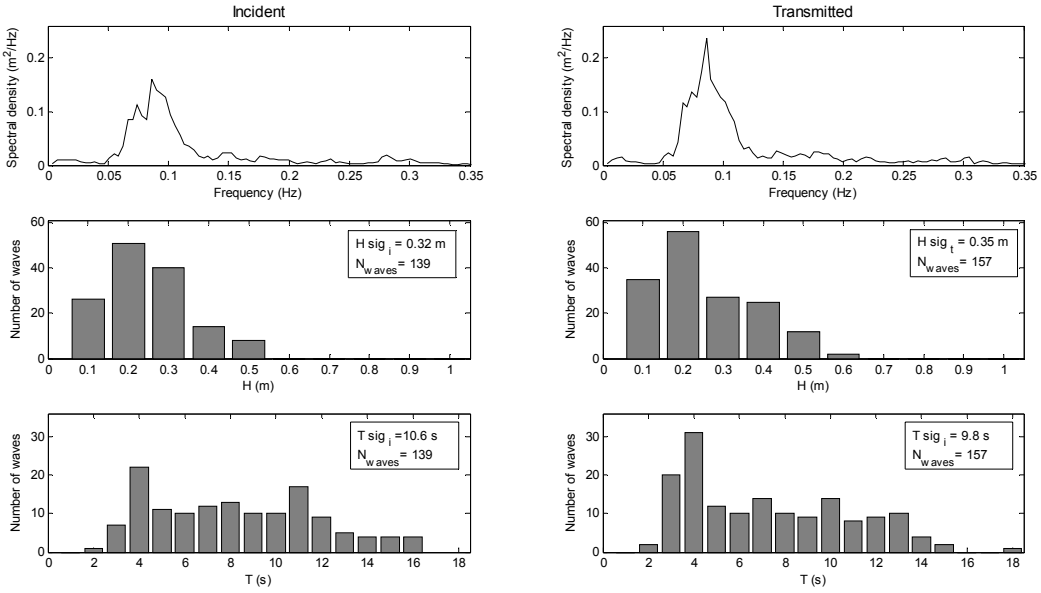

Figure 5.16. Incident and transmitted wave energy spectra, height distributions, and period distributions for small incident waves and a deep reef crest Rc=2.4 m (year day 242).

landward of the reef with relatively broad banded energy in the high frequency band. The effect of the peak energy reduction is the truncation of the height distribution at about H = 1 m. The decomposition of incident waves yielded about 70 additional secondary waves landward of the reef that appears to be distributed in the height and period range H = 0.2-0.5 m and T= 3-5 s respectively. This reduced the significant period by ~2 seconds.

b) Deep crest Rc=2.4 m, year day 244.1 (Figure 5.18).

The dissipation of primary peak energy of ~ 25% is less dramatic than for the shallow crest case. The secondary peak at ~ 0.15 Hz on the incident spectrum is dissipated, and a more distinct energy bulge develops at high frequency around 2 f_{peak} (~ 0.2 Hz) landward of the reef. Note that the event coincides with a maxima of the harmonic energy "line" visible on Figure 5.11 (period 3). Small and short waves are generated as visible in period and height distribution (~ 40 additional waves here). Due to milder dissipation conditions, the change of the height distribution is less evident than for the shallow crest case. A general shift to smaller heights is still observed.

5.3.6.3 Large Waves

a) Shallow crest Rc=1.6 m, year 243.3 (Figure 5.19)

This event is associated with the most intense wave dissipation conditions (Kt_{sig} = 0.58) of the experiment. The incident primary wave energy is relatively narrow banded (peak at 0.09Hz) and there are secondary peaks at higher frequencies. The peak energy dissipation is obvious in the transmitted spectrum (~ 75-80 % reduction). Secondary peaks are also reduced, with the high frequency energy becoming broader banded landward of the reef. The height distribution landward of the reef is truncated at H ~1.5 m and develops a 2-peak shape indicating 2 predominant groups of transmitted heights around ~1-1.5 m and ~ 0.2-0.5 m. The period distribution landward of the reef shows a reduction of the number of waves at longer periods and develops a peak around 3-5 seconds. The significant wave period is reduced by ~1.5 seconds.

b) Deep crest Rc=2.4 m, year day 243.1 (Figure 5.20).

This event is associated with the peak wave conditions measured during the field experiment. Incident energy was broad banded with a peak around 0.1-0.15 Hz

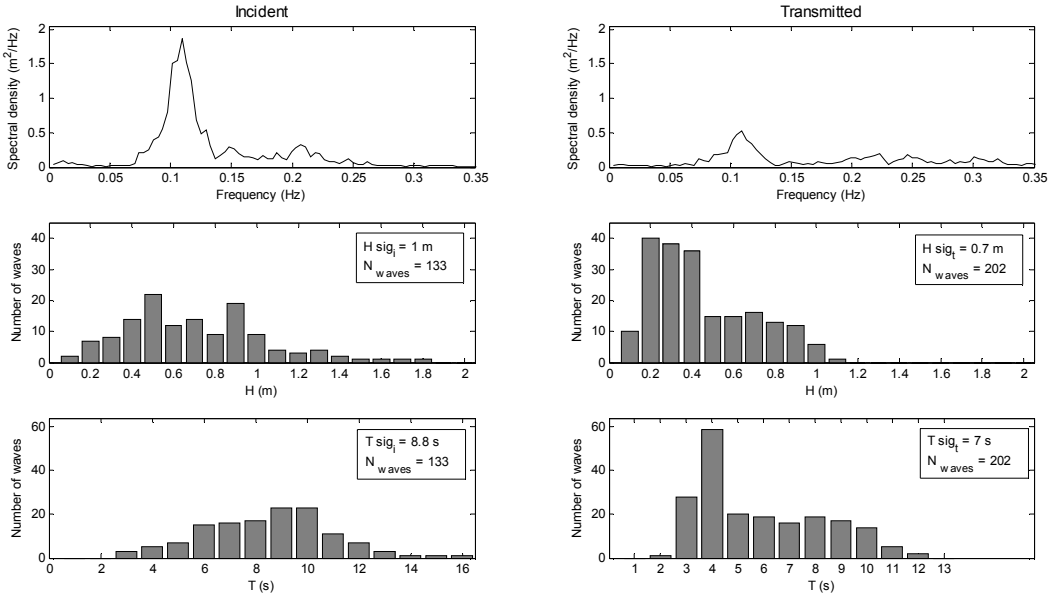

Figure 5.17. Incident and transmitted wave energy spectra, height distributions, and period distributions for medium incident waves and a shallow reef crest Rc=1.5 m (year day 243.9).

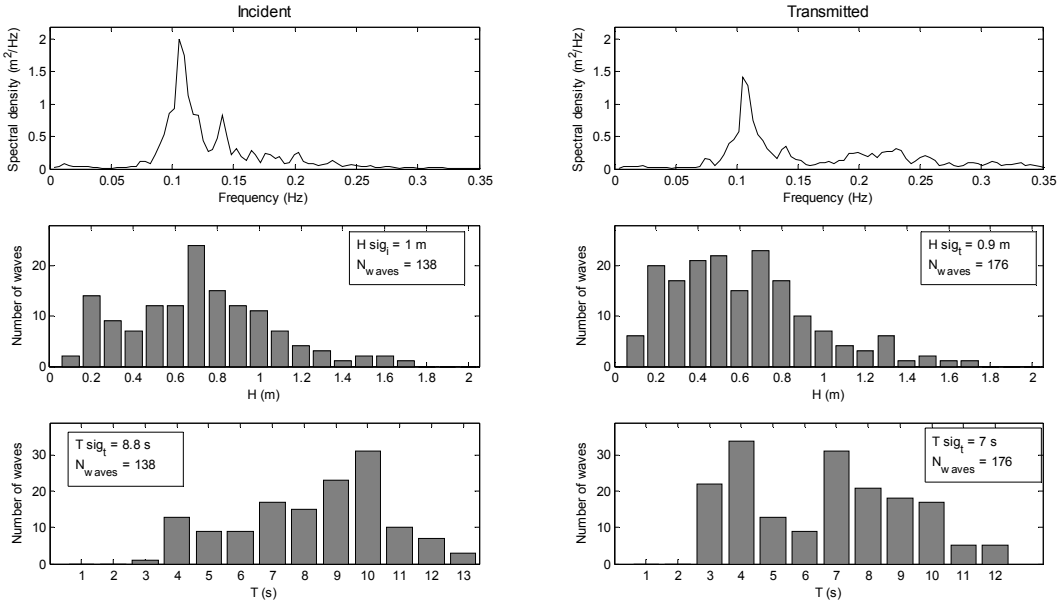

Figure 5.18. Incident and transmitted wave energy spectra, height distributions and, period distributions for medium incident waves and a deep reef crest Rc=2.4 m (year day 244.1).

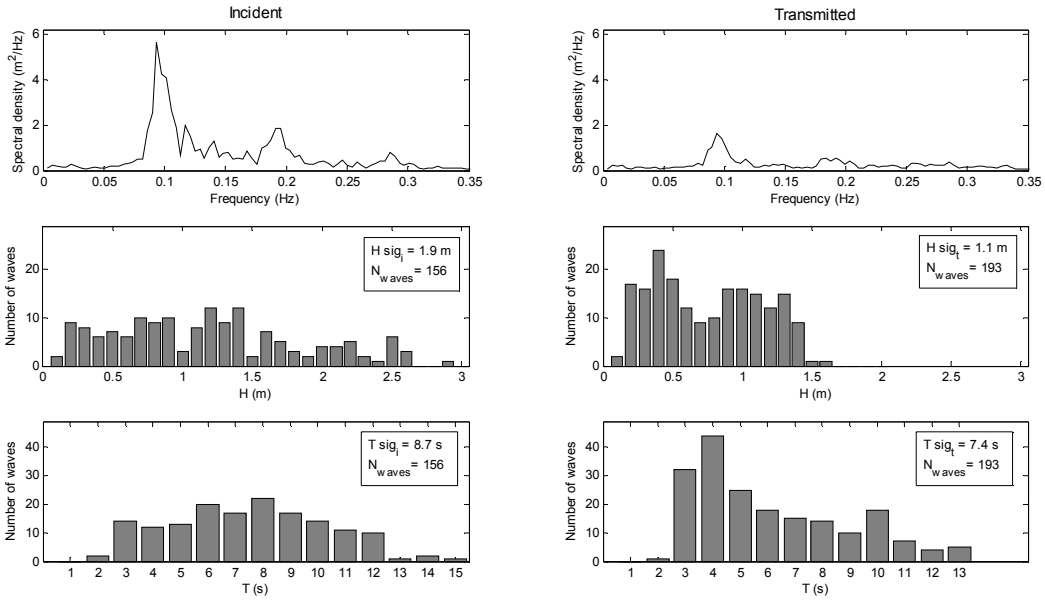

Figure 5.19. Incident and transmitted wave energy spectra, height distributions, and period distributions for large incident waves and a shallow reef crest Rc=1.6 m (year day 243.3).

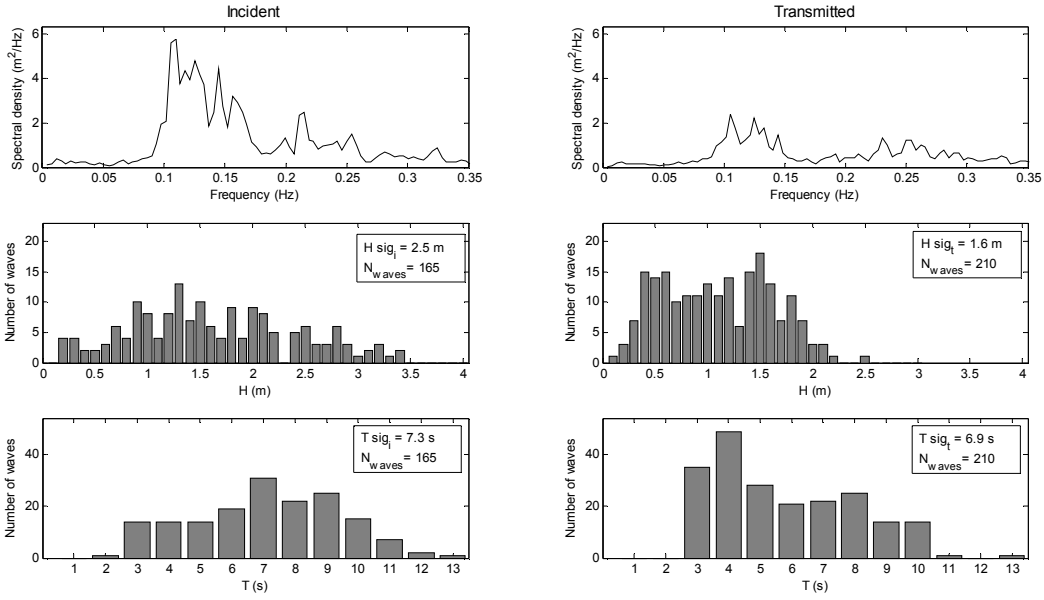

Figure 5.20. Incident and transmitted wave energy spectra, height distributions, and period distributions for large incident waves and a deep reef crest Rc=2.5 m (year day 243.1).

and secondary bulges around 0.2-0.25 Hz. The focus of the breaking-induced dissipation on the primary energy band (0.1-0.15 Hz) is well seen. As a result, the transmitted spectrum indicates a bimodal wave field with similar respective peak energies. Height and period distributions undergo changes similar to the precedent event on a shallow reef crest, including height distribution truncation (also becoming more bi-modal) and shift of period distribution to smaller periods.

5.4 DISCUSSION

5.4.1 WAVE HEIGHT TRANSMISSION

Wave height transmission has not been much studied specifically for multi-purpose reefs to date, however, this has been well examined for conventional submerged breakwaters (mostly in laboratory) by many researchers including GODA (1996), SEABROOK and HALL (1998), BLECK and OUMERACI (2002), FRIEBEL and HARRIS (2004), VAN DER MEER *et al.,* (2005) (among others). It was generally established that wave height transmission coefficients depended on incident wave conditions (i.e. height, steepness, direction), relative crest submergence, depth at toe of the structure, and relative crest width. In this study we focus on the influence of incident height and relative crest submergence but these are often found to be the parameters of primary importance (e.g. BLECK and OUMERACI, 2002; FRIEBEL and HARRIS, 2004). Note that these 2 parameters are related since an increased height at a fixed crest reduces the relative crest submergence.

The trend of increased height reduction for increasing incident wave heights and/or smaller relative crest submergence (under medium to large waves) is in agreement with the works on conventional submerged structures. The relationship between significant wave height transmission coefficient Kt_{sig} and incident significant wave height $H\,sig_{i}$ was correctly described by the Equation 5.9 (r^2=0.86) and could be used as a first order estimate of wave transmission over similar reef designs. More qualitatively, the overall relationship obtained with respect to the relative crest submergence (Figure 5.7) is in reasonable agreement with the relationship of BLECK and OUMERACI(2002) for a basic submerged rectangular smooth breakwater.

Figure 5.21. Reef-induced wave breaking at Tay Street, Mount Maunganui. Source: www.mountreef.co.nz (top); surf2surf.com, Copyright ©2009 SOURCE INTERLINK MEDIA™. All rights reserved (bottom).

BLENKINSOPP and CHAPLIN (2008) noted that since the majority of wave height decay occurs due to energy dissipation during wave breaking, the consistent dependence of height transmission on the relative crest submergence suggests that the nature of wave breaking vary as the relative crest submergence is varied. Based on experiments on a 2 dimensional physical model of submerged reef, they indeed found that waves would break in a more plunging and intense manner as the water depth over the reef was reduced. The increase in wave breaking intensity (e.g. level of turbulence, air entrainment, splash) resulted in increased wave energy dissipation. Intense plunging breakers are commonly observed at the site on lower tides (Figure 5.21) and quantitative results obtained here with respect to transmission coefficients seem consistent with these findings.

With respect to the magnitude of height reduction measured in the present study, the transmission coefficients Kt_{sig} ranging from 0.6 to 1 for relative crest submergence Rc / H_{sig_i} from 1 to 5 compare well with main datasets of transmission coefficients for conventional submerged breakwaters (from laboratory experiments) (see VAN DER MEER *et al*., 2005). In contrast though, in these datasets, a rapid drop in coefficients down to around 0.2 was observed as the relative crest submergence became inferior to 1. In the present results, smallest relative crest submergences experienced over the experiment ($Rc/ H_{sig_i} \sim 0.8$) do suggest an accelerated height reduction trend (Figure 5.8) but associated transmission coefficients remain still much larger, around 0.6. Potentially more relevant for the V-shaped reef studied here, TURNER *et al* (2001) provided height transmission coefficients versus incident heights based on experiments on a physical model of the multi-purpose reef of Narrowneck. Surprisingly, for the tested incident heights corresponding to the medium and large height ranges measured during the experiment, their transmission coefficients were much smaller (~0.2-0.5) than those obtained here. Besides, no dependence on the crest submergence was found.

Finally, an interesting feature of the collected data is the amplification of non-breaking small incident waves through shoaling over the reef crest. TURNER *et al.* (2001) did find that incident waves were amplified before breaking but the breaking process would then reduce the amplified heights. The pre-breaking shoaling likely occurs on the prototype reef too, but the amplification without subsequent breaking is different. This is associated with relatively small waves and mild energy but this could have long-term effects on the beach response, especially because the incident height range is often small at the study beach (e.g. SCARFE, 2008).

5.4.2 WAVE ENERGY TRANSMISSION AND IMPLICATION ON WAVE PERIOD

The comparison of incident and transmitted wave energy spectra (e.g. Figure 5.11) showed that the reef can modify the distribution of wave energy within the frequency domain. The result was an increased proportion of high frequency energy in the transmitted wave field under medium to large waves (e.g. Table 5.1). The 2 main mechanisms involved in the modification of the transmitted wave energy distribution are (i) the focus of breaking-induced dissipation on the primary energy (i.e. longer period waves), and (ii) the possible generation and

release of high frequency harmonic energy due to increased non linear interactions as waves propagate over the reef.

The energy transfer to higher harmonic frequency is related to the non linear character of waves that is firstly stimulated as waves reach shallower water over the reef ("more" non linear environment) and then relaxed in the deeper region past the reef ("less" non linear environment). As waves shoal on a sloping bottom, bound harmonic waves are amplified. They are initially phase-locked to the primary waves and change the wave shapes to steeper and more asymmetric profiles (SENECHAL *et al*., 2001). The release of the amplified bound harmonics as free secondary waves can possibly begin on the reef crest when waves have to adjust from a sloping bottom to an horizontal one (e.g. BEJI and BATTJES, 1993). This may generate so-called "dispersive tail waves" (MASSELINK, 1998; SENECHAL *et al*., 2001) travelling nearly at the same velocity of primary waves. Finally, more free harmonic energy will be released past the reef, due to increased water depth (MADSEN and SCHAFFER, 1999), where secondary waves will decompose from the primary waves (e.g. Figure 5.12). The scour hole in the direct lee of the reef where was located the landward measuring station (see Figure 5.1 and 5.2) provides a large deep water region after wave propagation over the reef.

It is noted that such a shift in wave energy partition will also progressively occur as waves propagate on natural profiles towards the beach. However, the feature of interest here is that, on the reef profile, the change in energy partition will occur relatively sharply, on a short distance (~ 80 m between ADV stations), and also further offshore (at least for the wave conditions experienced).

The main implication of the transformed wave energy partition is a transmitted wave field including smaller, shorter, and possibly more numerous waves, in turn reducing the wave period parameters landward of the reef (e.g. Figure 5 13). This is consistent with data collected on a barred beach profile (MASSELINK, 1998; SENECHAL *et al*., 2001) and a laboratory submerged reef (BLECK and OUMEARCI, 2002). The modification of the wave field has some likely effects on the subsequent wave energy dissipation in the surf zone in the lee of the reef. For example, SENECHAL *et al*. (2001) found that shorter waves transmitted after propagation over a sand bar inhibited wave breaking in the surfzone, and consequently delayed energy dissipation on the beach face. More theoretically, a reduction of the wave period also reduces the representative wave steepness, and

in turn the local surf similarity parameter (HEINEKE and VERHAGEN, 2007) used to describe a range of surfzone processes. For example, effects of a smaller surf similarity parameter includes more plunging or spilling breakers, reduced wave reflection from the beach, reduced breaker height index (i.e. less shoaling), and more numerous waves in the surfzone (e.g. BATTJES, 1974). Interestingly, this may also reduce the wave run-up (e.g. BATTJES, 1974; MASE, 1989).

5.5 CONCLUSIONS

A 5 day field experiment was undertaken in the vicinity of the multi-purpose reef near Tay Street at Mount Maunagnui. The deployment consisted of two ADV stations equipped with pressure sensors located 30 m seaward and just landward of the reef measuring incident and transmitted wave conditions. Incident and transmitted wave fields are compared focusing on (i) the transmission of significant wave heights, (ii) the modification of wave height distributions, and (iii) the transformation of wave energy spectra along with implications on wave periods. Main findings are:

- Significant height transmission coefficient Kt_{sig} is dependent on incident significant wave height $H\,sig_i$, and relative crest submergence $Rc/H\,sig_i$.

- Wave height amplification landward of the reef was observed for small incident waves ($H\,sig_i < 0.5$ m, no breaking). The transmission coefficient increased from 1 to 2.5 for decreasing crest submergence. This is attributed to a more efficient shoaling of incident waves on shallow reef crests.

- Wave height reduction landward of the reef was observed for incident wave height $H\,sig_i > 0.5$ m. Two sub-categories were identifiable for medium waves ($H\,sig_i = 0.5$-1.5 m), and large waves ($H\,sig_i = 1.5$-2.5 m), with respective transmission coefficients around ~ 0.7-1 and ~ 0.8-0.6. Smaller relative crest submergence $Rc / H\,sig_i$ were associated with more efficient wave height reduction.

- Transmission coefficients of significant wave height were found to be correctly described by the equation $Kt_{sig} = 0.21\,(H\,sig_i)^{-0.93} + 0.6$. ($r^2 = 0.86$). The equation could be used as a first approximation of wave

transmission over similar reef designs. It also provides a basis for calibration of numerical wave modelling over multi-purpose submerged reefs.

- The change of wave height distributions landward of the reef consisted of (i) a widening of the incident distribution up to 3 H_{sig_i} for small incident height (H_{sig_i} = 0-0.5 m), (ii) a shift of the distribution to reduced heights for medium incident waves (H_{sig_i} = 0.5-1.5 m), and (iii) a truncation of the distribution above ~1 H_{sig_i} for large waves (H_{sig_i} =1.5- 2.5 m).

- Comparison of incident and transmitted wave energy spectra showed that the reef can modify the wave energy distribution between the primary (0.05 Hz - 1.5 f_{peak}) and high frequency energy bands (1.5 f_{peak} - 0.35 Hz). Under medium to large waves, an increased proportion of high frequency energy in the transmitted wave field was identified. The 2 main mechanisms involved in the modification of the wave energy partition are (i) the focus of breaking-induced energy dissipation on the incident primary energy (i.e. longer period waves), and (ii) the possible generation and release of high frequency harmonic energy due to increased non linear interactions as waves propagate over the reef.

- The main implication of the transformed wave energy partition is the reduction of mean and significant period parameters landward of the reef for medium and large waves. The period reduction was found to increase on smaller relative crest submergence, and to a lesser extent for longer period incident waves. Peak periods were generally conserved and did not show consistent dependences on either relative crest submergence or incident wave period.

5.6 REFERENCES

BATTJES, J.A., 1974. Surf Similarity, *Proceedings of the 14th Coastal Engineering Conference* (Copenhagen, Denmark, ASCE), pp. 466–480.

BATTJES, J.A., JANSSEN, J.P.F.M., 1978. Energy loss and setup due to breaking of random waves. *Proceedings of the 16th International Conference on Coastal Engineering* (Hamburg, Germany, ASCE), pp. 569–587.

BEJI, S., and BATTJES, J.A., 1993. Experimental investigation of wave propagation over a bar. *Coastal Engineering,* 19, 151–162.

BLECK, M. and OUMERACI, H., 2002. Hydraulic Performance of Artificial Reefs: Global and Local Description. *Proceedings of the 28th International Conference on Coastal Engineering* (Cardiff, Wales, ASCE), pp 1778-1790.

BLENKINSOPP, C.E., and CHAPLIN, J.R., 2008. The effect of relative crest submergence on wave breaking over submerged slopes, *Coastal Engineering*, 55(12), 967-974.

BRODTKORB, P.A., JOHANNESSON, P., LINDGREN, G., RYCHLIK, I., RYDEN, J., and SJO, E., 2000. WAFO - a Matlab toolbox for analysis of random waves and loads. *Proceedings of the 10th International Offshore and Polar Engineering Conference* (Seattle,Washington), Vol 3, pp. 343-350.

ELGAR, S., RAUBENHEIMER, B., and GUZA, R.T., 2001. Current Meter Performance in the Surf Zone. *Journal of Atmospheric and Oceanic Technology*, 18, 1735-1746.

EMERY, W. J., and THOMSON, R. E., 1998. *Data Analysis Methods in Physical Oceanography*, 2nd edition. Elsevier, 634 p.

FRIEBEL, H.C., and HARRIS, L.E., 2004. A New Wave Transmission Coefficient Model for Submerged Breakwaters. *Proceedings of the 29th International Conference on Coastal Engineering* (Lisbon, Portugal, ASCE), pp.19–24.

GODA, Y., 1996. Wave Damping Characteristics of Longitudinal Reef System. *In*: CLIFFORD, J.E. (ed.), *Advances in Coastal Structures and Breakwaters*, Thomas Telford Publishing, London, Paper 12, pp.192–207.

HEINEKE, D., and VERHAGEN, H.J., 2007. On the use of the fictitious wave steepness and related surf-similarity parameter in methods that describe the hydraulic and structural response to waves. *Proceedings of the 5th Coastal Structures Conference, (Venice, Italy),* pp. 1057-1066.

HUTT, J.A., and BLACK, K.P., 1997. Vertical attenuation of wave-induced pressures. *Proceedings of the Pacific Coasts and Ports '97 Conference*, Christchurch, New Zealand, pp. 965-970.

HORIKAWA, K., 1988. *Nearshore Dynamics and Coastal Processes: Theory, Measurement, and Predictive Models*. Part I, Chapter 4, University of Tokyo Press, Japan, 522 p.

MADSEN, P.A., and SCHÄFFER, H.A., 1999. A review of Boussinesq-type equations for surface gravity waves. *In*: LIU, P.L.F., (ed.), *Advances in Coastal and Ocean Engineering,* Volume 5**,** pp. 1–95

MASE, H. 1989. Random Wave Runup Height on Gentle Slope. *Journal of Waterway, Port, Coastal, and Ocean Engineering*, 115(5), 649-661.

MASSELINK, G., 1998. Field investigation of wave propagation over a bar and the consequent generation of secondary waves. *Coastal. Engineering,* 33, 1–9.

NATIONAL INSTITUTE for WATER and ATMOSPHERIC RESEARCH, 2009a. National Climate Database, ClifFlo. Available at: http:\\cliflo.niwa.co.nz (station 1615) [Accessed on the 30th of October 2009].

NATIONAL INSTITUTE for WATER and ATMOSPHERIC RESEARCH, 2009b. Sea level at Moturiki Island tide gauge (http:\\www.niwa.cri.co.nz).

RUESSINK, B.G., 1998. Bound and free infragravity in the nearshore zone under breaking and non breaking conditions. *Journal of Geophysical Research*, 101, 25589-25597.

SCARFE, B.E., 2008. Oceanographic Considerations for the Management and Protection of Surfing Breaks. Hamilton, New Zealand: The University of Waikato, Ph.D. thesis, 307 p. + appendices.

SEABROOK, S.R., HALL, K.R., 1998. Wave transmission at submerged rubble mound breakwaters. *Proceedings of the 26th Coastal Engineering Conference* (Copenhagen, Denmark, ASCE), pp. 2000– 2013.

SENECHAL, N., BONNETON, P., and DUPUIS, H., 2002. Field experiment on secondary wave generation on a barred beach and the consequent evolution of energy dissipation on the beach face. *Coastal Engineering*, 46, 233-247.

SONTEK/YSI, 2001a. *Triton ADV Operation Manual, Firmware Version 1.0.* (available from Sontek, 6837 Nancy Ridge Drive, Suite A, San Diego, CA, 92121, USA), 117 p.

SONTEK/YSI, 2001b. *Triton ADV Software Manual, ViewTritonPro, Windows version 1.20.* (available from Sontek, 6837 Nancy Ridge Drive, Suite A, San Diego, CA, 92121, USA), 46 p.

SMITH, E.R., and KRAUS, N.C., 1991. Laboratory study of wave breaking over bars and artificial reefs. *Journal of Waterway, Port, Coastal and Ocean Engineering,* 117 (4), 307–325.

THORNTON, E.B., and GUZA, R.T.,1983, Transformation of wave height distribution. *Journal of.Geophysical Research,* 88 (C10), 5925–5938.

TURNER, I., LEYDEN, V., COX, R., JACKSON, A., and MCGRATH, J., 2001. Physical Model Study of the Gold Coast Artificial Reef. *In:* BLACK, K.P. (ed.), Natural and Artificial Reefs for Surfing and Coastal Protection. *Journal of Coastal Research, Special Issue No. 29*, 131-146.

VAN DER MEER, J.W., REGELING, H.J. and DE WAAL, J.P., 2000. Wave transmission: spectral changes and its effects on run-up and overtopping. *Proceedings of the 27th International Conference on Coastal Engineering* (Sydney, Australia, ASCE), pp. 2156-2168.

VAN DER MEER, J.W., BRIGANTI, R., ZANUTTIGH, B., WANG, B., 2005. Wave transmission and reflection at low crested structures: design formulae, oblique wave attack and spectral change. *Coastal Engineering*, 52, 915-929.

YOUNG, I.R.,1989. Wave transformation over coral reefs. *Journal of Geophysical Research*, 94, 9779-9789.

CHAPTER 6. HYDRODYNAMICS AT AN OFFSHORE SUBMERGED MULTI-PURPOSE REEF AT MOUNT MAUNGANUI, NEW ZEALAND

6.1 INTRODUCTION

The chapter presents analysis of hydrodynamics measured in the vicinity of the multi-purpose reef at Mount Maunganui, New Zealand during a 5 day field experiment. Two acoustic Doppler velocimeters measured near-bottom currents seaward and landward of the reef and an acoustic Doppler profiler measured current profiles landward of the reef. Hydrodynamic conditions experienced during the field experiment are described. The relationship between wave forcing and hydrodynamic response landward of the reef, including magnitude of mean current velocity and flow discharge, is then more specifically investigated.

6.2 METHODS

The field deployment consisted of an acoustic Doppler velocimeter (ADV) located 30 m seaward of the reef and co-located ADV and acoustic Doppler profiler (ADCP) landward of the reef to measure both undisturbed and reef-affected hydrodynamic conditions (see Figure 5.1). The 2 ADVs measured simultaneously 3 dimensional currents (east-west, north-south, and up-down) at 4 Hz for 1024 seconds every 30 minutes. Both sensors were 0.7 m above the seabed in a total water depth of ~ 5.2 m relative to mean sea level (Figure 6.1). The ADV data analysed consist in 231 burst measured from the 28th August 2009 at 2.30 pm to 2nd of September 2009 at 9.30 am. The ADCP measured 1 minute-averaged vertical current velocity profiles every 10 minutes. The sample profile was 5 m high and compartmented in ten 0.5 m bins. The sensors were 0.2 m above the seabed and had a blanking distance of 0.2 m so the centre of the first bin was at 0.65 m above the seabed. The top two bins were possibly above the surface at low tides and current profiles were accordingly corrected discarding the data sampled.

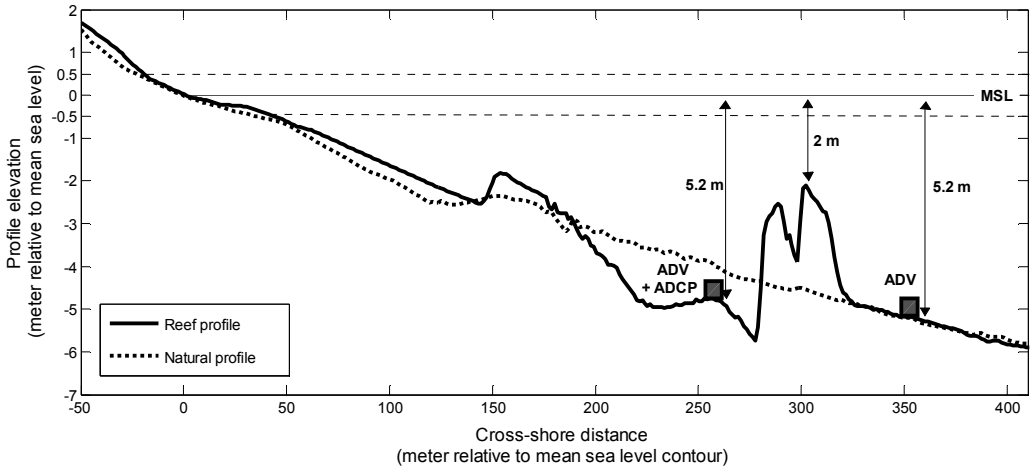

Figure 6.1. Reef profile with instrument depths and positions. Depths are relative to mean sea level (Moturiki vertical datum 1953, plain line). Highest and lowest water levels during the experiment are represented by the dashed lines. A natural profile located 300 m to the north of the reef profile is shown for comparison (thick dashed line).

The retrieval of instruments indicated important sediment accretion at the deployment sites (~ 0.2 m). The ADCP sensors were buried and data check indicated invalid measurements from the 4th day of the experiment. This data was discarded from the analysis. In total, 523 minute-averaged profiles measured from the 28th August 2009 at 2.30 pm to 1st September 2009 at 5.30 pm were used. Time is expressed as year day, with day 1 being the 1st January 2009. ADV data is therefore available from day 240.6 to 245.4, and ADCP data from day 240.6 to 244.3.

Both ADV and ADCP horizontal current components, east-west and north-south, were rotated by 48° (shore normal direction at the site) to provide cross (u) and long-shore (v) current velocities. The cross-shore currents (u) are positive landward, and the long-shore currents (v) are positive towards the southeast (see Figure 5.1 for reef orientation). Mean current magnitudes u_{mean} and v_{mean} were computed averaging current velocities over each burst. Mean current velocity $U_{mean} = \sqrt{u_{mean}^2 + v_{mean}^2}$ and mean current direction $\theta = \tan^{-1}(v_{mean}/u_{mean})$ were also determined. Current direction indicates the direction towards which the flow is moving (° to). A current direction of 0° indicates a flow fully cross-shore and directed landward. A positive current direction indicates a flow deviated towards the southeast while a negative direction a flow deviated towards the northwest.

The analysis is structured as follows: firstly, current conditions measured by the ADV and ADCP stations during the experiment are described. ADV and ADCP

datasets are then compared to test the validity of using near-bottom mean current velocity as a proxy for depth-averaged mean current velocity. The relationship between mean current velocity and wave forcing is then specifically investigated. Finally, water mass discharge landward of the reef is estimated and compared to wave-induced water mass flux on the undisturbed beach. An attempt is made to explain reef-induced water mass discharge as a function of incident wave-induced water mass flux on the reef crest.

6.3 RESULTS

6.3.1 CURRENT CONDITIONS DURING THE FIELD EXPERIMENT

Wave and burst-averaged bottom current conditions measured by the ADV stations are presented in Figure 6.2. With respect to the wave conditions, three periods can be identified during the experiment. Period 1 from day 240.6 to 242.5 consisted of small incident waves ($H\ sig_i$ = 0-0.5 m) that did not break on the reef crest and were instead amplified due to shoaling. A more significant wave event developed in period 2, with $H\ sig_i$ up to 2.5 m, during which important wave energy dissipation occurred on the reef (transmitted height reduction, see Figure 6.2, top). Incident wave energy decayed in period 3, with more medium sized waves ($H\ sig_i \sim 1$ m). Waves generally approached the reef with an oblique angle of incidence from the north to northeast (i.e propagating from ~10-30 ° relative to reef centreline). A more complete description of incident and transmitted wave conditions is provided in Chapter 5.

With respect to the corresponding mean wave-induced currents, period 1 is characterized by small current velocities both seaward and landward of the reef around 0.1 m/s or less. Seaward of the reef, current is initially long-shore directed, towards the southeast (~90°). Current directions landward of the reef are then very variable and show numerous reversals from +90° to -90°. On the second half of the period 1, currents seaward of the reef exhibit several direction reversals from + 90° to - 90°. This is firstly reproduced to some extent landward of the reef around day 241.5 – 242 but then becomes less evident for the end of the period.

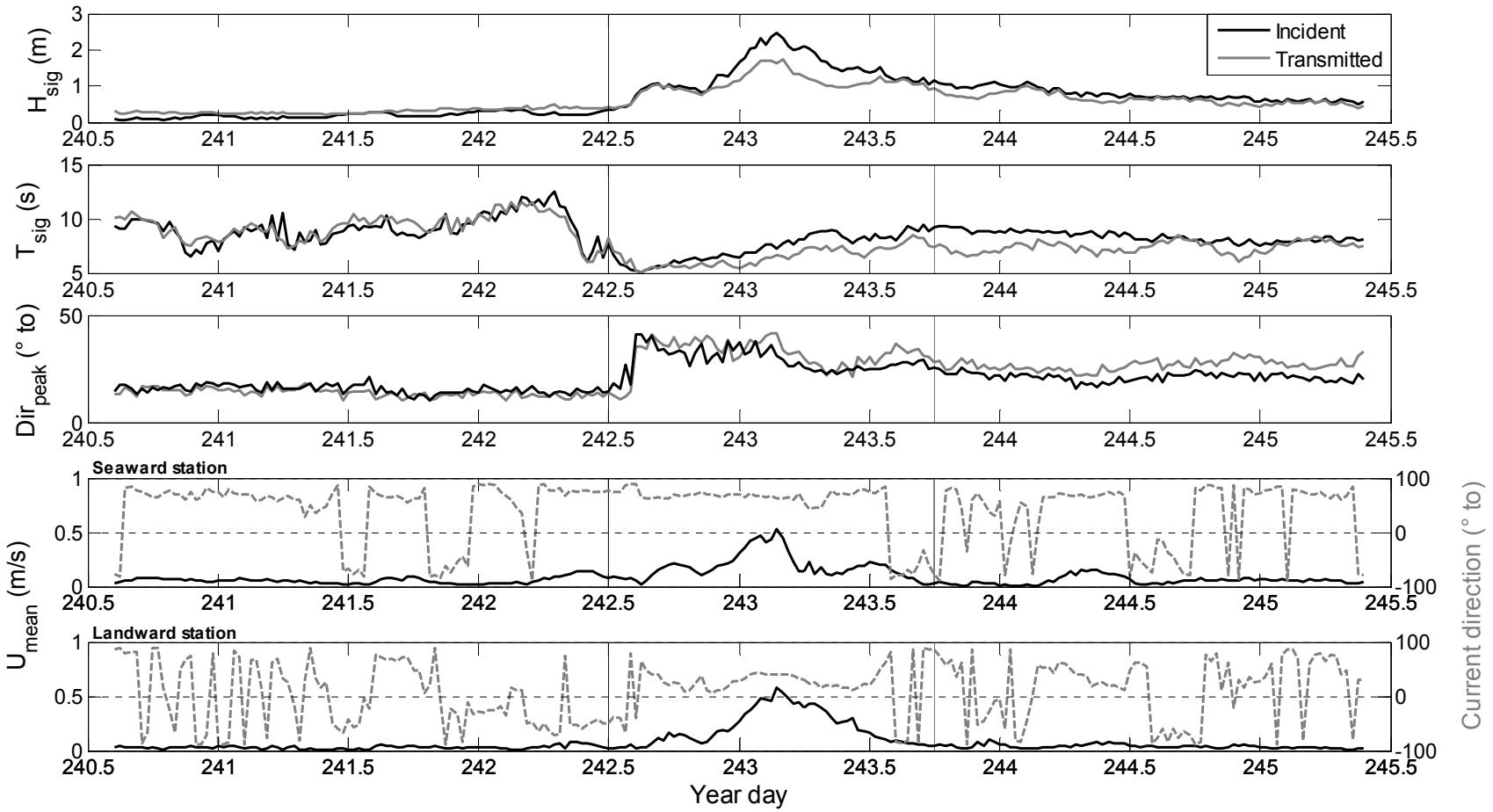

Figure 6.2. Wave and current conditions during the field experiment (ADV dataset). The top 3 graphics show incident (black lines) and transmitted (grey lines) wave height, period and direction. The two bottom graphics show mean current velocity (black lines) and direction (dashed grey lines) seaward and landward of the reef. Given current and wave directions correspond to the direction towards which a wave or current is propagating (i.e ° to). The 3 experiment periods are separated by the vertical lines.

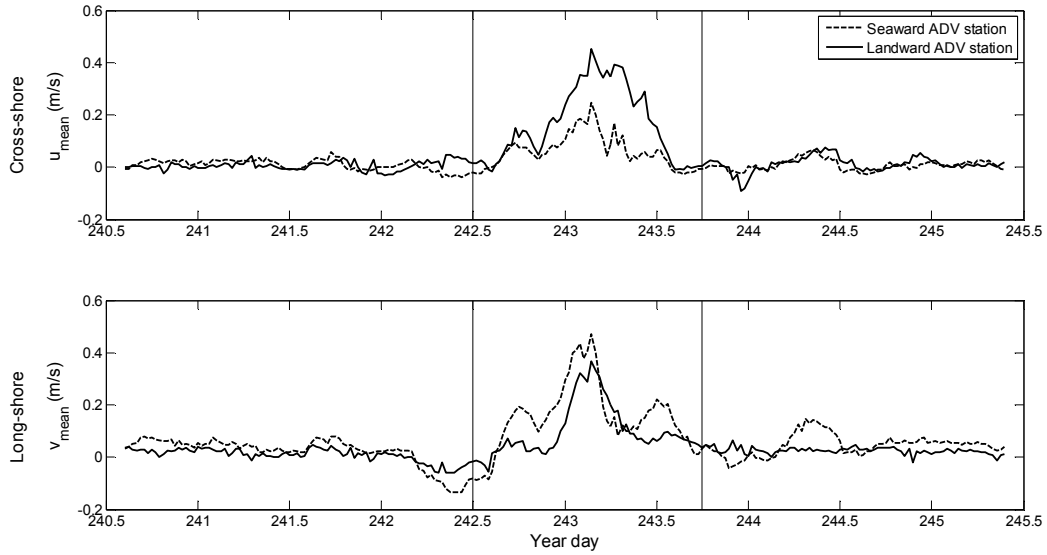

Figure 6.3. Cross and long-shore components of mean currents measured seaward (dashed) and landward (plain) of the reef (ADV dataset). Cross-shore currents are positive landward and long-shore current are positive southeastward. Experiment periods are delimited by the vertical lines (see Figure 6.2 for concurrent wave conditions). Note the stronger cross-shore currents landward of the reef in period 2 around day 243 (for $H sig_i$ ~1.5-2.5 m).

More significant mean current velocities develop in period 2 as incident wave heights increase. Concurrently, transmitted wave heights become significantly smaller than incident indicating important wave energy dissipation at the reef. Both seaward and landward mean currents reach their peak magnitude of ~ 0.5 m/s after day 243 under the maximum wave heights measured during the experiment. Mean current velocity seaward of the reef drops then at ~ 0.2 m/s shortly after the peak wave height, while current velocity of ~ 0.4 m/s is sustained landward of the reef. With respect to current direction, the flow is virtually long-shore directed seaward of the reef (+80°) and strongly deviated towards the shore landward of the reef (+ 10-30°). Mean current velocity decreases in period 3 to ~ 0.1 m/s and direction patterns become variable with frequent reversals. Note that these reversals are independent of the wave direction which is relatively stable throughout the period (as in period 1).

Cross and long-shore components of mean currents are shown in Figure 6.3. It is observed that the onshore flow deviation in period 2 landward of the reef (Figure 6.2, bottom graphic) is due to a an important increase of cross-shore current velocity landward of the reef, up to 0.5 m/s, that is not reproduced seaward of the reef (Figure 6.3, top). With respect to the long-shore component of current, differences between seaward and landward magnitudes are less obvious. Long-

shore currents are generally slightly weaker landward than seaward of the reef (Figure 6.3 bottom). They also seem less variable landward of the reef, and often do not reproduce oscillations of the seaward long-shore component.

The additional cross-shore current landward of the reef in period 2 is coherent with the concurrent important dissipation of incident wave energy (see Figure 6.2 top) that induce a cross-shore gradient in radiation stress and needs to be balanced by a onshore directed flow (e.g RANASINGHE *et al.*, 2006).

The vertical structures of the cross and long-shore currents measured by the ADCP are shown in Figure 6.4. Consistently with the ADV dataset, mean current velocities are generally small over the period 1 of the experiment, around + 0.1 m/s. There are greater velocities near the sea surface up to ~+ 0.3 m/s. These are well explained by the so-called "Stokes drift" that is the development of a net velocity in the direction of wave propagation. This drift results from the incomplete closure of water particles path as waves become more skewed and asymmetric through shoaling and non linear interactions (KOMAR, 1998). The wave shear near the sea surface is evident in individual vertical velocity profiles from day 240.5 to day 242 shown in Figure 6.5. The cross-shore current profiles clearly indicate stronger onshore directed flow within the top 2 m of the water column. Deeper in the water column, velocities are weaker but otherwise relatively depth uniform. Most of the long-shore current activity is also found within the top 2 m of the water column. Long-shore current velocities are predominantly positive indicating a flow towards the southeast, which is consistent with the wave direction (see Figure 6.2).

At the end of the period 1, from day 242 to 242.5, there is a short episode of offshore directed currents (Figure 6.4). These are most likely due to offshore winds (see Figure 5.3) rather than incident wave activity.

The transition to period 2 is characterized by an increase of both cross and long-shore mean current velocities. From day 242.5 to day 243, the top half of the water column is dominated by cross-shore currents of ~ 0.3 m/s, while the bottom half is dominated by long-shore currents (0.2-0.3 m/s). The maximum magnitudes of cross and long-shore currents are reached under peak incident wave conditions ($H\,sig_i$ ~ 2-2.5 m) between day 243 and 243.5 and are around 0.5-0.6 m/s.

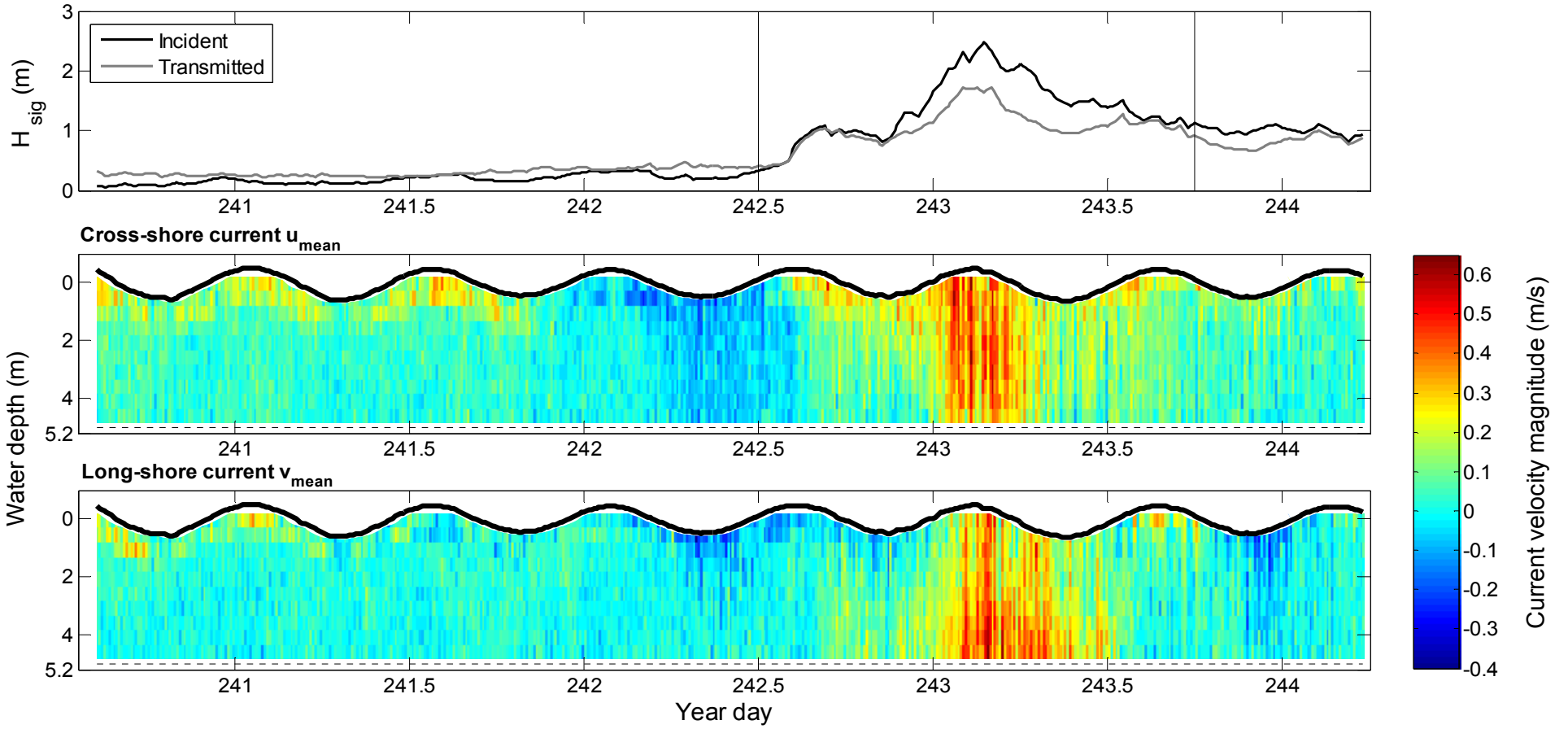

Figure 6.4. Cross and long-shore mean current profiles measured by the ADCP landward of the reef. Cross-shore currents are positive landward and long-shore currents are positive southeastward. Water depths are relative to mean sea level, and positive downward. On the bottom two graphics, the plain black line indicates the tide oscillations and the dotted line indicates the sensor height above the sea bed. For reference, the top graphic shows incident and transmitted significant wave heights (black and grey respectively), along with the 3 experiment periods (vertical lines).

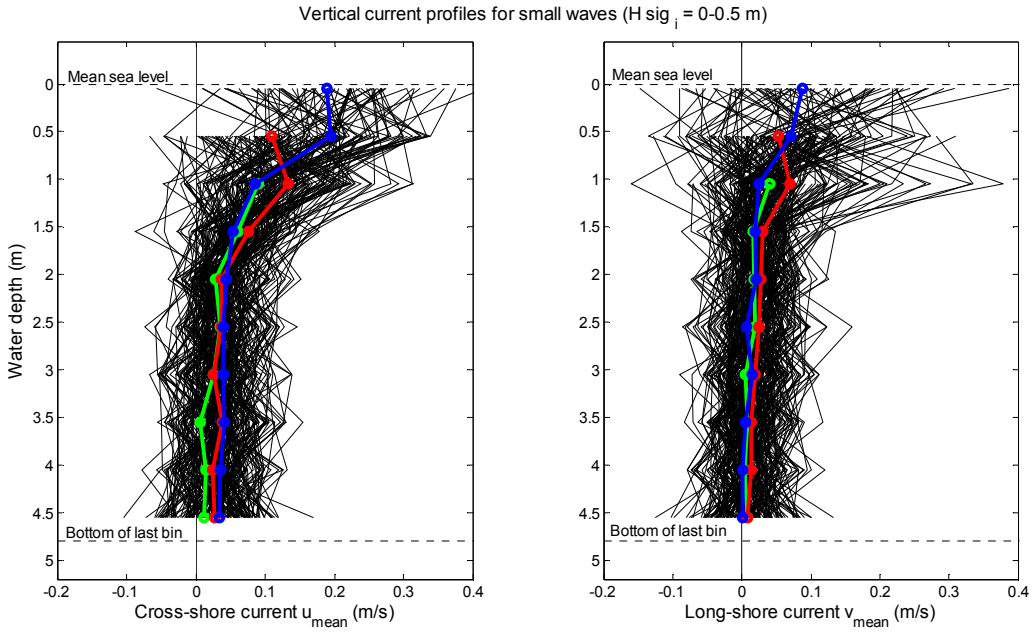

Figure 6.5. Individual cross and long-shore mean current profiles measured by the ADCP landward of the reef from day 240.5 to 242 in period 1 (H sig $_i$ = 0-0.5 m). The event of offshore currents between day 242 and 242.5 is not included (see Figure 6.4). Cross-shore currents are positive landward and long-shore currents are positive southeastward. Water depths are relative to mean sea level, positive downward. Thick color lines (blue, green and red) represent mean current profiles for each water level, and the dots represent the centre of each bin across the profile. Note the stronger cross and long-shore currents on the top half of the water column due to the Stokes drift induced by surface waves.

Current magnitude then seems relatively uniform across the water column. Individual current profiles measured for the interval from day 243 to 243.5 under these energetic wave conditions are shown in Figure 6.6. It is indeed observed that current profiles are relatively depth uniform. The main deviation is near the seabed where cross-shore currents are slightly weaker than across the water column and long-shore currents slightly stronger than across the water column.

In period 3 under decaying wave energy, the vertical structure of the flow becomes very similar to the one observed at the beginning of the wave event from day 242.5 to 243 (Figure 6.4). For completeness, individual current profiles for these transition periods, i.e. before and after peak wave conditions, are shown in Figure 6.8. The wave shear near the surface is observed on the cross-shore currents. More variability is present in the long-shore flow; near-bottom current magnitude seems generally stronger and more consistently positive (i.e southeastward) than across the water column.

As mentioned previously, a mechanism responsible for these relatively strong current velocities is development of gradients in radiation stress that need to be

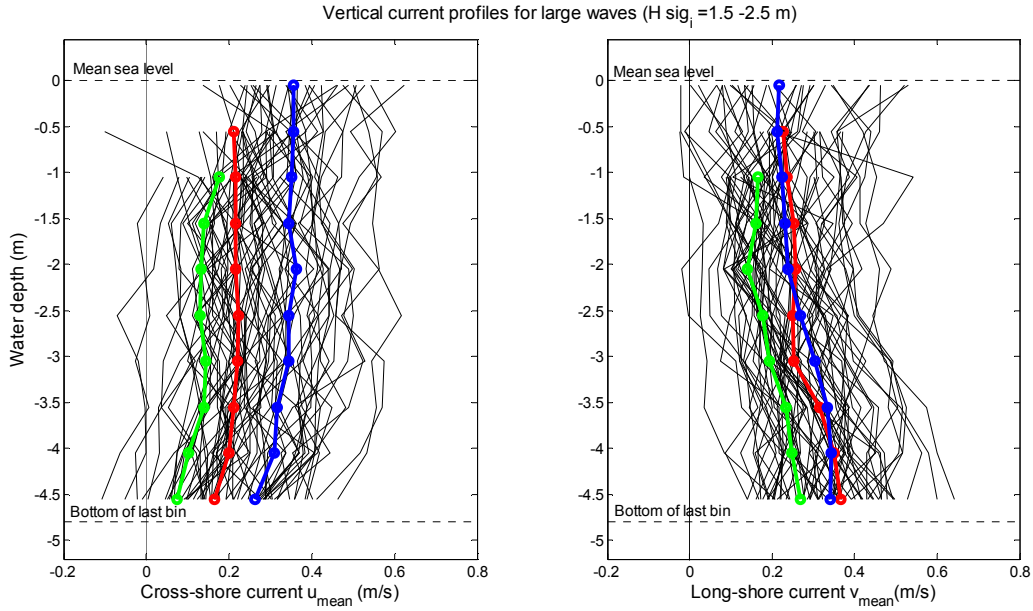

Figure 6.6. Individual cross and long-shore mean current profiles measured by the ADCP landward of the reef from day 243.5 to 243.5 for the peak wave conditions experienced during the experiment (H sig $_i$ = 1.5-2.5 m). Cross-shore currents are positive landward and long-shore currents are positive southeastward. Water depths are relative to mean sea level, positive downward. Thick color lines (blue, green and red) represent mean current profiles for each water level, and the dots represent the centre of each bin across the profile. Note the vertical profiles relatively depth uniform.

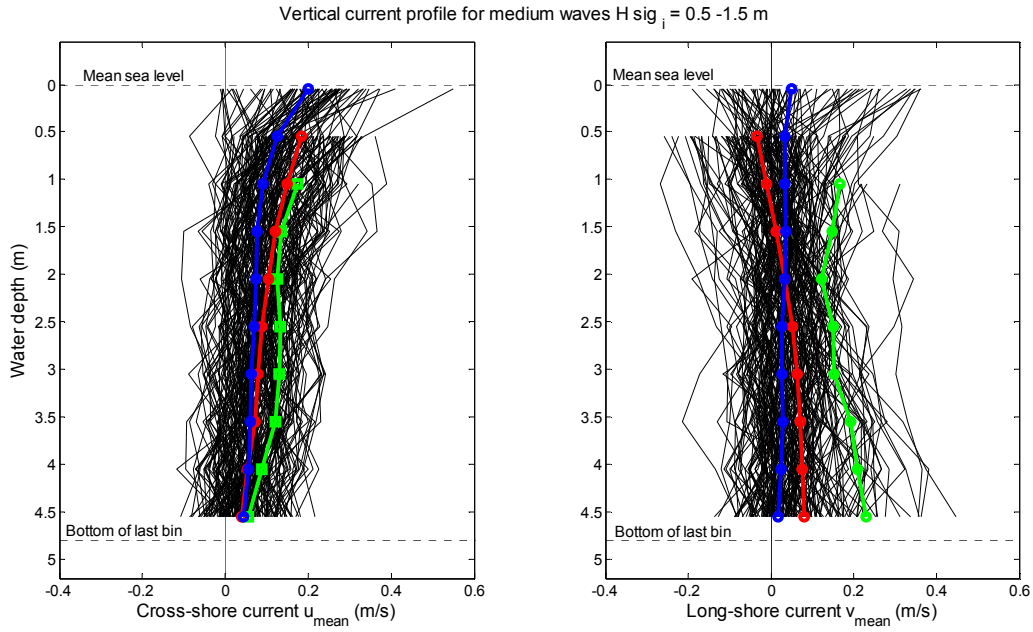

Figure 6.7. Individual cross and long-shore mean current profiles measured by the ADCP landward of the reef for medium waves from day 242.5 to 243 and from day 243.5 to the end of experiment (H sig $_i$ = 0.5-1.5 m). Cross-shore currents are positive landward and long-shore currents are positive southeastward. Water depths are relative to mean sea level, positive downward. Thick color lines (blue, green and red) represent mean current profiles for each water level, and the dots represent the centre of each bin across the profile.

compensated by change in the mean current field. According to the current profiles measured, there is also a likely contribution of the wave-induced mass transport due to Stokes drift. This would be combined with water mass transport due to wave rollers in the case of breaking waves (e.g. SVENDSEN, 1984). Under medium wave heights and mild energy dissipation, these processes may not extend through the entire water column thus explaining the near surface shear of stronger current velocities. For larger waves and more intense dissipative conditions, vertical current profiles become relatively depth uniform and suggest more saturated conditions.

6.3.2 COMPARISON OF DEPTH-AVERAGED AND NEAR-BOTTOM CURRENT VELOCITY

A valid and compact parameter to describe the current magnitude landward of the reef in response to wave forcing would be the depth-averaged current velocity. These current magnitudes can be obtained from the ADCP dataset. However ADVs measure currents at a single elevation relatively close to the seabed and consequently do not capture the vertical structure of the flow. That being, it was observed that the current profiles may become relatively depth uniform, particularly for strongest current velocities that are of more significant interest. As a result, the currents measured by the ADV at a single elevation near the bottom may still be representative of depth-averaged magnitude.

To test this hypothesis, current velocities measured on the bottom cell of the ADCP profile are compared to corresponding depth-averaged magnitudes in Figure 6.8. The centre of the lowest profile bin is at 0.65 m above seabed and is therefore similar to the ADV sensor height above seabed of 0.7 m

Depth-averaged current magnitudes were computed as:

$$u_{\text{depth av}} = \frac{1}{N}\sum_{i=1}^{N} u_i \qquad (6.1)$$

where u_i is the current velocity measured in bin i, and N is the number of bin considered for the profile (depending on the water level).

Figure 6.8 shows that the general agreement is qualitatively correct. Bottom and depth-averaged cross-shore velocities are reasonably correlated ($r^2 = 0.6$) with small bias ($m = 1.1$). The slightly larger depth-averaged magnitudes are explained

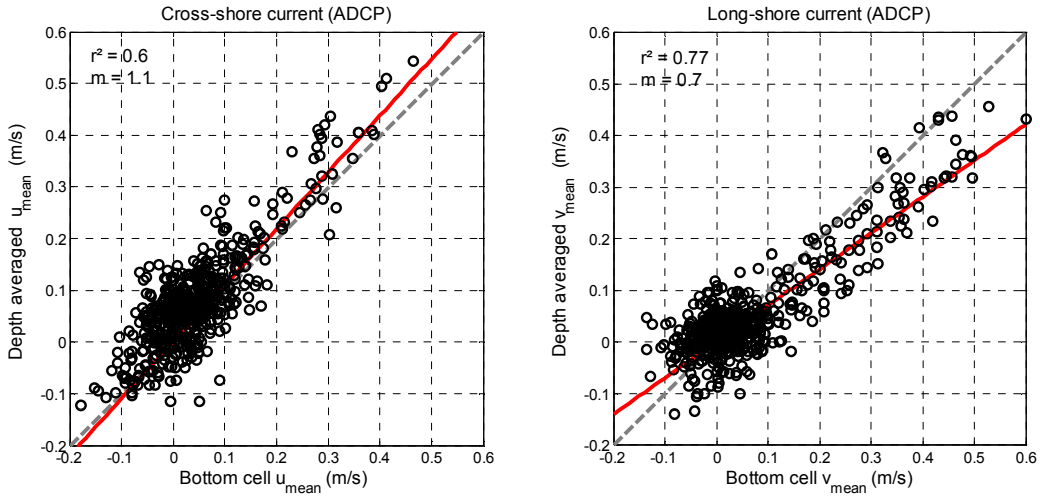

Figure 6.8. Cross and long-shore depth-averaged mean current as a function of mean current measured on the bottom cell of the profile (center of cell ~ 0.65 m above seabed). The grey dotted line represents unity of the two current magnitudes. The overall agreement is correct indicating that currents measured near the seabed are fairly representative of the depth-averaged flow. Cross-shore depth-averaged mean currents are biased high relative to those measured at the bottom cell (m = 1.1). Long-shore depth-averaged mean currents are biased low relative to those measured at the bottom cell (m = 0.7).

by the stronger current velocities generally observed near the surface (see Figure 6.4). A reasonable linear correlation is also observed for long-shore currents (r^2 = 0.77). However, the bias is larger (m = 0.7) which indicates that depth-averaged long-shore current magnitudes are consistently smaller than those measured near the bottom. Overall, the assumption that bottom currents provide a correct representation of the depth-averaged flow is not fully justified but still appears reasonable as a first approximation.

This is further tested in Figure 6.9 where the ADCP current dataset, including both depth-averaged and bottom cell mean currents, is compared to the ADV current dataset. The agreement is generally correct and importantly maximum mean current magnitudes are similar. However, there is a distinct difference between the 2 datasets around day 243.5 where the ADV cross and long-shore mean currents are respectively smaller and larger that the depth-averaged magnitudes. This is not due to a difference between bottom and depth-averaged current magnitudes since the pattern of the ADV data is not reproduced in the current measured in the bottom cell of the ADCP profile. The deviation may be due to the different averaging interval of instruments. The 1 minute interval used by the ADCP is relatively short and could induce some aliasing effects. Because of these differences between ADV and ADCP measured mean currents, it was

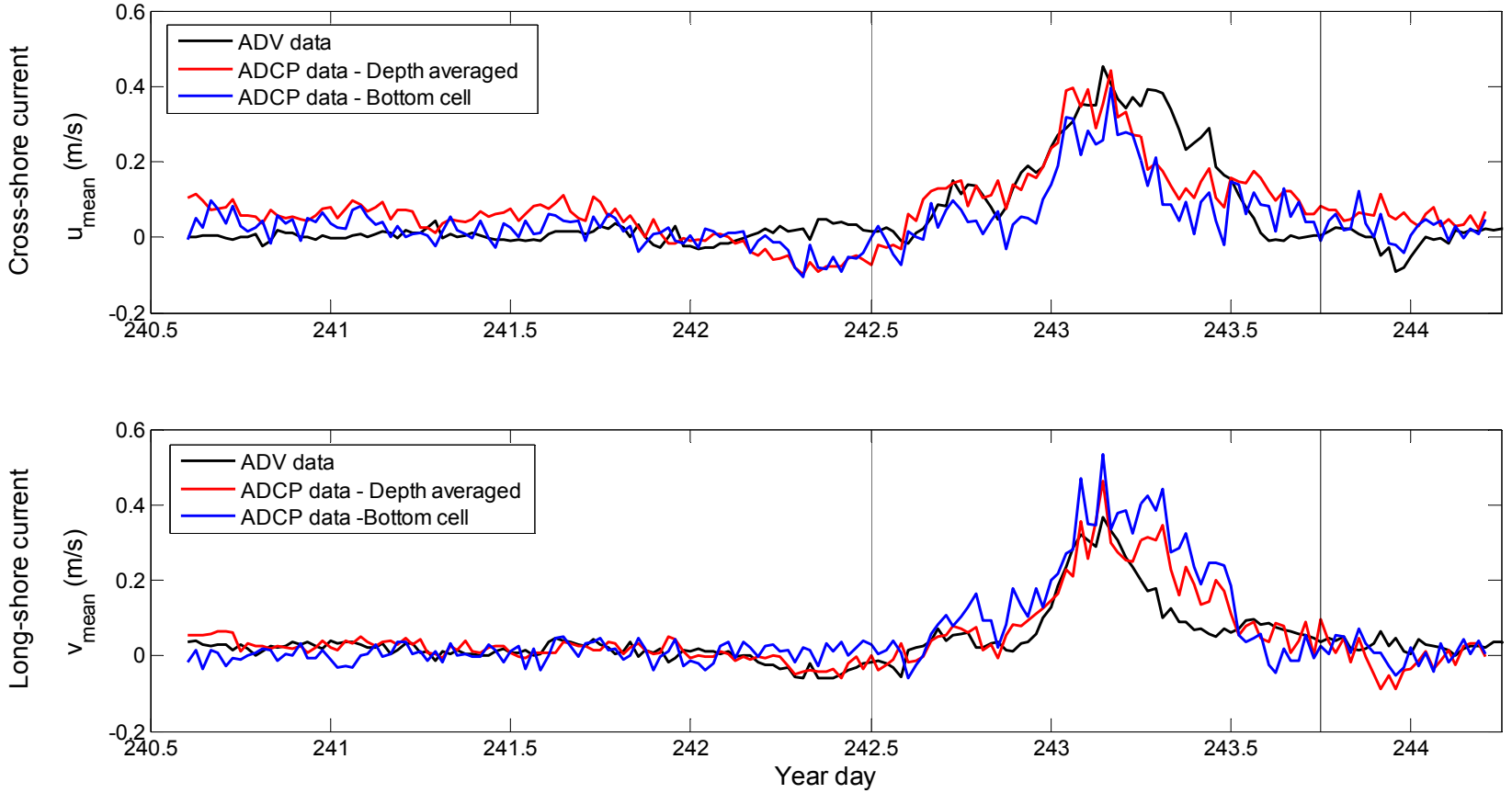

Figure 6.9. Cross and long-shore mean currents measured by the ADCP and ADV instruments landward of the reef. Cross-shore currents are positive landward and long-shore currents are positive southeastward. For the ADCP dataset, the depth-averaged and bottom cell mean current magnitudes are the red and blue lines respectively. The centre of the bottom cell of the ADCP profile is ~ 0.65 m above seabed. ADV mean currents (sensor height 0.7 m above seabed) are represented by the black lines. Experiment periods are delimited by the vertical lines (see Figure 6.2 for concurrent wave conditions). The overall agreement is close and maximum magnitudes are similar but a deviation is visible between day 243 and 243.5. This may be due to different averaging intervals of instruments (ADCP: 1 min, ADV: ~17 min).

decided to treat the two datasets separately in the following investigations on relationships between mean current magnitude and incident wave forcing.

6.3.3 Relationships between Mean Current Velocity and Wave Forcing

Depth-averaged (ADCP) and single point (ADV) mean current velocities $U_{mean}=\sqrt{u_{mean}{}^2 + v_{mean}{}^2}$ are compared to incident significant wave heights in Figure 6.10. The increase of mean current velocity in response to increased wave height is evident for both the ADV and ADCP datasets, however, the relationships are not linear. Currents are relatively weak (U_{mean} < 0.2 m/s) up to about H sig $_i$ = 0.8-1 m, and the increase in velocity is then clearly accelerated for waves larger than this threshold. Fitting of simple functions to the datasets indicated that the relationships were well described by a square function of the form:

$$U_{mean} = a.(H\ sig_{\ i})^{\ 2} \qquad (6.2)$$

with a_{ADCP}= 0.1, and a_{ADV}= 0.095. H sig $_i$ is the incident significant wave height.

The dependence of the mean current velocity U_{mean} on (H sig $_i$) ^{2} (Figure 6.10, bottom) suggests a linear response to the incident wave energy since:

$$E_{wave} = \frac{\rho.g}{8}.(H)^2 \qquad (6.3)$$

where ρ is the seawater volumic mass, g is the gravitational constant, and H is the wave height.

It is noted that the very close coefficients obtained for the 2 datasets (a_{ADCP} and a_{ADV}) indicate that the depth-averaged and single point current velocities respond approximately the same way to wave forcing. This further justifies the use of ADV single point currents as a proxy for depth-averaged current magnitudes.

It is evident from Figure 6.10 that incident wave height or energy is an important parameter to explain mean current velocity. However, there are other parameters such as the crest submergence or the depth landward of the reef that may also be important. To provide a more robust relationship between mean current velocity and wave forcing, dimensionless parameters including these characteristics are compared in Figure 6.11. Dimensionless parameters used are the mean current normalized by the wave phase speed (Equation 6.4), and the incident wave height

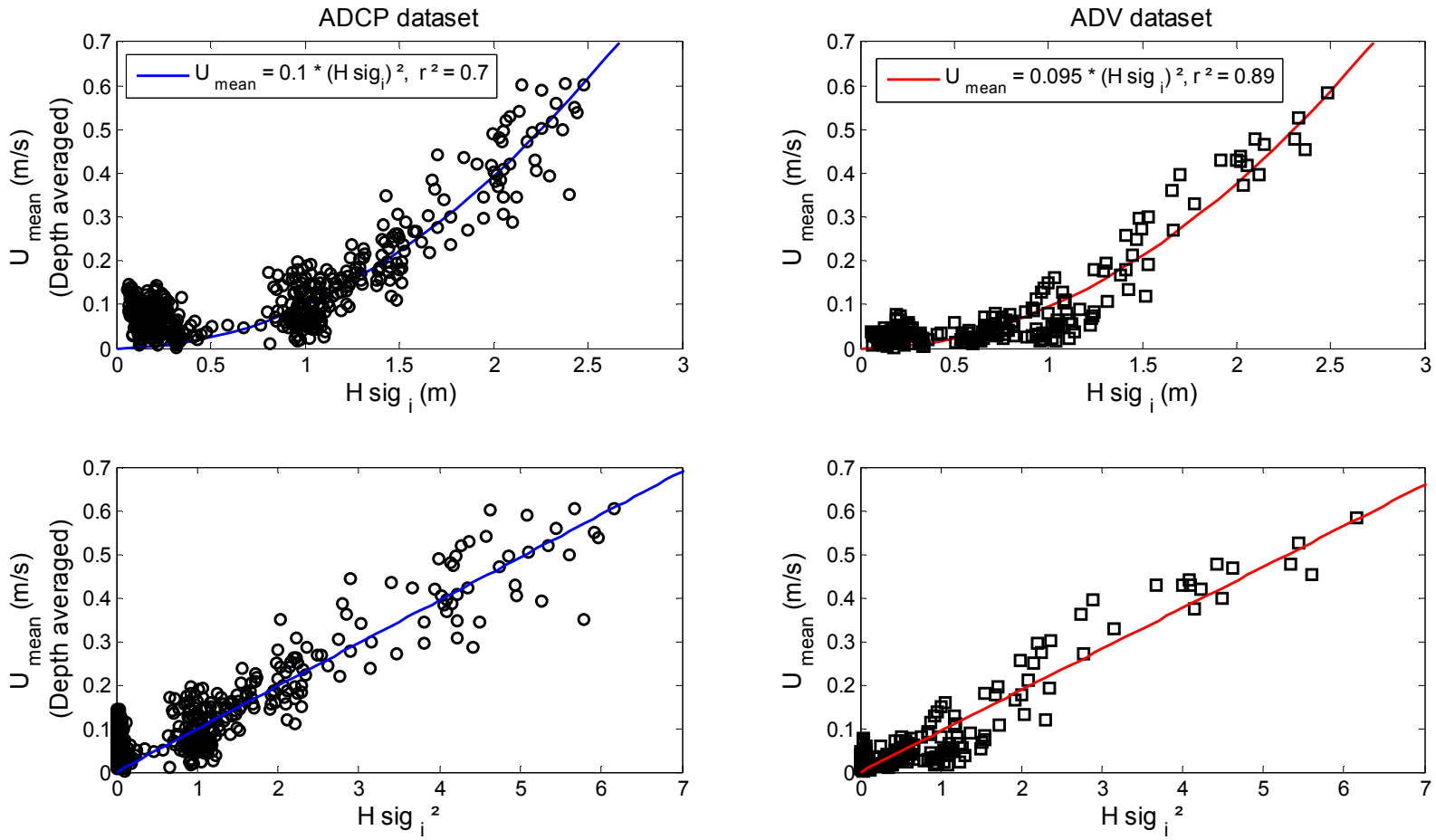

Figure 6.10. Mean current magnitude U_{mean} as a function of incident significant wave height $H sig_i$ and $(H sig_i)^2$ for the ADCP and ADV datasets. Mean current magnitude seems to increase linearly with the square of the incident significant wave height $H sig_i$ (top) suggesting a linear response to the incident wave energy (proportional to $(H sig_i)^2$, bottom).

normalized by the water depth over the reef (i.e. crest submergence) (Equation 6.5).

Dimensionless mean current velocity

$$\frac{U_{mean}}{C_{wave}} \tag{6.4}$$

where U_{mean} is the mean current velocity, and C_{wave} is the wave phase speed landward of the reef. C_{wave} is a function of water depth landward of the reef (h=5.2 m msl, tidally modified) and wave period (less significant for measured wave periods and water depths but still included in calculation). This parameter also corresponds to the Froude number that can be used as a proxy to describe flow regimes.

Dimensionless wave height

$$\frac{H\,sig_i}{Rc} \tag{6.5}$$

where H sig $_i$ is the incident significant wave height, and Rc is the water depth over the reef crest.

These parameters have been more commonly used to describe flow kinematics associated with rip current systems, particularly to relate the magnitude of offshore directed return currents to incident wave conditions (e.g. DRONEN *et al*., 2002; HALLER *et al*., 2002). They are found here to be appropriate to describe the (onshore) reef-induced flow in response to wave forcing for the present datasets.

Consistent with the Figure 6.10, increased wave forcing generally induces stronger mean (dimensionless) current velocity. The wave forcing threshold prior acceleration of current increase that was present in Figure 6.10 (H sig $_i$ ~0.8 – 1 m) roughly corresponds to ratios H sig $_i$ / Rc around 0.6-0.8 and can reasonably be attributed to the start of wave breaking on the reef crest. After this threshold, mean current magnitude increases with increasing wave forcing. The wave forcing threshold makes sense since the start of breaking-induced wave energy dissipation will induce radiation stress gradients subsequently compensated by mean currents.

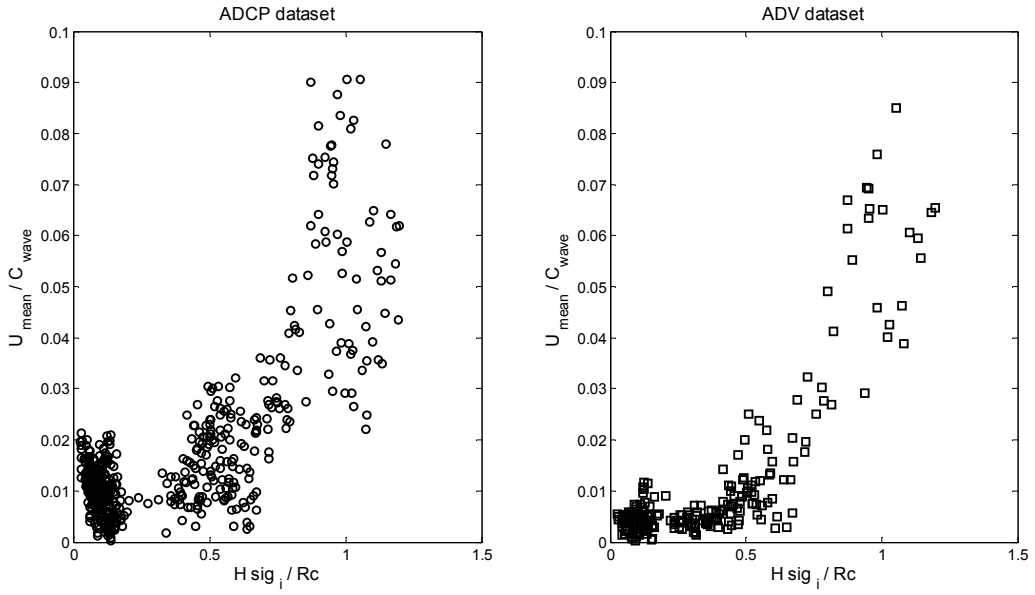

Figure 6.11. Dimensionless mean current magnitude landward of the reef U_{mean}/C_{wave} as a function of normalized incident significant wave height H sig $_i$ / Rc for the ADCP and ADV datasets. C_{wave} is the wave phase speed landward of the reef, and Rc is the water depth over the reef crest. The development of more significant (dimensionless) mean current begins for H sig $_i$ / Rc ~ 0.6-.8 and is reasonably attributed to start of wave breaking on the reef.

In linear wave theory, the radiation stress terms are directly related to the wave energy:

$$S_{xx} = E.\left[(n.\cos^2\theta + 1) - \frac{1}{2}.\right] \quad (6.6)$$

$$S_{yy} = E.\left[(n.\sin^2\theta + 1) - \frac{1}{2}.\right] \quad (6.7)$$

$$S_{xy} = \frac{E}{2}.n.\sin^2\theta \quad (6.8)$$

where E is the wave energy (Equation 6.3), n is the ratio of wave group speed to wave phase speed (n=Cg/C), and θ is the direction of wave propagation.

Assuming that cross-reef wave energy gradients (i.e. seaward/landward) can provide a gross measure of the radiation stress gradients, there should be a relationship with mean current magnitudes. Cross-reef wave energy gradients were estimated from incident and transmitted significant wave heights (using Equation 6.3 to compute wave energy) and are compared to mean current magnitudes in Figure 6.12. As expected, there are defined relationships for both the ADV and ADCP datasets, with a near linear response of mean current magnitude to increasing cross-reef wave energy gradient. This relationship indicates that the mean current magnitude will increase as the efficiency of the reef-induced wave energy dissipation increases. It is noted that, in addition to

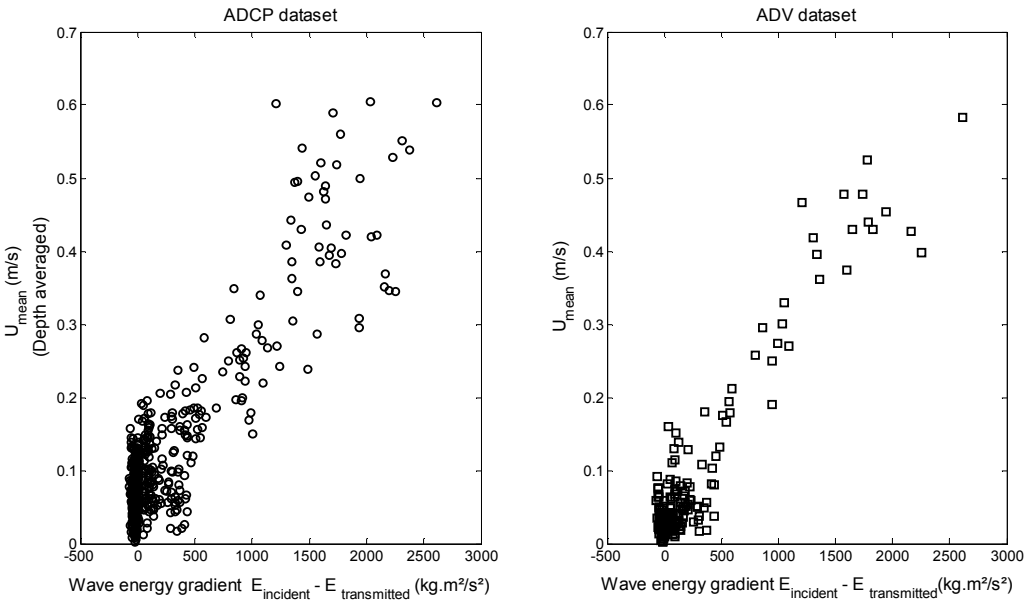

Figure 6.12. Mean current magnitude U_{mean} landward of the reef as a function of cross-reef wave energy gradient i.e. $E_{incident}$-$E_{transmitted}$ (E is the wave energy). Positive energy gradients correspond to wave energy dissipation at the reef (i.e H sig $_{transmitted}$ < H sig $_{incident}$). It is seen that mean current magnitude increases for increasing wave energy gradient. This is coherent since wave energy gradient can be seen as a crude proxy for radiation stress gradient that is expected to be an important driver for mean current at the reef.

gradients in radiation stress, other processes such as mass transport due to Stokes drift and wave rollers over the reef crest also likely contribute to the mean flow. Intensity of these processes is also described to some extents in the cross-reef wave energy gradients since more intense wave energy dissipation conditions will be associated with more intense breakers and consequently more important water mass transport due to wave rollers.

6.3.4 Estimated Water Discharge Landward of the Reef

The strong mean currents that develop landward of the reef indicate that an important flux of water is discharged in the lee of the reef. This feature is characteristic of submerged structures that allow wave and water transmission over their crest and is expected to govern the nearshore circulation in the structure lee side (e.g. Lesser *et al.*, 2003; Ranasinghe *et al.*, 2006; Ranasinghe and Turner, 2006).

To investigate the relative importance of the reef-induced water mass discharge at the study beach, mean water discharges landward of the reef were quantified from the measured mean current and compared to estimations of (i) wave-induced mass flux at the seaward measuring station i.e. incident flux, and (ii) wave-induced

mass flux expected at the same cross-shore position as the landward measuring station but on the undisturbed beach i.e. undisturbed flux.

Waves were unbroken at the seaward ADV station for the range of wave conditions experienced throughout the experiment (see Figure 5.5 for H sig $_i$ / h ratios) so the incident wave-induced mass flux (per unit width) $Q_{seaward\ ADV}$ was estimated as the mass flux due to the Stokes drift:

$$Q_{seaward\ ADV} = Q_{Stokes} = \frac{g.H\ sig_i{}^2}{8.C_{wave}} \quad (6.9)$$

where g is the gravitational constant, H sig $_i$ is the incident significant wave height, and C_{wave} is the wave phase speed at the landward instrument station. The water depth at the landward station is 5.2 m relative to mean sea level (tidally modified).

Landward of the reef, the mean water discharge (per unit width) Q_{reef} was computed as:

$$Q_{reef} = U_{mean}.\ h \quad (6.10)$$

where U_{mean} is the mean depth-averaged current velocity, and h is the depth at the landward ADV and ADCP stations (h=5.2 relative to mean sea level).

Actual depth-averaged magnitudes were used for the ADCP dataset, and near-bottom currents were assumed to be representative of the depth-averaged magnitudes for the ADV dataset.

To provide an estimate of the undisturbed water flux adjacent to the ADV station landward of the reef, a beach profile located 300 m to the north of the reef was considered (see Figure 6.1). The undisturbed water depth corresponding to the position of the landward ADV was ~ 4 m. For simplification, the same wave heights as those measured at the seaward station were used (shoaling and friction effects between the 2 water depths neglected).

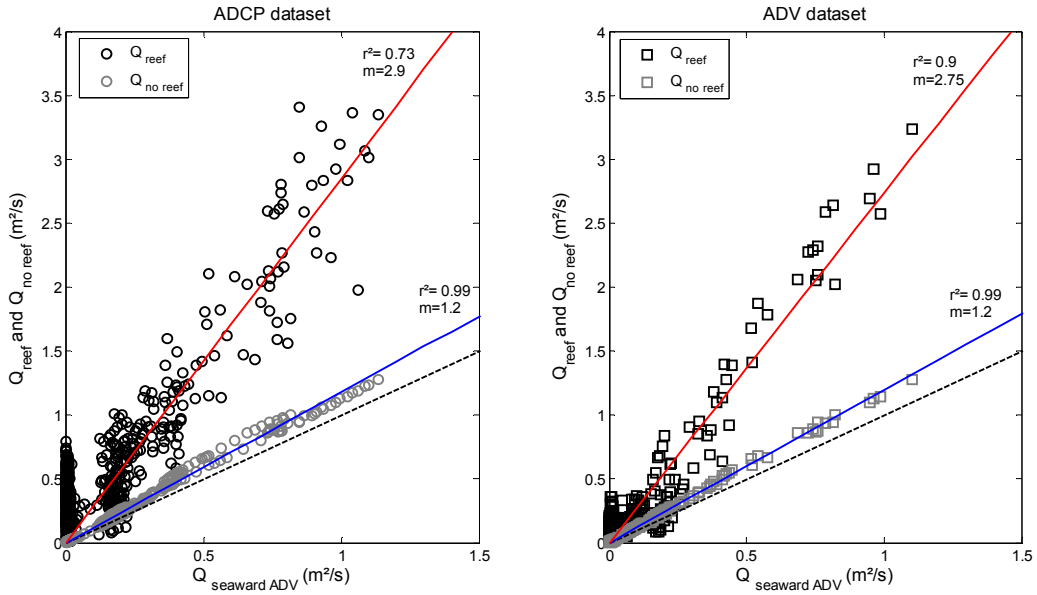

Figure 6.13. Mean water mass discharge landward of the reef Q_{reef} (black) and water mass flux at the same cross-shore position on the undisturbed beach, $Q_{no\ reef}$ (grey) as a function of incident water mass flux at the seaward station $Q_{seaward\ ADV}$. Fitted linear regressions for Q_{reef} and $Q_{no\ reef}$ are shown in red and blue respectively, and the black dashed line indicates equality between $Q_{seaward\ ADV}$ and transmitted fluxes Q_{reef}, or $Q_{no\ reef}$. It is observed that both the undisturbed and reef-induced mean water discharges seem to increase linearly with the incident water mass flux $Q_{seaward\ ADV}$. However, the mean water discharge landward of the reef Q_{reef} is about 2.5 times larger than the undisturbed one at a similar cross-shore position on the undisturbed beach ($Q_{no\ reef}$).

The maximum ratio $H\ sig_i$ / h was around 0.5 so no wave breaking was expected, and therefore the water mass flux $Q_{no\ reef}$ was estimated as the Stokes drift:

$$Q_{no\ reef} = Q_{Stokes} = \frac{g.H\ sig_i{}^2}{8.C_{beach}} \qquad (6.11)$$

where g is the gravitational constant, $H\ sig_i$ is the incident significant wave height, and C_{beach} is the wave phase speed at the ADV cross-shore position on the beach profile (h = 4 m, relative to mean sea level, tidally modified).

Reef-induced and undisturbed water discharge fluxes Q_{reef} and $Q_{no\ reef}$ are shown as a function of the incident water mass flux $Q_{seaward\ ADV}$ in Figure 6.13. The first feature of interest is that both the reef-induced and undisturbed water discharges seem to increase linearly with the incident water mass flux. Relationships are consistent for both datasets. According to linear regression slopes, the water discharge landward of the reef Q_{reef} is about 2.5 times larger than the one estimated at the same cross-shore location on the natural beach (i.e. $Q_{no\ reef}$). For example, for the maximum wave height measured of $H\ sig_i$ = 2.5 m, the incident water mass flux per unit width $Q_{seaward\ ADV}$ is 1 m²/s (seaward station) and becomes 1.2 m²/s on the natural beach at a cross-shore position equivalent to the

landward station. The concurrent water discharge in the lee of the reef is of 3 m²/s (per unit width). Considering the full width of the structure of 80 m and an equally wide undisturbed beach segment, respective flow discharges are 240 m^3/s and 96 m^3/s. This will have likely effects on the nearshore circulation in the lee side of the reef.

The difference between the reef-induced and undisturbed water mass fluxes will likely be the most significant when wave breaking is triggered on the reef outside of the natural surfzone. It can reasonably be hypothesized that this was the situation experienced throughout the experiment. Using the common wave breaking ratio of $\gamma = 0.78$ (e.g. KOMAR, 1998), the maximum breaking depth h_{break} is 3.2 m, and thus well landward of the reef on the "natural" beach profile shown in Figure 6.1.

Another feature to note is that the water depth used to compute Q_{reef} is in fact representative of the large scour hole that developed landward of the reef (Figure 6.1, see also Figure 4.5 and 4.8 for full beach bathymetries). The water depth at the landward toe of the reef was initially smaller and thus likely associated with stronger currents. Since the reef construction was extended in time and that the scour started to develop when only one arm was in place (see SCARFE 2008), the presently estimated discharges Q_{reef} for the completed reef may not be fully representative of the situation at that time. Nevertheless, if the reef had been completed quickly and assuming an initial depth at the toe of the reef of h = 4 m instead of h = 5.2 m (msl) (see Figure 6.1), a discharge Q_{reef} = 3 m²/s as experienced for H sig $_i$ ~2.5 m would correspond to current magnitudes around 0.8 m/s instead of 0.6 m/s (see Equation 6.10). Using the same reasoning and assuming mass conservation as waves propagates over the reef, current velocity magnitude over the reef crest can also be inferred. For a discharge Q_{reef} = 3 m²/s on the reef crest Rc ~2 m, corresponding current magnitude is ~1.5 m/s.

6.3.5 MODEL FOR ESTIMATION OF WATER DISCHARGE LANDWARD OF THE REEF

It would be valuable to develop a simple model able to explain the reef-induced water mass discharge Q_{reef}. Since the mean current magnitude landward of the reef was found to be dependent on the incident wave conditions (e.g. Figures 6.10 and 6.11) and efficiency of the reef-induced dissipation (i.e. wave energy gradients),

(Figure 6.12), there should be similar dependences with respect to the mean water mass discharge landward of the reef Q_{reef}.

SVENDSEN (1984) has shown that the amount of water carried onshore by the breakers is composed of two parts. One is associated with the mass transport in the waves Q_{Stokes} (Stokes drift, equation 6.11) and the other is due to the mass transport in wave rollers $Q_{roller.}$ (Equation 6.12). Since the main effect of the reef is to break incident waves due to its shallow crest, it should then be possible to explain the reef-induced discharge Q_{reef} in terms of the incident mass flux on the reef crest, as a combination of Q_{Stokes} and $Q_{roller.}$

The incident wave-induced water mass flux (per unit width) on the reef crest due to the Stokes drift is:

$$Q_{Stokes} = \frac{1}{8} \frac{g.(H\,sig_i)^2}{C_{reef}} \qquad (6.12)$$

where $H\,sig_i$ is the incident significant wave height , and C_{reef} is the linear wave phase speed on the reef crest, equal to $\sqrt{g.Rc}$. Rc is the water depth on the reef crest and g is the gravitational constant.

The water mass transport in wave rollers Q_{roller} can be estimated as (SVENDSEN, 1984):

$$Q_{roller} = \frac{A}{T} \qquad (6.13)$$

where T is the wave period, and A is the cross sectional area of the surface roller estimated by $A = 0.9\ H^2$ (H is the wave height). For the present application, $A = 0.9.(H\,sig_i)^2$ was assumed.

To apply the transport due to wave rollers only when relevant, a threshold was defined to indicate the start of breaking on the reef. A depth-limited criterion was used:

$$\frac{H\,sig_i}{Rc} = 0.8 \qquad (6.14)$$

where $H\,sig_i$ is the incident significant wave height, and Rc is the water depth on the reef crest.

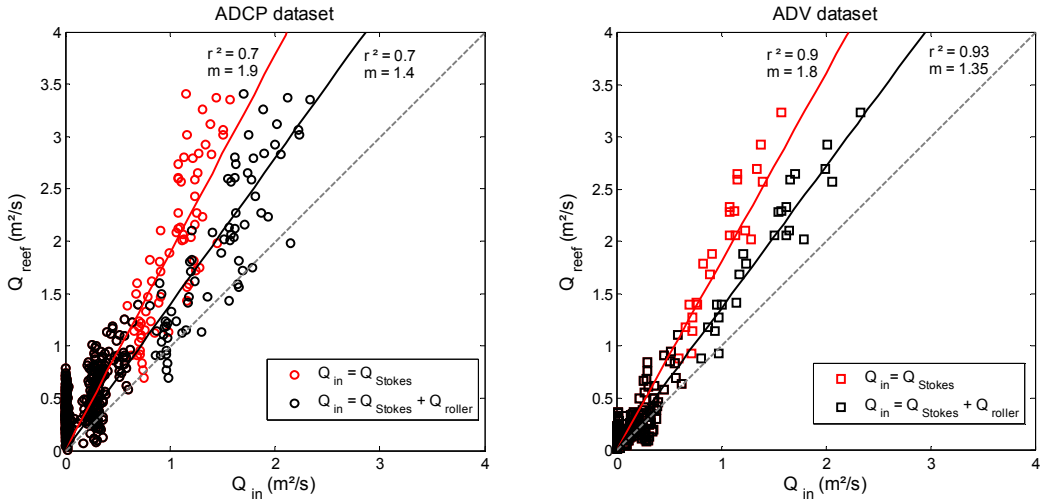

Figure 6.14. Mean water mass discharge landward of the reef Q_{reef} as a function of incident water mass flux on the reef crest Q_{in}. For comparison, Q_{in} was computed as the Stokes drift Q_{Stokes} only (red, Equation 6.11) and as the sum of the fluxes due to the Stokes drift Q_{Stokes} and wave rollers Q_{roller} (black, Equation 6.14). Fitted linear regressions are shown in red and black. The grey dashed line represents the unity Q_{in}= Q_{reef}. Q_{reef} seems linearly related but biased high relative to Q_{in}. The inclusion of the water transport due to wave rollers reduces the bias but Q_{reef} remains ~1.4 larger than Q_{in}.

The proportionality constant of 0.8 is close to the value of 0.78 generally used, and also consistent with recent experiments of wave breaking on submerged slopes (0.85, BLENKINSOPP and CHAPLIN, 2008).

As a result, the total incident water mass flux on the reef crest Q_{in} is determined as:

$$Q_{in} = Q_{Stokes} + \text{(if breaking) } Q_{roller} \quad (6.15)$$

The incident water mass flux on the reef crest Q_{in} is compared to the reef-induced water discharge Q_{reef} in Figure 6.14 for the ADCP and ADV datasets. Encouragingly, it is found that the water discharge landward of the reef Q_{reef} linearly increases with the incident water mass flux on the reef crest Q_{in}. Relationships are consistent for both the ADV and ADCP datasets. However, even when the water transport due to wave rollers is included, Q_{reef} remains biased high relative to Q_{in} (i.e regression slopes > 1). This indicates that the computed incident water flux on the reef crest Q_{in} only explains a fraction of the reef-transmitted discharge Q_{reef}. A possible explanation is that incident wave heights are likely being shoaled as they propagate over the shallow reef crest prior to breaking. As a result, the use of wave heights measured at the seaward ADV

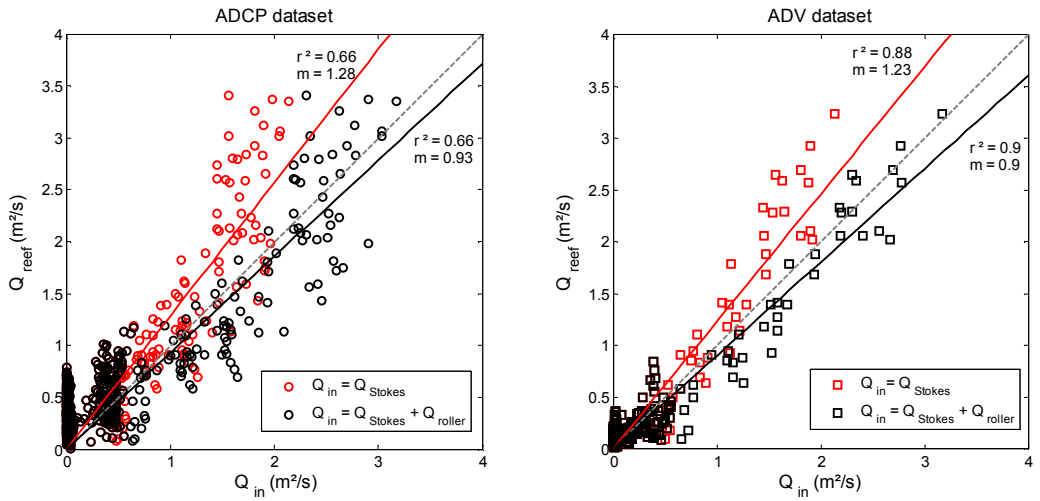

Figure 6.15. Mean water mass discharge landward of the reef Q_{reef} as a function of modified incident water mass flux on the reef crest Q_{in}. Here, Q_{in} was computed using significant wave heights measured at the seaward station (h=5.2 m msl) shoaled to the depth of the reef crest Rc (~2 m, msl). For comparison, Q_{in} was computed as the Stokes drift Q_{Stokes} only (red, Equation 6.11), and as the sum of the fluxes due to the Stokes drift Q_{Stokes} and wave rollers Q_{roller} (black, Equation 6.14). Fitted linear regressions are shown in red and black. The grey dashed line represents the unity $Q_{in} = Q_{reef}$. The use of shoaled wave heights reduces the bias between Q_{in} and Q_{reef}. The water mass discharge landward of the reef Q_{reef} can thus be approximated by the incident water mass flux on the reef crest Q_{in} (including mass transport due to wave roller) i.e. $Q_{reef} \sim Q_{in} = Q_{Stokes} + Q_{roller}$.

station in deep water (h=5.2 m, msl) in the computation of Q_{in} could underestimate the actual incident water flux on the shallow reef crest.

To try and reduce the bias, the incident water flux Q_{in} was recomputed using wave heights shoaled at the water depth on the reef crest (Rc). The shoaling coefficient $K_{shoal} = H_{reef} / H_{sig\ i}$ was determined using the method of NIELSEN (1982). It is observed in Figure 6.15 that the use of the shoaled wave heights effectively reduces the bias of Q_{reef} relative to Q_{in}. The computed incident water mass flux on the reef crest approximately equals the measured reef discharge i.e. $Q_{reef} \sim Q_{in} = Q_{Stokes} + Q_{roller}$ (Figure 6.15).

According to the linear regression coefficients, when the water mass transport due to wave rollers is included, the incident flux Q_{in} could in fact slightly overestimate the transmitted water discharge landward of the reef Q_{reef} ($m \sim 0.9 < 1$). A likely cause is that to be physically correct, the Q_{roller} should be included when breakers are saturated (e.g. AAGAARD *et al.*, 1997). Otherwise, in transitional conditions, the onshore water transport may be better described by the Stokes transport only. These breaking saturation conditions are hard to discriminate using a simple breaking criterion (Equation 6.13). It was possible to

obtain a regression coefficient slightly closer to unity (0.94) using a larger breaker ratio $H\,sig_i / Rc = 1$ to delay the inclusion of breaking roller to "more saturated" conditions but this also tended to scatter the data points. A similar regression coefficient was obtained using the reduction in wave height transmission coefficients i.e. $Kt_{sig} < 0.8$ to flag wave breaking and start including Q_{roller} (not shown).

These small deviations taken apart, it is expected that a good first order estimation of the water discharge landward of the reef can be obtained using the simple linear relationships shown in Figure 6.15. It may be useful to compare estimates obtained when the incident water flux on the reef crest Q_{in} is computed as Q_{Stokes} only or $Q_{Stokes} + Q_{roller}$ (using respective regression coefficients) to reduce uncertainties due to application of wave roller water transport. The simple relationships are interesting in that they link mean current magnitude landward of the reef to a range of important design parameters such as incident wave height, crest submergence, and water depth at the toe of the structure, implicitly included in water flux computations.

6.4 CONCLUSIONS

Analysis of hydrodynamics measured for 5 days in the vicinity of the multi-purpose reef at Mount Maunganui is presented. The field deployment consisted of an ADV station located 30 m seaward of the reef and co-located ADV and ADCP just landward of the reef. The stations measured current conditions simultaneously with the wave data analyzed in Chapter 5. Main findings are:

- The main feature of the data is the distinct onshore deviation of currents landward of the reef. Oblique wave incidence experienced throughout the experiment induced predominantly long-shore directed mean currents seaward of the reef (~80 ° relative to reef centerline). The flow was significantly deviated toward the shore landward of the reef (~ 10-30 ° relative to reef centerline). Mean current magnitude was of order 0.5 m/s when incident waves exceeded $H\,sig_i \sim 1.5$ m.

- Measurements of vertical current profiles indicated that the flow landward of the reef is relatively depth uniform under large waves ($H\,sig_i \sim 2$ m).

For small non breaking waves ($Hsig_i$ =0-0.5 m) or intermediate conditions ($Hsig_i$ =0.5-1.5 m), a wave shear is present near the surface (top 2 m) with stronger current magnitudes. As large waves are associated with most intense dissipative conditions, the depth uniformity of mean current magnitude is attributed to more saturated breaking conditions. Wave activity and energy dissipation may be more sensible near the surface for small (non breaking) and medium waves and would induce the observed shear near the surface.

- The mean current magnitude generally increased for increasing wave forcing. The relationship between mean current velocity and incident wave heights seemed to be well explained by a simple square function $U_{mean}=a.(H\ sig_i)^2$ suggesting a linear response of mean current magnitude to incident wave energy. A relationship between dimensionless parameters describing the mean current magnitude as the mean current U_{mean} normalized by the wave phase speed, and the wave forcing as the incident height $H\ sig_i$ normalized by the crest submergence Rc was found. The development of significant mean current started for ratios $H\ sig_i$ / Rc around 0.6-0.8 and can reasonably be attributed to the start of wave breaking on the reef. Mean current magnitude then increased for increasing ratios $H\ sig_i$ / Rc. Furthermore, the increase in mean current was found to be well explained by the development of more important cross-reef wave energy gradients (i.e. seaward /landward). This is coherent since the cross-reef wave energy gradient can be seen as a crude proxy for radiation stress gradient that is expected to be an important driver for mean currents.

- Mean water discharges landward of the reef were determined from the mean current magnitudes. Overall, water discharge landward of the reef is ~2.5 larger than the one expected at the same cross-shore location on a natural beach (when that is outside the surfzone). This has likely implications on the nearshore circulation in the lee of the reef.

- It was found that the mean water discharge landward of the reef Q_{reef} could be well explained by the incident wave-induced water flux over the reef crest Q_{in} that includes the water flux due to Stokes drift Q_{Stokes} and

the water flux due to wave rollers Q_{roller} for breaking waves (SVENDSEN, 1984). If incident wave heights measured at the seaward station were assumed for computation of the incident mass flux Q_{in}, Q_{reef} was linearly correlated but biased high relative to Q_{in} ($m \sim 1.4$). Using incident wave heights shoaled at the depth of the reef crest Rc, the mean water discharge landward of the reef was correctly approximated by $Q_{reef} \sim Q_{Stokes} + Q_{roller}$.

6.5 REFERENCES

AAGAARD, T.,B., GREENWOOD, B. and NIELSEN, J., 1997. Mean currents and sediment transport in a rip channel. *Marine Geology*, 140, 25-45.

BLENKINSOPP, C.E., and CHAPLIN, J.R., 2008. The effect of relative crest submergence on wave breaking over submerged slopes. *Coastal Engineering*, 55 (12), 967-974.

DRONEN, N., KARUNARATHNA, H., FREDSOE, J., SUMER, B.M., and DEIGAARD, R., 2002. An experimental study of rip channel flow. *Coastal Engineering,* 45 (3), 223-238.

HALLER, M.C., ROBERT A. DALRYMPLE, R.A., and SVENDSEN I.B., 2002. Experimental study of nearshore dynamics on a barred beach with rip channels. *Journal of Geophysical Research*, 107 (C6), 14-1:14-21.

KOMAR, P.D.,1998. *Beach processes and sedimentation*, 2nd Edition, Prentice Hall, 544 p.

LESSER, G.R., de VROEG, J.H., ROELVINK, J.A., de GERLONI M., and ARDONE, V., 2003. Modelling the morphological impact of submerged offshore breakwaters. *Proceedings of Coastal Sediments'03* (Clearwater Beach, Florida), 14 p. (CD ROM publication).

NIELSEN P., 1982. Explicit formulae for practical wave calculations. *Coastal Engineering*, 6, 389-398.

RANASINGHE, R., and TURNER, I.L., 2006. Shoreline Response to Submerged Structures: A Review. *Coastal Engineering*, 53, 65-79.

RANASINGHE, R., TURNER, I.L., and SYMONDS, G., 2006. Shoreline Response to Multi-Functional Artificial Surfing Reefs: A Numerical and Physical Modeling Study. *Coastal Engineering*, 53, 589-611.

SCARFE, B.E., 2008. Oceanographic Considerations for the Management and Protection of Surfing Breaks. Hamilton, New Zealand: The University of Waikato, Ph.D. thesis, 307 p. + appendices.

SVENDSEN, LA., 1984. Mass flux and undertow in a surf zone. *Coastal Engineering*, 8, 347-365.

CHAPTER 7. NUMERICAL MODELLING OF WAVES AND CURRENTS AROUND AN OFFSHORE SUBMERGED MULTI-PURPOSE REEF AT MOUNT MAUNGANUI, NEW ZEALAND

7.1 INTRODUCTION

This chapter presents results of numerical modelling of waves and currents around the offshore submerged multi-purpose reef at Mount Maunganui, New Zealand. The wave transmission over the reef was calibrated using the wave data collected seaward and landward of the reef during a 5 day field experiment. Simulated wave and current conditions during the field experiment are described to outline the large scale wave and circulation patterns that developed at the beach in response to the local transmission characteristics reported in Chapters 5 (wave) and 6 (hydrodynamics). The calibrated model was then used in predictive mode to simulate a range of representative wave events, and identify the main wave and circulation patterns expected at the site.

7.2 METHODS

7.2.1 2DBEACH MODEL DESCRIPTION

The numerical modelling was undertaken using the model 2DBEACH included in the 3DD® numerical model suites (BLACK, 2002). A complete description of the model structure and validation is provided in BLACK and ROSENBERG (1992). A brief description is provided below.

The model 2DBEACH consists of coupled wave and hydrodynamic modules. The wave module simulates the refraction, shoaling, and breaking of monochromatic waves. Time series of wave heights, periods, directions and water levels are specified at the offshore boundary of a rectangular computational grid and propagated through the model domain. The wave heights are obtained from the 2 dimensional energy flux conservation equation that is solved using a mixed Lagrangian/Eulerian solution. The technique was found to better handle wave

height propagation over complex topography, and the sharp height gradients across the breakpoint (see BLACK and ROSENBERG, 1992). The wave energy is dissipated in the model through bed friction, wave breaking, and wave-current interactions. Friction and wave breaking characteristics were modified during the calibration process, and therefore respective equations are provided for them.

The bed frictional resistance term used is of the form:

$$F_{friction} = \frac{2C_f}{3\pi}\frac{H^2}{g}\left[\frac{w}{\sinh(kh)}\right]^3 \quad (7.1)$$

where C_f is the bottom friction coefficient, H is the wave height, g is the gravitational constant, w is the radian frequency ($2\pi/T$, T wave period), k is the wave number ($2\pi/L$, L wave length), and h is the water depth. In the model, the bed friction is varied by changing the coefficient C_f.

The breaking wave height can be calculated using a user defined depth limited criterion:

$$\frac{H_b}{d_b} = \gamma \quad (7.2)$$

where H_b and d_b are breaking wave height and breaking depth respectively, and γ is a constant (theoretically 0.78 for solitary waves).

Alternatively, the criterion of MADSEN (1976) including the local bathymetry slope m can be chosen:

$$H_b = 0.72\, d_b(1 + 6.4\, m) \quad (7.3)$$

The wave energy dissipation after wave breaking, and subsequent wave height decay, are simulated using the model of DALLY *et al*. (1985):

$$F_{breaking} = \frac{K}{h}\left[EC_g - (EC_g)_{stable}\right] \quad (7.4)$$

where K is an empirical constant generally around 0.15-0.2, h is the total water depth, EC_g is the wave energy flux at a given point in the grid, and $(EC_g)_{stable}$ is the energy flux associated with a depth limited stable wave height in the surfzone. The stable wave height is of the form $H_{stable} = \Gamma h$, with $\Gamma \sim 0.4$ (half of the initial breaking value, $\gamma/2$).

The wave angles are solved assuming the conservation of wave numbers. The method implicitly accounts for wave-current interactions. In addition, a smoothing scheme in the form of a horizontal eddy viscosity term is applied to obtained wave angles to mimic diffraction effects. This was generally found to provide an acceptable substitute for the full diffraction equations in the model validation (BLACK and ROSENBERG, 1992). The output of the wave model consists of the wave height, wave angle, and radiation stress components at each grid point.

The hydrodynamic module (3DD) is mainly wave-driven and uses the height and radiation stress fields output by the wave module as input. The depth-integrated equations for conservations of mass and momentum in the 2 horizontal dimensions are solved to provide depth-integrated current velocities and sea levels in the computational grid. A more complete description of the hydrodynamic module is found in BLACK and HEALY (1998).

7.2.2. MODEL DOMAIN

The model domain used was a rectangular grid covering a beach segment of 1390 m in the long-shore direction and 780 m in the cross-shore direction, centred on the reef. The bathymetry grid was generated from the multibeam survey dataset collected in March 2009 (see Figure 4.8, bottom for high resolution bathymetric chart) using the software SURFER® (GOLDEN SOFTWARE INC.). A relatively coarse grid cell size of 10 x 10 m was used to keep simulation times reasonable, but the depth grid still resolved the main bathymetric features including the reef structure and associated onshore scour hole, along with the underlying long-shore bar and the small salient feature near the shoreline (Figure 7.1). The grid cells representing the reef were checked and manually edited to best fit the actual depths (see Figure 4.1) if needed.

A wave angle of 0° indicates waves approaching the reef and beach normally; the wave angle is positive for waves propagating towards the top of the grid, and negative for waves propagating towards the bottom of the grid (see Figure 7.1).

7.2.3 MODEL CALIBRATION

The numerical model was calibrated primarily with respect to the wave height transmission over the reef using the incident and transmitted wave height datasets collected around the reef (see Chapter 5). It is noted that the model cannot

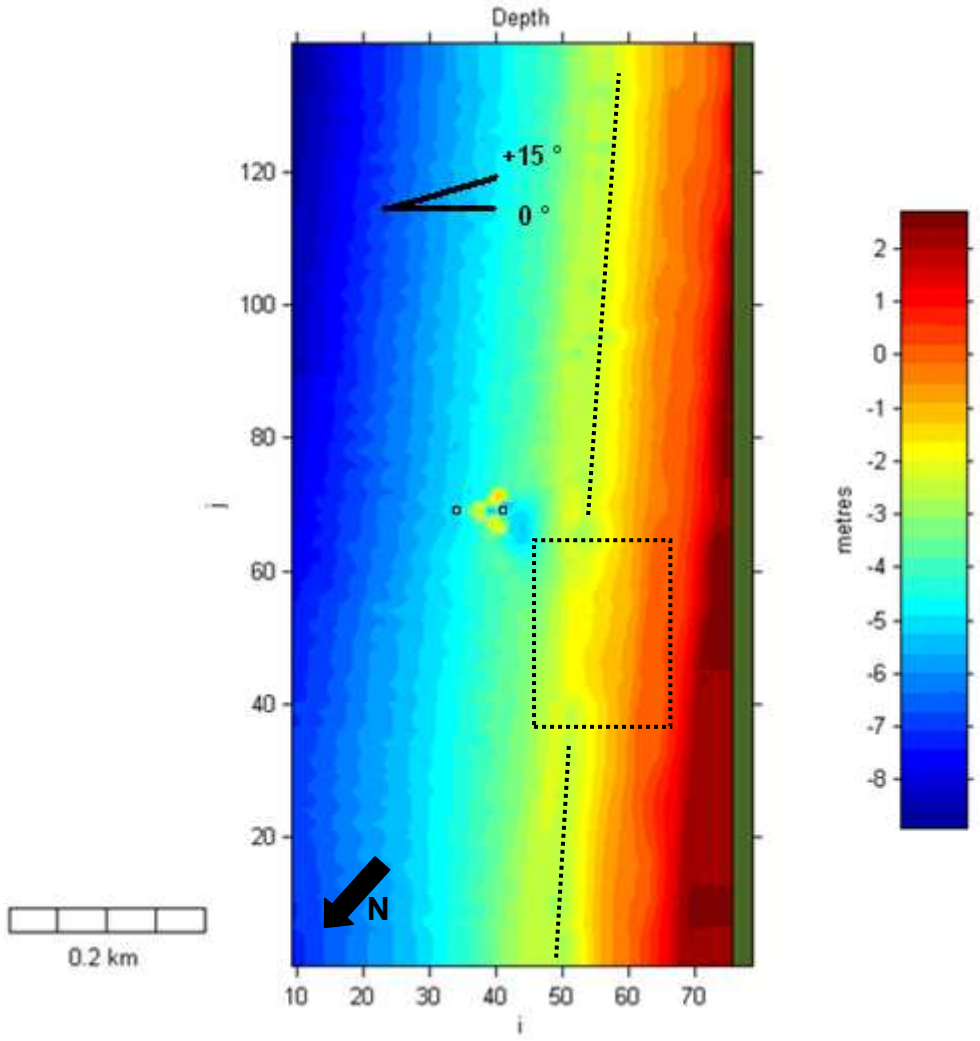

Figure 7.1. Bathymetry of the model domain. The cell size is 10 x 10 m and the grid dimensions are 139 cells in the vertical direction and 78 cells in the horizontal direction. For model calibration, model predictions were extracted at the positions indicated by the 2 symbols seaward and landward of the reef that correspond to the positions of instruments during the field experiment. The dashed rectangle below the reef centerline shows the small salient feature, and the dashed lines locate the underlying trough.

simulate the complex transformations of the irregular incident wave fields described in Chapter 5, including modification of the wave height and period distributions, and wave energy transfers within the frequency domain. Instead, the model was used to reproduce the overall magnitude of height transmission resulting from all these processes to get representative transmitted wave conditions in the lee of the reef.

Prior to the calibration, a first necessary step was to obtain wave conditions at the model offshore boundary since no wave data was available at that point. Wave heights and angles were estimated by back shoaling and back refracting wave conditions measured at the station seaward of the reef (see Figure 7.1 for measuring station positions). The methods of NIELSEN (1982) were used and

shore-parallel bathymetric contours were assumed. The same wave periods and tide levels as those measured at the station seaward of the reef were used. It was found that the computed offshore wave direction required a shift of ~ + 5° (i.e. to the West) to correctly reproduce the wave angle measured seaward of the reef. Wave heights and angles were then very well reproduced at the outer station position in the model grid.

The calibration of the wave height transmission was undertaken by testing a range of values for the model parameters describing the bottom friction, wave breaking, and horizontal eddy viscosity (i.e. angle smoothing) to best reproduce the measured transmitted wave heights and angles at the position of the landward station in the model grid (Figure 7.1). As a starting point, a set of reference parameter values were taken equal to those used in BLACK and MEAD (2007) for numerical modelling investigations at the same study site (Table 7.1, first line). Given the numerous combinations possible, a sensitivity analysis was conducted varying each parameter one at a time. This was done in the following order: a range of friction coefficients was first tested, and the best value was then used to test the effect of the horizontal eddy viscosity parameter. Using the best friction and eddy viscosity parameters, the effect of a modified wave breaking model, including incipient breaking criterion and intensity of wave energy dissipation (K constant of Dally's model), was finally investigated. The simulations are summarized in Table 7.1. The hydrodynamic module was less extensively calibrated by varying the roughness length while keeping the calibrated wave parameters constant (Table 7.2).

To identify the "best" parameter values, the goodness of fit of the model predictions to the measured time series was estimated using a relative squared error as in BLACK and ROSENBERG (1992):

$$\varepsilon^2 = \frac{\sum(X_p - X_m)^2}{\sum(X_m)^2} \qquad (7.5)$$

where X_p is the value predicted by the model, and X_m is the measured value.

Table 7.1. Relative squared errors ϵ^2 of predicted incident (subscript i) and transmitted (subscript t) wave heights and angles. The first line corresponds to the set of parameters used in BLACK and MEAD (2007) that served as a reference. The set of model parameters yielding the lowest error is highlighted in grey.

Friction factor Cf	**Eddy viscosity (m²/s)**	**Breaking criterion**	**Dally's model constant K**	**Resistance length (m)**	**Wave height errors**		**Wave angle errors**	
					ϵ^2 (H_i)	**ϵ^2 (H_t)**	**ϵ^2 (Angle $_i$)**	**ϵ^2 (Angle $_t$)**
0.01	10	Madsen	0.15	0.075	0.0148	0.0519	0.0034	0.0806
0.015	10	Madsen	0.15	0.075	0.0084	0.0467	0.0034	0.0808
0.02	10	Madsen	0.15	0.075	0.0047	0.0436	0.0034	0.0799
0.025	10	Madsen	0.15	0.075	0.0031	0.0410	0.0034	0.0797
0.03	10	Madsen	0.15	0.075	0.0032	0.0391	0.0034	0.0799
0.035	10	Madsen	0.15	0.075	0.0047	0.0395	0.0034	0.0804
0.04	10	Madsen	0.15	0.075	0.0073	0.0411	0.0034	0.0799
0.05	10	Madsen	0.15	0.075	0.0148	0.0418	0.0034	0.0790
0.03	0.1	Madsen	0.15	0.075	0.0032	0.0440	0.0034	0.0804
0.03	0.5	Madsen	0.15	0.075	0.0032	0.0441	0.0034	0.0816
0.03	1	Madsen	0.15	0.075	0.0032	0.0442	0.0034	0.0805
0.03	5	Madsen	0.15	0.075	0.0032	0.0428	0.0034	0.0802
0.03	10	Madsen	0.15	0.075	0.0032	0.0391	0.0034	0.0799
0.03	15	Madsen	0.15	0.075	0.0032	0.0407	0.0034	0.0799
0.03	20	Madsen	0.15	0.075	0.0032	0.0438	0.0034	0.0789
0.03	10	Madsen	0.15	0.075	0.0032	0.0391	0.0034	0.0799
0.03	10	Madsen	0.18	0.075	0.0032	0.0418	0.0034	0.0805
0.03	10	Madsen	0.2	0.075	0.0032	0.0429	0.0034	0.0799
0.03	10	$\gamma = 0.8$	0.15	0.075	0.0032	0.0426	0.0034	0.0796
0.03	10	$\gamma = 0.8$	0.18	0.075	0.0032	0.0436	0.0034	0.0787
0.03	10	$\gamma = 0.8$	0.2	0.075	0.0032	0.0440	0.0034	0.0785
0.03	10	$\gamma = 0.7$	0.15	0.075	0.0032	0.0438	0.0034	0.0792
0.03	10	$\gamma = 0.7$	0.18	0.075	0.0032	0.0444	0.0034	0.0792
0.03	10	$\gamma = 0.7$	0.2	0.075	0.0032	0.0451	0.0034	0.0796

7.2.4 WAVE EVENTS SIMULATED

The wave conditions and circulation patterns that developed at the site during the field experiment were first investigated using a numerical simulation with the parameters eventually selected after calibration (highlighted in grey in Table 7.1 and 7.2). The calibrated model was then used to simulate a range of wave events (Table 7.3) to identify the main wave and circulation patterns expected at the study beach.

7.3 RESULTS

7.3.1 MODEL CALIBRATION

The coefficients giving the best fits after the calibration runs are highlighted in grey in Table 7.1. The reference parameters used in BLACK and MEAD (2007) with respect to horizontal eddy viscosity and wave breaking characteristics provided the best predictions, however, the wave friction coefficient was increased to 0.03. An accepted reference value of the friction coefficient for sloping sandy beaches is 0.01 (e.g. THORNTON and GUZA, 1983), but the required increase seems acceptable since the reef surface, although smooth (i.e. geotextile), is relatively irregular (see Figure 1.4).

A consequent limitation of the present model is that since the friction coefficient is constant throughout the model domain, undisturbed waves outside the reef area may be subject to excessive attenuation due to friction. However, the value 0.03 is not dramatically greater than the reference value of 0.01, and it is expected that the correct reproduction of the reef transmission is more useful for this study than a possible slight under prediction of undisturbed wave heights. Furthermore, any excessive friction will become less significant near and in the surfzone as in these regions the bottom friction plays a negligible role in wave transformation when compared to shoaling and breaking (THORNTON and GUZA, 1983; DALLY *et al.*, 1985).

To supplement the direct comparison of relative errors (Table 7.1) and better outline the skills and limitations of the calibrated model, predicted wave heights

Table 7.2. Relative squared errors ϵ^2 of predicted incident (subscript i) and transmitted (subscript t) current speed and direction. The selected value is highlighted in grey.

Resistance length (m)	Current velocity ϵ^2	Current direction ϵ^2
0.005	0.5468	1.5874
0.01	0.3417	1.4869
0.05	0.2453	1.4768
0.075	0.1423	1.5333
0.1	0.2089	1.4989

and angles seaward and landward of the reef are shown in Figure 7.2. It is firstly observed that the wave heights and angles at the seaward station are very well reproduced by the model from the modified wave data applied at the model boundary.

Period 1 of the experiment was characterized by the shoaling of small incident waves ($H\,sig_i$ = 0-0.5 m), without breaking. In Chapter 5, the amplification of the transmitted wave heights was found to be relatively more efficient on lower tide levels because of the shallower reef crest, and consequently more intense shoaling. The predicted transmitted wave heights are correctly reproduced for high tide levels but consistently under predicted for low tide levels (Figure 7.4, time ~ 0-40 h). The predicted wave height evolution on the reef profile for the low tide levels generally indicated that the wave height was effectively amplified over the shallow reef crest, however, a significant height reduction was then observed in the deep scour hole in the lee of the reef. The predicted transmitted wave angles are larger by ~ 10° relative to measurements indicating waves propagating more obliquely in the model than measured. This was consistently obtained for the different simulations undertaken and could not be significantly modified.

For the wave event developing at time ~ 50 h (Period 2), the wave height transmission is correctly predicted. The measured tidal modulation of the height transmission resulting in smaller transmitted heights over the shallower reef crest is well reproduced by the model. The predicted wave angles are underestimated at the beginning of the wave event (time 50-60 h) (i.e. wave closer to shore normal incidence in the model than in reality) but correctly predicted afterwards.

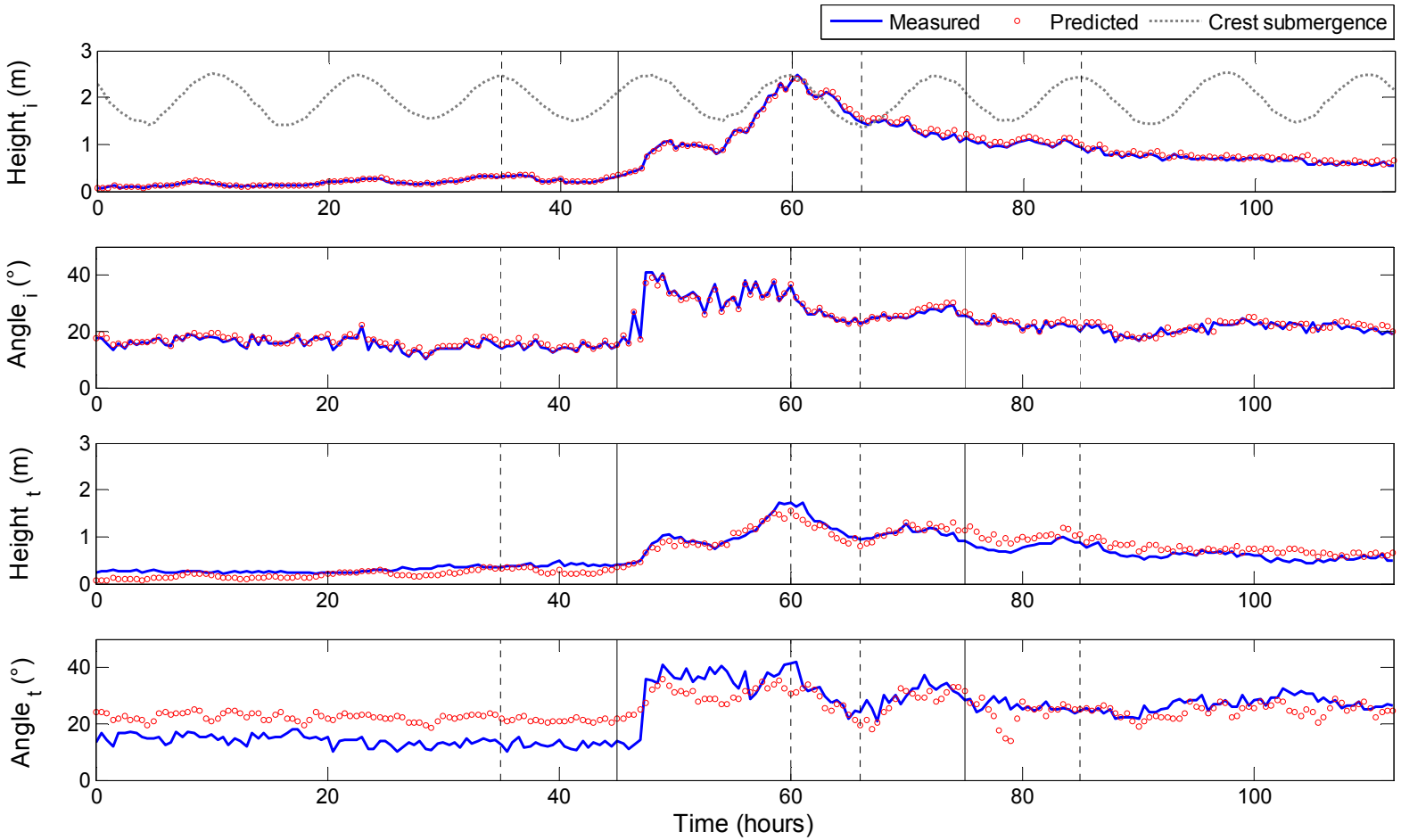

Figure 7.2. Comparison of measured wave heights and angles with predictions of the calibrated numerical model. The top 2 graphics show the incident wave conditions (subscript i) and the bottom 2 graphics show the transmitted wave conditions (subscript t). The water depth over the reef crest is plotted for reference on the top graphic (dashed grey line). The plain vertical lines separate the 3 periods of the experiment (i.e. small, medium, large waves), and the dashed vertical lines locate the 4 events described in Figures 7.5 to 7.11.

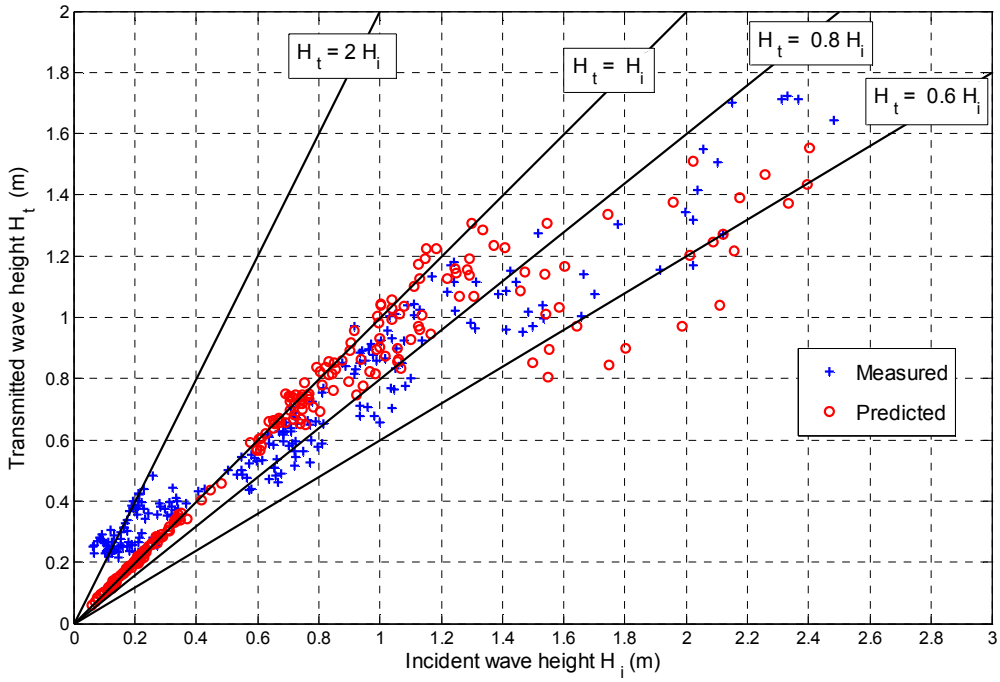

Figure 7.3. Measured and predicted transmitted wave height landward of the reef as a function of incident wave height seaward of the reef. The plain lines indicate some reference coefficients of wave height transmission.

For medium waves in period 3 (H sig $_i$ = 0.5-1.5 m), the predicted transmitted heights remain larger that measured; particularly on shallow reef crests. The fit of predicted / measured heights for period 3 was generally improved using a constant breaker coefficients of 0.8 or 0.7 that triggered the wave breaking "earlier" (i.e. in deeper waters or for smaller wave heights) in the model (the coefficient of MADSEN (1976) ranged from 0.9 to 1.3 over the reef). However, this also resulted in a significant underestimation of the transmitted heights in the precedent period 2 that would increase the overall error ϵ^2.

The ratio of transmitted to incident heights is illustrated in Figure 7.3 where measured and predicted transmitted heights are shown as a function of incident heights. It is observed that the model consistently under predicts transmitted heights in the lee of the reef for incident wave heights up to H_i = 0.5 m. Measured transmitted heights are then slightly smaller than those predicted for H_i = 0.5 -1 m. The agreement measured/transmitted is correct for H_i greater than 1 m, still with several cases of excessive reduction of the predicted transmitted wave heights.

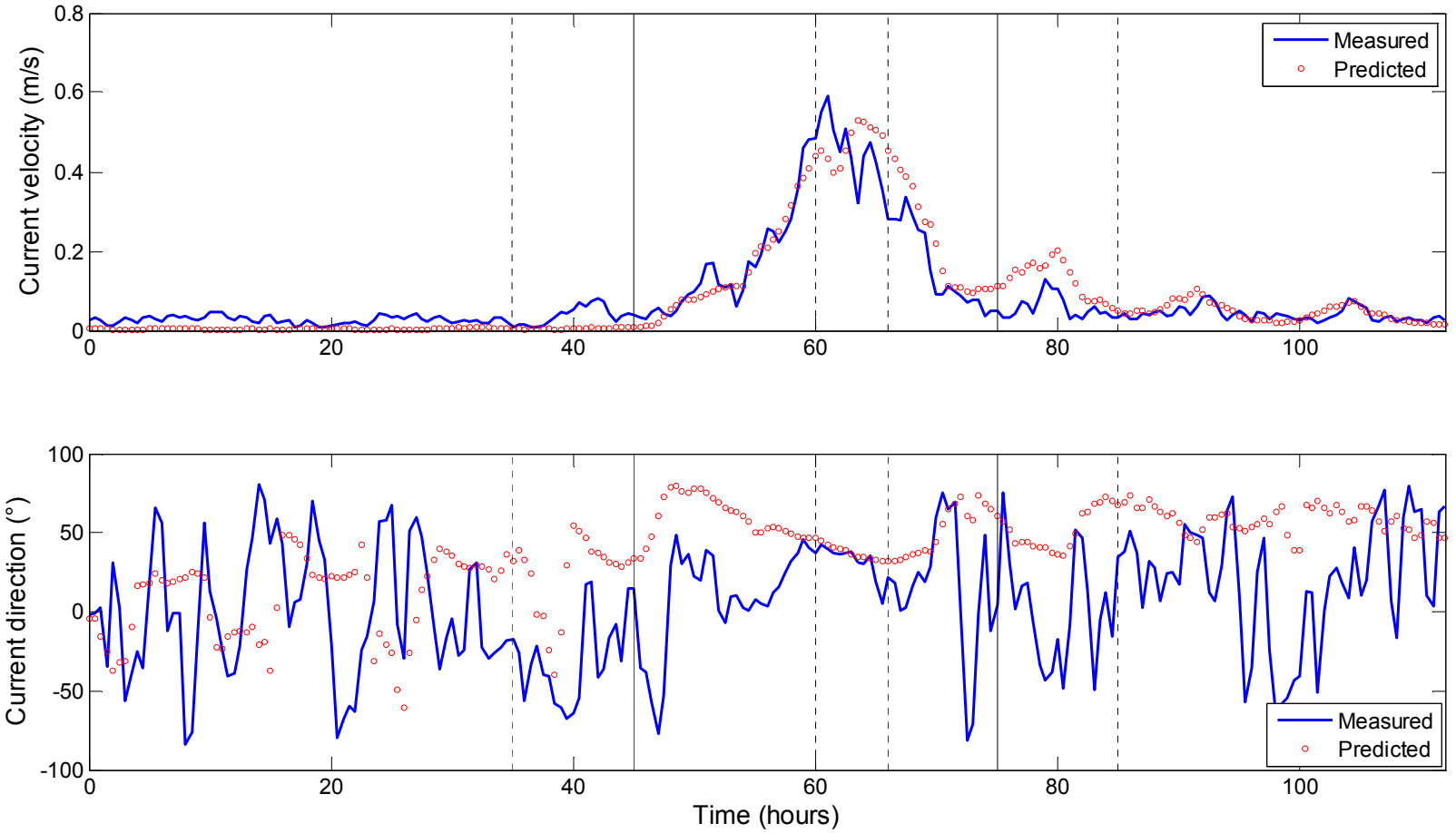

Figure 7.4. Measured and predicted current velocities and current directions landward of the reef. The direction reference is the same as that shown in Figure 7.1. The plain vertical lines separate the 3 periods of the experiment (i.e. small, medium, large incident waves, see Figure 7.2) and the dashed vertical lines locate the events described in Figures 7.5 to 7.11. The agreement measured/predicted is correct for the current velocity magnitude but more significant deviations are observed for the current direction.

The simultaneous current speeds and directions obtained from the hydrodynamic module are compared to measured currents in Figure 7.4. The calibration was less extensive and consisted in varying the roughness length parameter for the set of wave parameters selected. The parameter of 0.075 used in BLACK and MEAD (2007) eventually yielded the best overall prediction (Table 7.2). The magnitude of the current velocity was reasonably reproduced, but larger deviations were obtained for the predicted current direction. The direction pattern did not significantly change for the different roughness lengths tested so the calibration was mostly determined by the current velocity magnitude. It is noted that some deviation in current predictions were expected due to the use of monochromatic waves as a forcing while measured currents where measured under real (irregular) wave fields.

7.3.2 WAVE AND CURRENT CONDITIONS DURING THE FIELD EXPERIMENT

The wave and current patterns that developed at the beach during the field experiment are outlined here focusing on 4 events: (i) the peak wave height event at t = 60 h, (ii) the peak wave dissipation event (i.e. largest height reduction) at t = 66 h, (iii) the medium wave height event at t = 85 h, and (iv) the small wave height event at t = 35 h (see Figure 7.2).

The peak wave height event and peak wave dissipation events chosen occurred during period 2 and coincided with a high and low tide respectively. The respective predicted wave heights, angles, sea levels are shown in Figures 7.5 and 7.6, and circulation patterns are shown in Figures 7.7 and 7.8.

Height reduction in the lee of the reef is evident for both events. The strongest wave shadow zone develops in the first 100 m landward of the reef, and progressively weakens further landward. The sheltered area is orientated according to the incident wave direction for both cases, and is wider for the peak wave dissipation event that coincided with a lower tidal elevation and thus a shallower reef crest.

Wave angles are subject to significant modifications around, and in the lee of the reef. An oblique wave incidence implies that one arm of the reef is more normal to incident waves than the other. Further, there are abrupt wave angle changes at the reef arm extremities where there are sharp discontinuities in water depth. The incident waves are rotated towards the centreline of the reef by the arms, which

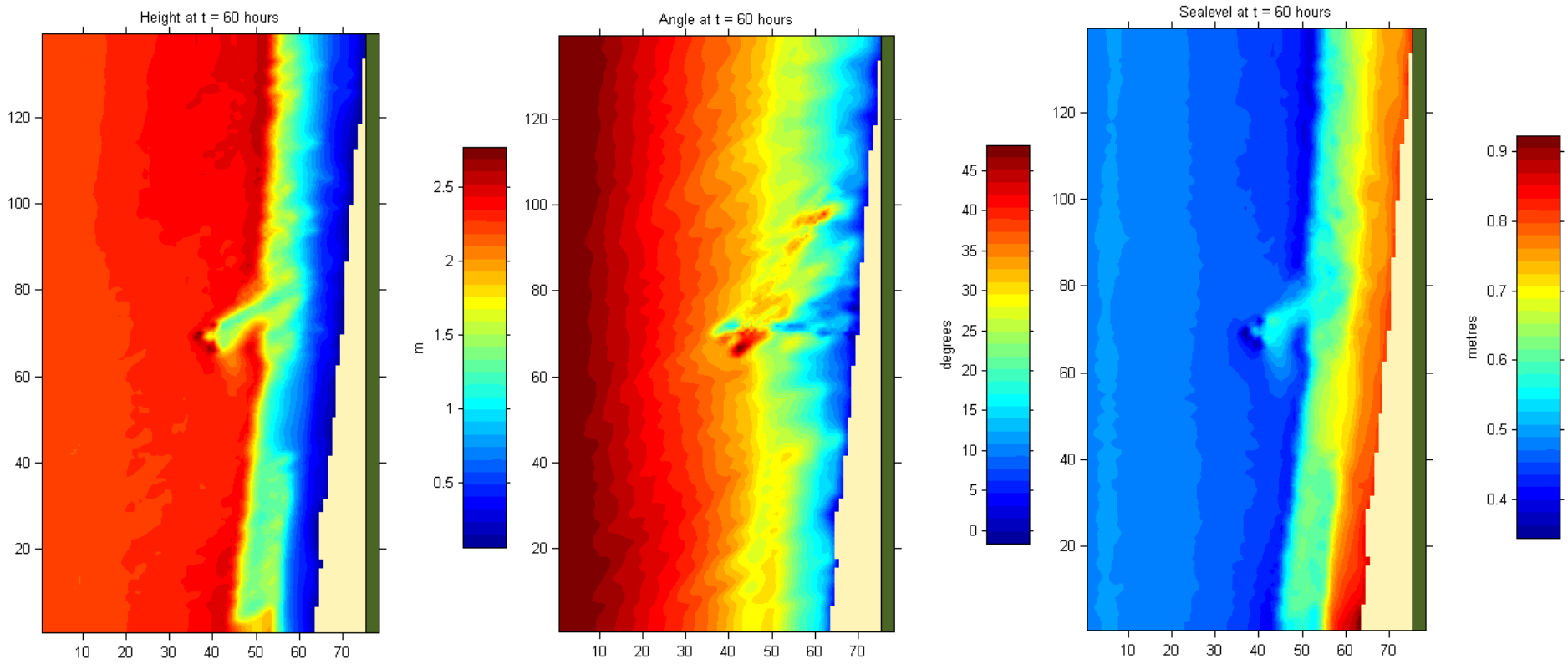

Figure 7.5. Predicted wave heights, wave angles, and sea levels (left to right) for the event of peak wave height at t = 60 h. The sharp color change from red to yellow (going landward) in the predicted heights (left) corresponds approximately to the wave breaking line (i.e. start of surfzone). There is a significant attenuation of the wave height in the lee of the reef (left) that is associated with a set-up of the water level (right). Note the wave rotation around the reef and the disturbed angle patterns in the lee side (middle).

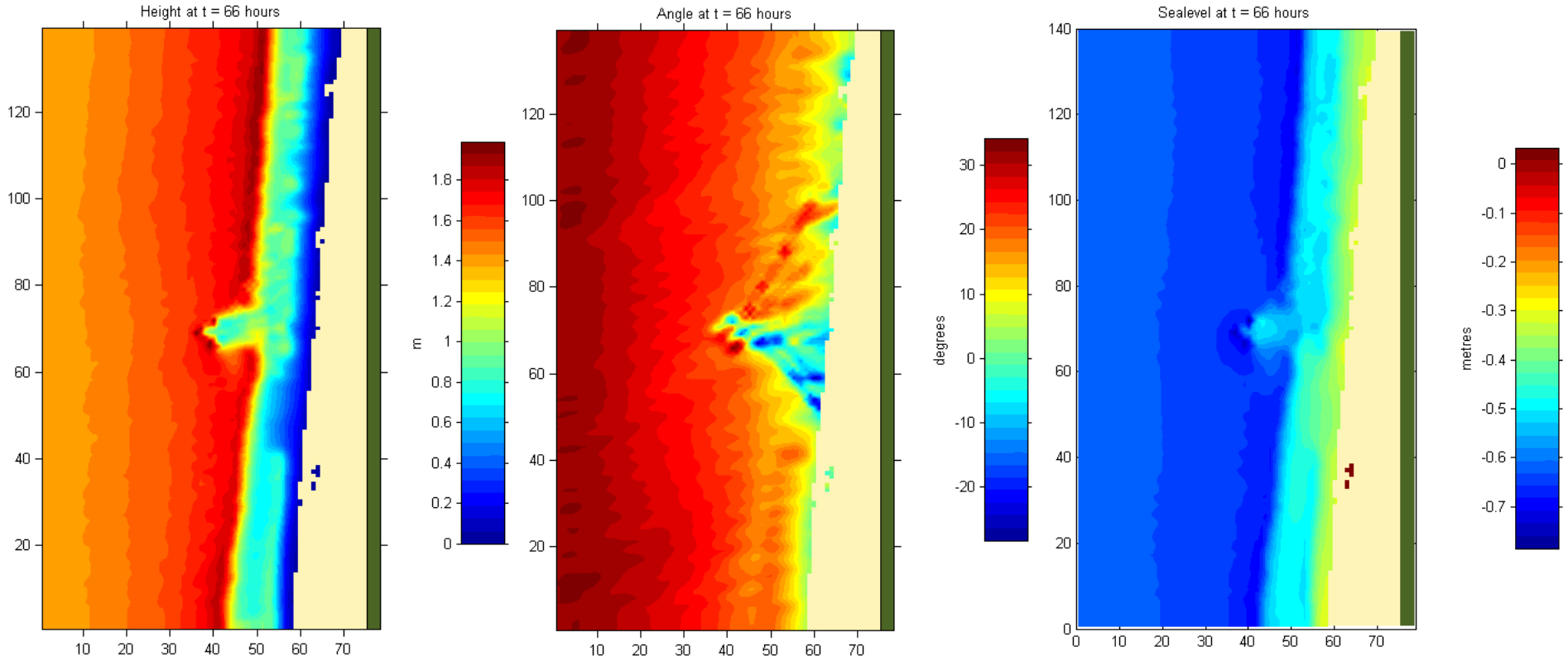

Figure 7.6. Predicted wave heights, wave angles, and sea levels (left to right) for the event of peak wave dissipation at t = 66 h. The sharp color change from red to yellow (going landward) in the predicted heights (left) corresponds approximately to the wave breaking line (i.e. start of surfzone). There is a significant attenuation of the wave height in the lee of the reef (left) that is associated with a set-up of the water level (right). Note the 2 distinct zones of diverging wave angles on either sides of the reef. Extent of the reef effect on wave angles appears to be around 600 m.

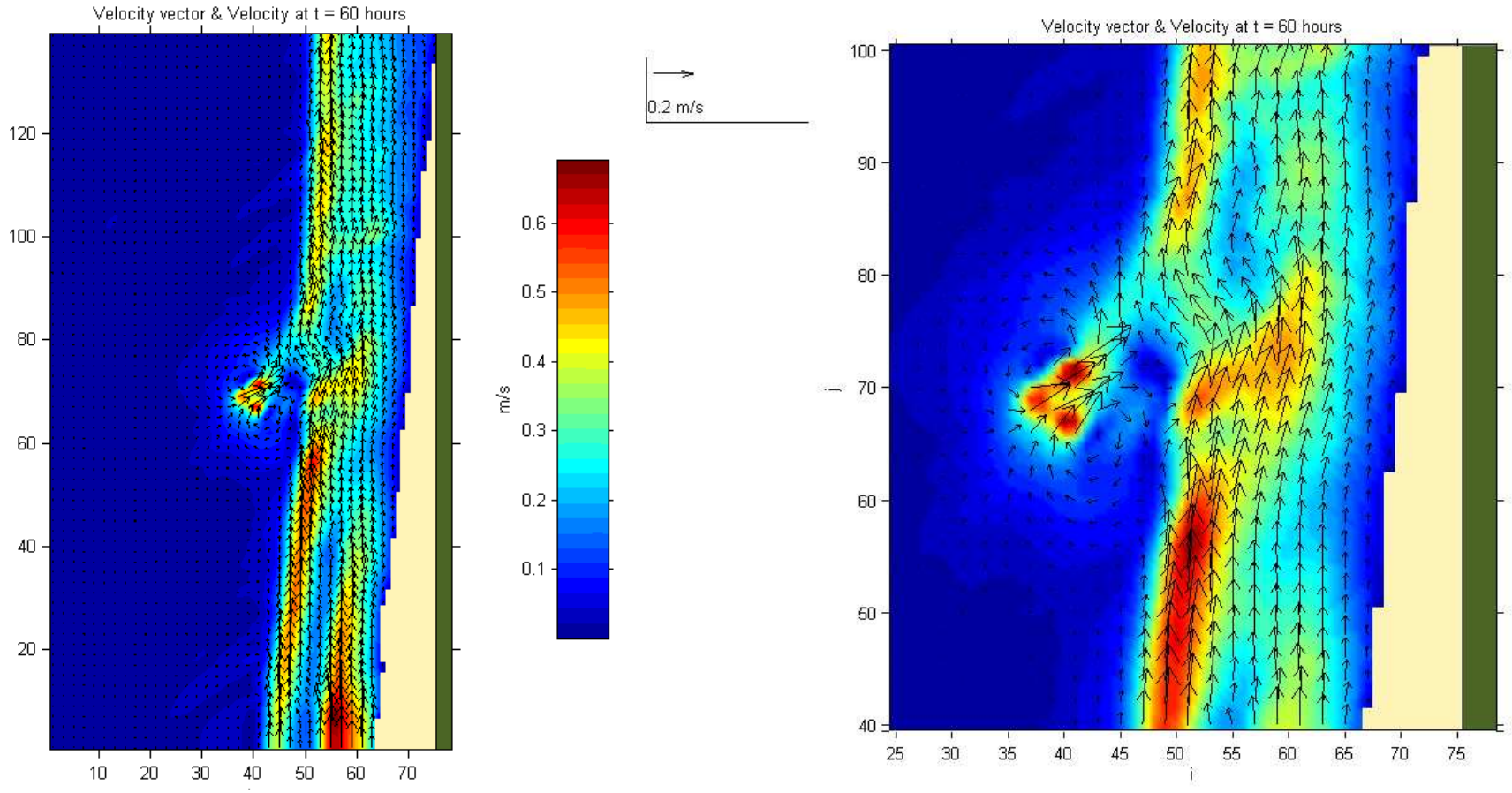

Figure 7.7. Predicted hydrodynamic circulation for the event of peak wave height at t = 60 h. The full domain circulation pattern is shown on the left, and a focus on the reef vicinity is shown on the right. The ambient long-shore flow developing due to the oblique wave incidence is deviated towards the shoreline in the lee of the reef due to the strong onshore flow over the reef, and the set-up of the water level in the lee of the reef (see Figure 7.5, right).

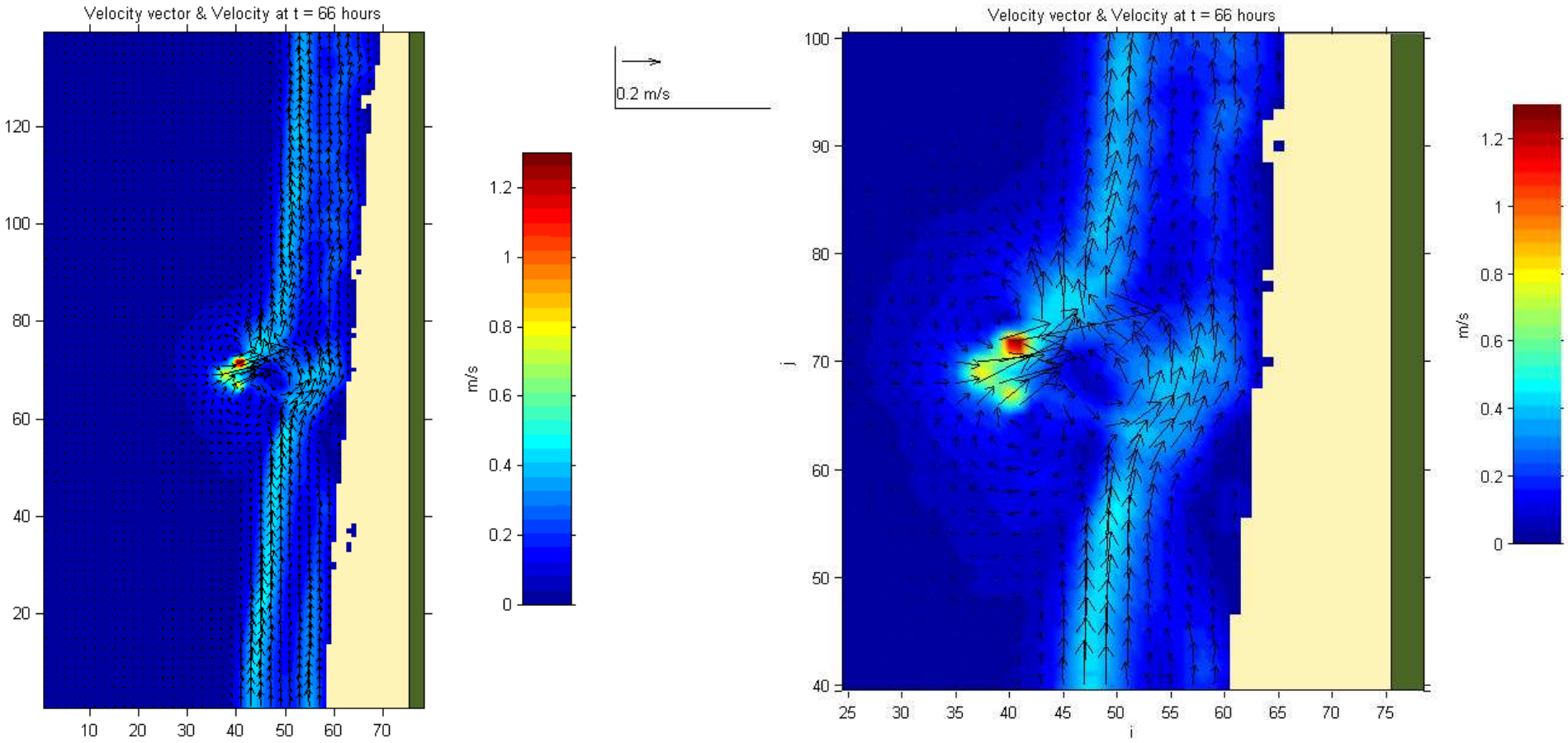

Figure 7.8. Predicted hydrodynamic circulation for the event of peak wave dissipation at t = 66 h. The full domain circulation pattern is shown on the left and a focus on the reef vicinity is shown on the right. The ambient long-shore flow developing due to the oblique wave incidence is deviated towards the shoreline in the lee of the reef due to the strong onshore flow over the reef and the set-up of the water level in the lee of the reef (see Figure 7.6, right).

results in two crossing wave fields in the lee of the reef that then create 2 zones of diverging wave angles near the shoreline. This pattern is the most obvious for the peak wave dissipation event at low tide (Figure 7.6, middle). However, the more oblique wave incidence for the peak wave conditions at high tide (Figure 7.5, middle) seems to induce a less significant crossing wave zone. Some interference patterns are visible in the lee of the reef. Overall, the extent of the reef effect on the wave angles for these 2 events seems to be around 600 m alongshore (i.e. 60 cells).

The hydrodynamic response to the modification of the wave field is consistent for the 2 events (Figures 7.7 and 7.8). The oblique wave incidence forces ambient long-shore currents in the direction of wave approach with a band of stronger velocity corresponding to the breaker line where driving radiations stress gradients are larger. The reef induces a strong onshore directed flow and a set-up of the water level in its lee (see Figure 7.5 and 7.6, right). The divergence of this flow and the additional water mass landward of the reef is observed to (i) block the incident long-shore flow updrift of the reef and force its deviation towards the shoreline, and (ii) feed the long-shore flow downdrift of the reef. Return currents develop on each side of the reef in response to the water level set-up.

The magnitude of long-shore currents near the shoreline in the lee of the reef is consequently increased relative to the undisturbed adjacent beach. Concurrently, an area of attenuated currents seems to develop updrift of the reef centreline (100-150 m), near the shoreline. Currents even oppose the ambient drift for the peak wave dissipation event (t = 66 h) (Figure 7.8). This zone coincides with the salient that likely weaken locally the long-shore flow but also with the zone of negative wave angles (i.e. opposing the long-shore flow) (Figure, 7.6, middle) suggesting a possible interaction.

The wave heights, wave angles, and sea levels for the medium and small wave events are shown in Figures 7.9 and 7.10. The respective circulation patterns are shown in Figures 7.11 and 7.12. The main difference between the medium and small wave events and the two peak events already discussed is that no wave breaking occurred on the reef. As a result, there is no significant height reduction in the lee of the reef and no enhanced set-up of the water level (Figures 7.9 and

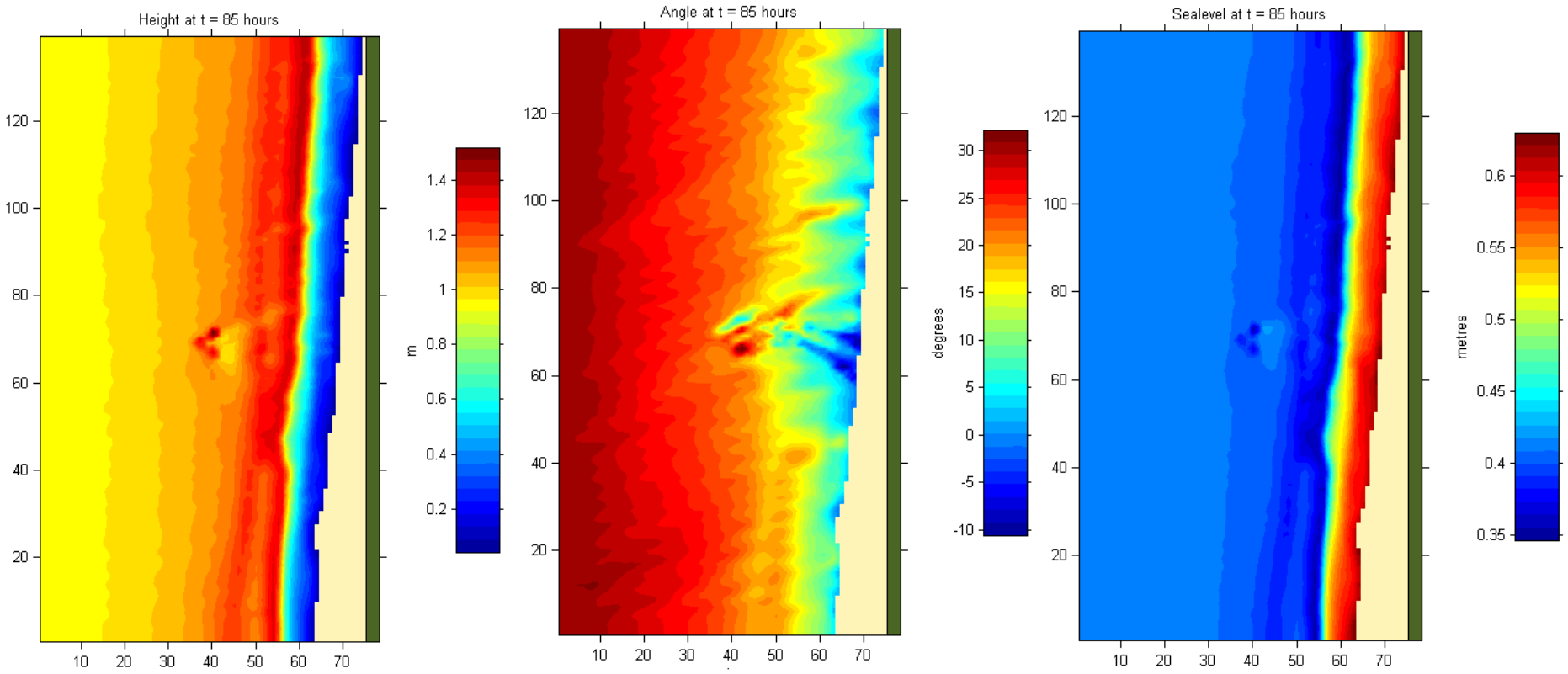

Figure 7.9. Predicted wave heights, wave angles, and sea levels (left to right) for the event of medium wave height at t = 85 h. The sharp color change from red to yellow (going landward) in the predicted heights (left) corresponds approximately to the wave breaking line (i.e. start of surfzone). The absence of wave breaking on the reef results in negligible height attenuation and sea level set-up in the lee of the reef. However, the wave rotation resulting in 2 zones of diverging wave angles at the shoreline in the lee of the reef is consistent with the Figures 7.5 and 7.6.

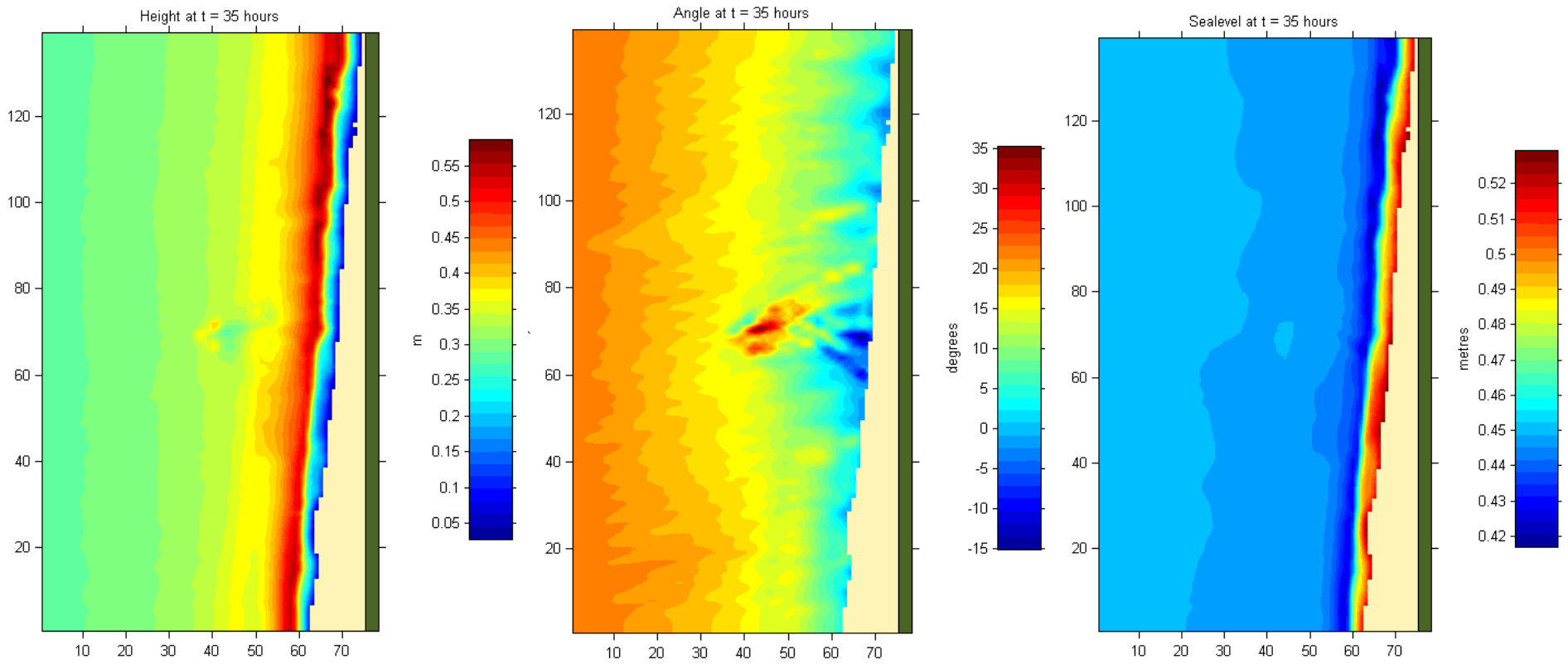

Figure 7.10. Predicted wave heights, wave angles, and sea levels (left to right) for the event of small wave height at t = 35 h. The sharp color change from red to yellow (going landward) in the predicted heights (left) corresponds approximately to the wave breaking line (i.e. start of surfzone). The absence of wave breaking on the reef results in negligible height attenuation and sea level set-up in the lee of the reef. However, the wave rotation resulting in 2 zones of diverging wave angles at the shoreline in the lee of the reef is consistent with the Figures 7.5 and 7.6.

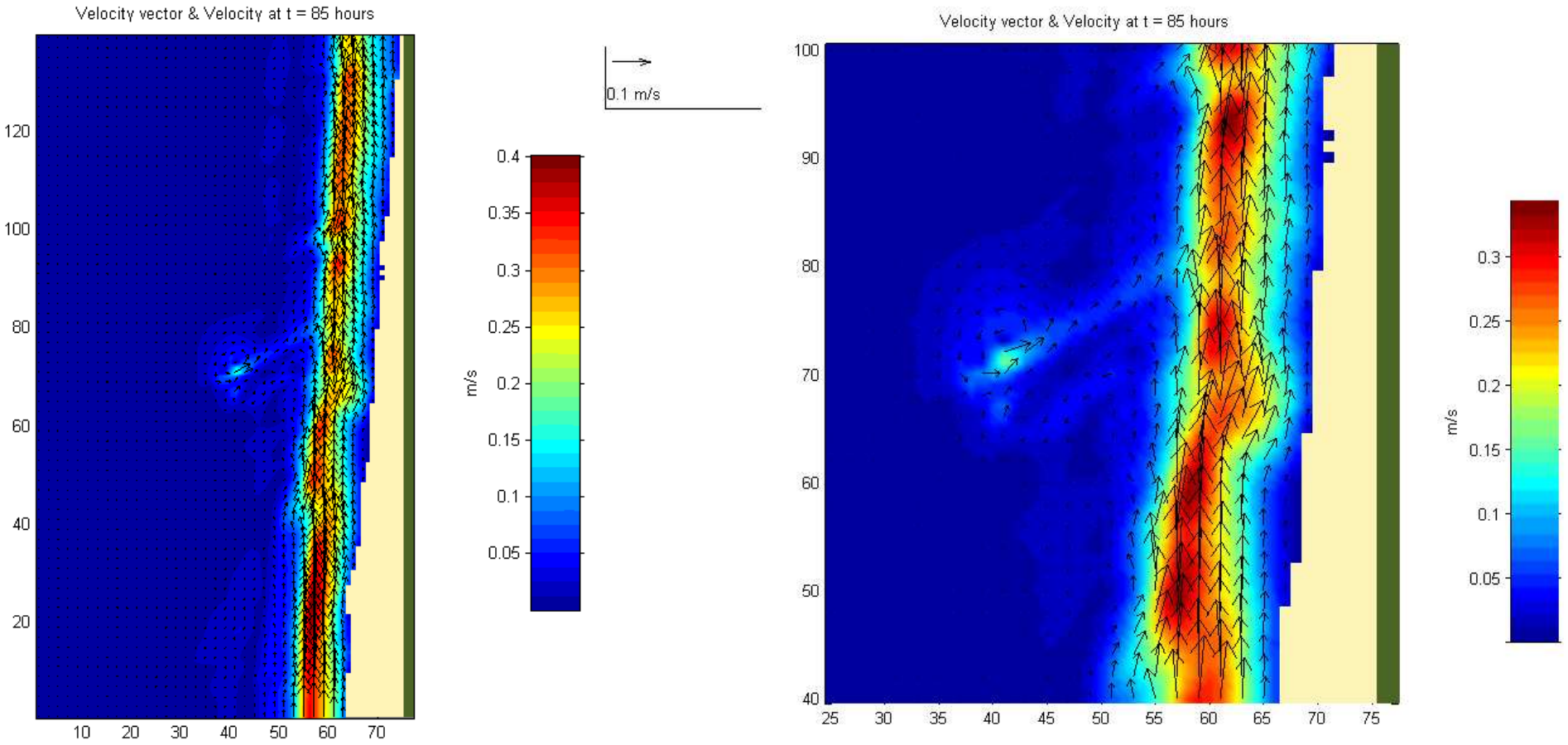

Figure 7.11. Predicted hydrodynamic circulation for the event of medium wave height at t = 85 h. The full domain circulation pattern is shown on the left and a focus on the reef vicinity is shown on the right. The absence of strong breaking-induced onshore flow over the reef results in a relatively undisturbed ambient hydrodynamic circulation.

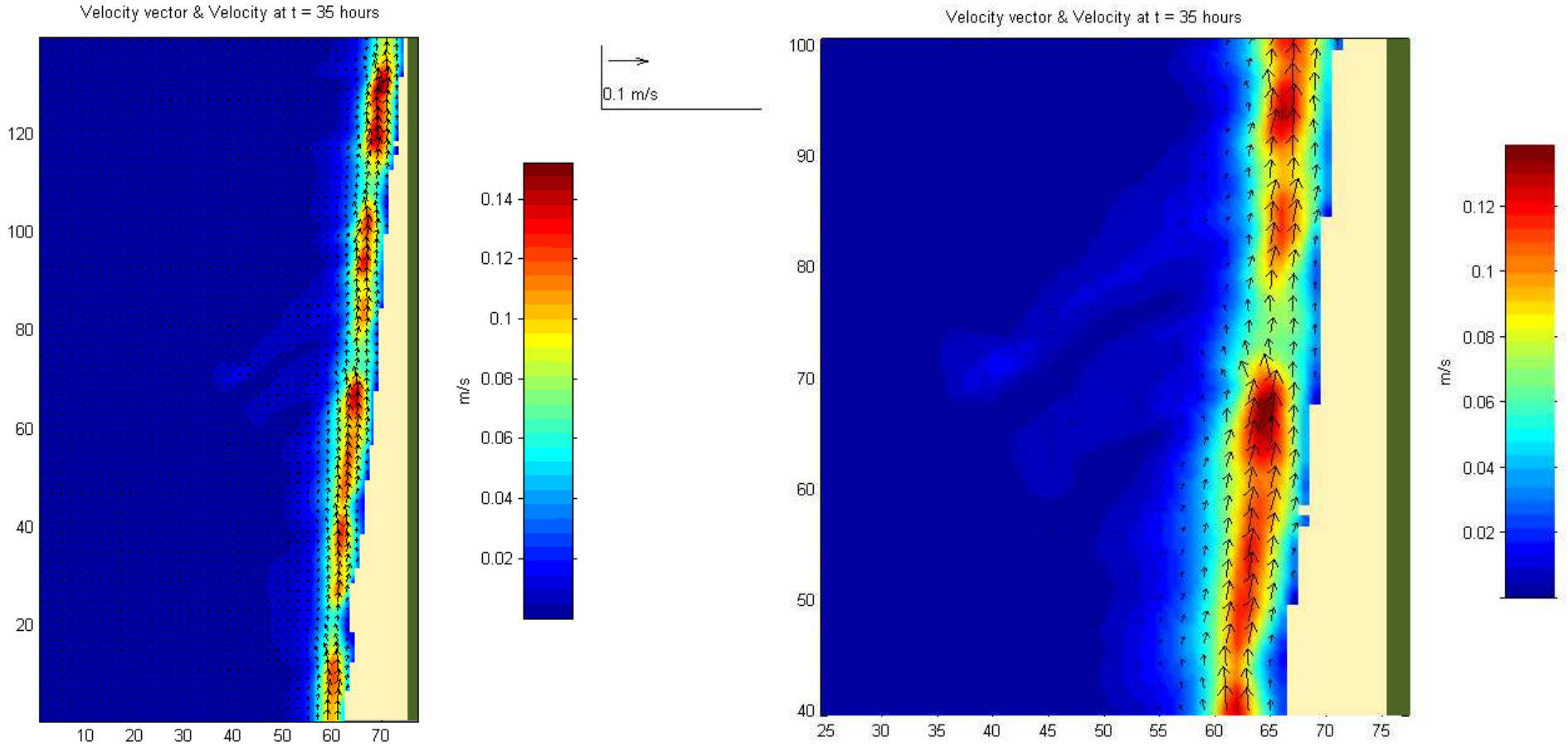

Figure 7.12. Predicted hydrodynamic circulation for the event of small wave height at t = 35 h. The full domain circulation pattern is shown on the left and a focus on the reef vicinity is shown on the right. The absence of strong breaking-induced onshore flow over the reef results in a relatively undisturbed ambient hydrodynamic circulation.

Table 7.3. Simulated wave events. The tide level was kept constant at mean sea level.

Height (m)	Angle (°)	Period (s)
1	0	9
2	0	9
3	0	9
1	15	9
2	15	9
3	15	9
1	30	9
2	30	9
3	30	9
1	-15	9
2	-15	9
3	-15	9
1	-30	9
2	-30	9
3	-30	9

7.10, left and right). The wave angle pattern is consistent with the 2 previous cases although it affects less the shoreline (Figures 7.9 and 7.10, middle). The absence of breaking-induced onshore flow over and landward of the reef results in virtually undisturbed ambient circulation patterns (Figures 7.11 and 7.12).

7.3.3 Wave and Current Patterns at Shore Normal and Oblique Wave Incidence

To extend the previous observations, a set of wave events with different heights and angles (at mean sea level) was simulated (Table 7.3). The following discussion of model results focuses on the 3 cases of shore normal waves and only one oblique incidence (15 °). However, comments are made about different oblique incidence cases when required. The complete set of model outputs is included in Appendix D.

7.3.3.1 Shore Normal Wave Incidence

a) Wave Height

The wave fields for incident wave height H = 1, 2 and 3 m are shown in Figure 7.13 (left to right). The effect of the reef is relatively limited for H = 1 m since no

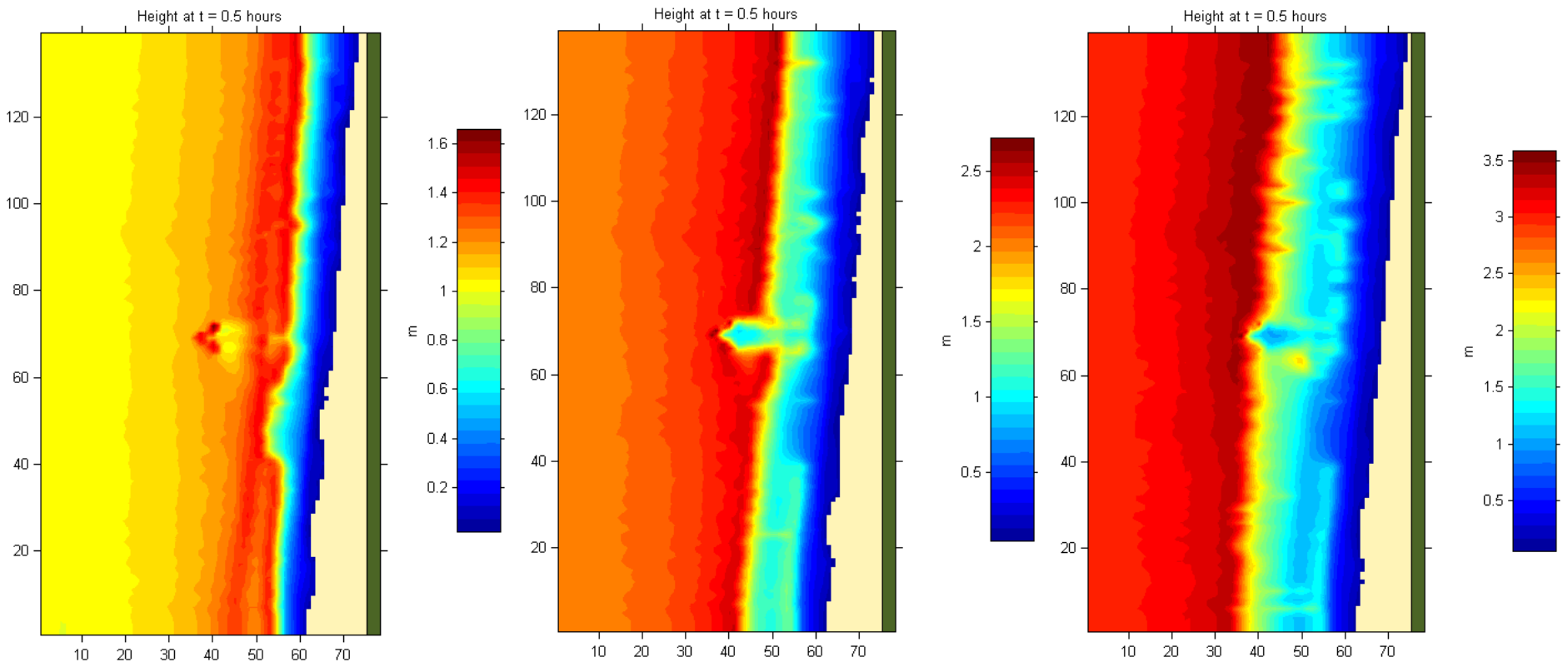

Figure 7.13 Predicted wave heights for the events of height H = 1, 2, 3 m (left to right), at shore normal incidence. The reef triggers wave breaking only for H = 2 and 3 m. The sharp color change from red to yellow (going landward) corresponds approximately to the wave breaking line (i.e. start of surfzone). Note the significant wave height attenuation for H = 2 m (middle) in the first 100 m landward of the reef. The wave shadowing zone is less evident for H = 3 m (right) as the breaker line is shifted offshore close to the reef position.

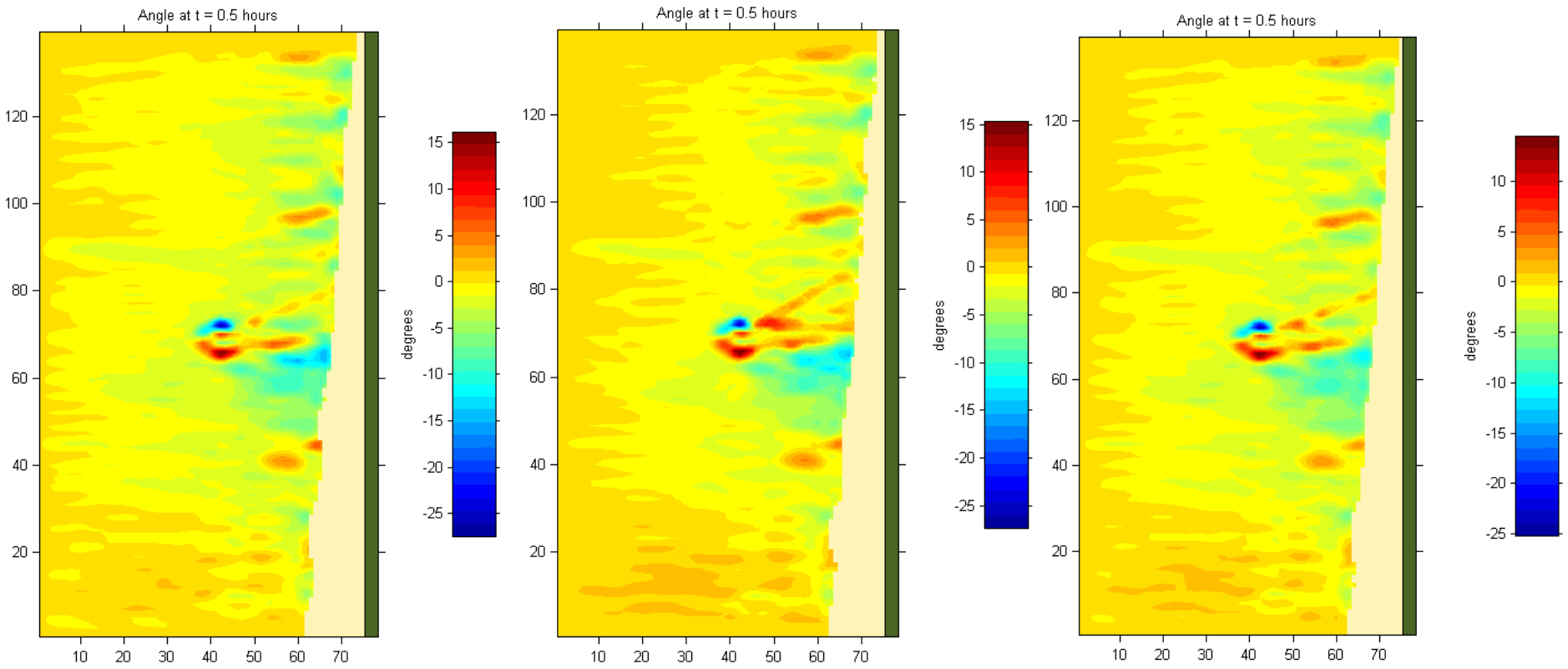

Figure 7.14. Predicted wave angles for the events of heights H = 1, 2, 3 m (left to right), at shore normal incidence. The refraction of waves over the reef induces 2 zones of diverging wave angles in the lee of the reef i.e. propagating towards the top of the grid above the reef centerline (+ 10 °), and propagating towards the bottom of the grid below the reef centerline (- 10 °) (see Figure 7.1 for angle convention). Some interference patterns due to diffractions effects are also visible. The pattern extent and magnitude (i.e. induced angles) are consistent for the 3 cases.

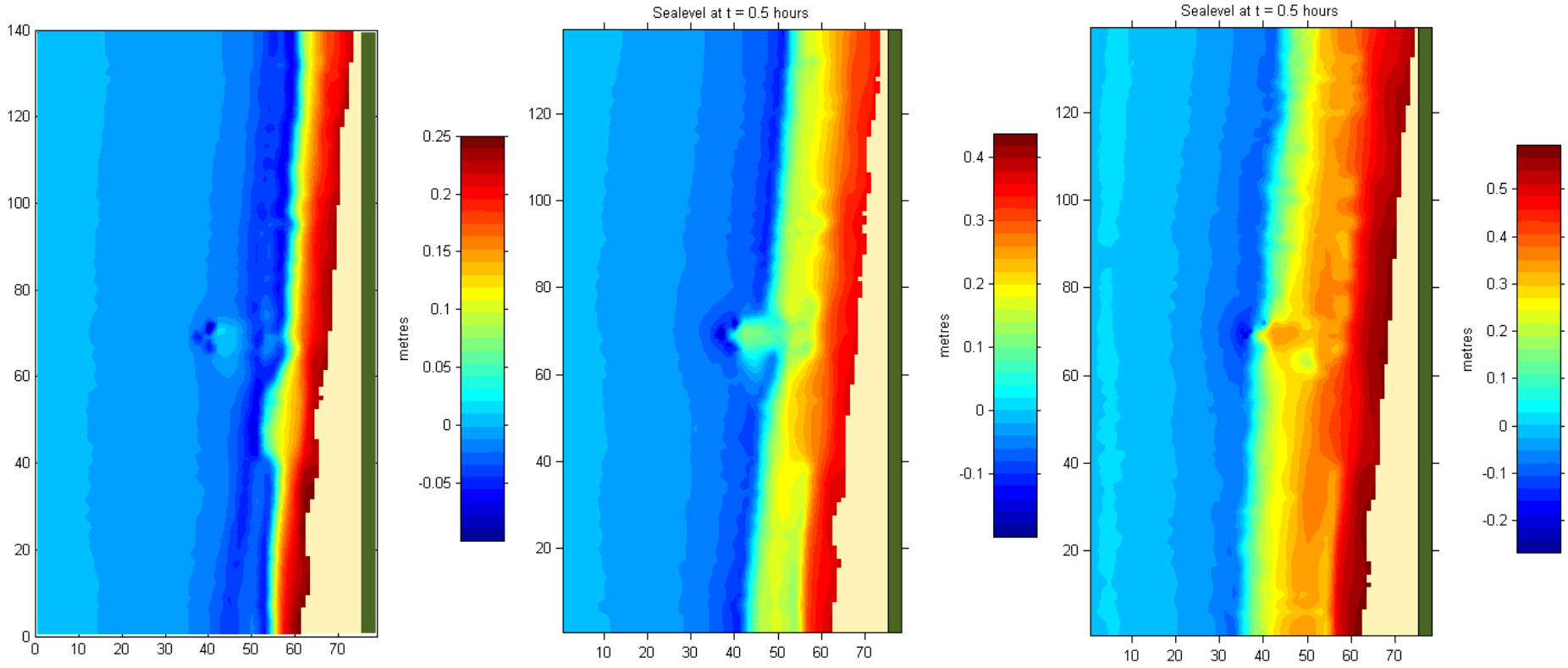

Figure 7.15. Predicted sea levels for the events of heights H = 1, 2, 3 m (left to right), at shore normal incidence. Note the most obvious set up of the sea level in the lee of the reef for H = 2 (middle).

wave breaking occurred on its crest. The wave heights increased as they approached the reef crest and subsequently decreased landward of the reef over the scour hole (no breaking). The process results in slightly reduced wave heights in the immediate lee of the reef relative to the undisturbed beach, but this is progressively compensated moving inshore. The small salient feature below the reef centreline breaks waves further seaward than along the rest of the beach.

For the 3 wave heights considered, the most obvious reef effect on the nearshore wave pattern is observed at H = 2 m when there is a clear reduction of the wave height in the lee of the reef relative to the undisturbed beach. This is due to the wave breaking occurring much further offshore on the reef profile than on the undisturbed beach. The most significant height gradients are found within the first 100 m landward of the structure, and the wave height shadow is then less evident further inshore. The height attenuation is still present, although less striking, for the case H = 3 m. This is because both reef-induced and natural wave breaking start roughly at the same cross-shore position. Since the ambient energy dissipation (and height reduction) is already important close to the reef, the height gradient in the lee side is consequently less significant.

b) Wave Angle

The predicted wave angle patterns (Figure 7.14) are relatively consistent for the 3 cases considered. Focusing on the reef vicinity, complex angle changes are observed over the reef and scour bathymetry. The apex and the two oblique reef arms initially induce a symmetric refraction of waves around the structure (from 0° to ± 5-10 °). The maximum wave angles are found at the landward extremities of the reef arms (± 15-20°), as the depth changes are sharper (i.e. transition reef arm to scour region). These transformations result in 2 crossing wave fields landward of the reef, propagating inward from each reef arm end. Near the shoreline, this consequently creates 2 zones of diverging wave angles i.e. oblique at about -10 ° below of the reef centreline, and oblique at about +10 ° above of the reef centreline. Some interference patterns are also visible in the lee of the reef.

The extent and magnitude of the pattern increase from H = 1 m to H = 2 m and decrease for H = 3m. This may be due to the wider surf zone damping the rotation process in the lee of the reef.

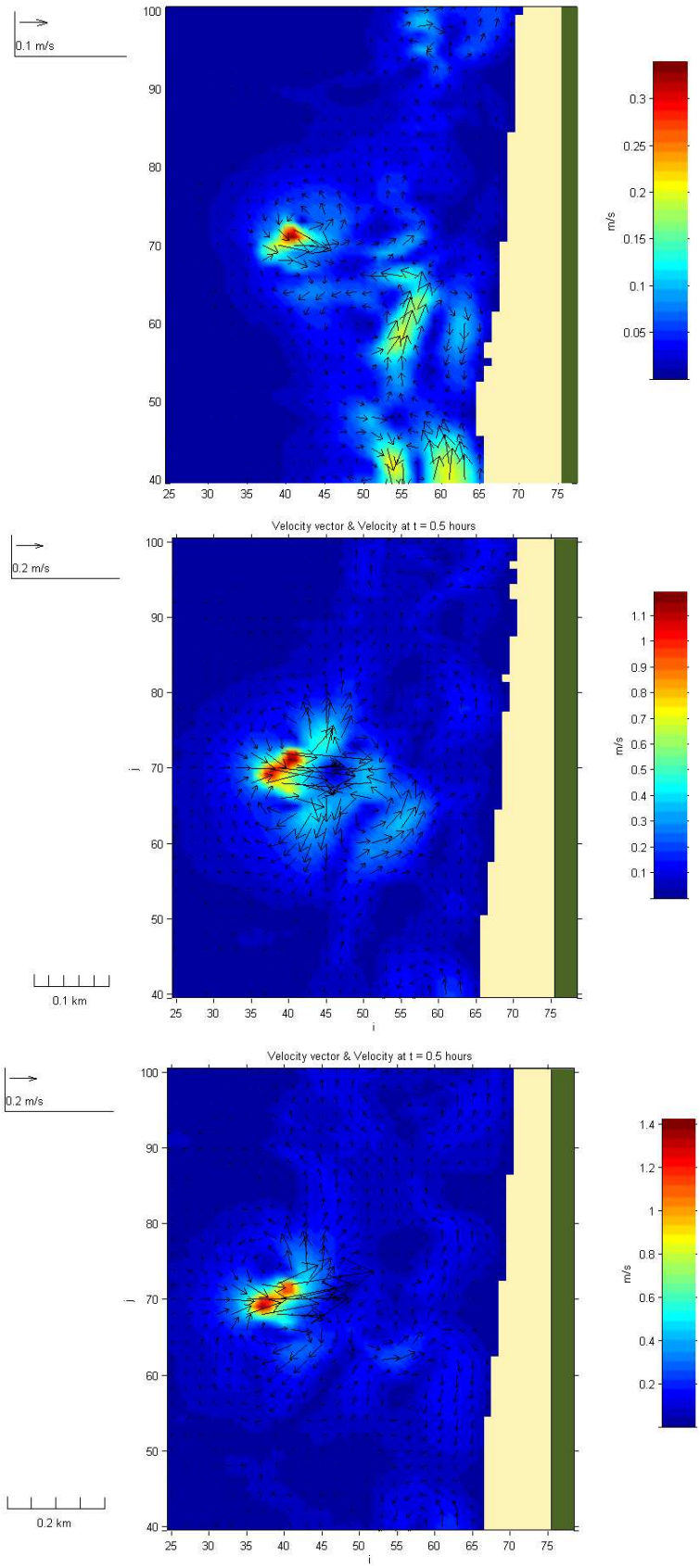

Figure 7.16. Predicted hydrodynamic circulations in the vicinity of the reef for the events of heights H = 1, 2, 3 m (top to bottom), at shore-normal incidence. Note the cellular circulations in the lee of the reef.

c) Hydrodynamics

Sea levels and circulation patterns are shown in Figures 7.15 and 7.16. For a wave height H = 1 m, with no wave breaking on the reef, the reef induces an onshore directed flow over the reef (~0.4 m/s) that diverges landward. Strong circulation cells tend to develop in the lee of the reef and in the vicinity of the small salient feature, and a more defined rip current is visible between the salient and the reef centreline. Changes in sea levels are very limited in the vicinity of the reef, with a very slight set down on the reef crest due to wave shoaling. There is also an area of higher water levels associated with the small salient feature that breaks waves further seaward than along the rest of the beach (see bathymetry in Figure 7.1).

The effect of the reef on the nearshore circulation becomes more significant for a wave height H = 2 m. A strong onshore directed flow develops over the reef in response to wave breaking (~ 1 m/s), and it spreads alongshore landward of the reef. This is associated with a set down of the water level over the reef crest of -0.2 m, and a matching set up of the water level landward of the reef (i.e scour hole) of about +0.2 m. Part of the diverging flow returns offshore, while the rest is directed onshore and forces circulation cells in the lee of the reef. A stronger anticlockwise cell is visible towards the salient and it induces an additional flux of water towards the shore. This results in diverging currents near the shoreline in the lee of the reef. Several weaker cells are observed along the shoreline further away from the reef. Overall, the disturbance of nearshore currents seems to extend ~ 400 m either side of the reef centreline. The underlying pattern is very similar for the case H = 3 m. The main circulation cell that developed towards the salient in the lee side is less defined than for H = 2 m.

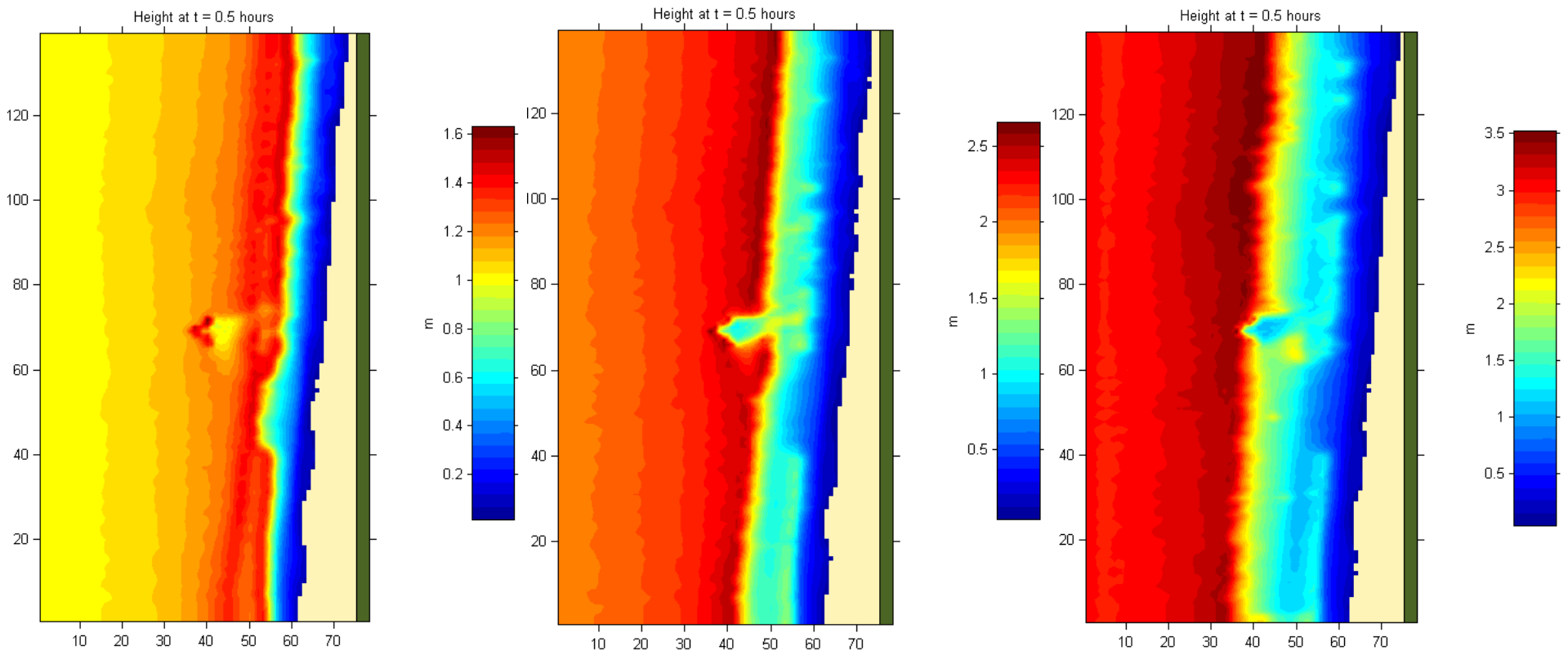

Figure 7.17. Predicted wave heights for the events of heights H = 1, 2, 3 m (left to right), at oblique incidence (+15 °). The reef triggers wave breaking only for H= 2 and 3 m. The sharp color change from red to yellow (going landward) corresponds approximately to the wave breaking line (i.e. start of surfzone). The main difference with respect to the shore normal cases is that the sheltered zone is reoriented according to the incident wave angle.

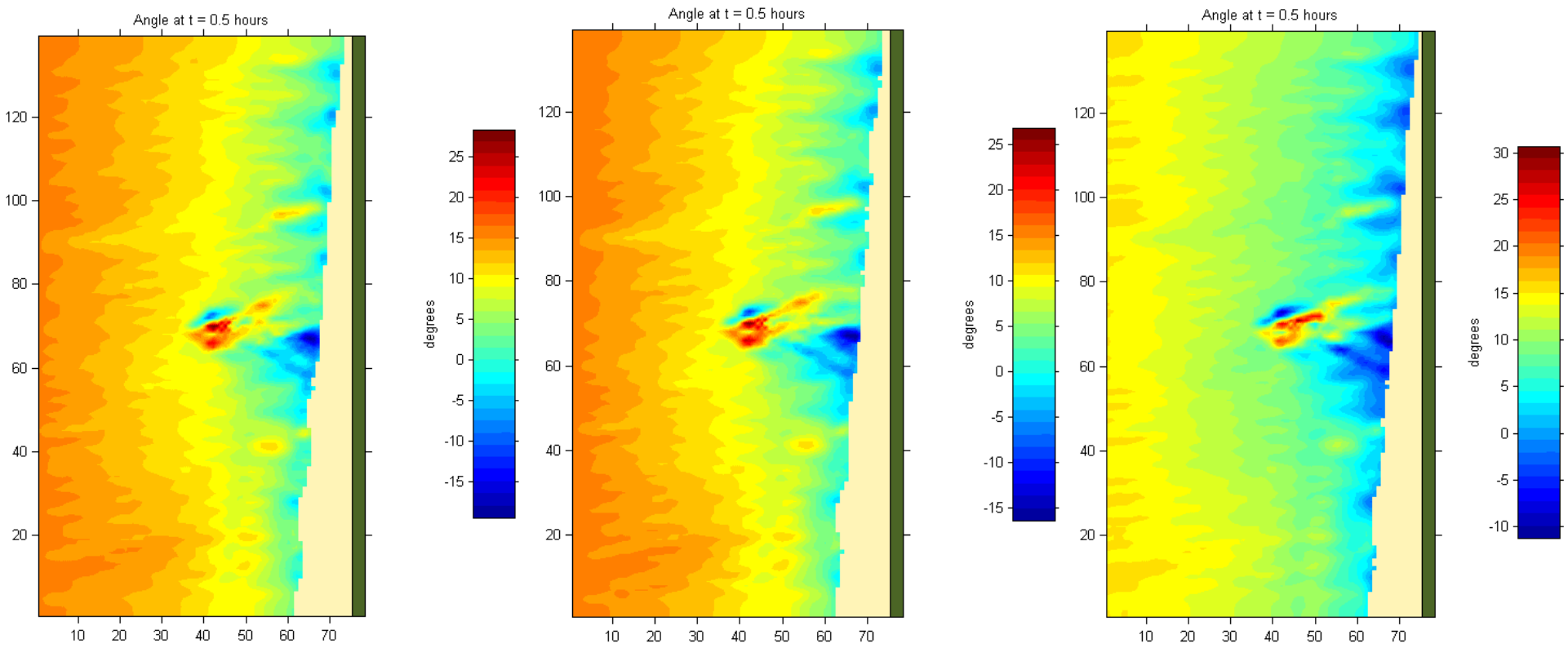

Figure 7.18. Predicted wave angles for the events of heights H = 1, 2, 3 m (left to right), at oblique incidence (15°). The angle pattern is slightly modified over the reef as one reef arm (the exposed arm) is approached more normally by incident waves. The 2 zones of diverging wave angles in the lee of the reef identified in the shore normal cases are observed in the 3 present cases (see Figure 7.1 for the angle convention). Some interference patterns due to diffractions effects are also visible (rhythmic bands landward of the reef).

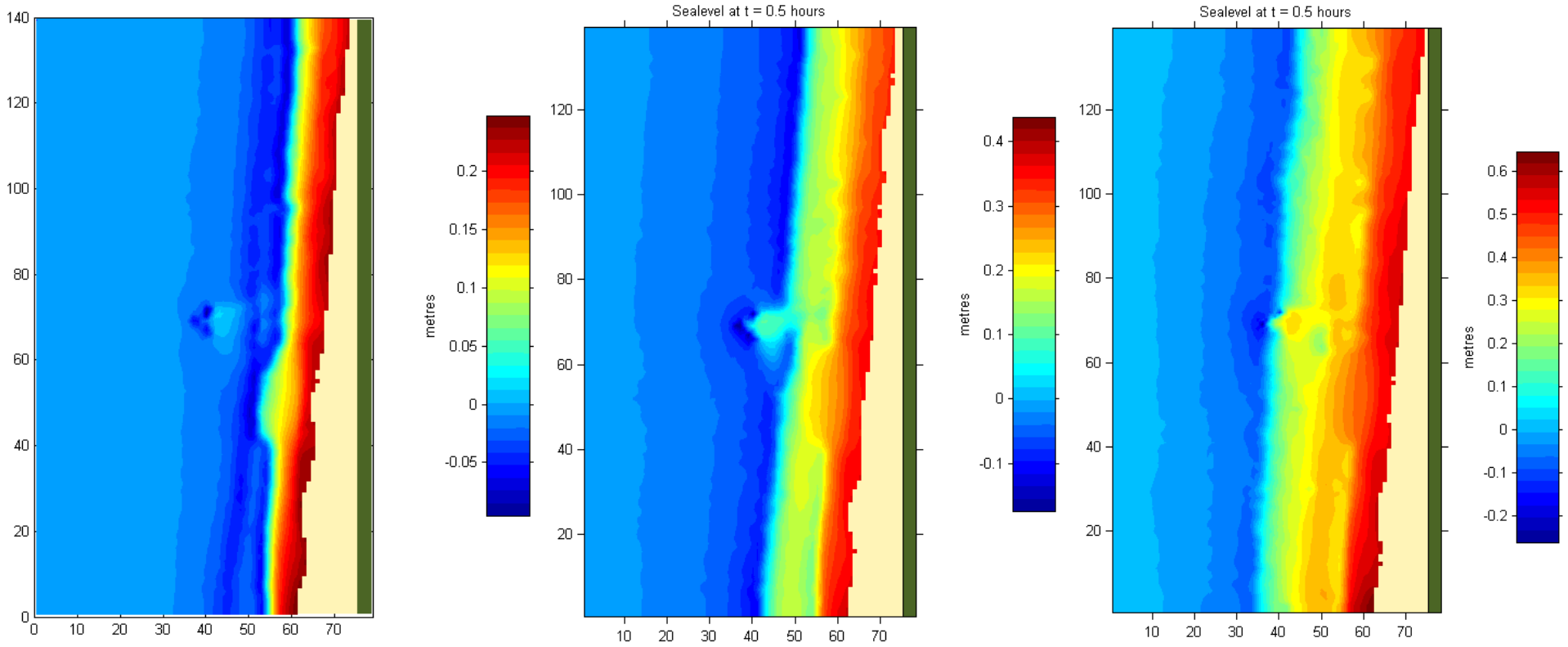

Figure 7.19. Predicted sea levels for the events of heights H = 1, 2, 3 m (left to right), at oblique incidence (15 °). Note the most obvious set up of the sea level in the lee of the reef for H = 2 (middle).

7.3.3.1 Oblique Wave Incidence (+ 15°)

a) Wave Height

The wave height patterns for the cases of oblique wave incidence (Figure 7.17) are consistent with those described for the shore normal cases. The main difference is that the sheltered zone in the lee of the reef is shifted downdrift of the reef centreline depending to the incident wave angle (i.e. away from the salient for the cases shown).

b) Wave Angle

An oblique wave approach changes the wave angle pattern over the reef, since the refraction and diffraction processes do not occur symmetrically around the reef centreline anymore (Figure 7.18). This was the situation observed for the simulated field experiment conditions. The oblique incidence implies that one reef arm (the exposed arm) is approached more normally by incident waves than the other. As a result, wave refraction occurs firstly around a reef arm rather than being conditioned by the reef apex. This results in increased wave angles (i.e. more oblique) at the landward end of the arm, and reduced wave angles (i.e. realigned with the shoreline) at the apex. For the section of wave crest rotated around the apex, the refraction process continues along the sheltered reef arm with wave eventually turning towards the reef centreline by around –5 ° at its' landward extremity. Concurrently, waves transmitted in between the reef arms (scoured region) are also refracted, predominantly towards the sheltered reef arm (shallower than the exposed arm). Consistently with the cases of normally incident waves, these transformations results in 2 crossing wave fields landward of the reef that subsequently induce 2 zones of diverging wave angles at the shoreline in the lee of the reef. Some interference patterns due to wave diffraction by the reef and these opposed wave fields are again visible in the lee of the reef (rhythmic bands).

Increasing the angle of incidence yielded greater opposing wave angles (see Appendix D, Figure D.15, middle). For the cases of negative wave incidence, the increased waves angles downdrift of the reef were evident as well, however the zone of opposing wave angles updrift of the reef appeared less defined (e.g. Appendix D, Figure D.27, middle). This is probably because the bathymetry shoreward of the reef is not symmetrical due to the presence of the salient.

Considering the wave angle patterns during the simulated field experiment conditions, it is noted that a shallower reef crest under waves at + 30 °, as observed for the peak wave dissipation event (t = 66 h, Figure 7.6 middle), could further increase the angle of the opposing waves (up to -20 ° for that event). In contrast, a deeper crest, and/or a larger incidence (+45 °), as experienced during the peak wave height event (t = 60 h, Figure 7.5, middle), may dampen the rotation process, and induce less evident zones of diverging angles.

c) Hydrodynamics

The main difference in the hydrodynamic circulations (Figure 7.20) for oblique wave incidence relative to shore normal wave incidence is that the reef-induced currents are now superimposed on ambient (unidirectional) long-shore currents. The set-up of water levels is similar to the shore normal cases (Figure 7.19) although reoriented according to the angle of wave incidence.

For a wave height H= 1 m and no wave breaking on the reef, the contribution of the reef consists of an additional onshore directed flow that feeds the ambient long-shore currents. Some of the reef-induced flow is also returned offshore. The rip current identified between the salient and the reef centreline in the shore normal case at H=1 m is again present.

The reef has a greater effect on the circulation patterns when wave breaking occurs, as in the case of a wave height H = 2 m (Figure 7.20, middle). The band of stronger long-shore currents ~ 100 m landward of the reef (i.e. near the breaker line) is perturbed by the strong onshore flow over and landward of the reef, along with the set-up of the water level (see Figure 7.19 middle). Updrift of the reef, the ambient long-shore flow is locally weakened and deviates towards the shoreline. Downdrift of the reef, the ambient long-shore flow is fed and strengthened by the reef-induced currents. Return currents also develop on each side of the reef.

For a wave height H = 3 m (Figure 7.20, bottom), the breaker line is shifted offshore and so is the band of stronger ambient long-shore currents. As a result, the strongest long-shore currents intersect the arms of the reef and the subsequent flow blocking is due to the structure itself, rather than reef-induced onshore flow as for the case H = 2 m.

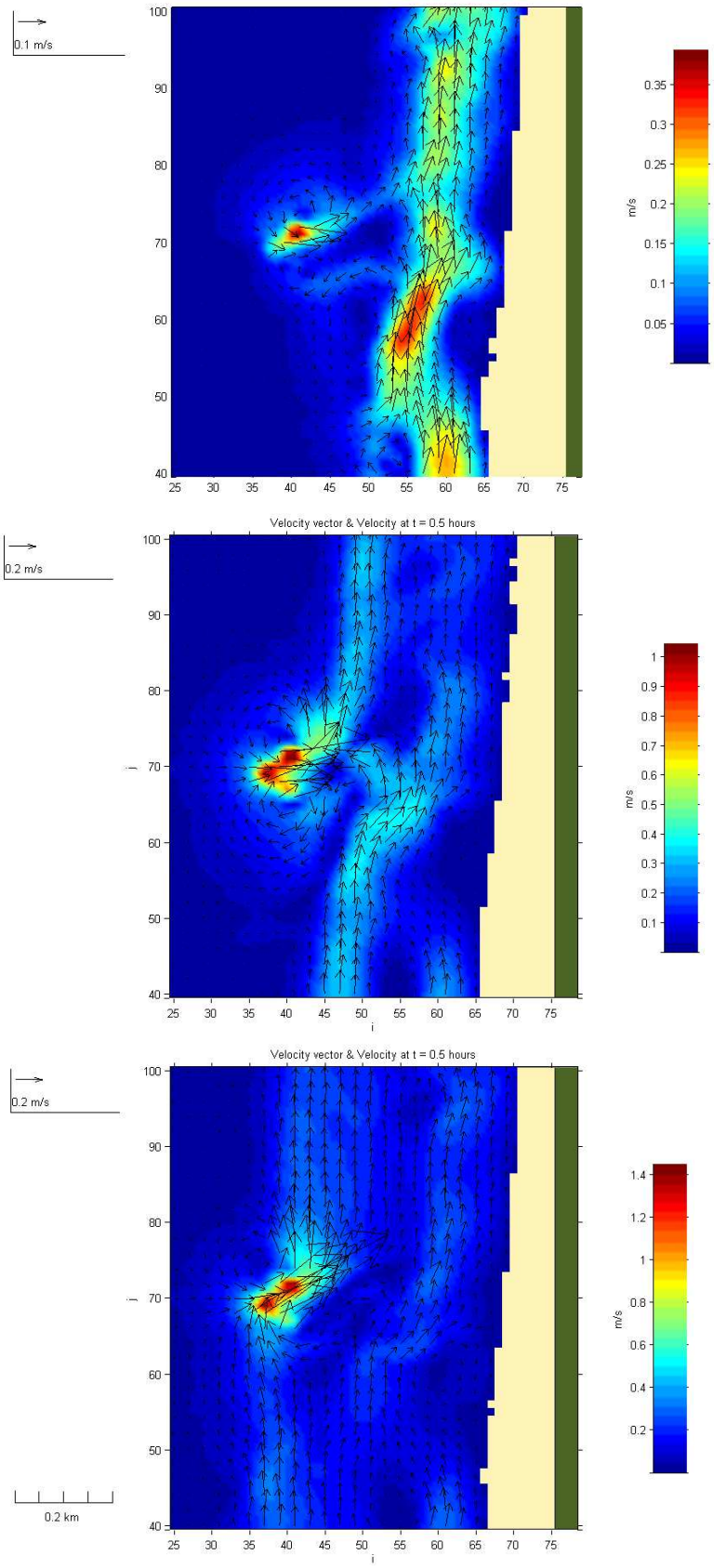

Figure 7. 20. Predicted hydrodynamic circulation in the vicinity of the reef for the events of heights H = 1, 2, 3 m (top to bottom), at oblique incidence (15°). Note the long-shore flow deviation towards the shoreline for the cases H = 2 and 3 m (wave breaking on the reef).

The underlying circulation pattern was generally similar for negative oblique wave incidences (see Appendix D, e.g. Figure D.28). However, the small salient feature tended to redirect the diverted long-shore flow seaward, rather than further focus it landward as for the positive incidence cases.

7.4 DISCUSSION

BLACK (2003) identified 4 important wave and hydrodynamic processes around submerged multi-purpose reefs, which are eventually expected to induce shoreline accretion. These are: (i) wave sheltering generating a shadow zone in the lee of the reef (viz. BLACK and ANDREWS, 2001), (ii) wave rotation over the reef reducing the long-shore currents by more closely aligning the wave crests at the breakpoint with the isobaths (viz. BLACK and MEAD, 2001), (iii) wave breaking on the reef reducing the set-up of water level at the shoreline, and (iv) development of counter clockwise vortices in the lee of the reef.

Wave height attenuation was consistently observed in the model results as soon as waves started to break on the reef. However, the resulting wave sheltering was most efficient within the first 100 m in the lee of the reef, and it was less evident approaching the shoreline. This means that a reef width of 80 m, located ~ 250 m from the shoreline, with the prototype height transmission characteristics (i.e. up to ~ 40 % reduction) would be insufficient to provide significant wave height reduction at the shoreline. This should be taken into account for future reef projects with a primary coastal protection function.

With respect to reef-induced wave rotation, the wave angle patterns obtained seemed more complex than a simple realignment of the wave crests with the shoreline. The reef did provide some control over the development of wave angles, as generally two zones of increased and diverging wave angles would develop in the lee of the reef. For incident shore normal waves, this may induce a long-shore current that is not desirable. However, for obliquely incident waves, which are more common, the results are beneficial as the updrift current is weakened promoting sediment accretion. The downdrift current is though strengthened.

The other two mechanisms of a relative reduction of the sea level at the shoreline in the lee of the reef, and reef-induced counter-rotating vortices were further confirmed by RANASINGHE *et al.* (2006) who provided detailed circulation patterns in the lee of an idealized multi–purpose reef on a planar sloping beach. They found that the starting point of the reef-induced circulation was the strong onshore flow generated over the reef, along with the set-up of the water level in its' immediate lee due to wave breaking on the reef crest. If the reef was sufficiently far from the shoreline (and surfzone), the divergence of this flow forced 2 counter-rotating cells between the reef and the shoreline (4-cell circulation, see Figure 2.9). When the reef caused wave breaking further offshore than that on the undisturbed beach, there was a reduction of sea level at the shoreline and this worked in combination with the circulation cells to force convergent currents at the shoreline in the lee of the reef, favouring sediment accretion. This underlying pattern was found to be relatively consistent for obliquely and normally incident waves.

Case H = 2 m (Figure 7.15) in this study is the most consistent with the simulated wave conditions of RANASINGHE *et al.* (2006) (H = 1.5 m). For this case, the onshore flow divergence and 2 offshore return cells are reproduced, but there are some differences in the lee of the reef. For shore normal waves, a counter rotating cell develops only on one side of the reef (near the salient). More importantly, the single cell seems to feed the region close to the shoreline with an additional flux of water that then results in divergent currents. Moreover, there are no obvious sea level gradients in the lee of the reef that could favour current convergence (Figure 7.16). Under oblique waves, a reduction of the sea level at the shoreline in the lee of the reef is likewise not obvious (Figure 7.19) and the circulation patterns suggest a local deviation of the ambient long-shore currents towards the shoreline rather than a significant forcing of nearshore circulation by the reef (Figure 7.20). It should be noted that the bathymetry in this study was not planar as assumed by RANASINGHE *et al.* (2006).

The absence of consistent circulation patterns that could be favourable for sediment accretion should be further investigated by coupling a morphological module to the wave and hydrodynamic modules used in the present study. The reef footprint at the study site does not seem to be large enough to force a large scale "organized" hydrodynamic circulation in its lee. However, BLACK and

MEAD (2007) identified a mechanism that is potentially important for shoreline accretion in the lee of the study reef involving the local fragmentation and onshore migration of sand bars in the vicinity of the reef, which they termed "reef bars". This relatively dynamic mechanism does not rely only on a modification of the surfzone hydrodynamics, but rather on morphological coupling, and therefore cannot be easily inferred from the wave and current patterns predicted here.

7.5 CONCLUSIONS

The chapter presented the results of numerical modelling of waves and currents around the multi-purpose reef at Mount Maunganui. Wave transmission over the reef was calibrated using the field datasets collected during a 5 day field experiment. Wave and current conditions experienced during the field experiment were described and a range of representative wave events was simulated to identify the main wave and circulation patterns expected at the site. Main findings are:

- The model calibration consisted of a sensitivity analysis of the measured versus predicted wave height transmitted landward of the reef by varying the wave friction coefficient, the horizontal eddy viscosity, and the wave breaking model characteristics, and assessing the goodness of fit in terms of the residual error. The set of parameters associated with the lowest error was a friction coefficient of 0.03, a horizontal eddy viscosity of 10 m^2/s, and the use of the breaking criterion of MADSEN (1976) with a dissipation constant K = 0.15 in the wave decay model of DALLY *et al.* (1985).

- Wave breaking over the reef created a shadow zone that was most evident in the first 100 m landward of the structure, and progressively diminished towards the shoreline. This wave shadowing was most efficient when the reef triggered wave breaking well offshore of the natural surfzone.

- The reef had a significant influence on wave angles and complex patterns were predicted around, and in the lee of the reef. For both normal and oblique wave incidence, wave refraction around the reef resulted in 2 crossing wave fields landward of the reef that then induced 2 zones of

diverging wave angles near the shoreline. Some interference patterns due to diffraction effects were superimposed.

- The hydrodynamic circulation became significantly disturbed by the reef when it started to break incident waves. The starting point of the reef-induced circulation was a strong onshore flow generated over the reef, along with the set-up of the water level in its' immediate lee. For shore normal waves, the divergence of this flow and additional water mass induced a cellular circulation in the lee of the reef along with two return currents on the reef sides. For oblique wave incidence, the reef-induced currents (i) deviated the ambient long-shore currents towards the shoreline updrift of the reef, and (ii) fed the ambient long-shore flow downdrift of the reef.

7.6 REFERENCES

BLACK, K.P., 2002. *The 3DD computational marine and freshwater laboratory. Model 2DBEACH, version W3.03*, ASR Ltd, Raglan, New Zealand, 69 p.

BLACK, K.P., 2003. Numerical Prediction of Salient Formation in the Lee of Offshore Reefs. *In:* BLACK, K.P., and MEAD, S.T. (eds.), *Artificial Surfing Reefs 2003: The 3rd International Conference,* (Raglan, New Zealand). CD publication. pp. 196-218, ISBN: 0-473-09801-06.

BLACK, K.P. and HEALY, T.R., 1988. Formation of ripple bands in a wave convergence zone. *Journal of Sedimentary Petrology*, 58 (2), 195-207.

BLACK, K.P., and ROSENBERG, M.A., 1992. Semi-empirical treatment of wave transformation outside and inside the breaker line. *Coastal Engineering*, 16, 313-345.

BLACK, K.P., and ANDREWS, C.J., 2001. Sandy Shoreline Response to Offshore Obstacles, Part 2: Discussion of Formative Mechanisms. *In:* BLACK, K.P.: (ed.), Natural and Artificial Reefs for Surfing and Coastal Protection. *Journal of Coastal Research, Special Issue No. 29*, 94-101.

BLACK, K.P., and MEAD, S.T., 2001. Wave Rotation for Coastal Protection. *Proceedings of the 2001 Coasts and Ports Conference* (Gold Coast, Australia), pp. 120-127.

BLACK, K.P., and MEAD, S.T., 2007. Sand Bank Responses to a Multi-Purpose Reef on an Exposed Sandy Coast. *In*: WALTHER, M. (ed.), Shore Protection and Surfing Dedicated Issue. *Shore and Beach,* 75(4), 55-66.

DALLY, W. R., DEAN, R. G., and. DALRYMPLE, R. A., 1985. Wave Height Variation Across Beaches of Arbitrary Profile, *Journal of Geophysical Research*, 90(C6), 11,917–11, 927.

GOLDEN SOFTWARE INC., SURFER, Version 6. Developed by Golden Software Inc. 809 14th Street, Golden, Colorado 80401-1866, U.S.A. (*www.goldensoftware.com*).

MADSEN, O.S., 1976. Wave climate of the continental margin: elements of its mathematical description. *In*: STANLEY, D.J., and SWIFT, D.J.P. (eds), *Marine Sediment Transport in Environmental Management.* Wiley, New York, NY, pp. 65-87.

NIELSEN P., 1982. Explicit formulae for practical wave calculations. *Coastal Engineering*, 6, 389-398.

RANASINGHE, R., TURNER, I.L., and SYMONDS, G., 2006. Shoreline Response to Multi-Functional Artificial Surfing Reefs: A Numerical and Physical Modeling Study. *Coastal Engineering,* 53, 589-611.

SCARFE, B.E., 2008. Oceanographic Considerations for the Management and Protection of Surfing Breaks. Hamilton, New Zealand: The University of Waikato, Ph.D. thesis, 307 p. + appendices.

THORNTON, E.B. and GUZA, R.T., 1983. Transformation of wave height distribution. *Journal of Geophysical Research*, 88, 5925-5938.

CHAPTER 8. MAIN FINDINGS AND CONCLUSIONS

8.1 CONTEXT

The innovative multi-purpose reef technology can combine a coastal protection function with recreational benefits such as improved surfing, diving or fishing, and therefore provides an appealing solution for the management and protection of beaches. However, since the concept is relatively new and real world reef prototypes scarce worldwide, the empirical knowledge about the method is still limited. In a coastal engineering context, there is consequently a lack of hindsight on the method performance compared to more conventional shore protection solutions. A necessary step for the widespread acceptance of the concept is the monitoring of existing reef prototypes to valid and/or refine the theoretical design practices. In line with this requirement, this thesis monitored the effect of the prototype multi-purpose reef constructed at Mount Maunganui in New Zealand on the local beach morphodynamics and oceanographic conditions. The research was primarily concerned with the modification of the beach system relevant to the coastal protection function of the concept, and the recreational functions have not been considered.

8.2 BEACH MORPHODYNAMIC RESPONSE TO THE REEF

The beach morphodynamic response to the reef was investigated using the beach bathymetric datasets collected prior to, and throughout reef construction in earlier work by SCARFE (2008), and a new post reef construction survey undertaken as a part of this research in March 2009. The shoreline response was specifically analyzed using an odd-even function analysis in Chapter 3, and the concurrent large scale morphological adjustments were treated in Chapter 4.

8.2.1 SHORELINE RESPONSE

The shoreline response to the reef was found to be dynamic, and in contrast with an equilibrium salient formation. Mean sea level contour analysis indicated that a small depositional feature of amplitude ~ 20 m extending ~ 150 m alongshore

could form at the shoreline in the lee of the reef. However, this shoreline advance pattern was superimposed on comparatively important natural fluctuations of the shoreline position, and was consequently transient throughout the monitoring period. The magnitude of the possible shoreline advance of ~ 20 m was found to be generally lower than predictions obtained using design relationships available to date for submerged reefs. This has evident implications for future reef projects whose designs should not rely only on these relationships.

In hindsight, it would have been beneficial to undertake surveys at a higher temporal resolution (weeks to months) to better capture the dynamic character of the shoreline response. Repetitive multibeam echosoundings and RTK GPS surveys of the complete bathymetry and foreshore as undertaken in the present study are likely not practically and financially realisable at such rate, but a focus on the intertidal area using RTK GPS surveying only seems achievable and sufficient to resolve the shoreline response.

8.2.2 MORPHODYNAMIC RESPONSE

Analysis of the pre and post reef construction beach bathymetries indicated that the reef disturbed the pre-existing beach state functioning including the onshore/offshore migration of the underlying long-shore bar, rather than caused a persistent salient response. The possible local shoreline advance mentioned above suggests that this process may have benefits for the shoreline stabilization. However any reef-induced morphological coupling and beach state modification needs to be further investigated to be controlled. This also suggests that a careful site by site assessment on the pre-existing beach state functioning is required during design.

Another important effect of the reef was that it provided a control point in the large scale long-shore sediment movement. The analysis of offshore bathymetric contours indicated that the reef obstruction to the natural long-shore sediment movement was able to induce a groin effect on the offshore beach morphology, accreting sediment updrift and eroding sediment downdrift. The accretion/erosion pattern extended up to 1400 m around the structure within the monitoring period. Although no adverse downdrift erosion was evident on the bathymetric charts or shorelines, this large scale effect requires attention particularly as reef structures get larger and/or are implemented in high magnitude drift environments.

8.3 MODIFICATION OF THE OCEANOGRAPHIC CONDITIONS

The effect of the reef on the local oceanographic conditions was monitored during a 5 day field experiment undertaken in the vicinity of the prototype reef during which incident and transmitted waves and currents were measured. The experiment provide the first oceanographic field dataset around a submerged multi-purpose reef. The analysis of the field data was supplemented by the numerical modelling of waves and currents to investigate the reef impact on the larger scale patterns of waves and circulations at the beach.

8.3.1 WAVE TRANSMISSION OVER THE REEF

A primary motivation of the field experiment was the quantification of the wave height and energy transmission over the reef (Chapter 5) since this is expected to be a dominant feature in the protection of the beach in the lee side.

The reef effect on the incident wave heights was twofold consisting of (i) transmitted wave height amplification for incident wave heights up to $H\,sig_i \sim 0.5$ m, and (ii) transmitted wave height reduction after this threshold. The height amplification was due to the wave shoaling on the reef and increased in intensity on shallower reef crests yielding transmitted wave heights larger than incident by up to a factor of 2. The height reduction began as waves started to break on the reef and was found to be increasingly efficient for larger incident wave heights and/or shallower reef crests, up to ~ 40 % reduction for the range of incident wave heights measured ($H\,sig_i = 0$ - 2.5 m). A strong relationship between the transmission coefficients of the significant wave height and the incident significant wave height was found ($r^2=0.86$), and could serve as a tool to provide a first order estimate of wave transmission magnitude over futures reef prototypes. Another potential application is for the calibration of numerical wave models, largely used for reef design, that require representative transmitted wave heights to yield valid results in the lee of the reef structure.

The reduction of the incident wave heights was consistently associated with a change of the wave energy distribution within the frequency domain. The breaking-induced energy dissipation was generally much more efficient in reducing the peak wave energy than that at higher frequencies thus increasing the relative proportion of high frequency wave energy within the transmitted wave

field. This was possibly further enhanced by harmonic energy generation due to non linear interactions during wave propagation over the reef. The shift in wave energy distribution resulted in shorter period transmitted waves in the lee of the reef that reduced the measured transmitted mean and significant wave periods by up to 3 seconds (~ 40 % of the incident period). The reduction of the transmitted wave periods has potential implications on the wave energy dissipation in the surfzone in the lee of the reef, and subsequent beach face morphodynamics.

8.3.2 HYDRODYNAMIC RESPONSE

An expected side effect of the incident wave energy reduction was the generation of mean currents in the lee of the reef, and these were treated in Chapter 6. The mean current velocity magnitude landward of the reef generally increased with increasing incident wave forcing (i.e. wave height, wave energy, or non dimensional wave height). The increase rate was however strongly accelerated when the reef started triggering wave breaking. The current direction landward of the reef was consistently deviated towards the shore relative to the ambient long-shore directed currents measured seaward of the reef. The maximum mean current velocities measured were around 0.6 m/s for incident significant wave heights ~ 2-2.5 m.

The increase in mean current velocity was also found to respond distinctly to increasing cross-reef wave energy gradients i.e. wave energy difference between the seaward and landward sides of the reef. These energy gradients can be seen as a crude proxy for radiation stress gradients which are a dominant driver for wave-induced mean currents.

The strong and onshore deviated flow measured landward of the reef is characteristic of submerged structures that allow water transmission over their crest, and is generally expected to the starting point of the hydrodynamic circulation in the lee side. Estimations of reef-induced and undisturbed flow discharges suggested that the flux of water landward of the reef was about 2.5 times greater than on an adjacent undisturbed area which has indeed likely implications on the circulation pattern in the lee of the reef.

8.3.3 NUMERICAL MODELLING OF WAVES AND CURRENTS

To gain insights on the larger scale wave and circulation patterns at the beach, numerical modelling of waves and currents was undertaken in Chapter 7. The collected field datasets provided a unique opportunity to calibrate and assess the numerical model with respect to the wave transmission, and subsequent current generation in the vicinity of a multi-purpose reef.

The first difficulty was to correctly reproduce the measured wave height transmission characteristics with a numerical model whose inherent simplifications (e.g. regular monochromatic waves, standard wave breaking model) seemed relatively crude when compared to the complexity of wave processes identified from the field data analysis. However, the model was found to perform generally well and a reproduction of most of the main features of field datasets was eventually achievable. Some difficulties still remained particularly regarding the treatment of small incident waves subject to shoaling only (without breaking) over the reef crest. The coupled wave-driven hydrodynamic model reproduced correctly the magnitude of reef-induced currents but important deviations were observed for predicted current direction.

To identify the main wave and circulation patterns at the site, a range of wave events was simulated. The main conclusions were:

- The height reduction was evident in the lee of the reef as soon as waves started to break on the reef crest, however, the wave shadow zone was the most evident in the first 100 m landward of the structure, and significantly decreased towards the shore. The wave sheltering was also less efficient as the reef became included in the natural surfzone.

- Under both breaking and not breaking conditions, the reef had a significant influence on incident wave angles that generally resulted in two zones of diverging waves fields near the shoreline in the lee of the reef.

- The resulting hydrodynamic circulation in the lee of the reef was strongly influenced by the strong onshore flow over the reef crest due to wave breaking, and the associated sea level set-up. The reef-induced flow (i) forced a cellular circulation in the lee of the reef under shore normal waves, and (ii) significantly diverted the ambient (unidirectional) long-

shore flow towards the shoreline under obliquely incident waves. The resulting currents at the shoreline were either divergent or relatively accelerated, and thus did not suggest obvious templates for sediment accretion.

The wave height shadow was obviously expected and consistent with previous research, however the hydrodynamic circulation and wave angle patterns obtained were not readily comparable to available investigations on hydrodynamic circulations (e.g. BLACK, 2003; RANASINGHE *et al.*, 2006) or wave rotation processes (BLACK and MEAD, 2001) around multi-purpose reefs. Although the proposed mechanisms are robust, the present results suggest that there may be significant interferences to their developments on actual beach bathymetries that should be considered.

8.4 RECOMMENDATIONS FOR FUTURE RESEARCH

Some recommendations for future research following on from the work undertaken as a part of this thesis follow:

- An area that would require further attention is the monitoring of the short-term beach morphodynamics at the reef site (and future reef sites), on a scale from weeks to months. More regular field surveys using maybe less demanding survey techniques, such as RTK GPS surveying only, may be an option. Another option that can provide the required temporal resolution (and even further) is the use of video monitoring stations. These can provide short-term shoreline positions, intertidal topographies, and sand bar positions, and would significantly facilitate the monitoring of the beach response. Such stations should be considered for future reef projects.

- It would be valuable to undertake a more comprehensive and longer field deployment at the site, including arrays of wave and current meters from the reef position to the shoreline on both the reef profile and an "undisturbed" beach profile. Measurements of a wider range of incident wave conditions (i.e. height, period, direction) would allow investigating the effects of additional parameters on wave transmission such as wave period, wave steepness, and wave angle. This would supplement the

characteristics outlined from the field experiment undertaken as a part of this research that focused on incident height and crest submergence (Chapter 5). Additional instruments landward of the reef would allow relating the local reef transmission characteristics with the eventual wave and current conditions near the shoreline in the lee of the reef, and importantly compare them to these observed on the undisturbed adjacent beach.

- The next logical step with respect to the numerical modelling undertaken in the present study would be the coupling of a morphological module to investigate sedimentary patterns at the beach, and any coupling between perturbed sand bars and shoreline/intertidal morphology. The bathymetric and oceanographic datasets now available provide a robust basis to undertake further field-based numerical modelling on a realistic reef system. This could provide valuable supplements to the theoretical investigations available to date.

8.5 REFERENCES

BLACK, K.P., 2003. Numerical Prediction of Salient Formation in the Lee of Offshore Reefs. *In:* BLACK, K.P., and MEAD, S.T., (eds.), *Artificial Surfing Reefs 2003: The 3rd International Conference,* (Raglan, New Zealand). CD publication. pp. 196-218, ISBN: 0-473-09801-06.

BLACK, K.P., and MEAD, S.T., 2001. Wave Rotation for Coastal Protection. *Proceedings of the 2001 Coasts and Ports Conference* (Gold Coast, Australia), pp. 120-127.

RANASINGHE, R., TURNER, I.L., and SYMONDS, G., 2006. Shoreline Response to Multi-Functional Artificial Surfing Reefs: A Numerical and Physical Modeling Study. *Coastal Engineering,* 53, 589-611.

SCARFE, B.E., 2008. Oceanographic Considerations for the Management and Protection of Surfing Breaks. Hamilton, New Zealand: The University of Waikato, Ph.D. thesis, 307 p. + appendices.

APPENDICES

APPENDIX A: Paper on Shoreline Analysis Presented at the Coasts and Ports Conference 2009 (Wellington, NZ).

APPENDIX B: Matlab Code for Odd-Even Function Analysis

APPENDIX C: Samples of Matlab Codes for Wave Data Analysis

APPENDIX D: Simulated Wave Events at Mount Maunganui, New Zealand. Numerical Model: 2DBEACH (3DD suite).

The appendices are included as a CD at the end of the thesis.

APPENDIX A. PAPER PRESENTED AT THE COASTS AND PORTS CONFERENCE 2009 (WELLINGTON, NEW ZEALAND).

WEPPE, S.B., HEALY, T.R., SCARFE B.E., and IMMENGA, D., 2009. Shoreline response to an offshore submerged multifunction reef at Mount Maunganui, New Zealand. *Coasts and Ports Conference 2009 (Wellington, New Zeland)*, 7 p.

Shoreline response to an offshore submerged multifunction reef at Mount Maunganui, New Zealand

Simon Weppe, Terry Healy, Brad Scarfe and Dirk Immenga
Coastal Marine Group, University of Waikato, Hamilton, New Zealand

Abstract
Shoreline response to an offshore submerged multifunction reef is investigated using an odd-even function analysis. The method is used to separate natural (e.g. cyclic erosion/accretion) and structural modes (e.g. salient formation, groin effect) of shoreline changes. The shoreline dataset allows analysis of both pre and post construction shoreline change functions. Results for the pre construction interval depicted a complex pre-existing shoreline with possible fluctuations of 20-30 m, including an underlying alongshore gradient in shoreline change. Post construction analysis indicated a more crenulated response since structure implementation with growth of two bar features located around the reef centreline. Combined with a local groin effect, this has led to an additional net shoreline (MSL contour) advance of ~20 m extending ~150 m alongshore to the north of the reef. The identified pattern is masked at times by ambient fluctuations in shoreline position, suggesting a transient character of shoreline response to the structure.

1 Introduction

Multifunction offshore submerged reefs are potentially able to provide beach protection while enhancing local surfing conditions, with a low impact on coastal zone aesthetic (Black, 2001). With respect to coastal protection, structure function is similar to conventional offshore submerged structures and aims at reducing incident wave energy and rearranging waves and currents to promote sedimentation in the lee side (e.g. salient formation). The characteristic of the concept is that instead of common shore parallel single or segmented designs, the structure shape is optimised to break waves in way suitable for surfing. The desired beach response is the development of a salient in the landward side, widening the beach and providing additional buffer during high energy erosive wave events. Observations of salient features in the lee of natural offshore obstacles (Black and Andrews, 2001) supported by numerical and physical modelling results (e.g. Turner et al., 2001; Black, 2003; Ranasinghe et al., 2006) provide robust arguments for such formation to occur. In contrast, Ranasinghe and Turner (2006) still suggested important unpredictability in beach response to submerged structures with 7 out of 10 major projects to date resulting in net erosion. Encouragingly though, the Narrowneck reef (Australia), first example of multifunctional design was among the 3 accretive cases (see Turner, 2006).

The present study focuses on the other example of multifunctional design to date, which is the submerged reef constructed at Mount Maunganui in New Zealand. The project is somewhat unique since it was undertaken primarily for research purposes rather than for addressing a significant erosion problem. The objective to test the beach protection aspect of the concept was to induce formation of a small salient feature which would have negligible impact on adjacent beaches (Mead and Black, 1998). In this paper we investigate the shoreline response to the structure.

Although comparison of pre/post construction shoreline can give insight of system response,

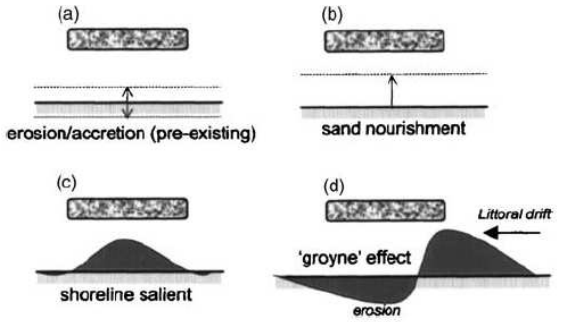

Figure1. Different modes of shoreline response to offshore structures: Natural variability (a), Artificial nourishment (b), Structural effects (c) and (d) (from Turner, 2006).

"interwoven" natural variability may be hard to discriminate, which complicates the quantification of net structure impacts. To account for the pre-existing variability of a beach system, Turner (2006) used an odd-even function analysis to monitor shoreline adjustment to the construction of the Narrowneck reef. The method has been used previously to assess the alongshore extent of impacts of engineering projects such as inlets (e.g. Dean and Work, 1993; Rosati and Ebbersole, 1998) but application on a smaller scale to the Narrowneck site proved it to be a robust tool to discriminate different modes of shoreline response i.e. natural erosion/accretion, salient growth, or secondary groin effect (Figure 1). This allows separate assessment of natural and structural signals and thus more accurately quantify net structure effects. To quantify net shoreline adjustment at Tay Street, Mount Maunganui, we will apply the odd-even function analysis to available shoreline data collected by Scarfe (2008).

2 Study site

The multifunction reef has been constructed near Tay Street in Mount Maunganui, which is located on the Bay of Plenty on the north-eastern coast of New Zealand (Figure 2). The V-shaped submerged structure is located at about 250 m offshore and has an alongshore width of 80 m. Local wave conditions consist predominantly of locally generated small

Figure 2. Features of interest around the reef site including dredged channel and dredge disposal sites. Shorelines have been extracted from surveys by Scarfe (2008) of the study site.

waves (H<1 m) but with the possibility of more energetic swell events due to subtropical disturbances (Pickrill and Mitchell, 1979). The net drift is towards the southeast through the Bay of Plenty with magnitude of order 60 to 80.000 m^3/ year (Healy, 1980). Frequent reversals are expected in response to the reigning climatic system or individual high energy events (Mead and Black, 1998; Scarfe, 2008). As a result, the net movement may be small relative to gross movement along the site. Antecedent coastal engineering projects in the site vicinity include maintenance dredging of the Tauranga Harbour channel, 4 km to the northwest, and subsequent dredge disposals to the north of the study area (Figure 2).

3 Methods

3.1 The dataset

The site benefits from a pre-construction baseline bathymetric and foreshore survey using multibeam echsosoundings and RTK GPS (Scarfe and Healy, 2005). Throughout construction, Scarfe (2008) collected additional surveys for comparison with the baseline (Table 1). To apply the odd-even function analysis, shoreline contours, taken as mean sea level (MSL) contours, have been extracted from the surveys. The study zone was defined as a 1400m portion of the shoreline centred on the reef axis. Six complete shoreline contours were available for this zone (Table 1). A reference line in the backshore provided a measure of the beach width and contours were then interpolated and smoothed to yield evenly-spaced data (every 10m) as required to apply the proposed method.

3.2 Odd-Even function analysis

The basic principle of the odd-even analysis is to decompose shoreline change data into its symmetric and asymmetric components about a point of significance (Rosati and Ebbersole, 1998). The reference point corresponds typically to a coastal structure (here the reef) or inlet position. Such decomposition potentially allows discrimination of distinct depositional modes (Figure 1) and estimation of extent and magnitude of structural effects. Natural shoreline changes are expected to occur homogeneously alongshore while structural effects will be likely limited to the vicinity of the structure. Moreover, salient formation (symmetric) and potential secondary groin effect (asymmetric) can be separated thanks to the signal decomposition. Importantly, this may require re-centring shoreline data relative to salient apex in the case of an alongshore offset (Turner, 2006). The reader is directed towards Rosati and Kraus (1997) and Turner (2006) for a complete outline of calculation procedure and interpretation.

Table 1. Surveys dates around the Tay Street reef and stage of reef completion. * symbol indicates surveys for which a complete shoreline contour (MSL) is available (from Scarfe, 2008).

Survey date	Reef completion
19/08/2004 *	0%
28/10/2004	0%
26/04/2005	0%
08/09/2005	0%
17/11/2005*	10%
20/04/2006	25%
15/08/2006 *	25%
23/01/2007 *	70%
15/05/2007 *	70%
14/03/2009 *	100%

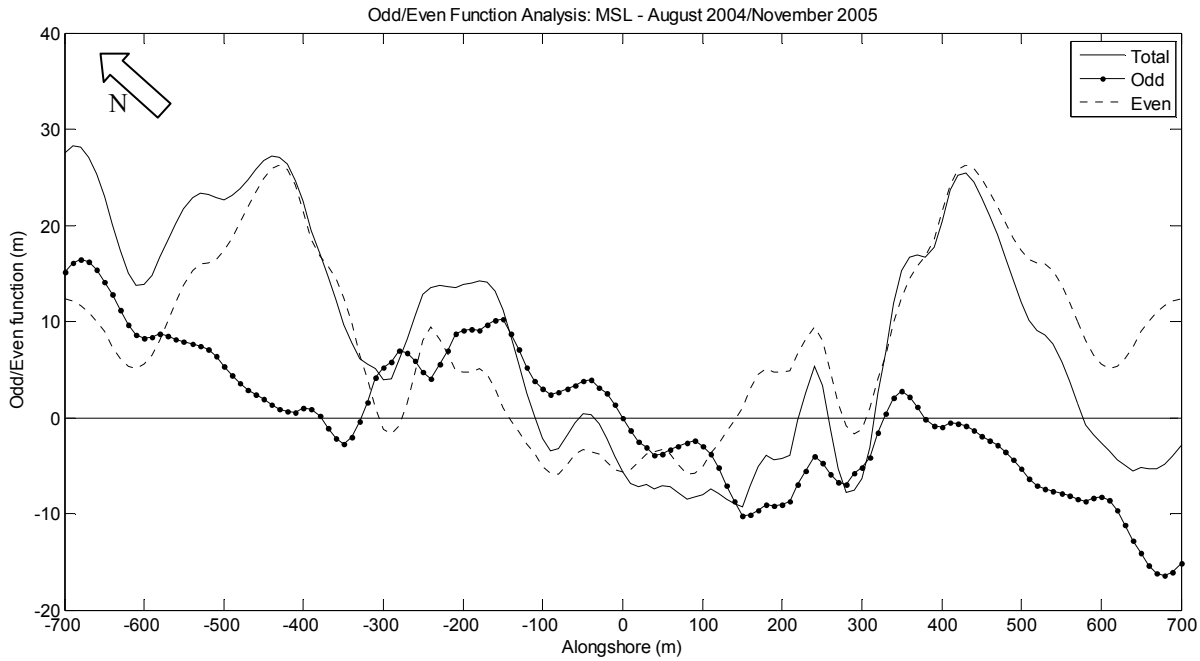

Figure 3. Odd-even function analysis results for the pre-construction interval, from August 2004 to November 2005. The total function is the sum of the odd (dotted) and even (dashed) components. The alongshore origin (x=0) corresponds to the reef centreline. Note the negative gradient in shoreline advance towards the southeast described by the odd function.

A strength of the dataset is that the first two available contours i.e. August 2004 and November 2005, provide a shoreline change function representative of the pre-construction shoreline behaviour. Reef construction began towards the end of 2005 and 10% of the reef was actually completed during the survey in November 2005, but we can still reasonably assume minimal interaction with the beach system. Therefore, to serve as a basis for further interpretation, we can apply the analysis to a pre-construction interval. This is valuable as it may be able to identify any pre-existing alongshore gradient in shoreline change at the site. These may occur in places where incident wave energy is naturally modulated along the coast (e.g. offshore islands, focusing shoals). It is potentially relevant for the site and such a signal may be hard to discriminate from structure effects if only a pair of pre/post shorelines are available (Walton, 2002), which is often the case.

The next logical interval to study is the period from November 2005, virtually pre reef construction, to March 2009, post construction (the reef was completed in June 2008). Salient formation and any secondary groin effect can thus be investigated on the longest term possible given the available data. This is supplemented by additional analysis focusing more closely on the post construction period.

4 Results

4.1 Pre-construction interval

The decomposition of the shoreline change function between August 2004 and November 2005 is given in Figure 3. The even function is predominantly positive indicating net accretion over the period. It is characterized by two more prominent depositional features (symmetric) located at about ± 400m with a magnitude of about +25 m. The central part of the function consists of two secondary symmetric peaks (+10 m) at about ± 200 m separated by a zone of shoreline retreat (-5 m). The offset in accretion in the central 400 m may be related to a modulation of the incident wave energy. Scarfe et al. (2009) identified distinct bands of wave focusing offshore of the site that can vary in location depending on wave direction. The localized zones of enhanced wave energy (e.g. wider surfzone as observed by Scarfe and Healy, 2005) could have effects on the pre-construction shoreline adjustment.

Looking now to asymmetrical shoreline adjustments (Figure 3), we can see that the odd function, although undulating, tends to indicate a negative gradient in shoreline advance as we go towards the southeast. Overall, this involves about 10 m of accretion to the northwest of the zone progressively switching to erosion of similar magnitude to the southeast.

The alongshore gradient is consistent with the earlier observation of overall decrease in beach width towards the south east (Scarfe, 2008). It is important to note that, as a pre-existing characteristic of the system, it may potentially be present in the next applications, interwoven with structure effects. This highlights the necessity of having independent baseline data (see Scarfe and Healy, 2005) to apply the odd-even method. The observed gradient may arise from sheltering effect of offshore islands (see Scarfe (2008) for modelling). Another likely cause is the proximity of dredge disposal (Figure 2). The gradient may then be due or enhanced by onshore migration of this additional sediment (e.g. Spiers and Healy, 2007).

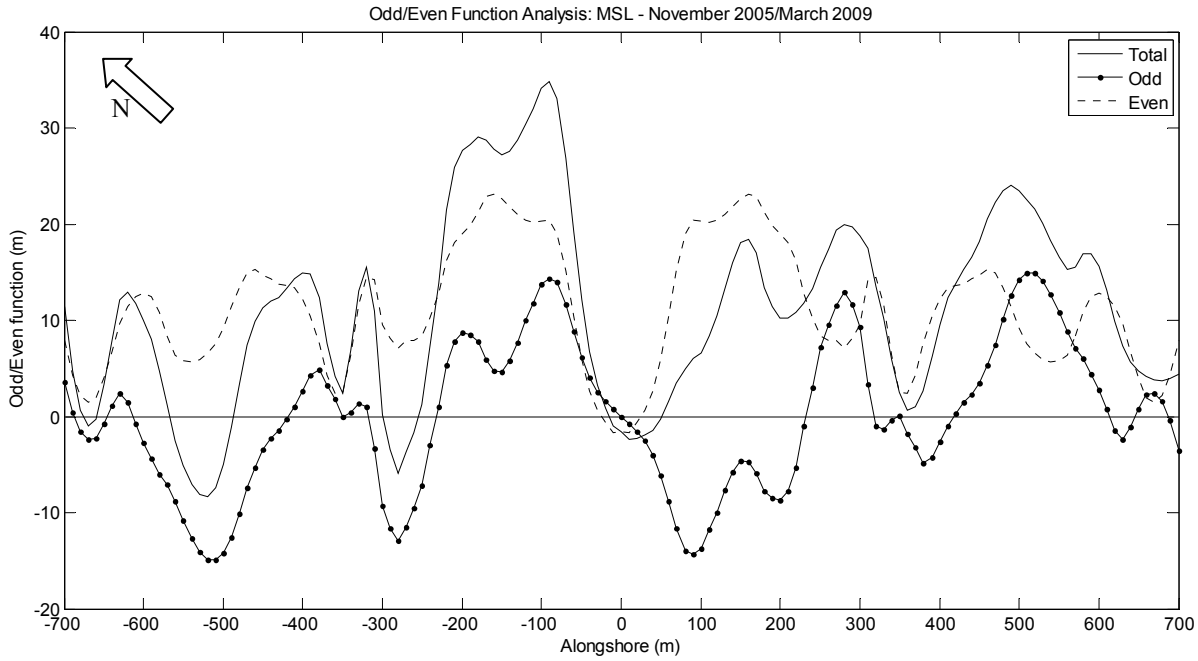

Figure 4. Odd-even function analysis results for shoreline change function computed from the November 2005 (pre construction) and March 2009 (post construction) shorelines. The total function is the sum of the odd (dotted) and even (dashed) components. The alongshore origin (x=0) corresponds to the reef centreline. Two more prominent features can be identified in the central 400 m (even) along with a local groin effect (odd). This explains the distinct depositional feature to the north of the reef.

4.2 Pre/Post construction interval

Shoreline change from November 2005 to March 2009 allows investigating structural effects during the longest time frame allowed by the dataset. Given that the major phase of the reef construction was completed at the January 2007 survey, we can assume that for the last survey in March 2009, the beach has had more than 2 years to adjust to the structure. The salient was expected to form within a year (Mead and Black, 1998) so this time interval is reasonable to identify the adjusted state.

Figure 4 presents results of the odd-even function analysis for the interval considered. Even component of shoreline change function indicates a positive mean shoreline advance of about 10 m, likely associated with a natural fluctuation (e.g. Figure 1 (a)). The function is however found to significantly oscillate around this mean trend with features spacing of 100-300 m. Features observed here appear to be more regular and closer together than they were for the pre-construction interval and this distinctive crenulated character was not as obvious in the pre-construction even function. Although undulations developed all along the study site, thus limiting direct discrimination of a structural effect, the more crenulated aspect of the even component still suggests a modification of the beach system response which it is tempting to attribute to the structure since it coincides with its implementation. In the vicinity of the structure, two more prominent features (+20 m) are found on both sides of the reef at approximately ± 200 m. These 2 more marked advances are separated by a low in the central 50-100 m in the immediate lee of the reef, with virtually no change. Here, the signal contrasts with classic salient growth as a symmetric and localized shoreline advance (Figure 1 (c)). This consequently limits the relevance of a readjustment of shoreline data relative to salient position as in Turner (2006). That being, the central pattern still tends to stand out from the function shape and would indicate a structural effect.

Any secondary groin effect can be investigated in the corresponding odd function. A first observation that can be made is that the negative gradient identified in the precedent interval is absent. In fact, although oscillating, the function mean trend has straightened up and thus not reproduces any distinct gradient in the alongshore direction. An implicit assumption to observe again the gradient initially identified in Figure 3 is a condition of stationary wave climate/sediment supply over the period (Walton, 2002) that cannot be resolved here. As a result, it can hardly be resolved whether this absence is induced by the structure or rather related to natural causes (e.g. better balance in gross sediment transport with less net effects, lessened supply, or ENSO effect).

Between ± 200m alongshore, an interesting feature is the sharp gradient in shoreline position change that occurs around the reef centreline. This results in accretion of ~10 m to the north side matched by similar erosion to the south (Figure 4). The odd function describes undulations at some distance of the reef, however, it is stressed that no such magnitude of erosion/accretion is found further alongshore, indicating that the structure does have a

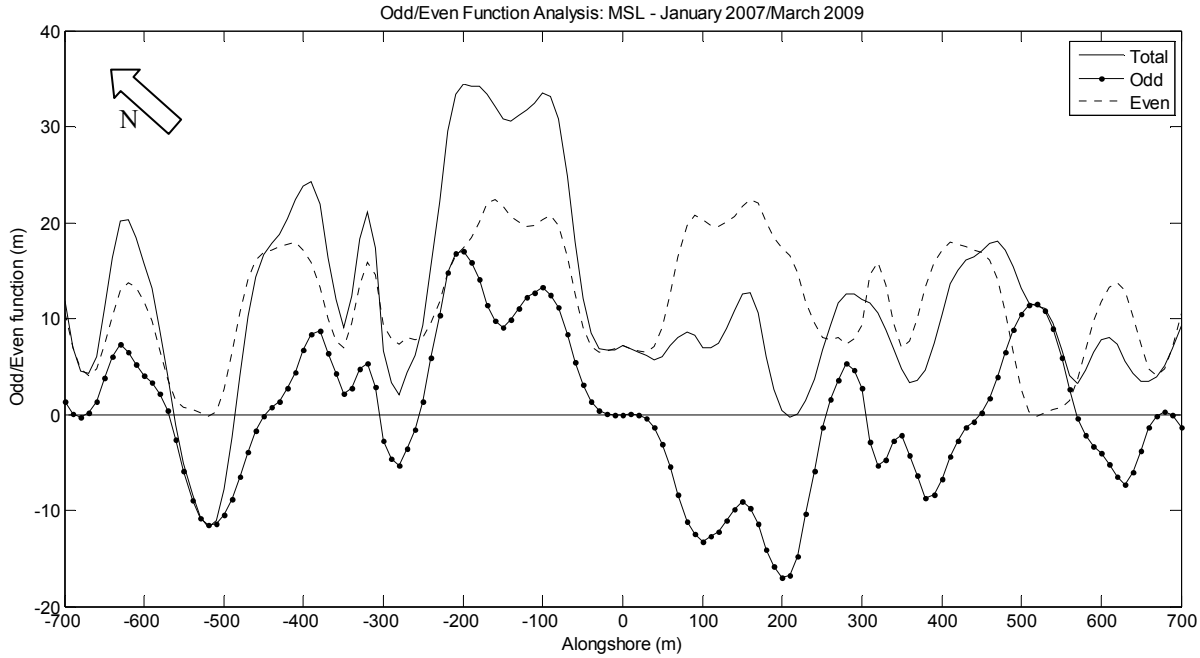

Figure 5. Odd-even function analysis results for shoreline change function focusing on post construction, i.e. from January 2007 to March 2009 when 70% to 100% of the structure was in place. The total function is the sum of the odd (dotted) and even (dashed) components. The alongshore origin (x=0) corresponds to the reef centreline. The central pattern is fully consistent with Figure 4 and the magnitude of changes indicates that most of the net changes shown in Figure 4 have occurred during this interval.

role on the observed changes, even if limited. Since the net drift direction is to the south east, the signal i.e. updrift accretion and downdrift erosion is consistent with a local groin effect.

Also, given that the net drift is potentially small compared to gross movement, groin effect signature may be present to some degree in the even function, as a symmetric impoundment of sediment around the structure centreline (Rosati and Kraus, 1997). That would actually be in agreement with the more marked accretion of the shoreline around the reef centreline.

The groin pattern coincides with the two depositional features in the lee of the reef (even function). The combined effects are shown in the total function and result in the greater growth of the depositional feature to the northwest of the reef, benefiting from additional accretion, while the symmetric feature to the south is offset due to the matching erosion. This yields a distinct advance of the MSL contour of up to 35 m to the north west of the structure (total function).

The 2-feature pattern and groin effect that induce greater accretion to the north of the reef are not considered to be a coincidence. As additional shoreline contours are available within the period (Table 1), it is interesting to consider shoreline adjustments over different intervals to further validate and/or refine the identified pattern.

Analysis of successive shorelines indicated that the central pattern observed in Figure 4 is not the result of a progressive adjustment through the entire pre/post construction interval. The shoreline position appears to be primarily governed by natural fluctuations through the period from November 2005 to January 2007. On January 2007, the beach was in an eroded state with a linear shoreline and reduced beach width (see Scarfe, 2008). In contrast, the last survey in March 2009 imaged a beach full and well accreted. Analysis of shoreline change between these two distinct beach states (Figure 5) yields odd and even functions fully consistent with Figure 4. Magnitudes indicate that most of the net accretion observed during the entire interval has occurred during this 2 year period from January 2007 to March 2009.

Removing the mean "natural" advance of ~10 m of the even component, the 2 more prominent symmetric features provide additional 10 m of shoreline advance around the reef centerline. The local groin effect superimposes and gives rise to the distinct depositional feature to the north west of the reef with an overall net additional advance estimated at ~20 m extending ~150 m alongshore. As this happened while structure footprint on the system was larger, this increases our confidence in relating the pattern to the structure.

In contrast, the linear eroded shoreline of January 2007 still suggests that the depositional features may be more prominent for accreted beach states and subsequently eroded under high wave energy conditions. This would explain the relative absence of any significant shoreline adjustments over the first part of the interval (November 2005 to January 2007) that may have been masked by larger scale ambient morphology.

5 Discussion

Although complexity of the natural shoreline has to be kept in mind, the structure impact appears to be twofold: (1) more crenulated response associated with 2 more prominent features around the structure centreline, and (2) development of a localized groin effect.

With respect to the first impact, Scarfe (2008) already identified more prominent undulations in post construction shorelines that were found to be linked to rhythmic bar and rip features. This evolution may be the expression in the morphology of a more cellular surfzone circulation induced by the structure (Short, 1999). By triggering wave breaking, the reef induces a local gradient in wave height driving strong flows over the structure (e.g. Ranasinghe et al., 2006). This likely stimulates the development of circulation cells that may then be expressed in the beach morphology into stronger rips, crescentic features, or development of crenulated shoreline (Short, 1999).

Furthermore, morphological modelling of the beach system by Black and Mead (2007) showed that the structure would drive bar formation in its vicinity much faster that on other parts of the beach. Two main bar features would grow along the side of the reef and migrate inshore to eventually merge with the shoreline. This is coherent with the 2 larger depositional features identified in the lee of the reef, possibly indicating a signature of such mechanism. That being, as the rhythmic character is consistently present in the full extents of even functions we can still expect that the proposed mechanism either has some effects even at some distance from the structure, or is a localized expression of a larger scale modification of the surfzone such as more cellular circulation (Short, 1999; Scarfe, 2008) or development of wave interference patterns (Turner et al., 2001).

The second identified impact is a shoreline change signal that indicates a local groin effect. The question that arises is how the structure develops this effect on the shoreline. A first possible explanation is that the structure acts as a physical barrier to the overall motion of sediment, able to trap sediment updrift. Such effect was observed on the offshore bar (Scarfe, 2008) and although obviously expected to be greater in the direct vicinity of the reef, the process might be relevant at some distance from the structure. Secondly the groin effect may be due to the structure induced circulation. The strong onshore flows over the structure interact with longshore currents to weaken currents updrift and enhance them downdrift (Ranasinghe and Sato, 2001; Turner et al., 2001; Ranasinghe and Turner, 2006). This may create a local gradient in longhsore transport rate and subsequent deposition/erosion that would be consistent with the groin signal. Finally, the pattern may be a secondary effect of the depositional features identified, acting as actual submerged groins (Turner, 2006).

The combination of these two effects gives rise to a distinct depositional feature to the north of the reef and thus on the updrift side of the structure (Figure 4 and 5). Although on a smaller scale and likely masked by natural variability “noise”, the pattern could then resemble an episode of proto-salient formation as observed on physical modelling of the Narrowneck site (Turner et al., 2001) and subsequently identified during the first year of shoreline response monitoring (Turner, 2006). This was expected to be a temporary phase with subsequent merging of features into an equilibrium salient, offset downdrift relative to the structure centreline. With respect to our case, this may suggest a shoreline still adjusting. However, given the significant time period allowed, the identified pattern is more likely representative of the adjusted state. This would then indicate a more complex and transient character of shoreline response that contrasts with equilibrium salient formation.

Subsequent research that could be undertaken using the existing datasets would be to undertake an odd-even analysis on the contour immediately offshore of the reef. This would help understand the groin effect on the offshore bar identified by Scarfe (2008) and seen in the shoreline analysis presented here. Future shoreline surveys over the next years would also be of interest to further monitor shoreline adjustment. Moreover, more accurate understanding of the shoreline response would likely benefit from observations of the system at a higher temporal resolution, as for example through individual high energy events and recovery periods.

6 Conclusion

Shoreline response to the multifunction reef constructed at Mount Maunganui has been tested using an odd-even function analysis. The shoreline dataset includes a pair of contours representative of the pre-construction behaviour along with several post-construction shorelines. This allowed application of the method to investigate the pre-existing variability of the system. Results for this pre-construction interval indicated a complex pre-existing shoreline with possible fluctuations of order 20-30 m, including an underlying negative alongshore gradient in shoreline change from the northwest to the southeast. Analysis for the pre/post construction shoreline change function depicted a more crenulated character of shoreline adjustment with the growth of two prominent features in the vicinity of the structure (even component) along with the development of a localized groin effect (odd component). Analysis of successive shoreline adjustment within the period indicated that most obvious net adjustments occurred while the structure was in place, and thus provided a favourable argument to relate the pattern to the structure. However, the shoreline feature(s) are superimposed on large scale natural fluctuations, and may be more prominent on accreted beach states and reset on more eroded states. Although this transient response contrasts with equilibrium salient formation, the identified pattern still provided a net additional advance estimated at ~20 m along ~150 m of

shoreline (MSL) to the northwest of the reef. Due to the complexity of the shoreline system, odd-even analysis in conduction with 3D erosion-accretion analysis, modelling and site visits are recommended.

7 Acknowledgements

The Broad Memorial fund is acknowledged for providing monetary support for this research.

8 References

Black, K.P., 2001. Artificial Surfing Reefs for Erosion Control and Amenity: Theory and Application. *In:* Healy, T.R. (ed.), International Coastal Symposium (ICS2000). *Journal of Coastal Research, Special Issue,* 34, 1-14.

Black, K.P., 2003. Numerical Prediction of Salient Formation in the Lee of Offshore Reefs. *In*: Black, K.P., and Mead, S.T. (eds.), *Artificial Surfing Reefs 2003: The 3rd International Conference, Raglan, New Zealand.* CD publication, pp. 196-218.

Black, K.P., and Andrew, C.J., 2001. Sandy Shoreline Response to Offshore Obstacles, Part 1: Salient and Tombolo Geometry and Shape. *In:* Black, K.P.: (ed.), Natural and Artificial Reefs for Surfing and Coastal Protection. *Journal of Coastal Research, Special Issue*, 29, 82-93.

Black, K.P. and Mead, S.T., 2007. Sand Bank Responses to a Multi-Purpose Reef on an Exposed Sandy Coast. *In*: Walther, M. (ed.), Shore protection and surfing dedicated issue: *Shore and Beach*, 75(4), 55-66.

Dean, R.G., and Work, P.A., 1993. Interaction of navigational entrances with adjacent shorelines. *Journal of Coastal Research,* 18, 91–110.

Healy, T.R., 1980. Erosion and Sediment Drift on the Bay of Plenty coast. *Soil and Water*, August, pp. 12-14.

Mead, S.T. and Black, K.P., 1999. A Multipurpose, Artificial Reef at Mount Maunganui Beach, New Zealand. *Coastal Management,* 27, 335-365.

Pickrill, R. A., and J. S. Mitchell. 1979. Ocean wave characteristics around New Zealand. *New Zealand Journal of Marine and Freshwater Research,* 1, 501–520.

Ranasinghe, R., and Turner, I.L., 2006. Shoreline Response to Submerged Structures: A Review. *Coastal Engineering*, 53, 65-79.

Ranasinghe,, R., Turner, I.L., and Symonds, G., 2006. Shoreline Response to Multi-Functional Artificial Surfing Reefs: A Numerical and Physical Modeling Study. *Coastal Engineering*, 53, 589-611.

Ranasinghe, R., and Sato, S., 2007. Beach morphology behind single impermeable submerged breakwaters under obliquely incident waves. *Coastal Engineering Journal*, 49 (1), 1-24.

Rosati, J. D., and Ebersole, B. A., 1998. Littoral impact of Ocean City Inlet, Maryland, USA, *Proceedings of the 25th International. Conference. on Coastal Engineering*, ASCE, New York, pp. 2779–2792.

Rosati, J. D., and Kraus, N. C., 1997. Even–odd analysis of shoreline position and volume change, *Coastal Engineering Technical Note IV-10*, Coastal and Hydraulics Laboratory, United States Army Corps of Engineers Waterways Experiment Station, Vicksburg, Mississipi, 8p.

Scarfe, B.E., and Healy, T.R., 2005. Baseline Bathymetric Data Collection for Monitoring of Bar, Rip and Salient Response to an Artificial Surfing Reef - Mount Maunganui, New Zealand. *In*: Townsend, M. and Walker, D. (eds.), *Proceedings for the 2005 Coasts and Ports Australasian Conference* (Adelaide, South Australia), pp. 459-464.

Scarfe, B.E., 2008. Oceanographic Considerations for the Management and Protection of Surfing Breaks. Hamilton, New Zealand: The University of Waikato, Ph.D. thesis, 307p. + appendices.

Scarfe, B.E., Healy, T.R., Rennie, H.G., and Mead, S.T., 2009. Sustainable Management of Surfing Breaks: Case Studies and Recommendations. *Journal of Coastal Research*, 25(3), 684-703.

Short, A.D., 1999. Beach Modification: Natural impacts and beach Morphodynamics. *In*: Short, A.D. (ed.), *Handbook of Beach and Shoreface Morphodynamics*. West Sussex, England: John Wiley & Sons Ltd, pp. 253-270.

Spiers, K.C., and Healy, T.R., 2007. Beach Renourishment through Spoil Disposal Downdrift of a Dredged Entrance Channel. *In*: Kraus, N.C. and Rosati, J, D. (eds.) *Coastal Sediments '07,* pp. 2358-2371.

Turner, I.L., Leyden, V., Cox, R., Jackson, A., and McGrath, J., 2001. Physical Model Study of the Gold Coast Artificial Reef. *In:* Black, K.P. (ed.), Natural and Artificial Reefs for Surfing and Coastal Protection. *Journal of Coastal Research, Special Issue,* 29, 131-146.

Turner, I.L., 2006. Discriminating Modes of Shoreline Response. *Journal of Waterway, Port, Coastal and Ocean Engineering*, 132(3), 180-191.

Walton, T.L., 2002. Even-odd analysis on a complex shoreline. *Ocean Engineering*, 29, 711–719.

APPENDIX B. MATLAB CODE FOR ODD-EVEN FUNCTION ANALYSIS

```
% ODD EVEN FUNCTION ANALYSIS
%This program decomposes beach width changes between two times
%into an odd and an even function. The calculation procedure
%follws the method oultined in Rosati and Kraus, 1997.

clear all
close all

%INPUT

%load beach width (bw) matrix
%( X (alongshore grid), bw0408, bw0511, bw0608, bw0701, bw0705,
bw0903)

load MSL_contours.mat

%Choice of interval analysed

b_width1=bw0511; %beach width at t1
b_width2=bw0701; %beach width at t2

%net change in beach width between t1 and t2
delta_bw=(b_width2-b_width1);

%Even and odd function computation

%variables creation
delta_odd=zeros(length(b_width1),1);
delta_even=zeros(length(b_width1),1);

for i=1:1:length(b_width1)

    delta_even(i,1)=0.5.*(delta_bw(i,1)
    +delta_bw(length(b_width1)-i+1,1));
    %equivalent to equation (8)
    delta_odd(i,1)=0.5 .* (delta_bw(i,1)
    -delta_bw(length(b_width1)-i+1,1));
    %equivalent to equation (9)

    %delta_bw(i,1) represents delta_bw(-x)
    %delta_bw(length(b_width1)-i,1) represents delta_bw(+x)

end

figure(1)
plot(X,delta_bw,'k')%
hold on
plot(X,delta_odd,'k.-')%
hold on
plot(X,delta_even,'k--')%
xlim ([-700 700])
xlabel ('Alongshore (m)')
ylabel ('odd - Even function (m)')
title ('Odd - Even Function Analysis ')
legend('Total','Odd ','Even ')
```

APPENDIX C. SAMPLES OF MATLAB CODES FOR WAVE DATA ANALYSIS

The appendix includes samples of Matlab codes used for the wave data analysis in Chapter 5 and a comparison of crossing-derived and spectrally-derived significant wave heights.

C.1 PRESSURE TIME SERIES TO SURFACE ELEVATION TIME SERIES

```
clear all
close all
%INPUT DATA
load ADV_PUV_DATA.mat

% create ADV_PUV_OFF and ADV_PUV_IN and burst_index in the
workspace
% data in 3 column P U V, get burst number n using ADV_PUV_OFF
(burst_index(:,X),:)
% 4096 pts/burst sampled at 4Hz during 1024 seconds

%CONSTANT
dt=0.25;
fs=4;
fNyq=2;
nfft=4096;
n=4096;
f_vect=(((0:n/2)'*fs)/n);
relative_t=0:dt:(nfft/4)-dt;
instr_elev=0.7;
rho=1025;%volumic mass of seawater kg/m3
g=9.81; %gravity constant
cutoff_high=0.35; %high frequency cut off
cutoff_low=0.05; %low frequency cut off

for kk=1:231

    p=ADV_PUV_IN(burst_index(:,kk),1);

    %Detrend presssure record
    data=detrend(p); %remove tidal oscillation
    %fft of pressure timeseries
    Y=fft(p,nfft);
    %sorting of real and imaginary parts
    Re_Y1=real(Y(1))/nfft;
    Re_Y2=real(Y(2:end-1))/(nfft/2);
    Re_Y3=real(Y(nfft/2))/nfft;
    Re_Y=[Re_Y1' Re_Y2' Re_Y3'];
    Im_Y=-imag(Y(1:end))/(nfft/2);

    %Transfer of fft coefficient back to a timeseries
    %the frequency component i is stored in timeseries (i,:)
```

```
    for i=1:nfft/2

      timeseries(i,:)=Re_Y(i).*cos(2.*pi.*f_vect(i).*relative_t)+I
      m_Y(i).*sin(2.*pi.*f_vect(i).*relative_t);
    end

    %water depth
    h=mean(p)+instr_elev; %total water depth
    z=-(h-instr_elev);%depth at which we look i.e. instrument
elevation

    find_cutoff_high=find(f_vect>=cutoff_high,1);
    find_cutoff_low=find(f_vect<=cutoff_low,1);

    %Computation of attenuation coefficient for each frequency
component
    for j=1:length(f_vect)-1
    %k for for range of frequency of fourier transforms
    k=2*pi.*dispersion(f_vect(j),h);
    %frequency dependent attenuation with depth
    att(j)=(cosh((k).*(z+h))./cosh(k.*h));
    end

    %Transfer function pressure/surface elevation

    Kt=(rho*g).*att./10000;
    %Generation of surface elevation time series
    for ii=find_cutoff_low:1:find_cutoff_high
    eta(ii,:)=timeseries(ii,:)./Kt(ii);
    end
    eta_matrix(kk,:)=sum(eta);

end  %end of first loop
eta_off=eta_matrix;
save eta_off.mat eta_off
```

C.2 DETERMINATION OF REPRESENTATIVE WAVE PARAMETERS

```
function [H Hs H10 Hrms Hmax T Ts T10 Tmean]=wave_param(eta,fs)

% Calculate wave parameters from pressure sampling using crossing
analysis
% calls dat2crossind function from WAFO toolbox to determine down
crossing %index
% INPUT: surface elevation time series (p), sampling frequency
%
% OUTPUT
%   H wave heights
%   Hs mean of 1/3 of highest waves
%   H10 mean of 1/10 of highest waves
%   Hrms 1/nwaves *sum(H²)
%   Hmax max wave height
%   Simon weppe (20/09/09)

data=eta;
t=1/fs:1/fs:length(data)/fs; %time vector

%find (best)index for down crossing relative to specified level
```

```
% u for up crossing, d for down crossing > down crossing is better
for surfzone due to wave profile horikawa 1988;

[ind, Nc]= dat2crossind(data,mean(data),'d');
% create wave height and period matrix > if NC index then there
are (NC-1) % waves
H=zeros(Nc-1,1);
T=zeros(Nc-1,1);
for i=1:Nc-1
    index=ind(i):ind(i+1); %i th wave segment
    [hmax indmax]=max(data(index)); %find the crest
    [hmin indmin]=min(data(index));%find the trough

    H(i,1)=hmax+abs(hmin); %Wave height matrix
    T(i,1)=length(index).*(1/fs);
end    %for end

%HEIGHT output

H_sort=sort(H,'descend');
n=length(H_sort);
nsig=round(n/3);
n10=round(n/10);

Hs=mean(H_sort(1:nsig,1));
H10=mean(H_sort(1:n10,1));
Hmax=max(H_sort);
Hrms=sqrt((1/n)*sum(H_sort.^2));

%PERIOD output

limsig=H_sort(nsig); %last height considered for significant wave
height
ind_sig=find(H>=limsig);  %get  index  of  height  used  for  Hs
computation
Ts=mean(T(ind_sig)); %significant period > mean period of 1/3
highest waves
lim10=H_sort(n10);%last height considered for H10
ind_10=find(H>=lim10);  %get  index  of  height  used  for  H10
computation
T10=mean(T(ind_10));
Tmean=mean(T);

end %function end

% dat2crossind function : WAFO TOOLBOX

%BRODTKORB, P.A., JOHANNESSON, P., LINDGREN, G., RYCHLIK, I., RYDEN,
%J., and SJO, E., 2000. WAFO - a Matlab toolbox for analysis of
%random waves and %loads. Proceedings of the 10th International
%Offshore and Polar %Engineering Conference (Seattle,Washington),
%Vol 3, pp. 343-350.


function [ind , Nc]= dat2crossind(x,v,wdef)
%DAT2CROSSIND Finds indices to level v down and/or upcrossings
from data
%
%  CALL:  [ind, Nc]= dat2crossind(x,v,wdef/cdef);
%
% ind  = indices to the level v crossings of the original sequence
x.
```

```
% Nc   = number of crossings (i.e.length of ind).
%  x   = the surface elevation data.
%  v   = the reference level (default  v = mean of  x).
% wdef = defines the type of wave. Possible options are
%        'dw', 'uw', 'cw', 'tw' or 'none'. (Default 'none').
%        If wdef='none' all crossings will be returned,
%        otherwise only the crossings which defines a
%        wave according to the wave definition will be returned.
% cdef = defines the type crossings returned. Possible options are
%        'd' 'u' or 'all'. (Default 'all').
%        If def='d' all down-crossings will be returned.
%            Similarly if def='u' only the up-crossings will be
returned
%        otherwise 'all' the crossings will be returned.
%
% Example:
%   t = linspace(0,7*pi,250);
%   x = sin(t);
%   [ind, Nc] = dat2crossind(x,0.75,'u')
%   plot(t,x,'.',t(ind),x(ind),'o')
%
% See also  findcross, wavedef, crossdef

%tested on: Matlab 6.0, 5.3, 5.2, 5.1
% History:
% revised pab Feb2004
% revised by pab 12.06.2001
%  -added check on ind returned from findcross.
% Revised by jr 02.04.2001
% - Added example, updated help
% By Per A. Brodtkorb 07.07.1998,  27.07.1998,

error(nargchk(1,3,nargin))
xn=x;

[n m]= size(xn);
if n<m
 b=m;m=n;n=b;
 xn=xn';
end

if n<2,
  error('The vector must have more than 2 elements!')
end

istime=1;

switch m
 case 1, istime=0;
 case 2, xn= xn(:,2);% dimension OK!
 otherwise, error('Wrong dimension of input! dim must be 2xN, 1xN,
Nx2 or Nx1 ')
end

if ((nargin<3) | isempty(wdef)),
  wdef='none';
end

if ((nargin<2) | isempty(v)),
  v = mean(xn);
  disp(['   The level v is set to: ', num2str(v)])
end
```

```
% find level v down-crossings and/or up-crossings
% according to wdef or cdef
ind = findcross(xn,v); % faster than find

if isempty(ind), %added pab 12.06.2001
   Nc = 0;
   txt = sprintf('No level v = %0.5g crossings found in x',v)
   warning(txt)
   return,
end

switch wdef   % switch wdef/cdef
  case 'd', %downcrossings only
    if xn(ind(1)+1)>v,
      ind =ind(2:2:end);
    else
      ind =ind(1:2:end);
    end

 case 'u',%upcrossings  only
   if xn(ind(1)+1)<v,
      ind =ind(2:2:end);
    else
      ind =ind(1:2:end);
    end

  case {'dw','uw'},
    % make sure that the first is a level v down-crossing if wdef
== 'dw'
    % or make sure that the first is a level v up-crossing if wdef
== 'uw'

    if xor(((xn(ind(1))>xn(ind(1)+1))),strcmp(wdef,'dw')),
      ind(1)=[];
    end
    Nc=length(ind); % number of level v crossings
    % make sure the number of troughs and crests are according to
the
    % wavedef, i.e., make sure length(ind) is odd
    if ~(mod(Nc,2)), % if Nc is even do
      ind(end)=[];
    end
  case {'tw','cw'},
    % make sure that the first is a level v down-crossing if wdef
== 'tw'
    % or make sure that the first is a level v up-crossing if wdef
== 'cw'

    if xor(((xn(ind(1))>xn(ind(1)+1))),strcmp(wdef,'tw')),
      ind(1)=[];
    end
    Nc=length(ind); % number of level v crossings
    % make sure the number of troughs and crests are according to
the
    % wavedef, i.e., make sure length(ind) is even
    if (mod(Nc,2)), % if Nc is odd do
      ind(end)=[];
    end
  case {'du','all','none'},
    % do nothing
```

```
 otherwise,  error('Unknown wave/crossing definition!')
end
if nargout>1,
  Nc=length(ind); % number of level v crossings
end
 return
```

C.3 DETERMINATION OF WAVE HEIGHT AND PERIOD DISTRIBUTIONS

```
function [prob X_vect]=distrib(X,dX)

%INPUT
%set of H or T
%dX, bin interval
%OUTPUT
%Probability of occurrence prob of wave in each bin
%bin vector X_vect

%interval definition

X_vect=0:dX:ceil(max(X));
ntot_X=length(X);%number of measurement



for i=1:length(X_vect)-1
    ind=find(X>=X_vect(i) & X<X_vect(i+1));
    prob(i)=length(ind)/ntot_X;
end

X_vect=X_vect+(dX/2);

end
```

C.4 COMPUTATION OF ONE DIMENSIONAL WAVE ENERGY SPECTRUMS

```
function [S f]=onedspec(data_raw,fs,win_sec)
%compute the one dimensional spectra of 'data' sampled at fs
following
%method by Emery and Thompson,1997
%
%we consider 1024 s timeseries. The spectra is obtained by
averaging 7
%spectral estimates computed on 256-second window,
tappered(hanning) and %detrended with 50 % overlapping

%INPUT
%data: pressure data timeseries
%fs: frequency sampling
%win_sec:Window size in seconds
%OUTPUT
%S spectral estimates of sea surface elevation
%f frequency vector



%DATA PREPARATION-----------------------------------------------
%Data filtering
cutoff=0.35;
[data]=butt_filt(data_raw,cutoff,2,4,'low');

%Data segmentation
```

```
winsize_pt=win_sec*fs;

if (win_sec==512)
    win_num=3;
    else if (win_sec==256)
         win_num=7;
         else if (win_sec==128)
              win_num=15;
              else ('problem size window')
              end
        end
end

win=zeros(winsize_pt,win_num);

   win(:,1)=1:winsize_pt;
   i=2;
while  (win(end,i-1)<=1024*fs-winsize_pt/2)  %last  index  of  last
window smaller than half of last window
    start_pt=win(end,i-1)-(winsize_pt/2) +1;
    win(1:winsize_pt,i)=start_pt:1:start_pt+winsize_pt-1;
    win(1:winsize_pt,i)./4;
    i=i+1;
end

%Detrend and tapper data segments

seg=zeros(winsize_pt,win_num);

for i=1:win_num
seg(:,i)=detrend(data(win(:,i)));
seg(:,i)=hann(winsize_pt).*seg(:,i);
end

n=winsize_pt;%length of data segment

%FOURIER TRANSFORM OF EACH SEGMENT--------------------------------
--------
E=zeros(winsize_pt,win_num);
for i=1:win_num
F=fft(seg(:,i));%  Fast fourier transform
%Rescaling  of  estimate  to  account  for  loss  of  energy  due  to
windowing
F=F.*sqrt(8/3);
E(:,i)=abs(F).^2;% estimates of two-sided periodogram
end
%Averaging
for j=1:winsize_pt
    S(j)=mean(E(j,1:win_num));
end
S=S';% still two sided

%TRANSFER FUNCTION to SURFACE ELEVATION spectra-------------------
---------

% transfer function K based on linear theory
% uses dispersion.m (K.Bryan)
instr_elev=0.7;
h=mean(data_raw)+instr_elev; %total water depth
z=-(h-  instr_elev);%depth  at  which  we  look  i.e.  instrument
elevation
rho=1025;%volumic mass of seawater kg/m3 (between 1020-1035)
```

```
g=9.81; %gravity constant
k=2*pi.*dispersion(f,h); %k for for range of frequency of fourier
transforms
att=(cosh(k.*(z+h))./cosh(k.*h));%frequency dependent attenuation
with depth
Kt=(rho*g).*att./10000;  %Transfer  function  from  pressure  to
surface elevation

%SURFACE ELEVATION SPECTRUM ----------------------------------------
---------
amp=sqrt(S); %back to amplitude
%     ind=find(f>=cutoff);
%     amp(ind)=0;
% zeroth amplitude above frequency cutoff
% pressure already filtered but zeroth spectral densities
amp=amp./Kt; %apply transfer function
% Define first half of  spectral density fct
select = [1;ones((n/2)-1,1).*2;1];
Seta=amp.^2;
Seta=Seta.*select; % Power estimates of one-sided spectral density
Seta=Seta./(fs*n);% Normalizing for Parseval's theorum

%OUTPUT-------------------------------------------------------------
---------
% %remove first value f=0
cut_spec=find(f>=cutoff,1);
S=Seta(2:cut_spec);
f=f(2:cut_spec);

%Dispersion function by Karin Bryan 28/01/99

function [kk]=dispersion(f,d);

% This is a function for calculating the dispersion properties of
waves in
% and depth of water. f can be a vector or a single frequency. f
and k
% are in cycles per s (Hz) and cylces per m respectively  and d is
the depth in metres.
% The program works by going through each f, suggesting a k,
% calculating ERR=(2*pi*f(j)).^2-2*pi*k.*g.*tanh(2*pi*k*d); If the
ERR is +ve, than the
% suggested k is too small, and k is increased, if ERR is -ve,
than k is too
% large and it is decreased. Tol determines when the answer is
close enough, which is set
% at 0.003.
%
% Written by K. Bryan, 28/01/99


%Setting up matrices to store the results
    kk=zeros(size(f));
    ERR=zeros(2,1);
    g=9.812;
    tol=0.003;
    'Calculating Wavenumber for Depth Correction';

%Stepping through each frequency loop
    for j=1:length(f);
    %if rem(j,100)==0,j,end
```

```
% You know that the new wavenumber is always going to be larger
than
% the one you have just found, so might as well save time and
start looking there

      if j>1;
        k=kk(j-1);
      else
        k=0;
      end

      dk=0.001;
      found=0;

      ERR(1)=(2*pi*f(j)).^2-2*pi*k.*g.*tanh(2*pi*k*d);
      ERR(2)=ERR(1);
        if ERR(1)<=tol,dk=0;end;

% This is if the right k is not found immediately, it checks to
see whether k is too
% small or too large and adjusts this by setting the sign of dk

        while abs(ERR(1))>tol
          if ERR(1)/ERR(2) <= 0
            dk=-dk/2;
            found=1;
          else
            if found==0
              dk=1.5*dk;
            end
          end

% Storing the old results so you can check it the next time around
         ERR(2)=ERR(1);
             ERR(1)=(2*pi*f(j)).^2-2*pi*k.*g.*tanh(2*pi*k*d);
             k=k+dk;

% Sometimes if k is very small, adjusting it makes it negative so
this line stops that
         while k<0,k=(k-dk),dk=dk/2;,k=k+dk;,end
       end

       kk(j)=k-dk;
    end

%Butterworth filter

function [data_filt]=butt_filt(X,cutoff,Nyq,n,choice)

%INPUT
    % data to filter X
    % cut off frequency in Hz
    % Nyquist frequency
    % n order of filter
    % Choice low or high

data=detrend(X);
wn=cutoff/Nyq;
%Filter design > Butterworth
tf = strcmp('high',choice);
if (tf==1)
[b a]=butter(n,wn,'high');
```

```
else if (tf==0)
        [b a]=butter(n,wn,'low');
    end
end

data_filt_forward=filter(b,a,data);
data_filt_backward=filter(b,a,wrev(data_filt_forward));
data_filt=wrev(data_filt_backward); %zero phase shift

end
```

C.5 COMPUTATIONS OF WAVE ENERGY SPECTRUMS AND ENERGY FLUX DISTRIBUTIONS

```
%Energy Spectrums and energy flux partition

load ADV_PUV_DATA.mat

% create ADV_PUV_OFF and ADV_PUV_IN and burst_index in the
workspace
%data in 3 column P U V, get burst number X using ADV_PUV_OFF
(burst_index(:,X),:)
% 4096 pts/burst sampled at 4Hz during 1024 seconds

%CONSTANT CHOICE
%choice of window size for onedspec
win_size=256; %128s 256s or 512s with decreasing smoothing
spec_length=90;
instr_elev=0.7;
[burst_length burst_num]=size(burst_index);
fs=4;

%VARIABLE CREATION
spec_full_off=zeros(231,spec_length);
spec_full_off_NORM=zeros(231,spec_length);
Hmo_off=zeros(231,1);

spec_full_in=zeros(231,spec_length);
spec_full_in_NORM=zeros(231,spec_length);
Hmo_in=zeros(231,1);

wdepth_off=zeros(231,1);
wdepth_in=zeros(231,1);

%LOOP for spectrums calculation

for i=1:burst_num

    po=ADV_PUV_OFF(burst_index(:,i),1);
    [So f]=onedspec(po,fs,win_size);
    spec_full_off(i,1:end)=So;
    df=f(5)-f(4);
    ind=find(f>=0.05);
    Hmo_off(i,1)=4*sqrt(sum(So(ind))*df);
    [Somax_in indfp_off]=max(So);
    Tp_off(i,1)=1/f(indfp_off);
    norm_fact=max(So); % NORMALIZATION by incident peak spectral
density
    spec_full_off_NORM(i,1:end)=spec_full_off(i,1:end)./norm_fact;
```

```
    pi=ADV_PUV_IN(burst_index(:,i),1);
    [Si f]=onedspec(pi,fs,win_size);
    spec_full_in(i,1:end)=Si;
    %norm_fact1=max(Si);
    spec_full_in_NORM(i,1:end)=spec_full_in(i,1:end)./norm_fact;
    % normalization
    Hmo_in(i,1)=4*sqrt(sum(Si(ind))*df);
    [Simax_in indfp_in]=max(Si);
    Tp_in(i,1)=1/f(indfp_in);

    %water depth for determination of energy flux
    wdepth_off(i,1)=mean(po)+instr_elev;
    wdepth_in(i,1)=mean(po)+instr_elev;


end

%Energy flux Table 5.1

tot_off=zeros(231,1);
tot_in=zeros(231,1);
prim_band_off=zeros(231,1);
prim_band_in=zeros(231,1);
harmo_band_off=zeros(231,1);
harmo_band_in=zeros(231,1);

Cg_off=zeros(231,spec_length);
Cg_in=zeros(231,spec_length);

for kk=1:231

%OFF
Cpha_off=f./dispersion(f,wdepth_off(kk,1)); %phase velocity
A=4.*pi.*dispersion(f,wdepth_off(kk,1)).*wdepth_off(kk,1);%interme
diate variable
Cg_off(kk,:)=(Cpha_off./2).*(1+(A./(sinh(A)))); %group velocity
%%IN
Cpha_in=f./dispersion(f,wdepth_in(kk,1)); %phase velocity
B=4.*pi.*dispersion(f,wdepth_in(kk,1)).*wdepth_in(kk,1);
%intermediate variable
Cg_in(kk,:)=(Cpha_in./2).*(1+(B./(sinh(B)))); %group velocity

end
    for jj=1:231

    [Somax_in indfp_off]=max(spec_full_off(jj,1:end));

    indprim=find(f>=0.05 & f<=1.5*f(indfp_off)); %maybe add limit
0.05
    indharmo=find(f>1.5*f(indfp_off) & f<=0.35);
    indtot=find(f>=0.05 & f<=0.35);

prim_band_off(jj,1)=sum(Cg_off(jj,indprim).*spec_full_off(jj,indpr
im).*df);
harmo_band_off(jj,1)=sum(Cg_off(jj,indharmo).*spec_full_off(jj,ind
harmo).*df);
tot_off(jj,1)=sum(Cg_off(jj,indtot).*spec_full_off(jj,indtot).*df)
;

prim_band_in(jj,1)=sum(Cg_in(jj,indprim).*spec_full_in(jj,indprim)
.*df);
```

```
harmo_band_in(jj,1)=sum(Cg_in(jj,indharmo).*spec_full_in(jj,indhar
mo).*df);
tot_in(jj,1)=sum(Cg_in(jj,indtot).*spec_full_in(jj,indtot).*df);

    end

%% Normalization by total energy flux

prim_band_off=prim_band_off./tot_off;
harmo_band_off=harmo_band_off./tot_off;

prim_band_in=prim_band_in./tot_off;
harmo_band_in=harmo_band_in./tot_off;
tot_in=tot_in./tot_off;

%Ratio computations
indsmall=find(Hs_off<=0.5 & Ts_off<20);
indmed=find(Hs_off>0.5 & Hs_off<=1.5);
indlarge=find(Hs_off>1.5);

SMALL_TOT_OFF=mean(tot_off(indsmall))
SMALL_PRIM_OFF=mean(prim_band_off(indsmall))
SMALL_HARM_OFF=mean(harmo_band_off(indsmall))
SMALL_TOT_IN=mean(tot_in(indsmall))
SMALL_PRIM_IN=mean(prim_band_in(indsmall))
SMALL_HARM_IN=mean(harmo_band_in(indsmall))

MEDIUM_TOT_OFF=mean(tot_off(indmed))
MEDIUM_PRIM_OFF=mean(prim_band_off(indmed))
MEDIUM_HARM_OFF=mean(harmo_band_off(indmed))
MEDIUM_TOT_IN=mean(tot_in(indmed))
MEDIUM_PRIM_IN=mean(prim_band_in(indmed))
MEDIUM_HARM_IN=mean(harmo_band_in(indmed))

LARGE_TOT_OFF=mean(tot_off(indlarge))
LARGE_PRIM_OFF=mean(prim_band_off(indlarge))
LARGE_HARM_OFF=mean(harmo_band_off(indlarge))
LARGE_TOT_IN=mean(tot_in(indlarge))
LARGE_PRIM_IN=mean(prim_band_in(indlarge))
LARGE_HARM_IN=mean(harmo_band_in(indlarge))
```

C.6 COMPARISON OF SIGNIFICANT WAVE HEIGHTS FROM WAVE CROSSING AND SPECTRAL ANALYSIS

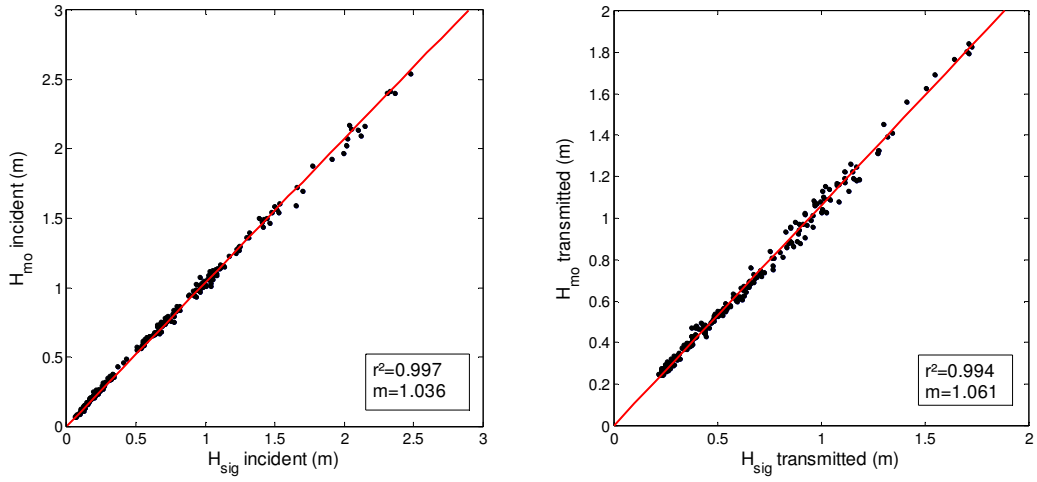

Figure C.1. Comparison of significant wave heights obtained from wave crossing analysis H_{sig} and spectrally-derived significant heights H_{mo}.

APPENDIX D. SIMULATED WAVE EVENTS AT MOUNT MAUNGANUI, NEW ZEALAND

The appendix includes predicted wave heights, wave angles, sea levels, and nearshore circulation patterns for the wave events simulated (Table 7.3) using the numerical model 2DBEACH (Chapter 7).

Table 7.3. Simulated wave events. The tide level was kept at mean sea level.

Height (m)	**Angle (°)**	**Period (s)**
1	0	9
2	0	9
3	0	9
1	15	9
2	15	9
3	15	9
1	30	9
2	30	9
3	30	9
1	-15	9
2	-15	9
3	-15	9
1	-30	9
2	-30	9
3	-30	9

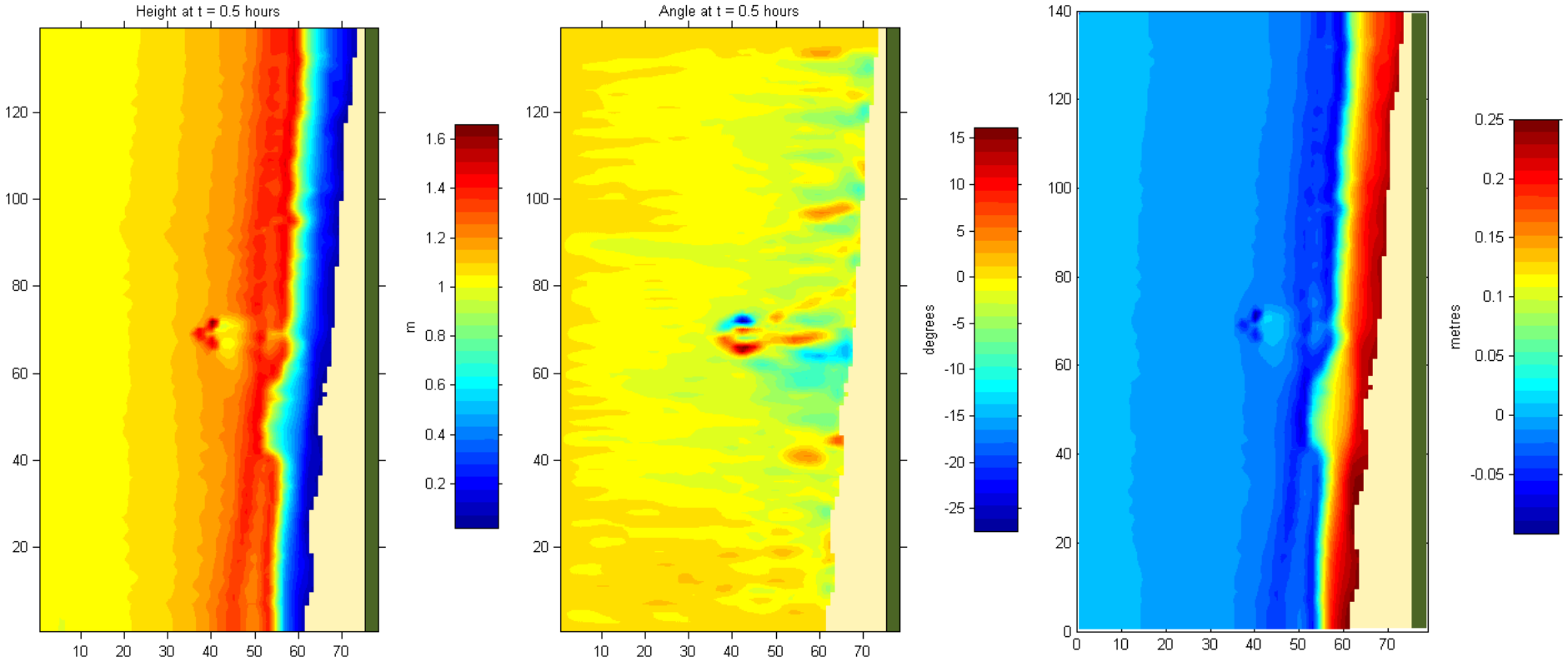

Figure D.1. Predicted wave heights, wave angles, and sea levels for the wave event H = 1m and angle = 0° (i.e. shore normal waves).

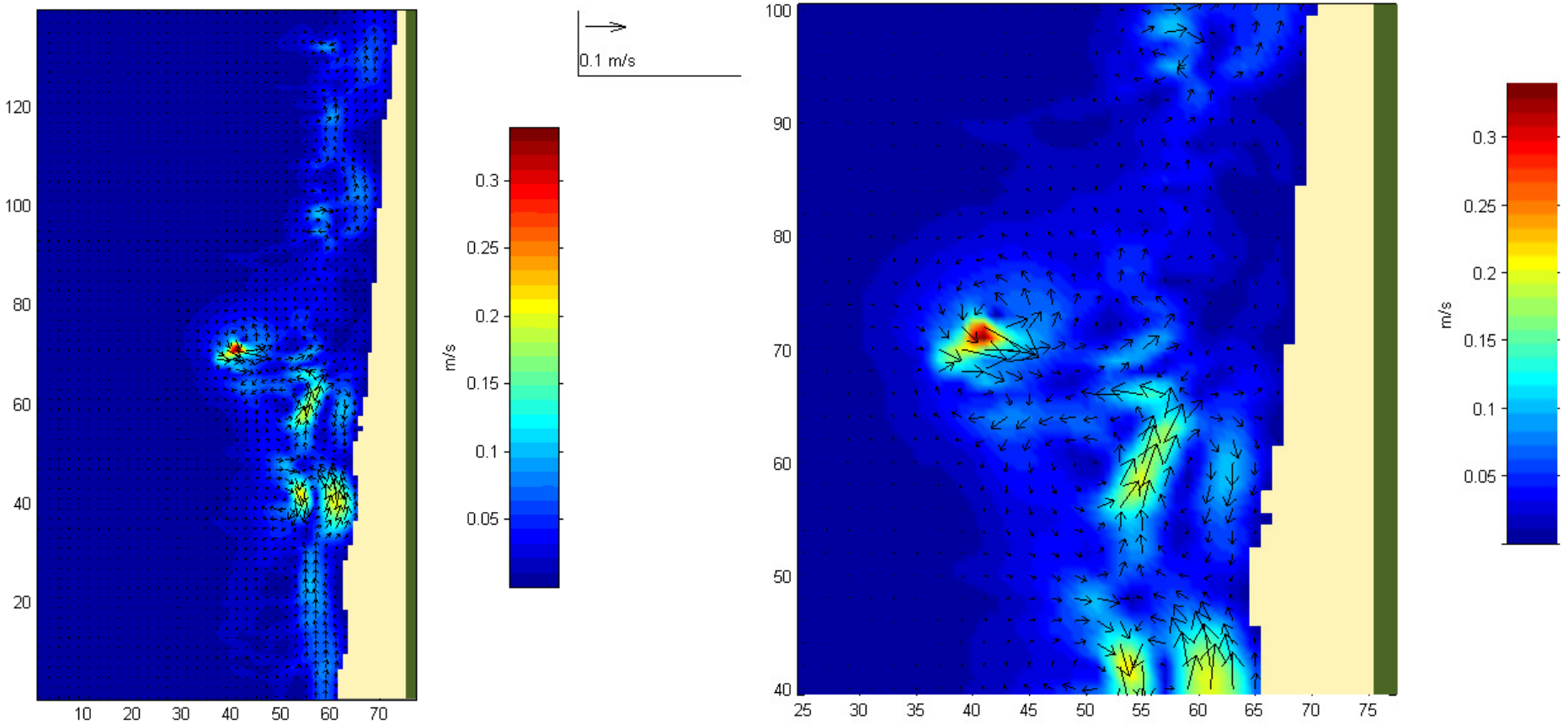

Figure D.2. Predicted hydrodynamic circulation for the wave event H = 1 m and angle = 0° (i.e. shore normal waves). The full domain circulation is shown on the left and a focus on the reef vicinity is shown on the right.

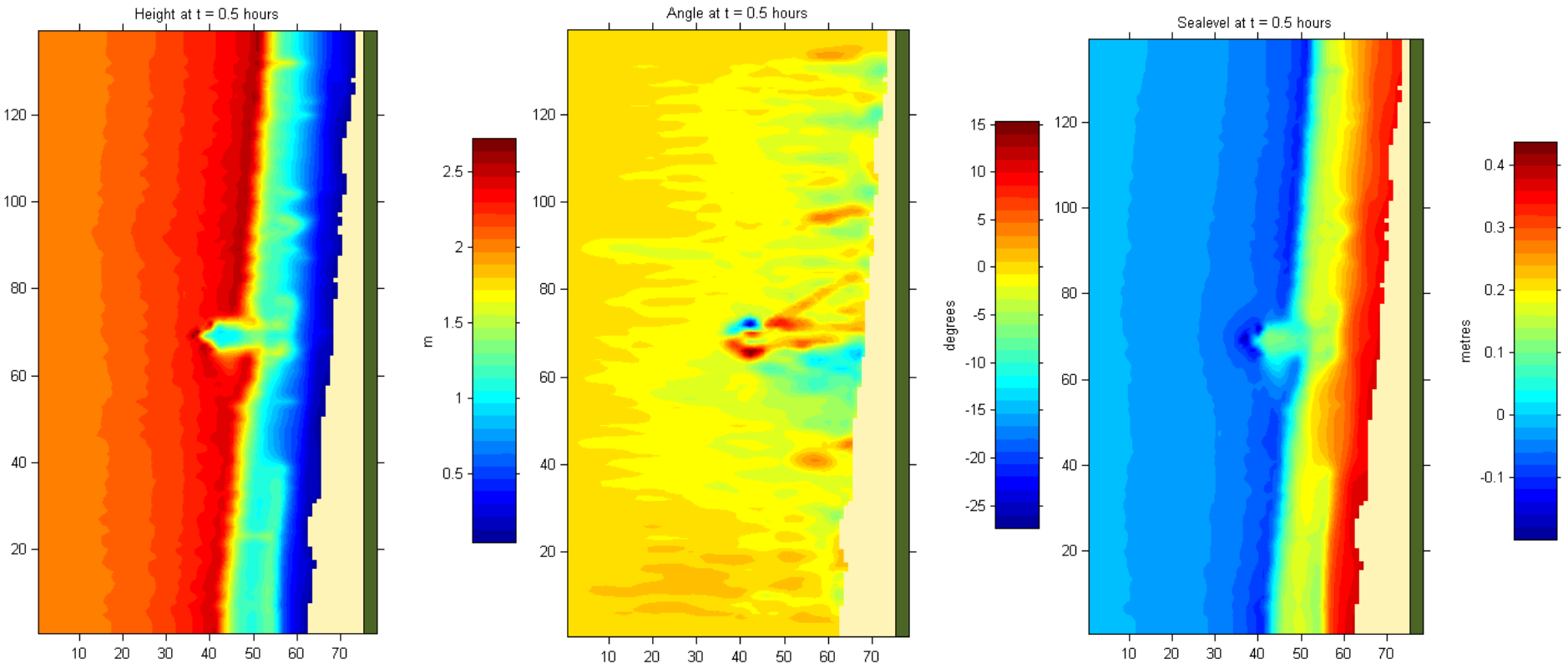

Figure D.3. Predicted wave heights, wave angles, and sea levels for the wave event H = 2 m and angle = 0° (i.e. shore normal waves).

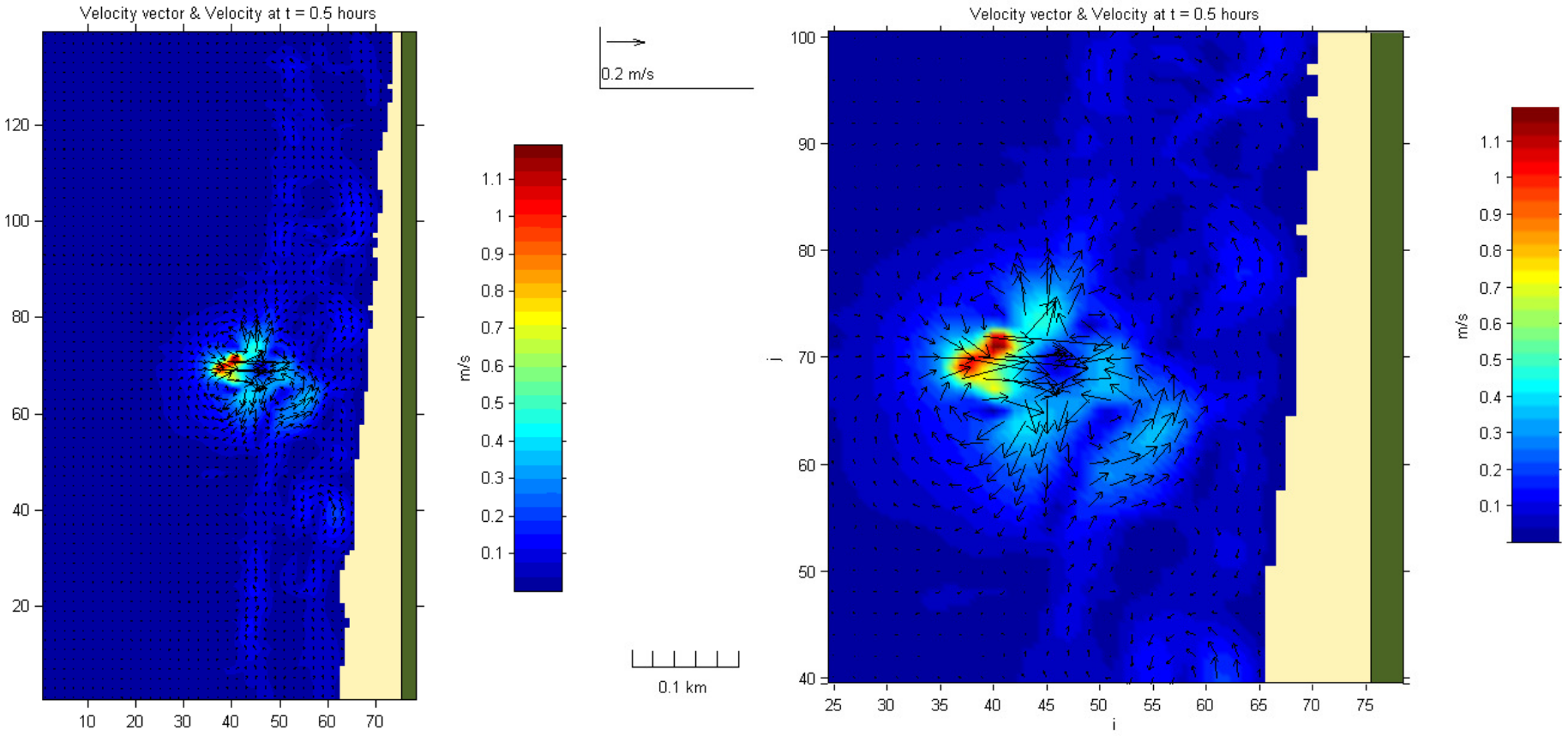

Figure D.4 Predicted hydrodynamic circulation for the wave event H = 2 m and angle = 0°. The full domain circulation is shown on the left and a focus on the reef vicinity is shown on the right.

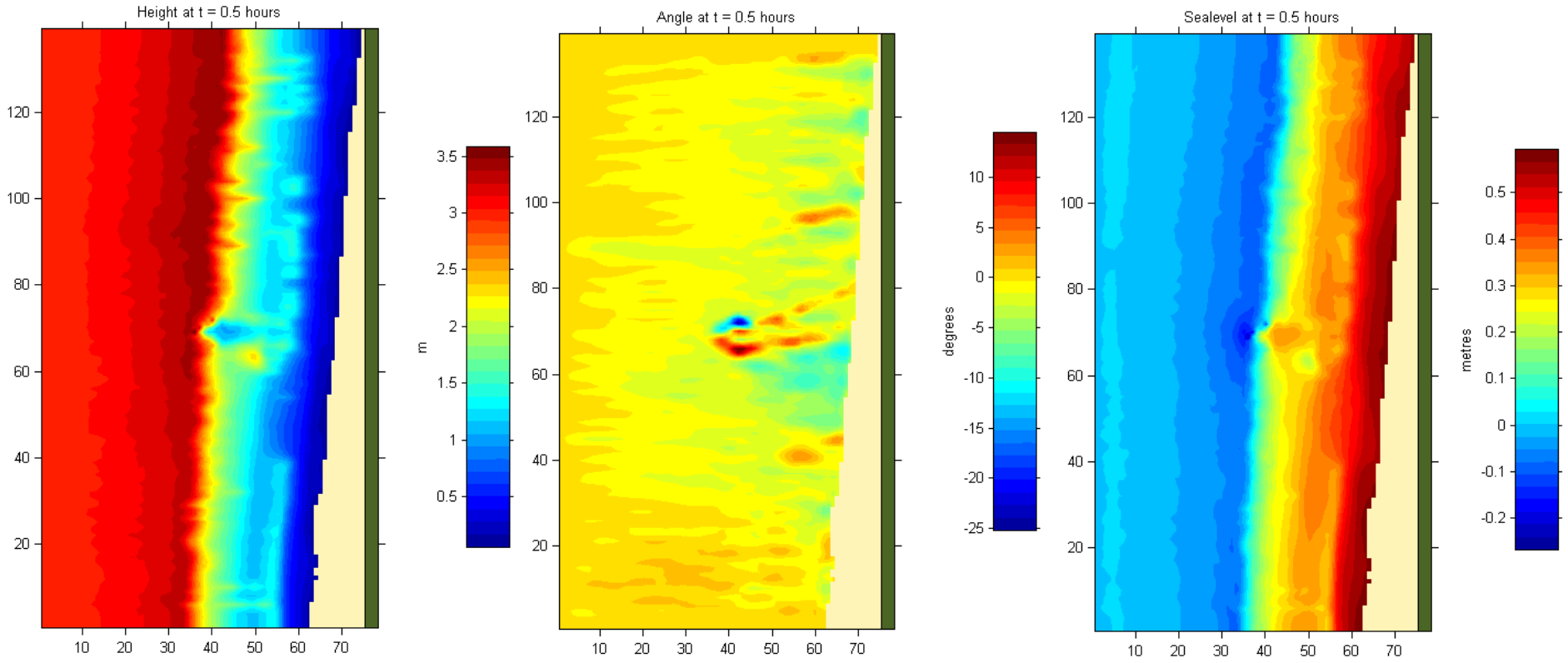

Figure D.5. Predicted wave heights, wave angles, and sea levels for the wave event H = 3 m and angle = 0° (i.e. shore normal waves).

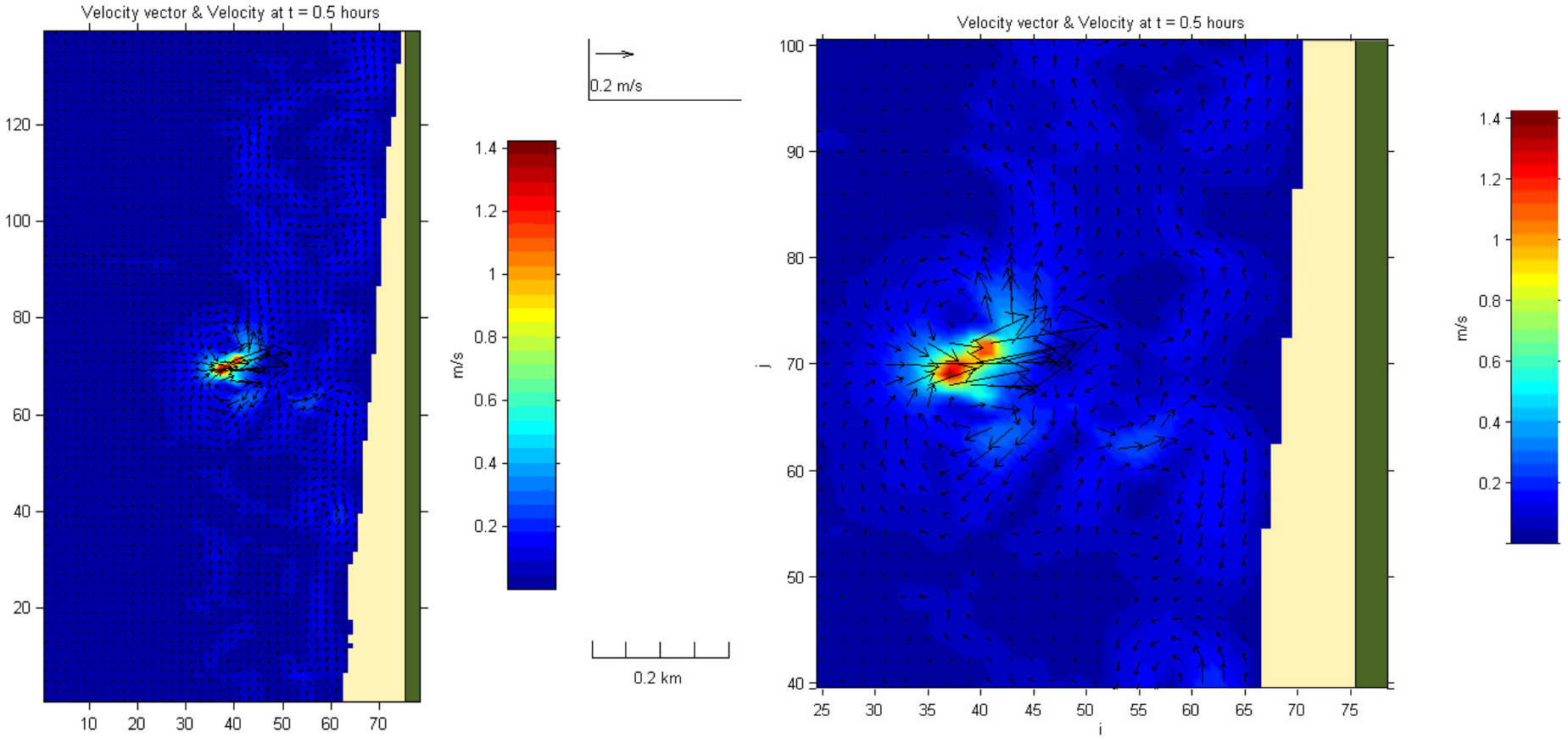

Figure D.6. Predicted hydrodynamic circulation for the wave event H = 3m and angle = 0°. The full domain circulation is shown on the left and a focus on the reef vicinity is shown on the right.

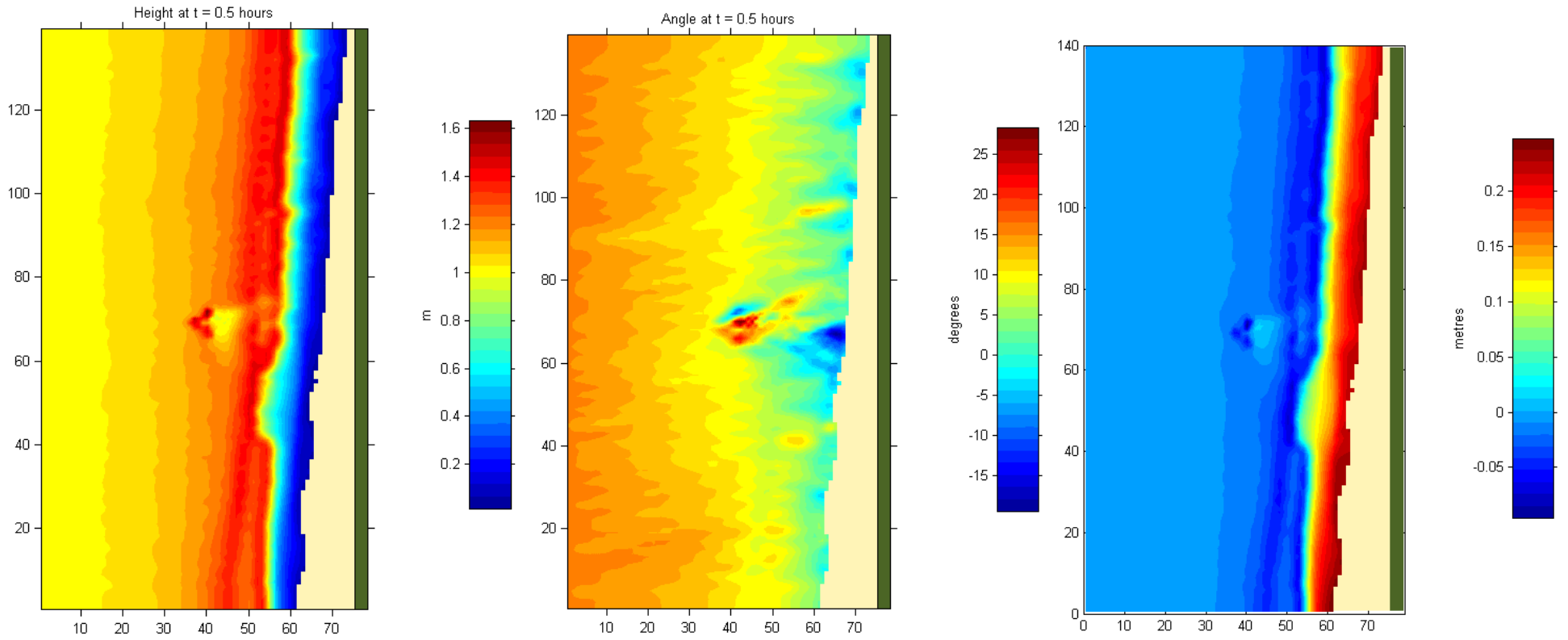

Figure D.7. Predicted wave heights, wave angles and sea levels for the wave event H = 1 m and angle = 15°.

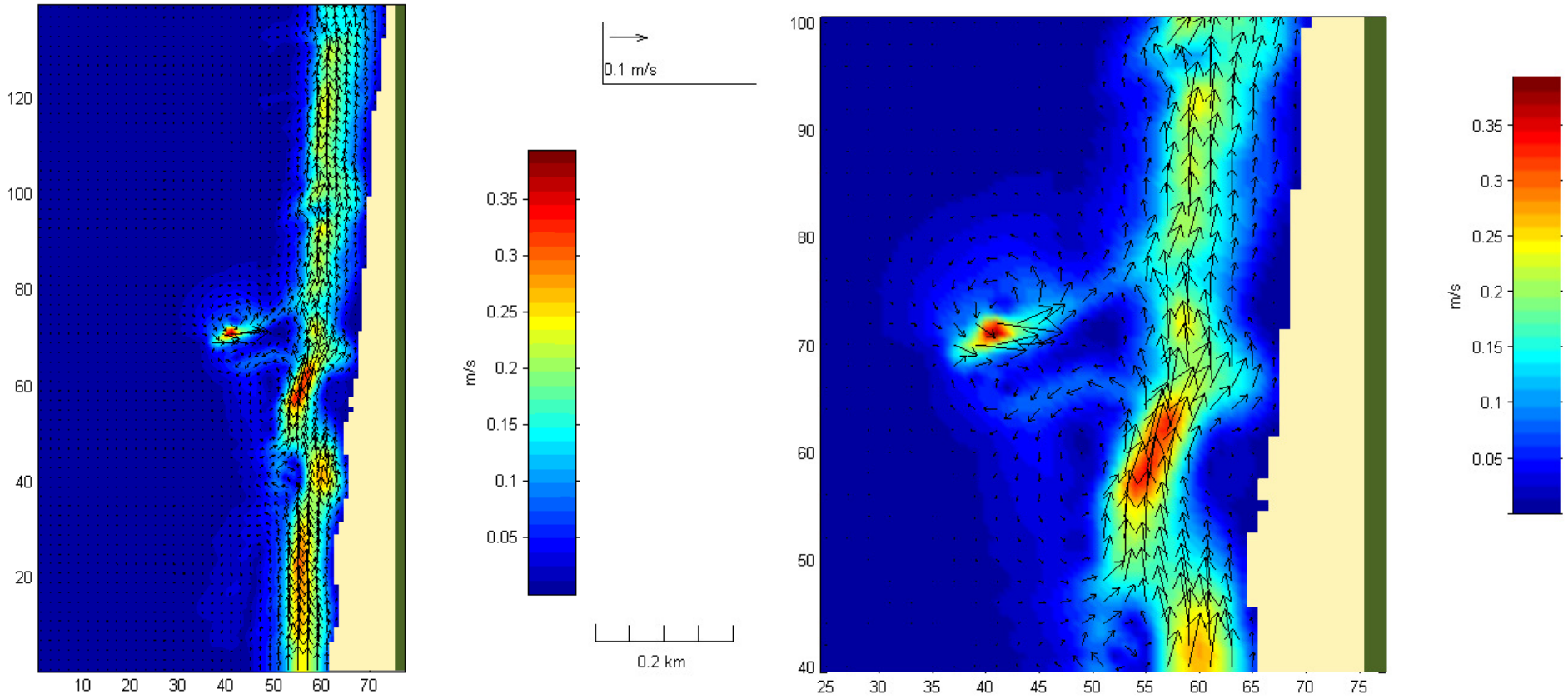

Figure D.8. Predicted hydrodynamic circulation for the wave event H = 1 m and angle = 15°. The full domain circulation is shown on the left and a focus on the reef vicinity is shown on the right.

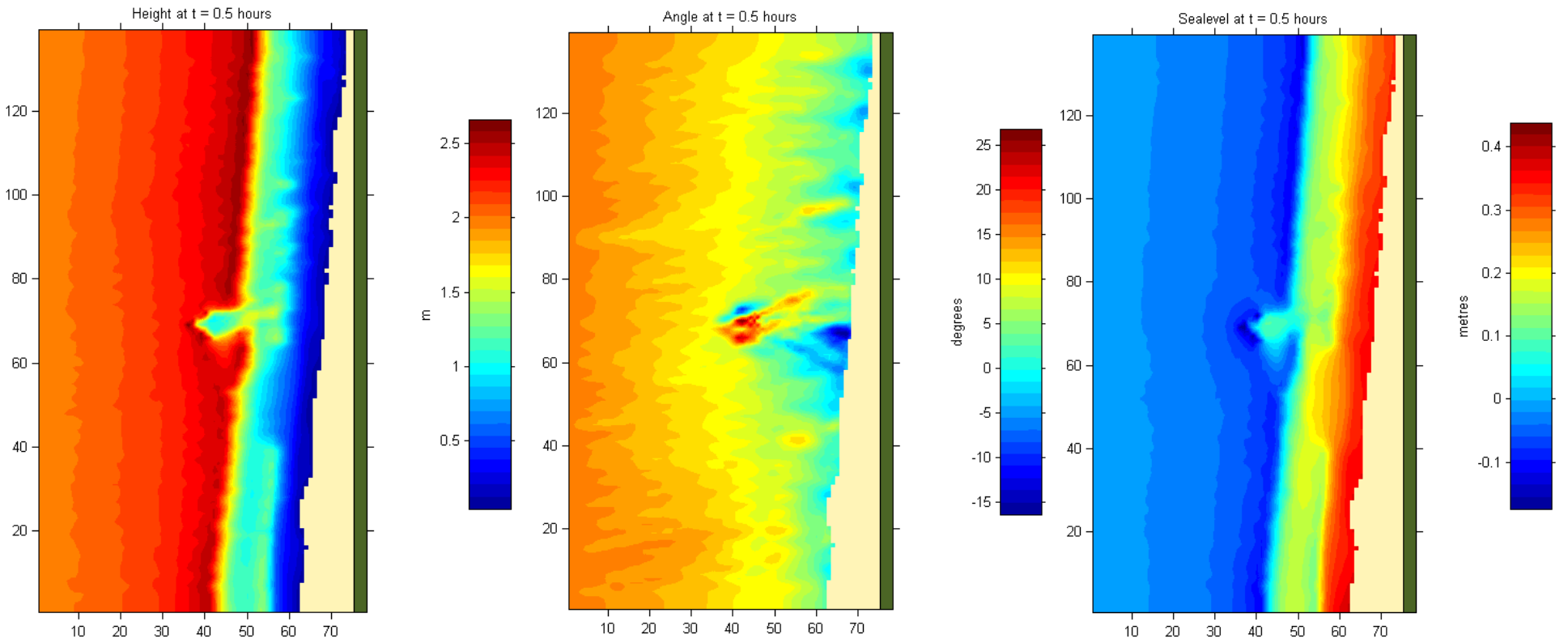

Figure D.9. Predicted wave heights, wave angles and sea levels for the wave event H = 2 m and angle = 15°.

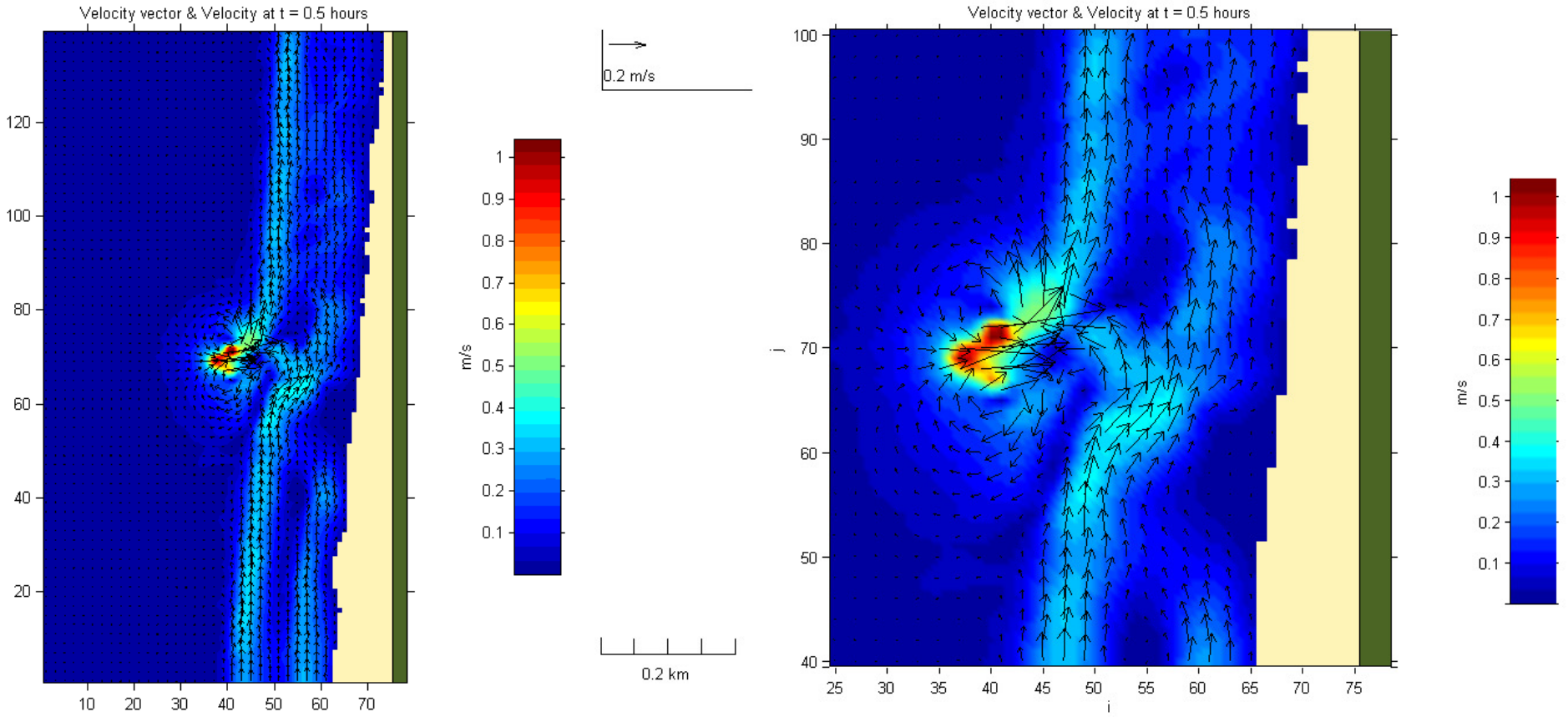

Figure D.10. Predicted hydrodynamic circulation for the wave event H = 2 m and angle = 15°. The full domain circulation is shown on the left and a focus on the reef vicinity is shown on the right.

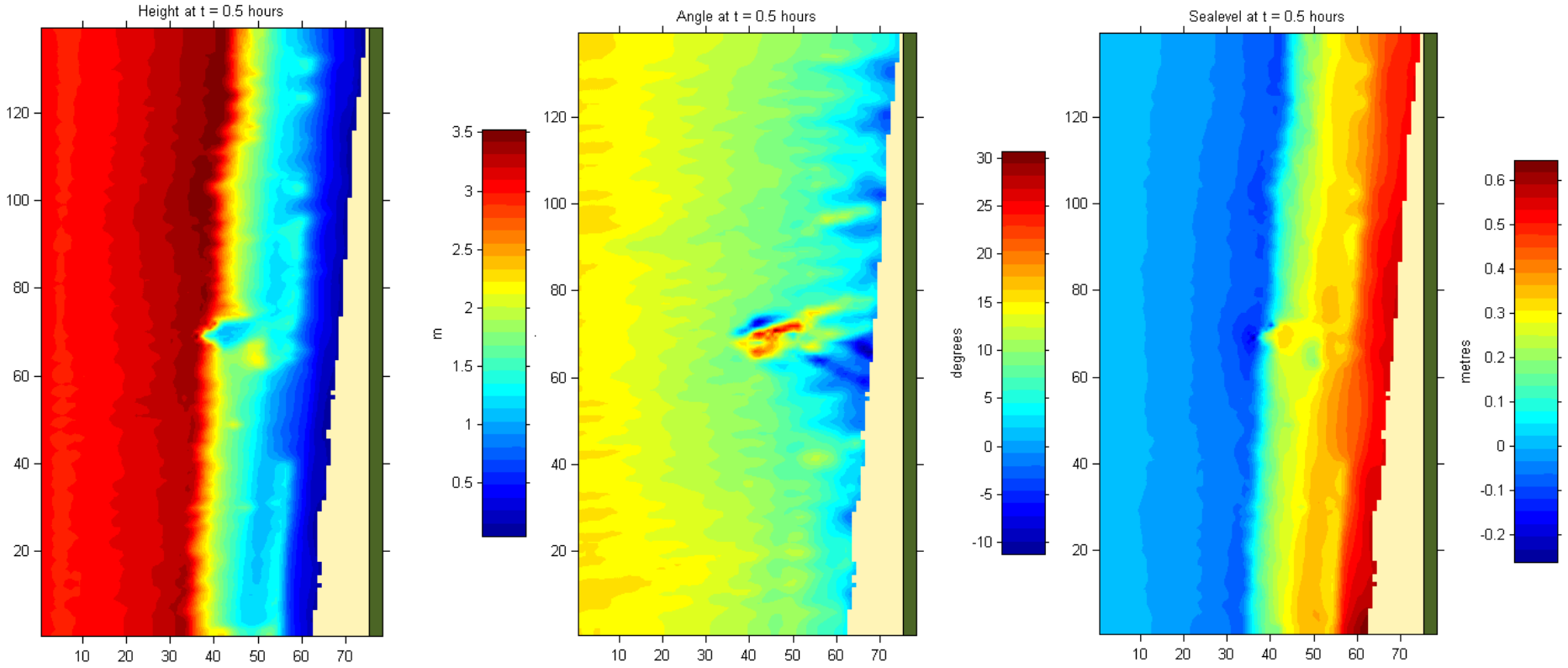

Figure D.11. Predicted wave heights, wave angles and sea levels for the wave event H = 3 m and angle = 15°.

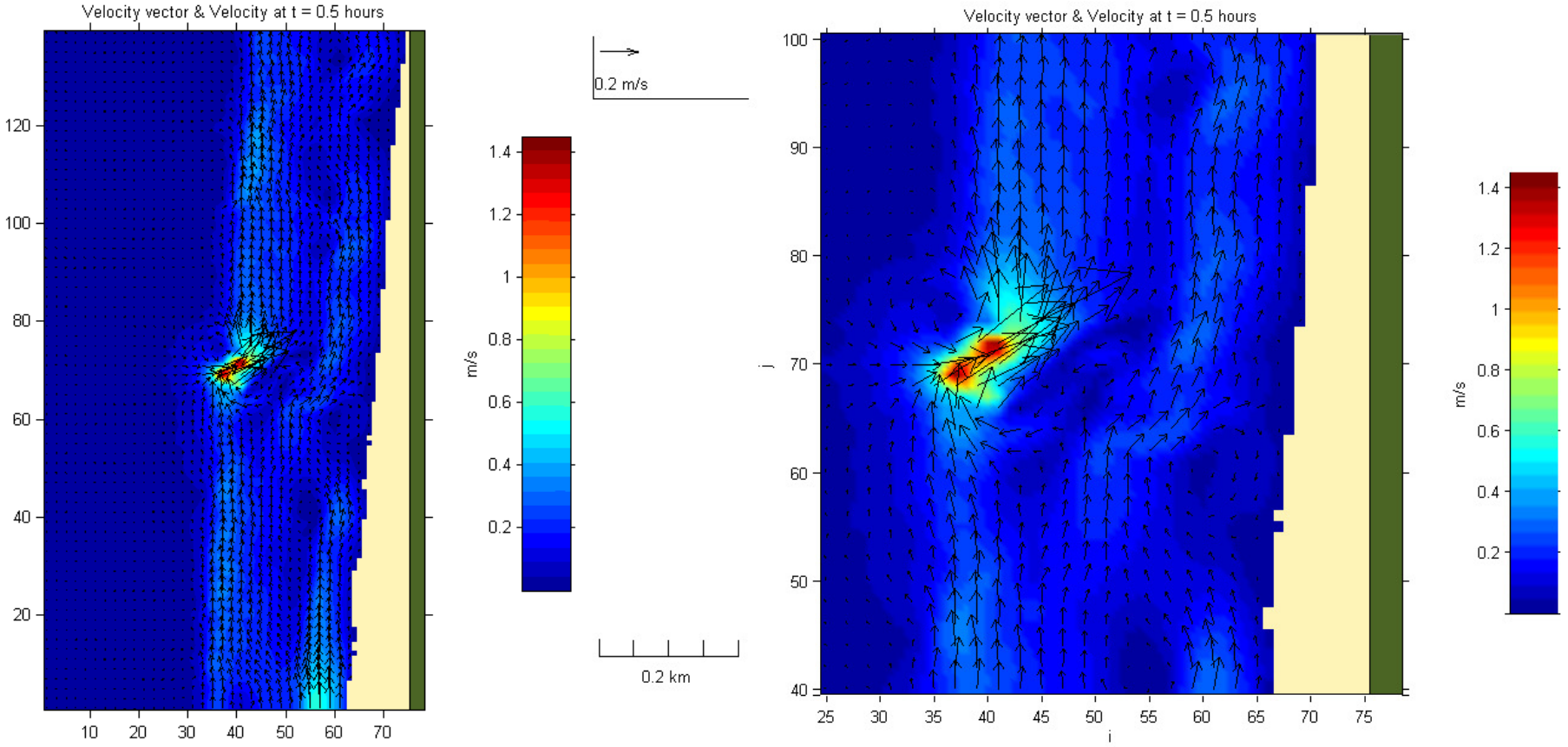

Figure D.12 Predicted hydrodynamic circulation for the wave event H = 3 m and angle = 15°. The full domain circulation is shown on the left and a focus on the reef vicinity is shown on the right.

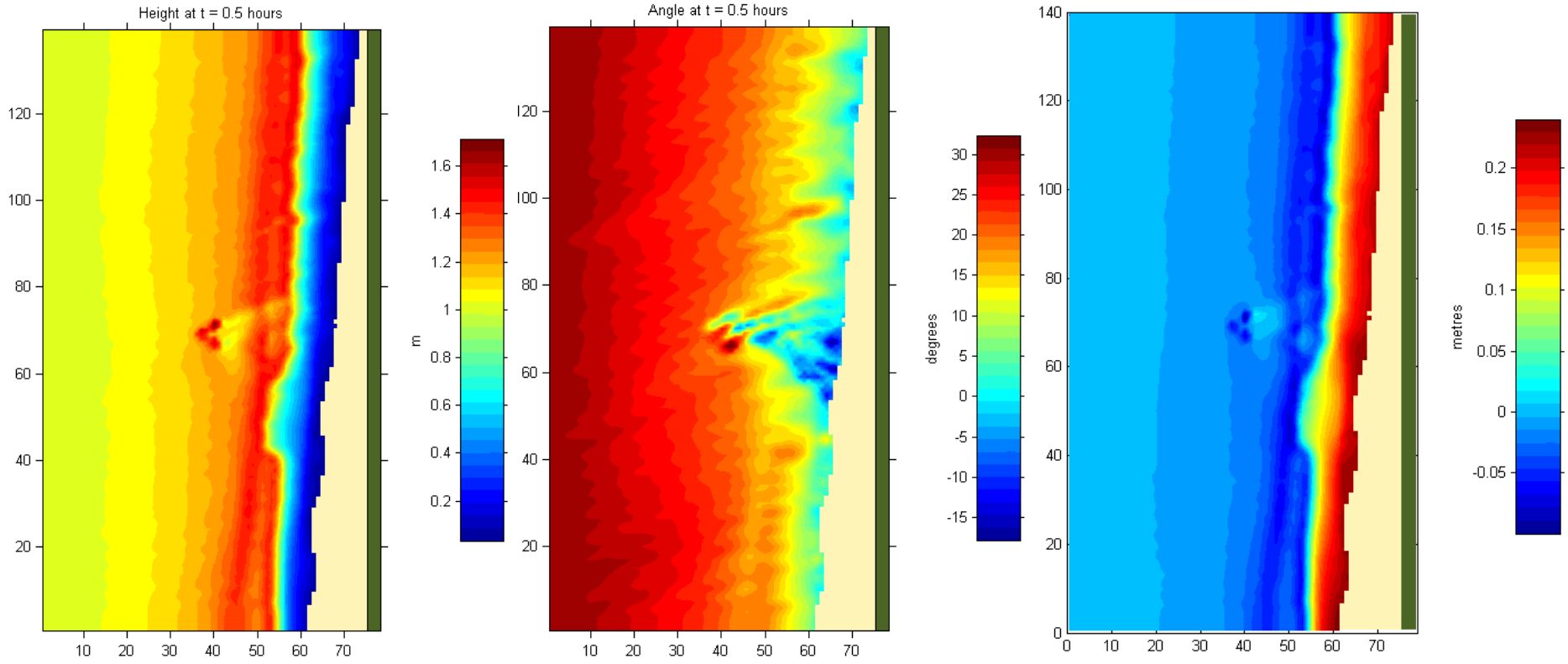

Figure D.13 Predicted wave heights, wave angles and sea levels for the wave event H = 1m and angle = 30°.

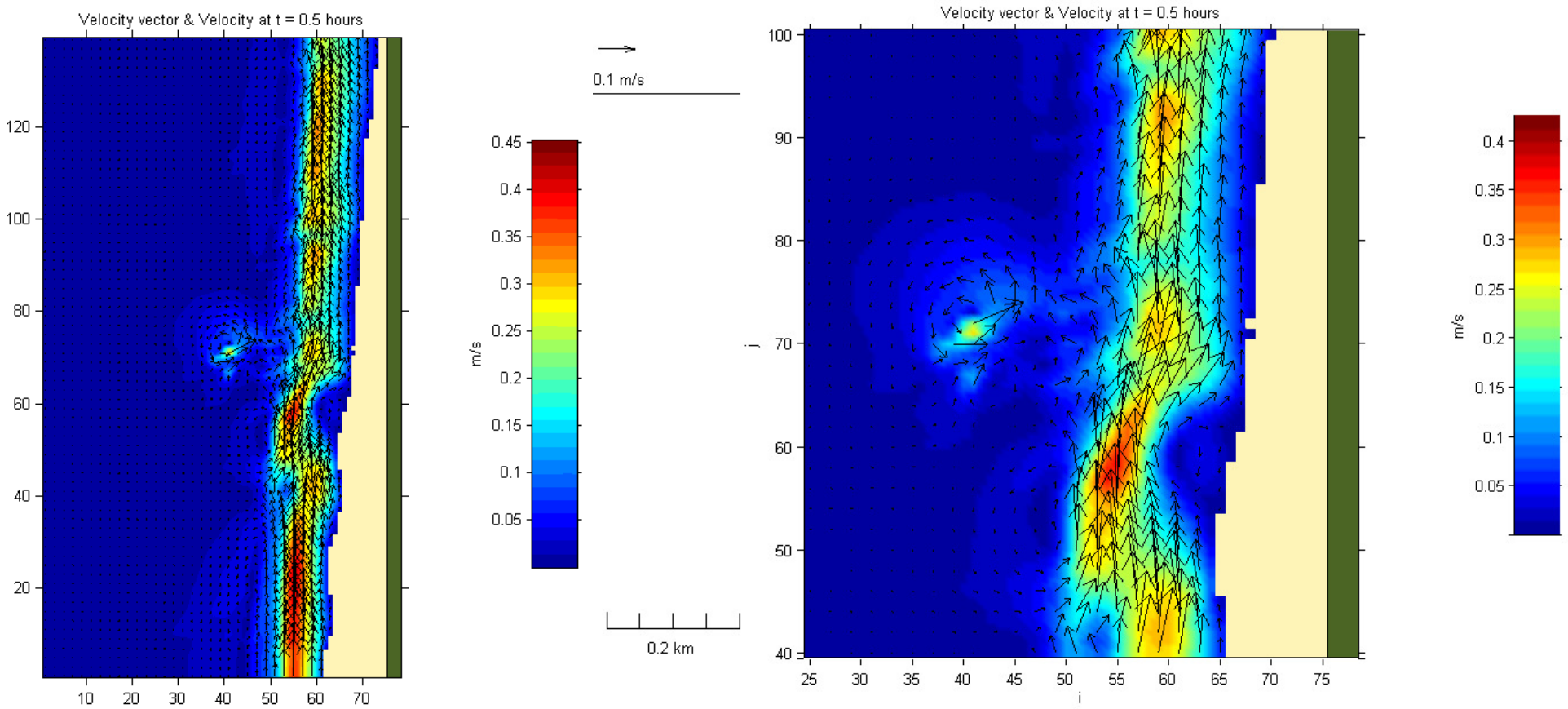

Figure D.14. Predicted hydrodynamic circulation for the wave event H = 1 m and angle = 30°. The full domain circulation is shown on the left and a focus on the reef vicinity is shown on the right.

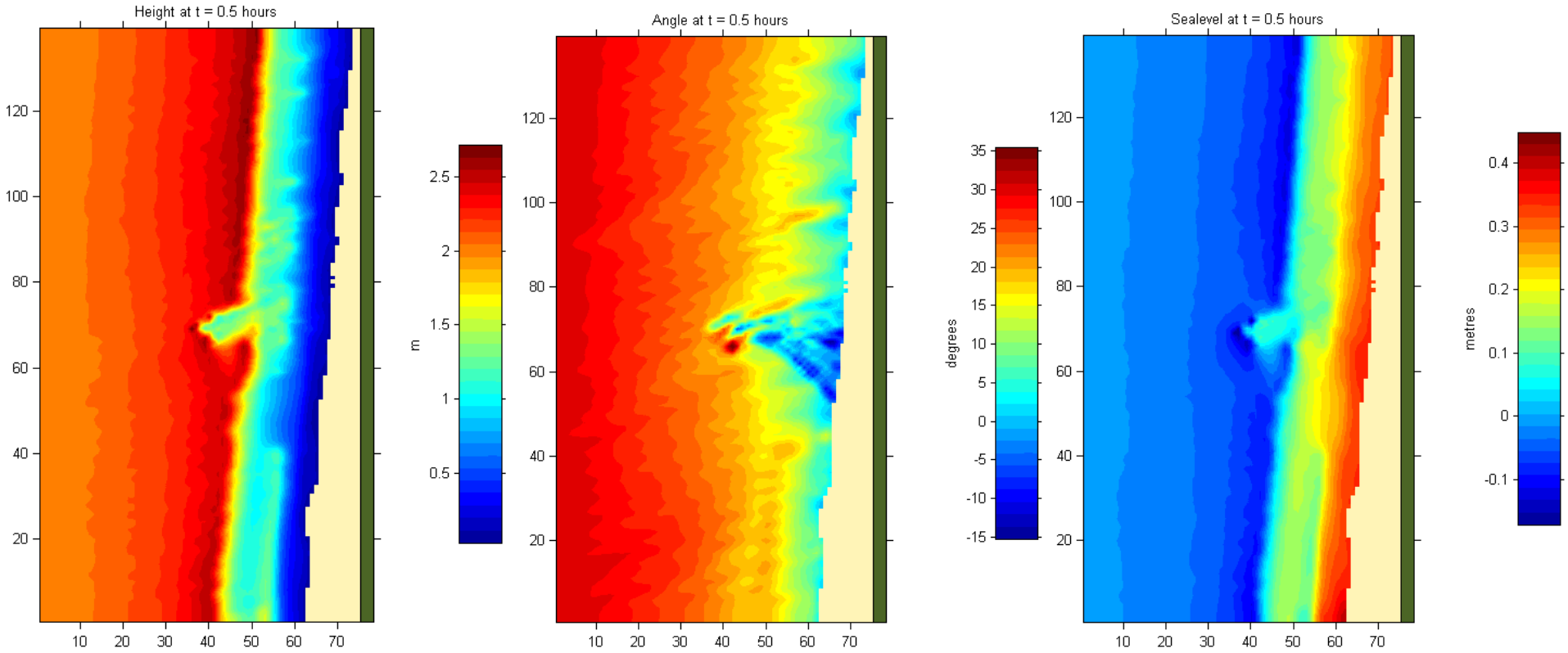

Figure D.15. Predicted wave heights, wave angles and sea levels for the wave event H = 2 m and angle = 30°.

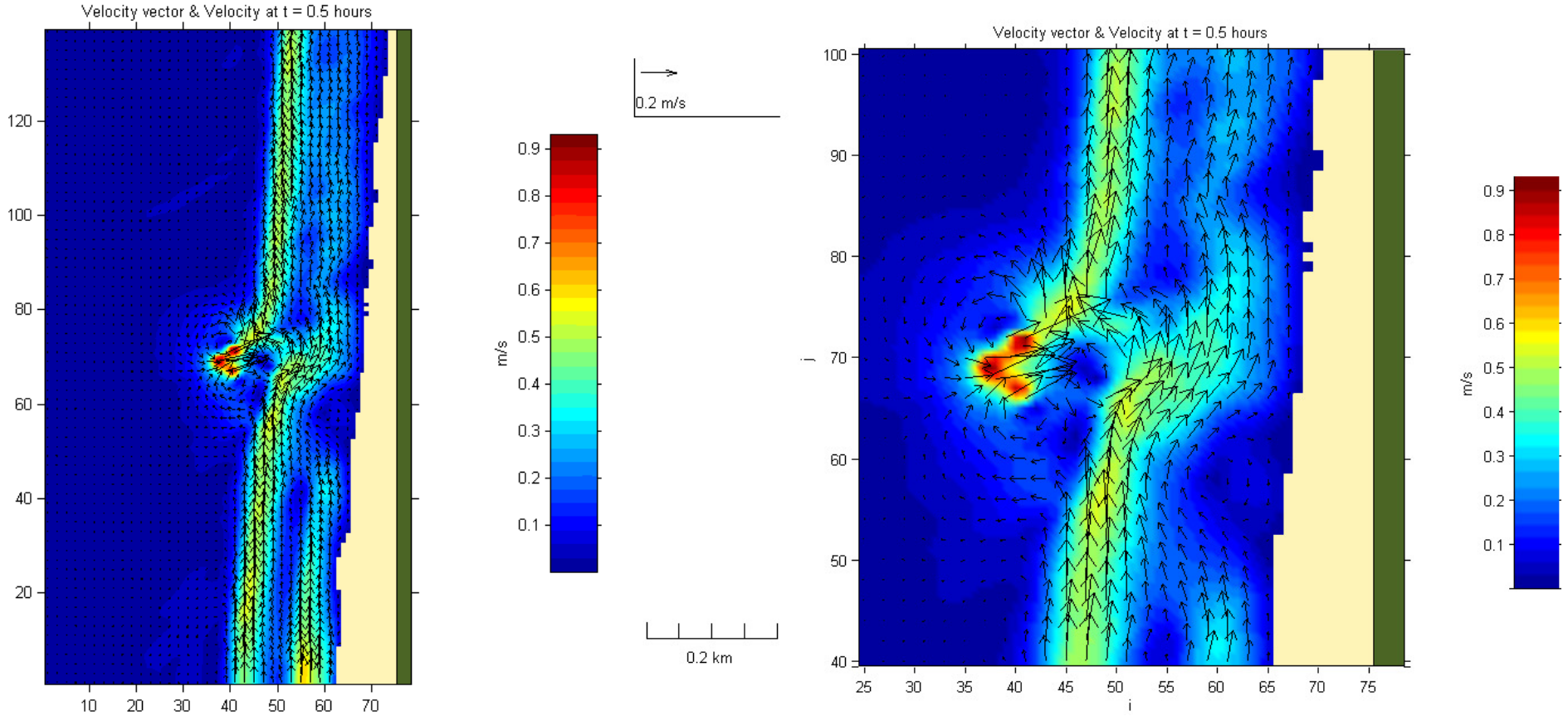

Figure D.16 Predicted hydrodynamic circulation for the wave event H = 2 m and angle = 30°. The full domain circulation is shown on the left and a focus on the reef vicinity is shown on the right.

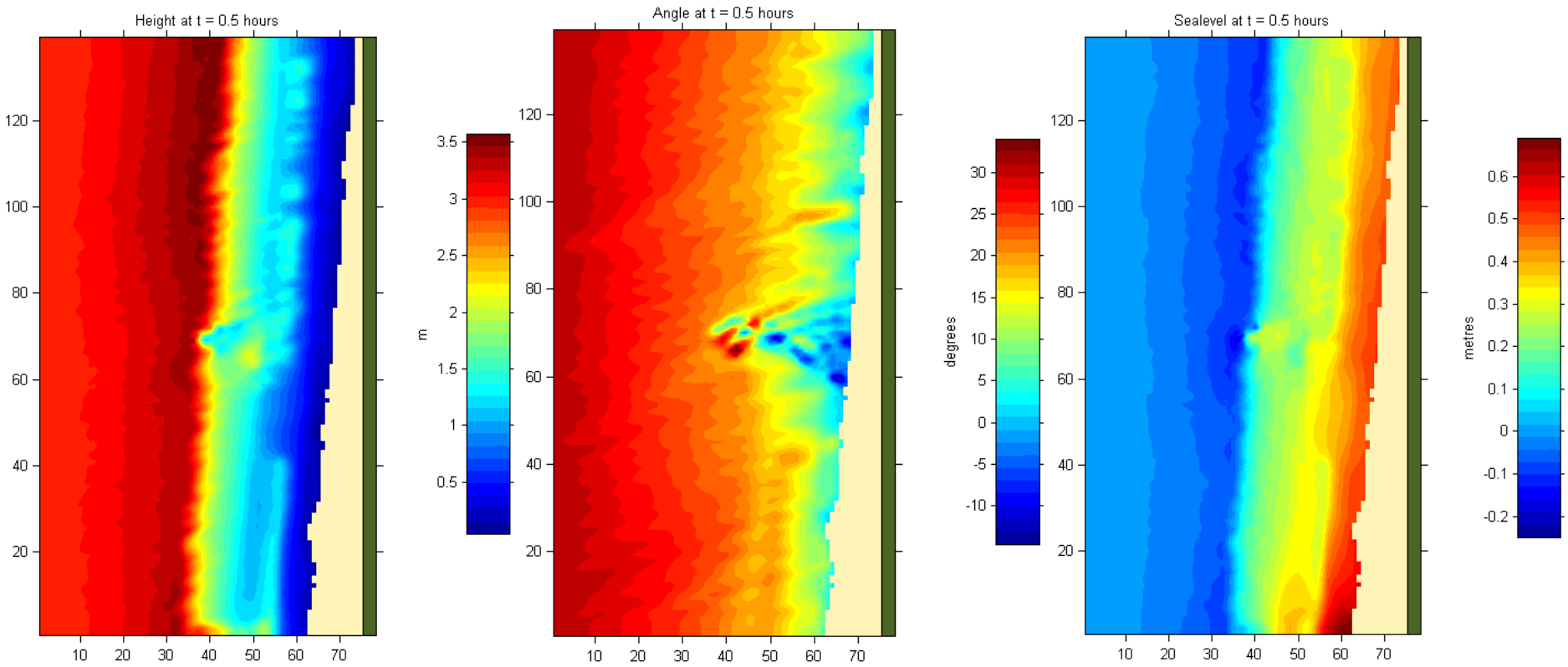

Figure D.17. Predicted wave heights, wave angles and sea levels for the wave event H = 3m and angle = 30°.

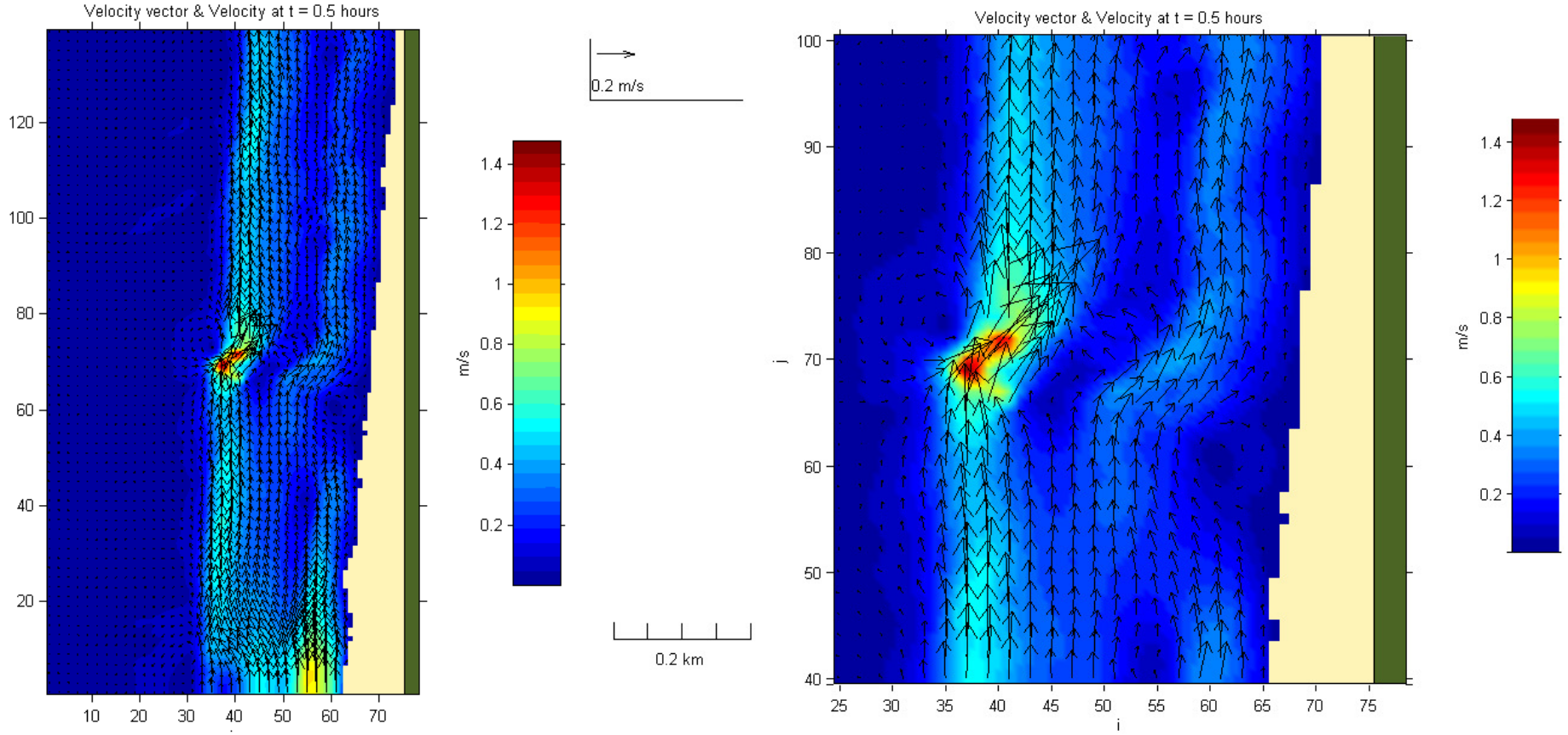

Figure D.18. Predicted hydrodynamic circulation for the wave event H = 3 m and angle = 30°. The full domain circulation is shown on the left and a focus on the reef vicinity is shown on the right.

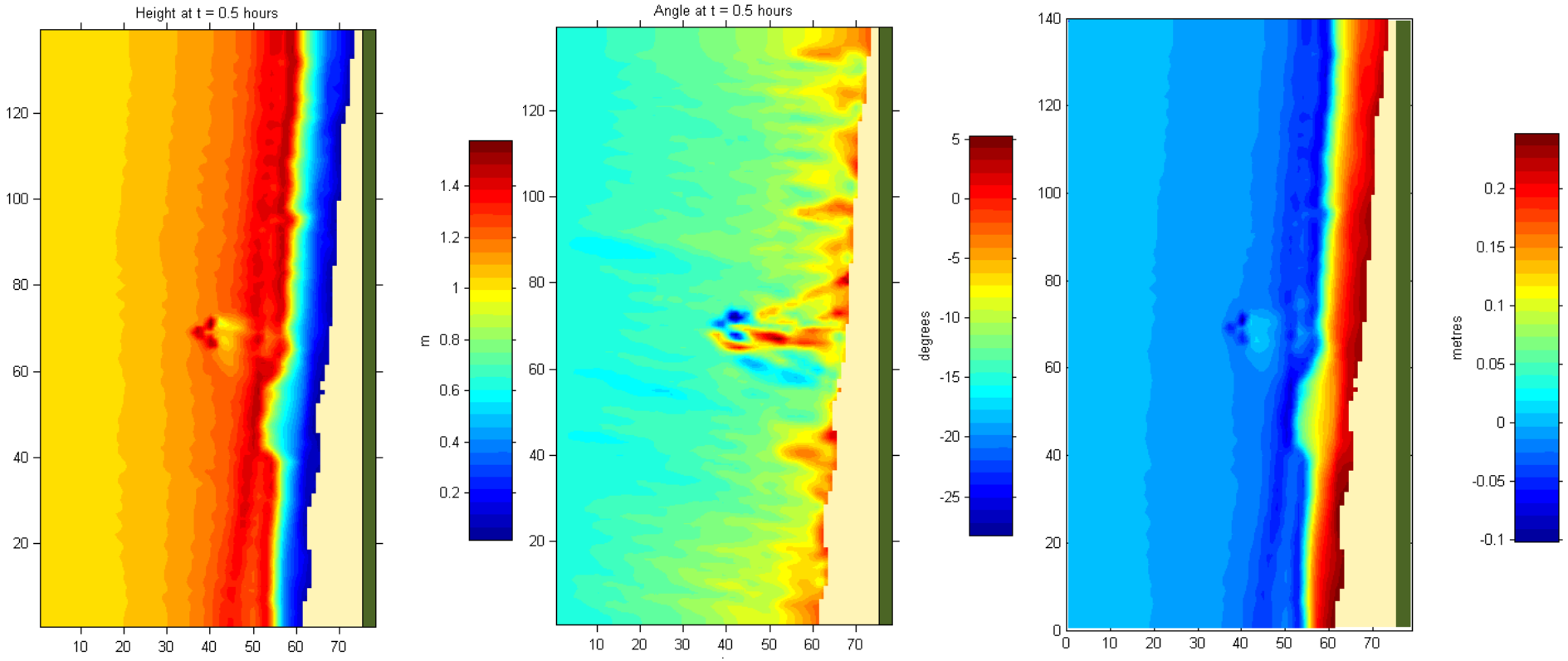

Figure D.19. Predicted wave heights, wave angles and sea levels for the wave event H = 1m and angle = -15°.

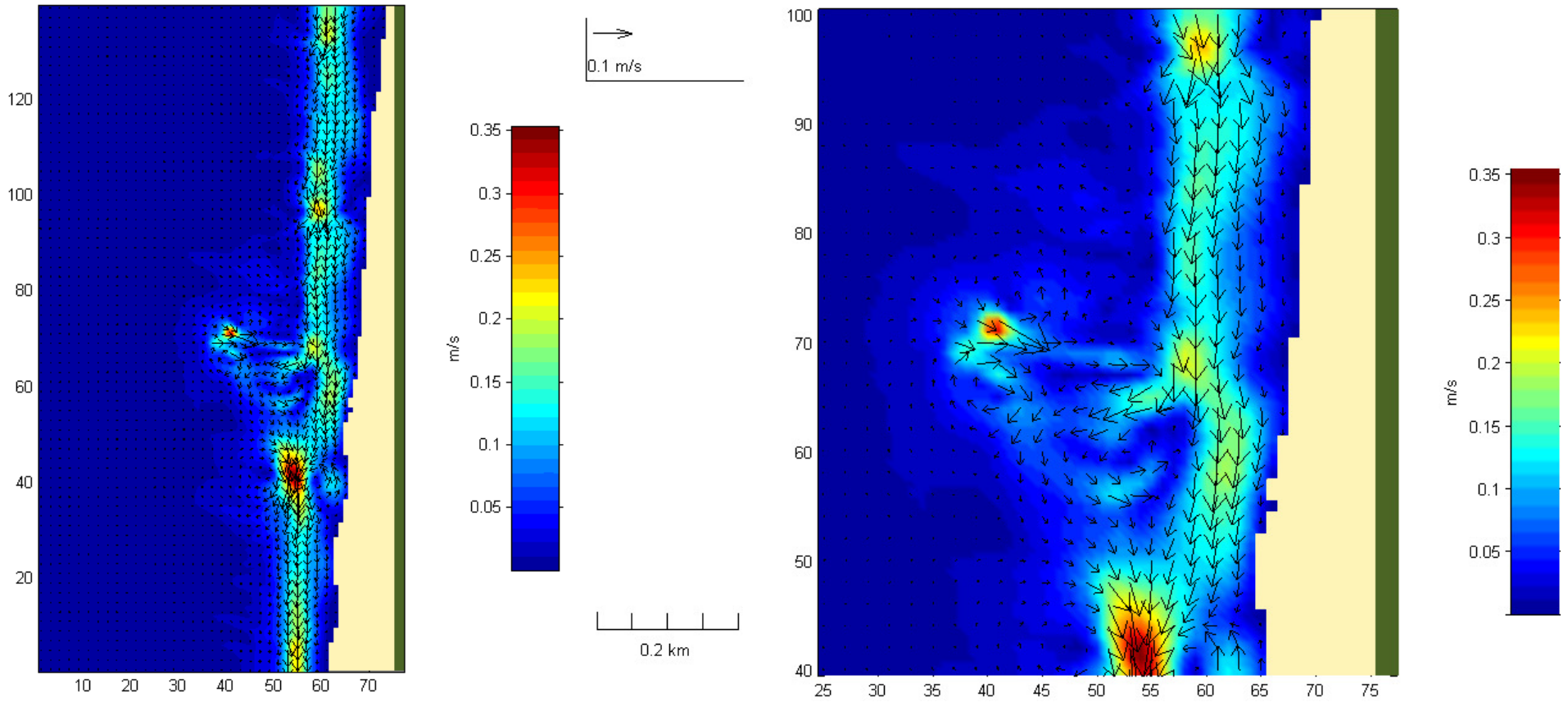

Figure D.20. Predicted hydrodynamic circulation for the wave event H = 1 m and angle =- 15°. The full domain circulation is shown on the left and a focus on the reef vicinity is shown on the right.

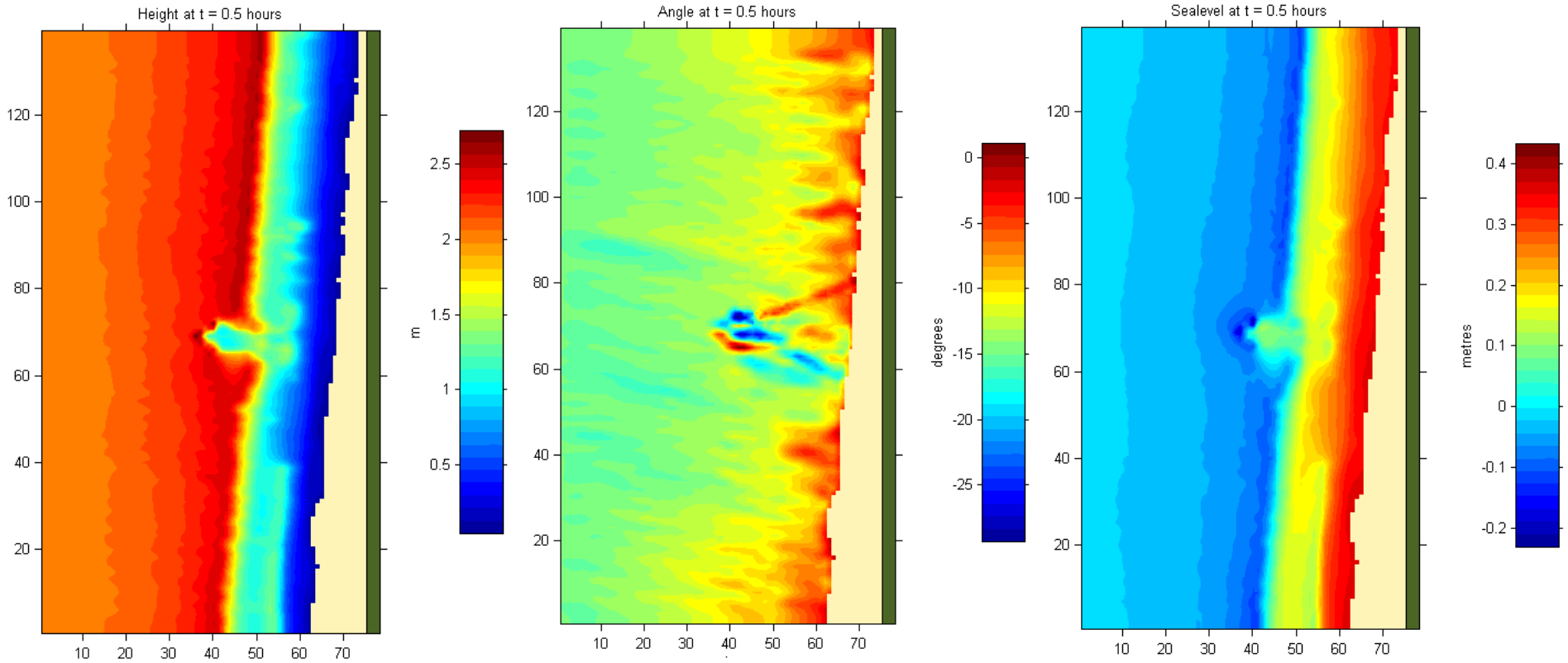

Figure D.21. Predicted wave heights, wave angles and sea levels for the wave event H = 2m and angle = -15°.

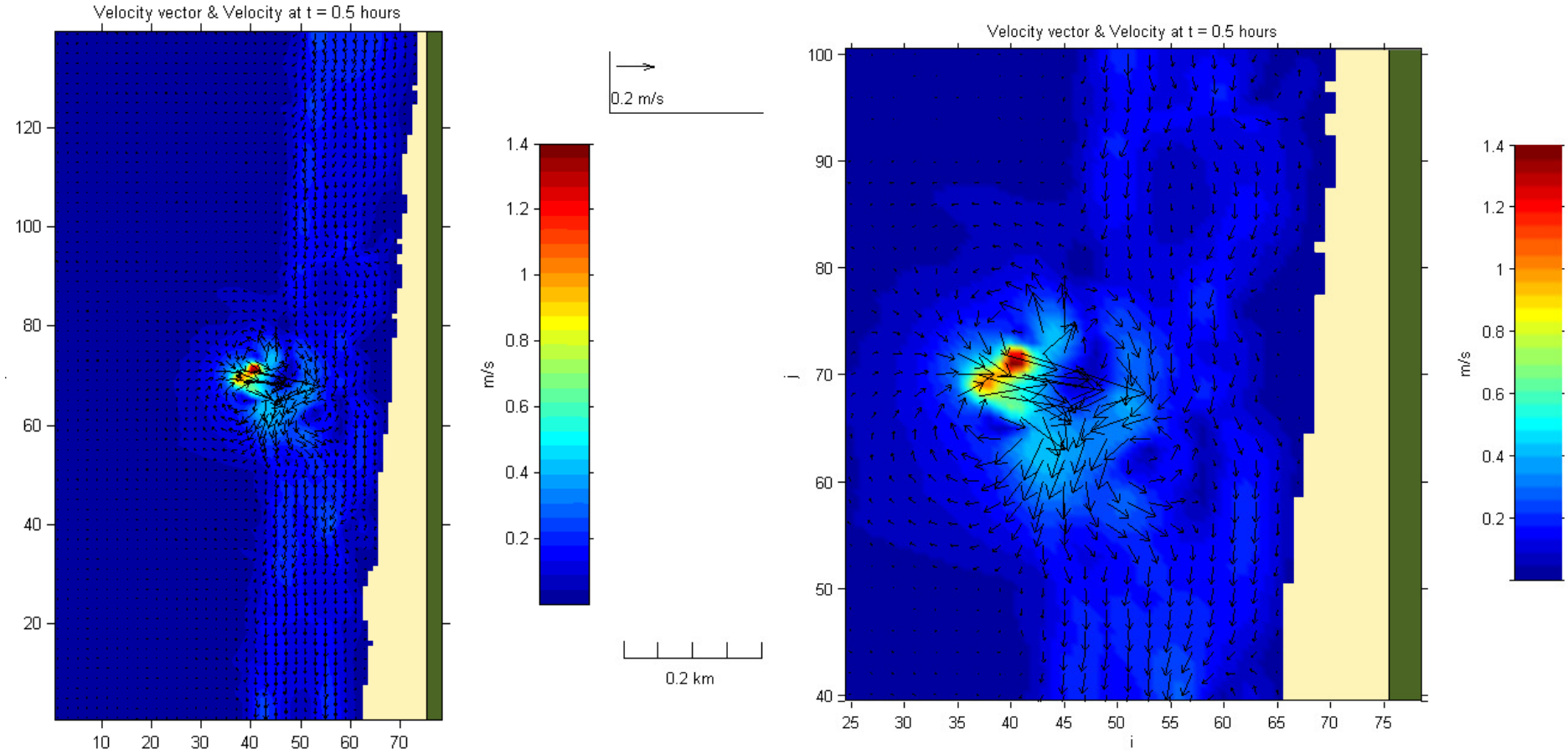

Figure D.22. Predicted hydrodynamic circulation for the wave event H = 2 m and angle = -15°. The full domain circulation is shown on the left and a focus on the reef vicinity is shown on the right.

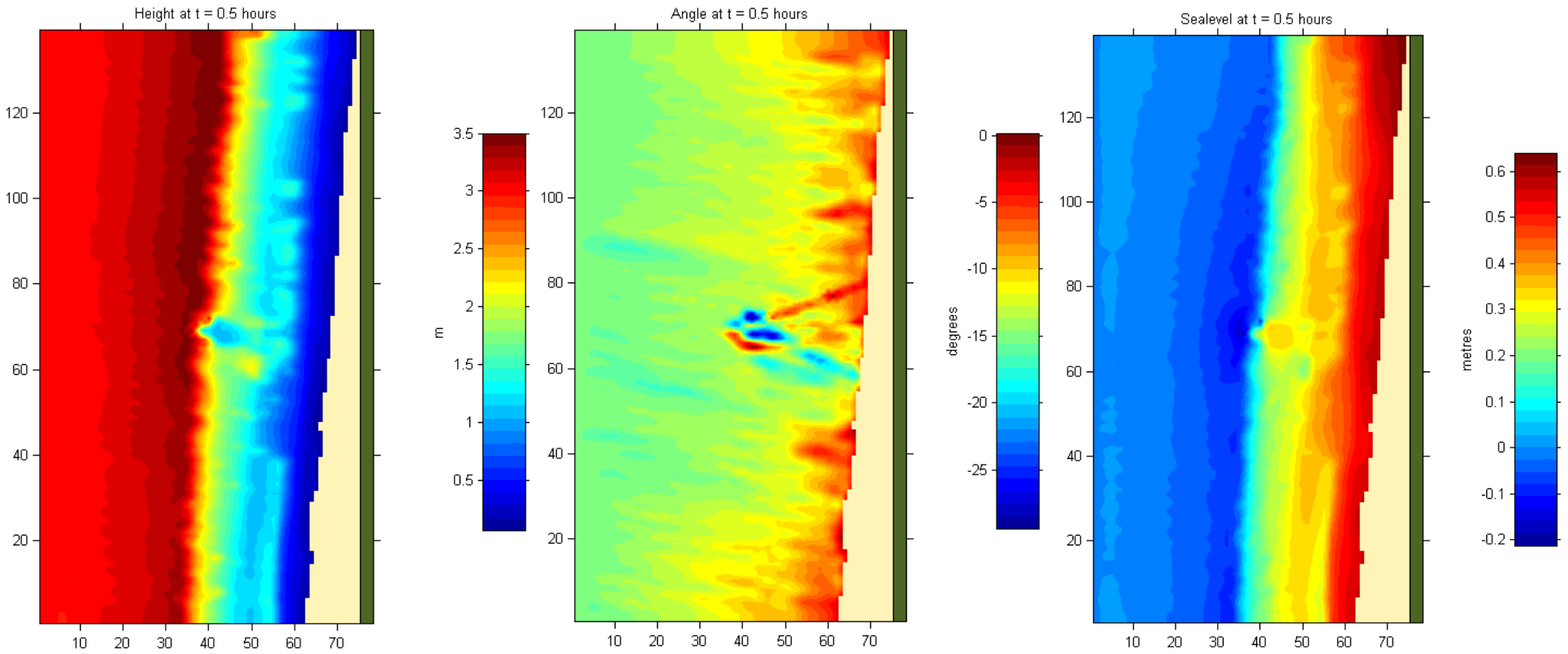

Figure D.23. Predicted wave heights, wave angles and sea levels for the wave event H = 3m and angle = -15°.

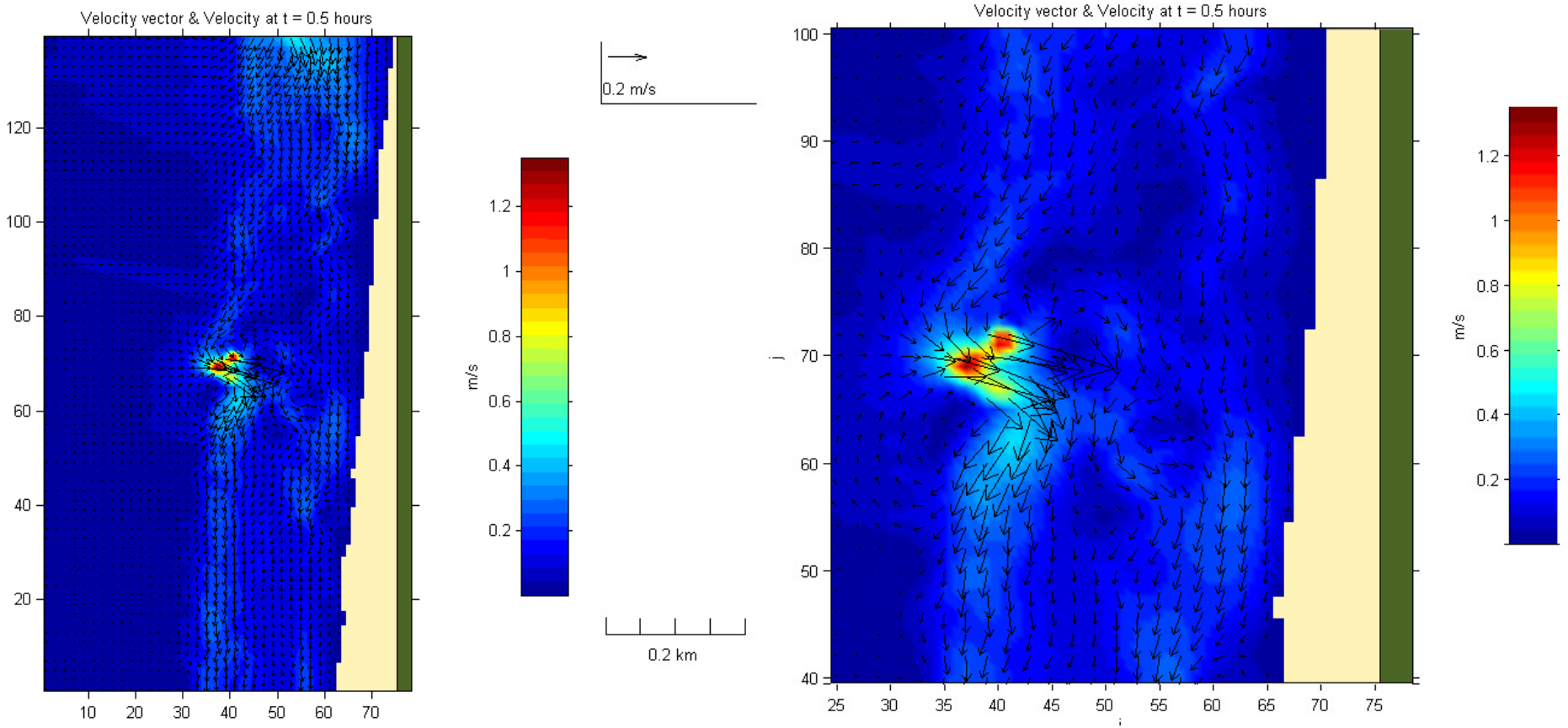

Figure D.24. Predicted hydrodynamic circulation for the wave event H = 3 m and angle = -15°. The full domain circulation is shown on the left and a focus on the reef vicinity is shown on the right.

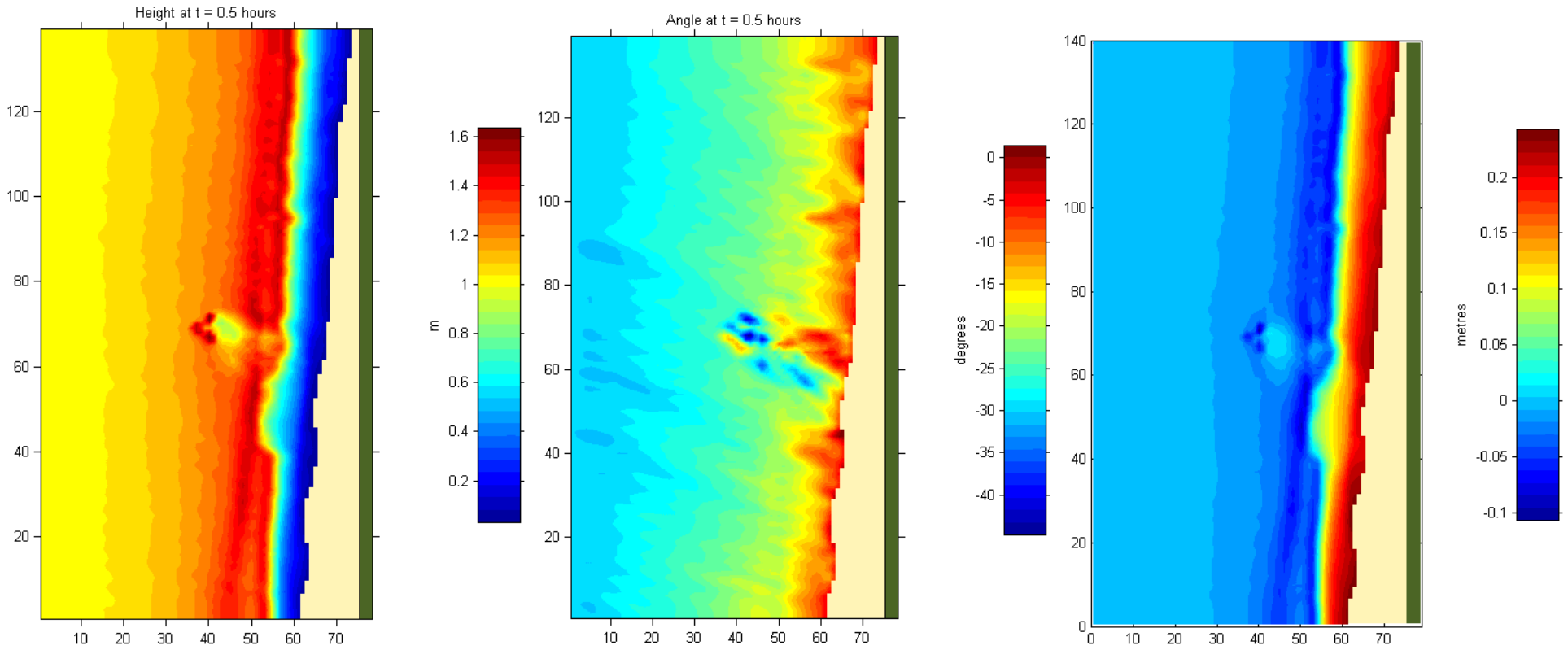

Figure D.25. Predicted wave heights, wave angles and sea levels for the wave event H = 1m and angle = -30°.

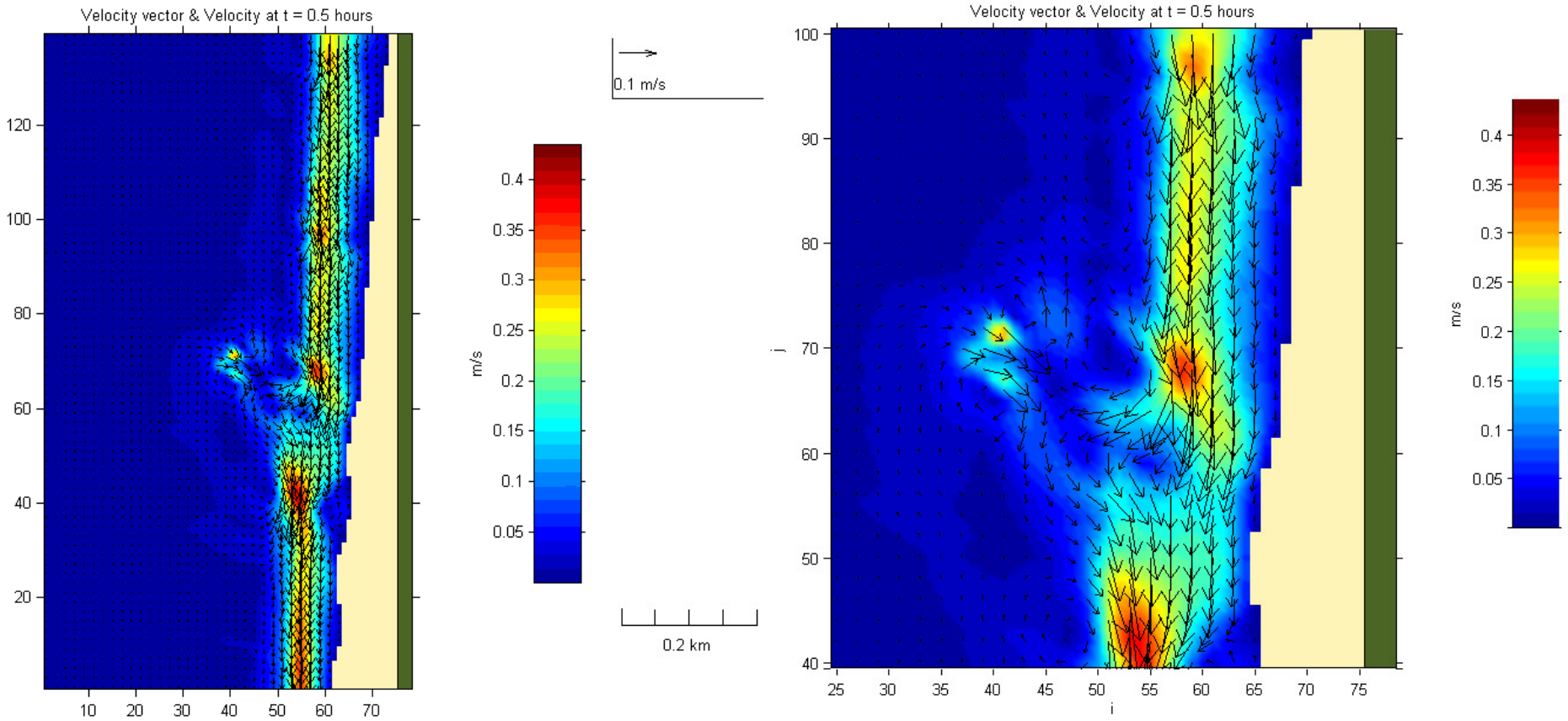

Figure D.26. Predicted hydrodynamic circulation for the wave event H = 1 m and angle = -30°. The full domain circulation is shown on the left and a focus on the reef vicinity is shown on the right.

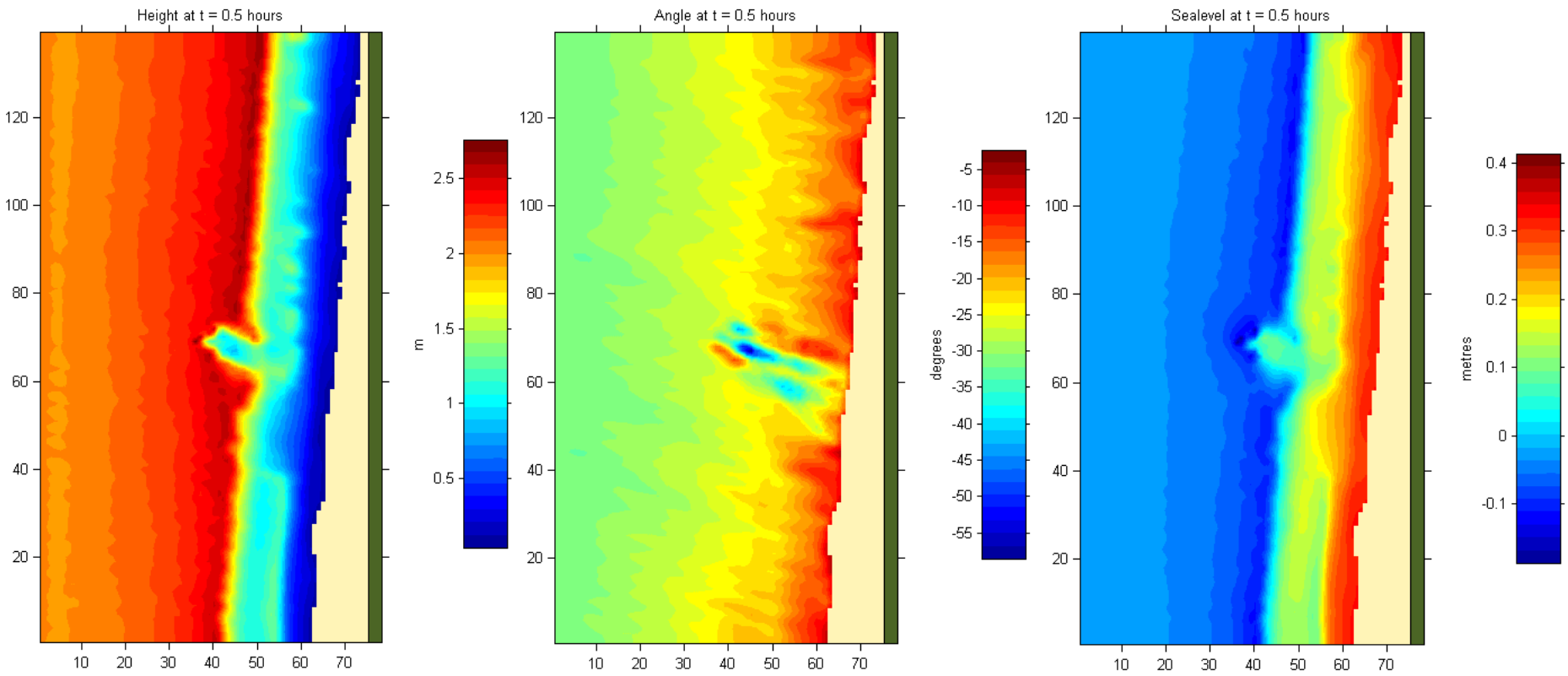

Figure D.27. Predicted wave heights, wave angles and sea levels for the wave event H = 2m and angle = -30°.

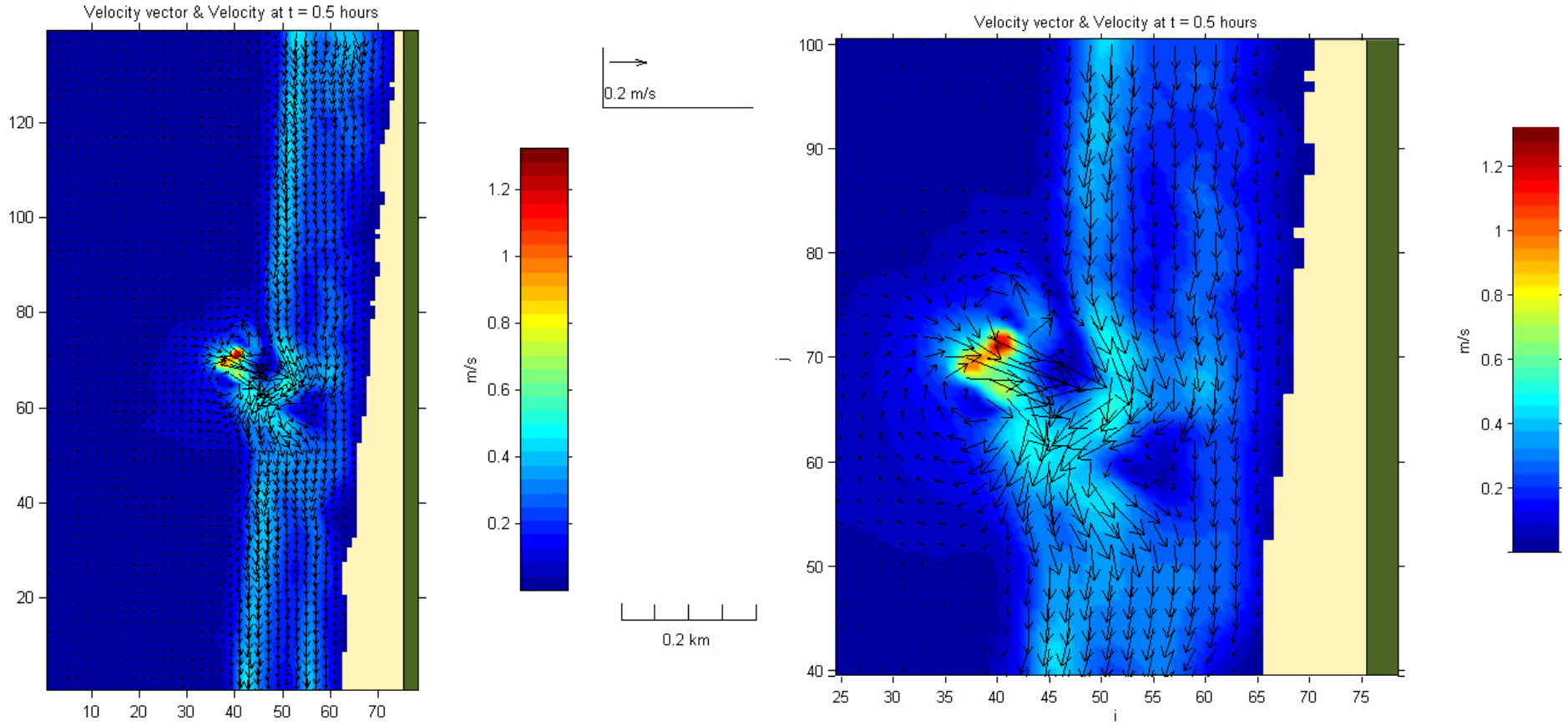

Figure D.28. Predicted hydrodynamic circulation for the wave event H = 2 m and angle = -30°. The full domain circulation is shown on the left and a focus on the reef vicinity is shown on the right.

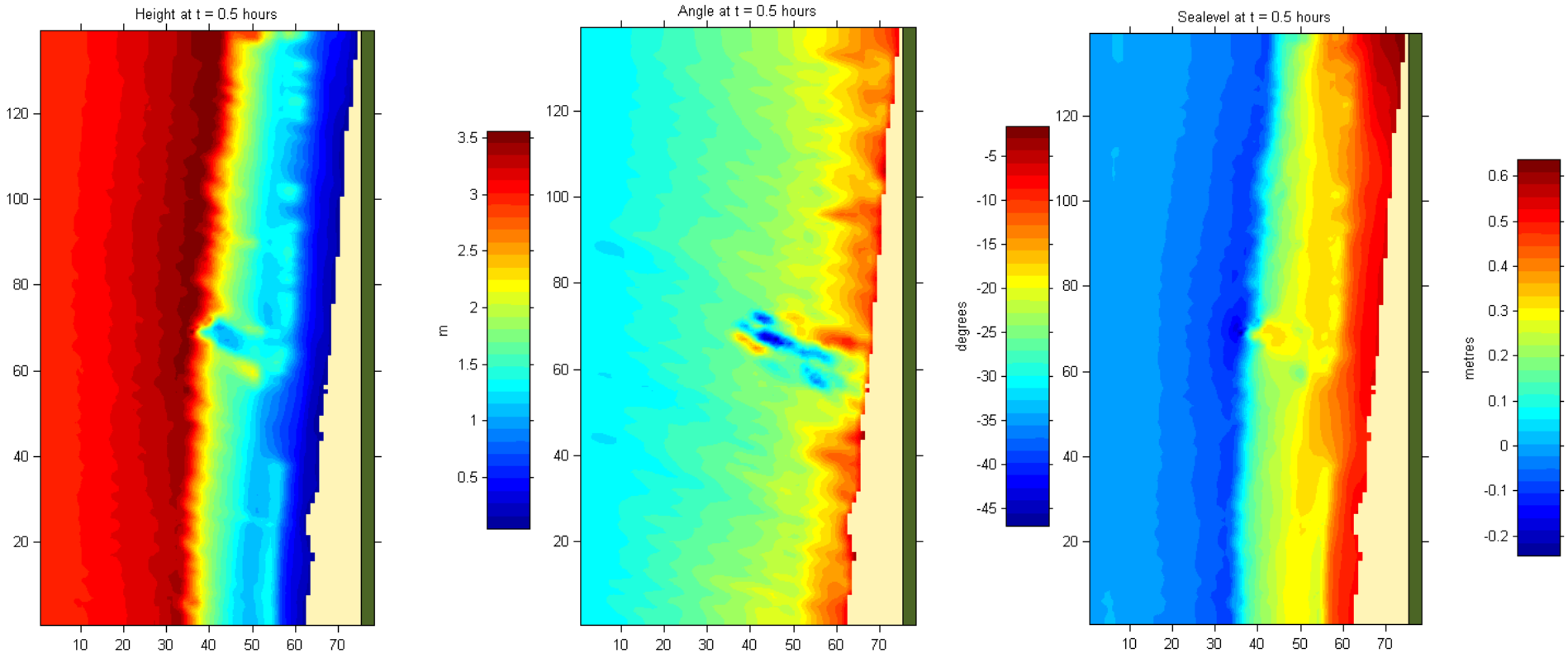

Figure D.29. Predicted wave heights, wave angles and sea levels for the wave event H = 3m and angle = -30°.

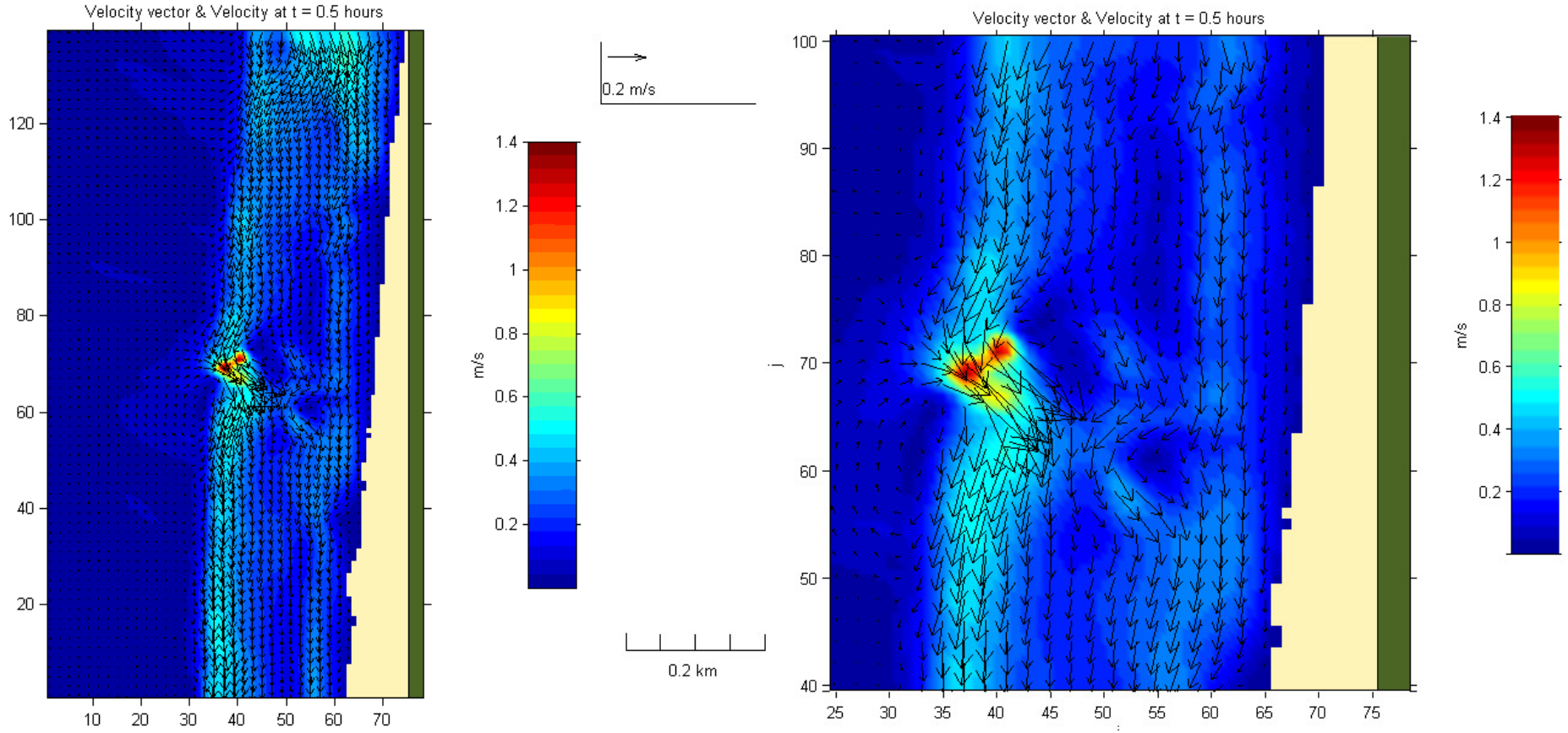

Figure D.30. Predicted hydrodynamic circulation for the wave event H = 3 m and angle = -30°. The full domain circulation is shown on the left and a focus on the reef vicinity is shown on the right.